Faculty of Sciences
Department of Geography

MODELLING THE WORLD IN 3D

Aspects of the acquisition, processing, management and analysis of spatial 3D data

Cornelis Stal

Promoter: Prof. Dr. ir. Alain De Wulf
Co-promoter: Prof. Dr. Philippe De Maeyer

Supported by the Fund of Scientific Research (FWO, G.0823.09N)

Dissertation submitted in accordance with the requirements for the degree of Doctor of Sciences: Geomatics and Surveying

Modelling the world in 3D: aspects of the acquisition, processing, management and analysis of spatial 3D data

Het modelleren van de wereld in 3D: aspecten rond de acquisitie, verwerking, beheer en analyse van ruimtelijke 3D data

Cornelis Stal
Department of Geography, Ghent University, Belgium

Supported by the Fund of Scientific Research (FWO, G.0823.09N)

Dissertation submitted in accordance with the requirements for the degree of Doctor of Sciences: Geomatics and Surveying

Promoter:
Prof. Dr. ir. Alain De Wulf
Department of Geography, Ghent University, Belgium

Co-promoter:
Prof. Dr. Philippe De Maeyer
Department of Geography, Ghent University, Belgium

Reading committee:
Dipl.-Ing. Dr.techn. Christian Briese
Department of Geodesy & Geoinformation, Vienna Technical University, Vienna, Austria

Prof. Dr. Roland Billen
Department of Geography, University of Liège, Liège, Belgium

Prof. Dr. Rudi Goossens
Department of Geography, Ghent University, Belgium

Examination board:
Prof. Dr. Nico Van de Weghe
Department of Geography, Ghent University, Belgium

Prof. Dr. ir. Sidharta Gautama
Department of Telecommunication and Information Processing, Ghent University, Ghent, Belgium

Prof. Dr. ing. Greta Deruyter
Department of Industrial Technology and Construction, Ghent University, Ghent, Belgium

Acknowledgements

The work presented in this dissertation is made possible with thanks to many people and institutions. First of all, I would like to express my sincere gratitude to the Fund for Scientific Research Flanders (FWO) for funding this research as part of a larger project entitled "3D CAD-modelling of spatial architectural volumes using terrestrial and airborne laser scanning" (G082309N). I would also like to thank Prof. Dr. ir. Alain De Wulf, who is the promoter of my work and Prof. Dr. Philippe De Maeyer, who is the co-promoter. I am very grateful for their guidance and advice during the process, but also for their time, patience, trust and most of all the opportunity to perform this research. It truly was a pleasure working with and for them. The project as a whole was co-promoted by Prof. Dr. Nico Van De Weghe, Prof. Dr. ir. Sidharta Gautama, Prof. Dr. Ronald De Meyer and Arch. Mario Mattys and I thank them for their participation in the project.

I would also like to express my appreciation and thankfulness to many colleagues who supported me during the research with interesting discussions, suggestions and support. In particular to Helga Vermeulen and Timothy Nuttens, but also to many other office colleagues and friends: Ann Vanclooster, Marijn Hendrickx, Leen Carlier, Bart De Wit, Dr. Amaury Frankl, Dr. Frederik Tack, Dr. Nasem Badreldin, Kim Van Liefferinge, and many others.

All the co-authors who participated in this research, like Prof. Dr. Rudi Goossens, Prof. Dr. Roald Docter, Prof. Dr. Jean Bourgeois and all the others are kindly thanked for their contribution to this work. The reviewers of the papers presented in this dissertation, the examination board and the journal editors are also acknowledged for their suggestions and critical view. Moreover, the promoters of my internship in Vienna, Univ.Prof. Dipl.-Ing. Dr.techn. Norbert Pfeifer, Dipl.-Ing. Dr.techn. Christian Briese and Dipl.-Ing. Dr.techn. Peter Dorninger, are gratefully thanked for their support.

Last but not least, I would like to thank my family and friends for their support, sympathy and prayers, in particular for my wife, Joke Stal, my father and mother, Huub and Yvonne Stal, my brother and sister, Bram and Lot Stal, and of course my grandmother Tinie Rigter. Bram Smets and Wouter Braet are also very trustful friends who supported me during the last few years of this work. I suppose it was not always a pleasure to live with a guy working on a Ph.D.

My sincere thanks to all these people, and many others who assisted me in this interesting research.

Cornelis Stal

“I can do all this through him who gives me strength”
Philippians 4:13 (NIV)

"Ik vermag alle dingen in Hem, die mij kracht geeft."
Filippenzen 4:13 (NBG)

Samenvatting

Het gebruik van virtuele 3D-modellen is van essentieel belang voor een groot aantal toepassingen, waaronder ruimtelijke planning, het aansturen van stedelijke voorzieningen, kadastrale kartering in 3D, toerisme, cultureel erfgoed en het organiseren van openbare dienstverlening. Modellen van ons leefmilieu, maar in het bijzonder 3D-stadsmodellen[1], ondersteunen de besluitvorming en worden gebruikt als communicatiekanaal tussen de overheid en het publiek. Er is een grote en groeiende vraag naar hoog-nauwkeurige 3D-stadsmodellen van complexe bebouwde gebieden, maar eveneens van grote landelijke gebieden. De mate waarin deze modellen op een geautomatiseerde wijze gemaakt worden is echter zeer laag. Daarnaast dient het productieproces van 3D-modellen het resultaat te zijn van een moeilijk evenwicht tussen enerzijds de gewenste graad van detail en anderzijds de performantie van het resulterende model. De beschikbaarheid van 3D-modellen wordt in grote mate gehinderd door deze kenmerken. Ten gevolge van deze kenmerken is het voor veel gebruikers van ruimtelijke data weliswaar mogelijk om zeer grote 3D-datasets in te winnen. Het daadwerkelijke gebruik van deze data ten behoeve van 3D-stadsmodellering blijft vaak buiten de mogelijkheden van de gebruikersgroep. Dit is zeker het geval wanneer meerdere datasets geïntegreerd dienen te worden voor de modellering in 3D.

In dit proefschrift worden verschillende elementen behandeld betreffende de acquisitie, het verwerken, de analyse en het beheer van ruimtelijke data voor 3D-modellering. De doelstelling van dit proefschrift is onder meer het optimaliseren van deze verschillende aspecten voor de constructie van 3D-stadsmodellen. Bijzondere aandacht wordt hierbij besteed aan het beschrijven en het behouden van de datakwaliteit, alsook aan de uitwisselbaarheid van de 3D-modellen. De verschillende onderdelen van het proces worden uitvoerig besproken en geïllustreerd aan de hand van een aantal toepassingen. Deze toepassingen hebben uiteraard betrekking op stadsmodellering, maar behelzen eveneens voorbeelden uit het cultureel erfgoed en de archeologie. De lessen die uit deze projecten geleerd kunnen worden, bieden uiterst noodzakelijke kennis en ervaring voor 3D-stadsmodellering. Daarnaast wordt de multidisciplinariteit van het gebruik van ruimtelijke 3D-data en de daaruit afgeleide modellen aangetoond door deze toepassingen.

In eerste instantie zullen meerdere 3D-data acquisitie sensoren en technieken besproken worden. Hierbij zal de nadruk worden gelegd op de theorie van de laserscanning en op gebruikelijke toepassingen van deze techniek. Ook fotogrammetrie en andere op foto's gebaseerde 3D-reconstructietechnieken waarbij gebruik gemaakt wordt van *Structure from Motion* en *MultiView Stereo* (SfM-MVS), zullen behandeld worden. Tot slot wordt een korte analyse gemaakt van het gebruik van conventionele topografische technieken voor oppervaktemodellering. Enerzijds worden *Airborne Laser Scanning* (ALS, laserscanning vanaf een vliegend platform) en luchtfotografie op grote schaal gebruikt voor het modelleren van oppervlakken en het

[1] Aangezien er geen ondubbelzinnige vertaling bestaat voor de term '*environmental model*', zal de term '3D-stadsmodel' gebruikt worden ter verwijzing naar 3D-modellen van ons leefmilieu in een ruime context.

systematische aanmaken van digitale hoogtemodellen (*Digital Elevation* Model, DEM [2]). Anderzijds is SfM-MVS recentelijk geïntroduceerd als een techniek voor het 3D-modelleren, waarbij de afstand tussen de camera en het te modelleren object beperkt is. Ter illustratie van het gebruik van SfM-MVS voor de 3D-modellering van kleine en complexe objecten wordt een innovatieve methode beschreven, waarbij 3D-modellen zijn gemaakt van historische globes. In dit geval zijn een groot aantal foto's gebruikt voor het digitaal reconstrueren van twee globes van Gerardus Mercator uit de 16de eeuw. Deze reconstructie was een grote uitdaging, aangezien het modelleren van kleine bollen geen alledaagse toepassing is, en de precisie en de kwaliteit van de textuur zeer hoog moeten zijn. Op deze manier wordt de wetenschappelijke reikwijdte van dit type patrimonium aanzienlijk vergroot. Tijdens een vergelijkende studie zijn verschillende technieken gebruikt om de optimale 3D-reconstructietechniek te kunnen selecteren voor deze globes.

Het resultaat van de 3D-reconstructie van de globes was duidelijk in het voordeel van SfM-MVS. De geometrische kwaliteit van deze modellen dient gekwantificeerd te worden vooraleer deze techniek daadwerkelijk aangewend kan worden voor het maken van 3D-stadsmodellen. Zodoende zijn verschillende DEM's aangemaakt op basis van ALS data, luchtfotogrammetrie en SfM-MVS voor twee verschillende testzones. Een eerste zone betreft een gebied met dichte bebouwing in Gent, en een tweede zone betreft een landelijk gebied in Kooigem (België). Voor deze vergelijking wordt verondersteld dat het tijdsverschil van twee jaar tussen verschillende opnamen geen invloed heeft op de resultaten. De ALS data worden gebruikt als referentie en worden vergeleken met de op foto's gebaseerde 3D-modellen. Een geometrische punt-naar-punt vergelijking biedt hierbij afstanden die voor de analyse gebruikt worden. Om de invloed van ongelijke puntendichtheden tussen de verschillende datasets te minimaliseren wordt een tweede punt-naar-mesh vergelijking uitgevoerd tussen de op foto's gebaseerde modellen en de getrianguleerde referentiedataset. Uit deze analyse blijkt dat de geometrische kwaliteit van het stedelijke testgebied veel lager is dan die van het landelijke gebied (respectievelijk ongeveer drie keer de pixelgrootte en één tot twee keer de pixelgrootte). Zowel voor de fotogrammetrie als voor de SfM-MVS zijn deze geometrische afwijkingen per studiegebied redelijk gelijkaardig. Naast de analyse van de geometrische kwaliteit van de modellen, zijn de mogelijkheden om de op foto's gebaseerde modellen te gebruiken voor het maken van Digitale Terrein Modellen (DTM) onderzocht. Voor het extraheren van grondpunten uit de puntenwolken is een gestandaardiseerde filterprocedure gebruikt op zowel het fotogrammetrische DEM alsook op het SfM-MVS gebaseerde DEM. Een statistische vergelijking tussen de gefilterde DTM's is uitgevoerd met behulp van een kruisvalidatie. De resultaten hiervan wijzen op een goede overeenkomst tussen de SfM-MVS en de op ALS gebaseerde puntenwolken voor het stedelijke gebied, en zelfs op een zeer goede overeenkomst voor het landelijke gebied. De correspondentie voor de fotogrammetrische puntenwolk is laag voor het stedelijke gebied en zelfs afwezig voor het landelijk gebied. Derhalve kan geconcludeerd worden dat SfM-MVS een betrouwbaar alternatief is voor conventionele oppervlak reconstructietechnieken, vooral wanneer een DTM nodig is.

[2] De verschillende modellen worden afgekort vanuit het Engels. Vrije vertalingen voor het DEM en DSM zijn respectievelijk DHM (Digitaal Hoogtemodel) en DOM (Digitaal Oppervlaktemodel)

In een tweede vergelijking tussen ALS gegevens en fotogrammetrische digital oppervlaktemodellen (*Digital Surface Model*, DSM) worden eveneens verticale verschillen geanalyseerd voor de stad Gent (België). In tegenstelling tot het eerste onderzoek wordt bij deze vergelijking aangenomen dat geometrische verschillen tussen de modellen veroorzaakt worden door het tijdverschil van negen jaar tussen de beide opnamen. Een verschilmodel wordt hierbij aangemaakt door beide DSM's van elkaar af te trekken. Vervolgens worden de waarden in dit model geëvalueerd om een onderscheid te maken tussen verschillen veroorzaakt door fouten in het model en verschillen veroorzaakt door een gewijzigde topografie. De verschillen veroorzaakt door fouten in het model kunnen worden geëlimineerd door gebruik te maken van beeldverbeteringprocedures. Hierdoor ontstaat een nieuw model dat enkel (stedelijke) veranderingen weergeeft. Zodoende bevat dit model gebouwen, of delen van gebouwen, die gesloopt of opgetrokken zijn in de tijdspanne van negen jaar. Uit dit onderzoek blijkt duidelijk het potentieel van zowel ALS-gegevens als van luchtfoto's voor de (geautomatiseerde) detectie van veranderingen in stedelijke gebieden. Het detecteren en modelleren van stedelijke verandering is zeer belangrijk voor de handhaving van de bouwreglementering en voor de opsporing van overtredingen van deze regels.

Een classificatie of filteringprocedure is noodzakelijk om DEM's converteren naar DTM's en DSM's. Helaas is het met de meest gangbare classificatiealgoritmen slechts mogelijk om enkele duidelijk omschreven klassen (grond, gebouwen, vegetatie) toe te wijzen. Voor wat betreft de semantische beschrijving van objecten belemmert deze beperking de flexibiliteit van geautomatiseerde procedures voor stadmodellering. Om die reden is er een innovatieve classificatieprocedure ontwikkeld op basis van Binomiale Logistische Regressie (BLR) analyse. Op basis van de evaluatie van een berekende probabiliteit wordt een punt toegewezen aan een door de gebruiker gedefinieerde klasse. De kans dat een punt tot een zekere klasse behoort, wordt geschat door het opstellen van een binaire logit functie, waarin een aantal parameters uit een '*feature space*' verwerkt zijn. Hoewel de '*feature space*' bepaald wordt voor elk punt in functie van een groot aantal geometrische kenmerken van de lokale puntenwolk, wordt er voor iedere klasse een afzonderlijke BLR-analyse uitgevoerd. Hierbij wordt gebruik gemaakt van een manueel samengestelde training set. De resultaten van deze gecontroleerde classificatieprocedure voor zowel een stedelijk gebied (Gent, België) als voor een landelijk gebied (Ctiněves, Tsjechië) zijn zeer goed, met type-I fouten variërend van 0.4% tot 7.7% en type-II fouten van 0.5% tot 6.4%. Deze resultaten tonen de mogelijkheden van deze methode aan voor geautomatiseerde semantische 3D-modellering.

De mogelijkheden om snel en accuraat virtuele representaties te genereren met behulp van efficiënte 3D-modelleringsprocedures is noodzakelijk voor de documentatie van snel veranderende omgevingen of objecten. Steden zijn dynamische omgevingen op een macroschaal, maar archeologische opgravingen zijn dit des te meer op een microschaal. Voor het opstellen van tijdreeksen wordt het gebruik van 3D-modellering op basis van foto's onderzocht voor een archeologische site. De site van Thorikos (Griekenland) is hierbij gebruikt als test-case, waarbij dagelijks een aantal fotorealistische 3D-modellen zijn gemaakt ter ondersteuning van het toezicht en documenteren van een lopende opgraving. De interactie tussen de 3D-modellen wordt mogelijk gemaakt door een beheersysteem op basis van een Harris matrix. Deze matrix

functioneert als een intermediair tussen een grafische gebruikersinterface en het databanksysteem, ten behoeve van de visualisatie en analyse van de 3D-modellen. Bovendien worden twee toepassingen voor deze 3D-modellen uiteengezet, gericht op volumeberekeningen of in-situ kartering van relicten van stenen muren. Het gepresenteerde management systeem, het koppelen van 3D-modellen aan gegevens van de opgraving, alsook het gebruik van 3D-modellen als een wetenschappelijk onderzoeksinstrument, tonen de veelzijdige mogelijkheden van 3D-data voor tijd-ruimtelijk onderzoek aan. De gepresenteerde applicaties kunnen met behulp van deze methode worden geïmplementeerd om historisch-geografische toepassingen mogelijk te maken, zoals het karteren van stadsontwikkeling in 3D op basis van gescand historisch beeldmateriaal.

Op basis van voorgaande conclusies wordt een innovatieve methode voor het opstellen van digitale 3D-stadsmodellen gepresenteerd. ALS-puntwolken, luchtfoto's en gegevens uit een digitaal 2D-kadaster worden gebruikt in een geïntegreerde aanpak voor 3D-stadsmodellering. De procedure wordt gevalideerd aan de hand van ruimtelijke gegevens van de steden Gent en Geraardsbergen (België). De datasets hebben een hoge dichtheid en een hoge nauwkeurigheid. De procedure steunt op het gebruik van gekende geografische en fotogrammetrische software. Bovendien wordt een grote mate van automatisering mogelijk gemaakt door scripts uit te voeren. De voorgestelde workflow start met de verwerking van de puntenwolk en met de detectie van gebouwen en van grond uit deze puntenwolk. Daarna wordt de geometrie van de gedetecteerde gebouwen beschreven door een vereenvoudigd triangulair model en wordt een afbeelding gemaakt voor het correct visualiseren van ieder object. Nadat het model aan de kadastrale databank is gekoppeld, beschikt ieder object in het model over de nodige semantiek. De resultaten van de voorgestelde procedure kunnen worden beheerd en geanalyseerd in een CityGML-database, waarna verschillende afgeleide modellen en visualisaties kunnen worden gegenereerd. Dit verhoogt het bereik en uitwisselbaarheid van deze 3D-stadsmodellen aanzienlijk.

Tot slot wordt een overzicht gegeven van de conclusies uit dit proefschrift. Deze conclusies situeren zich rond de hierboven besproken onderwerpen, en geven een concreet antwoord op een aantal belangrijke onderzoeksvragen:

- Welke data acquisitie methoden en platformen zijn in staat om ruimtelijke data aan te maken voor het opstellen van 3D modellen?
- Welke geometrische nauwkeurigheden kunnen worden behaald dankzij deze verschillende technieken, en wat is de performatie van de dataverwerking?
- Er van uitgaande dat puntenwolken gebruikt worden voor 3D-stadsmodellering, hoe kan dan informatie uit deze puntenwolk geëxtraheerd worden?
- Hoe kunnen ruimtelijke data worden beheer, met de nadruk op het gebruik van ruimtelijk-temporele databanken met verschillende datasets, en overeenkomstig een gegeven data model?
- Hoe kunnen ruimtelijke data worden gebruikt voor het opstellen van 3D stadsmodellen waarbij gebruik gemaakt wordt van een geïntegreerde en semi-automatische procedure?
- Wat is het doel van het modelleren van het leefmilieu, steden of andere modellen in 3D, en hoe kunnen deze modellen bijdragen tot multidisciplinair onderzoek?

Ter ondersteuning worden de belangrijkste bevindingen in een brede context geplaats, om de praktische reikwijdte van dit werk te benadrukken. Ook worden mogelijkheden en kansen besproken voor toekomstig onderzoek. Hoewel er dus nog werk aan de winkel is, kan wel worden gesteld dat dit werk een significante bijdrage levert aan het onderzoek rond data acquisitie, processing, management en analyses ten behoeve van 3D-modellering.

Summary

The use of virtual 3D models has gained a significant importance for a wide range of applications, like spatial planning, urban facility management, 3D cadastre mapping, tourism or the organization of public services. Environmental models and 3D city models facilitate decision making processes and they are used as communication channel between the government and the public. In spite of the growing demand for high quality 3D city models of complex urban areas, but also for large rural areas, the degree of automation for generating these models is rather low. Moreover, the construction process is the result of a difficult equilibrium between the desired level of detail on the one hand and model performance on the other hand. These properties are substantial bottle necks for the availability of the models. As a result, spatial data users are able to obtain very large 3D data sets, but the use of 3D city models derived from these data is frequently out of range. This is especially the case when multiple data sources are used to obtain these 3D models.

This dissertation covers different elements of the acquisition, processing, analysis and management of spatial data for 3D modelling. The aim of this research is the optimization of the various aspects of the workflow for 3D city model generation. A special focus is also given to the assessment and preservation of the quality of the data, but also on exchangeability. The different phases of the workflow are elaborated and illustrated with applications that are also beyond 3D city modelling, like 3D reconstruction for cultural heritage management and archaeology. The lessons learnt from these projects result in indispensable knowledge for environmental mapping and 3D city modelling. Furthermore, these extended applications demonstrate the multidisciplinary of the use of 3D spatial data and their derived models.

At first, multiple 3D data acquisition sensors and techniques are elaborated, focussing on the theory of laser scanning and applications of this technique. Photogrammetry and image based 3D reconstruction techniques using Structure from Motion and Multi-View Stereo (SfM-MVS) are also discussed, next to the use of conventional topographic techniques. On the one hand, Airborne Laser Scanning (ALS) and airborne photogrammetry are traditionally used for the systematic construction of Digital Elevation Models (DEM). On the other hand, SfM-MVS is recently introduced for (close range) 3D modelling applications, where the appearance of a 3D model is of great importance. As an example of the use of SfM-MVS for 3D reconstructions of small and complex objects, the technique is applied for the 3D modelling of historical globes. In this case, a large number of images are used for the digital representation of two 16th century globes, made by Gerardus Mercator. This reconstruction project is a great challenge, since the modelling of small

spheres is not a common application, where both the precision and the quality of the texture mapping have to be high. If the texture maps of these models correspond with the real appearance of the globes, it is possible to perform historical and cartographic research on these objects without actually possessing the globes. This significantly increases the scientific range of this patrimony. A feasibility study is performed for the 3D reconstruction, using different image based techniques and laser scanning.

The results of the globe reconstruction project are very satisfactory in favour of SfM-MVS. However, in order to use this technique for environmental modelling, the geometric quality has to be assessed. Hence, DEMs based on ALS data, airborne photogrammetry and SfM-MVS are generated for two test sites, covering a heavily built-up area in Ghent and a rural area in Kooigem (Belgium). For this comparison, it is assumed that the temporal difference of two years between the data sets does not have an influence on the results. The ALS-based models are used as reference data and geometrically compared with the image based 3D models. A point-to-point comparison is performed for this analysis. In order to minimize the influence of unequal point densities of the different data sets, the reference point cloud is triangulated and another comparison is performed using a point-to-mesh comparison. The analysis made clear that the geometric quality of the urban area is much lower (two or three times the pixel size, ~0.30-0.45 m) than of the rural area (around one time the pixel size, ~0.20-0.40m). However, for both the image based reconstruction techniques, these geometric deviations are very similar per study area. Next to the analysis of the geometric quality of the models, the ability to use the image based point clouds for the construction of Digital Terrain Models (DTM) is explored. For the extraction of ground points, a standard point cloud filtering procedure is executed on both the photogrammetric DEM and the SfM-MVS-based DEM. The statistical comparison between the filtered image based point cloud and the ALS-based point cloud is determined using cross validation, indicating a good correspondence between the SfM-MVS and ALS-based point clouds for the urban test site and very good correspondence for the rural test site. For the photogrammetric point clouds, this correspondence is low for the urban test site and even absent for the rural area. Therefore, it can be concluded that SfM-MVS is a reliable alternative for conventional surface reconstruction techniques, especially when DTMs are required.

An additional comparison between ALS data and photogrammetrically derived Digital Surface Model (DSM) is also presented for the city of Ghent (Belgium). The vertical differences between the models are mainly caused by the temporal shift of nine years between the two acquisition campaigns, in contrast with the previous research. Thus, a pixel-wise difference model is generated by subtracting the two DSMs. Thereafter, the magnitude of the differences is evaluated in order to distinct erroneous differences in the model and differences caused by changed topography. Pixels that represent unchanged areas indicate the same errors as described in the previous comparison. After performing a series of image enhancement procedures, like morphologic filtering, change models can be generated. These models contain all constructed and destroyed structures in the study area for the time frame between the two acquisition models. Hence, this research clearly demonstrates the potential of both ALS data and airborne imagery for the (automated) detection of changes in urban areas. Urban change modelling is a very important

tool for the enforcement of the building regulations and for the detection of violations of these regulations.

A classification or filtering procedure is required to convert DEMs to DTMs and DSMs. Unfortunately, most available classification algorithms only allow the assignment of clearly defined point classes (ground, buildings, vegetation). This hampers the flexibility of automated city modelling procedures in terms of semantic description of features in these models. To overcome this limitation, an innovative classification procedure is presented based on Binomial Logistic Regression (BLR) analysis. A point is assigned to a user-defined class, based on probability evaluation. The probability that a point belongs to a class is estimated by the construction of a binary logit function, containing a series of parameters derived from a feature space. Whereas the feature space is calculated for each point as a function of a large number of neighbourhood variables, the BLR analysis makes use of a manually generated training point cloud for each class. The results of this supervised classification procedure are very good for both an urban study area (Ghent, Belgium) and a rural test site (Ctiněves, Czech Republic), with type-I errors ranging from 0.4% to 7.7 % and type-II errors ranging from 0.5% to 6.4%. Thus, the great potential of the proposed classification methodology for automated semantic 3D modelling is obvious.

The ability to generate fast and accurate virtual representations using efficient 3D modelling procedures is required for the documentation of rapidly changing environments. Cities are dynamic environments, but archaeological excavations all the more on a micro scale. The possibility of using image-based 3D modelling for the construction of time series is explored for the archaeological site of Thorikos (Greece). In order to monitor the on-going of the excavation and to document the findings on the site, photorealistic 3D models are generated on a daily base. The interaction with the 3D models is enabled by a management system. This system is implemented as a consultation and analysis application using a Harris matrix. The matrix functions as an intermediate between a graphical user interface and the database system. Additionally, two applications of these 3D models are presented, focussing on capacity calculations and in-situ mapping (orthophoto mapping) of stone wall relicts. The presented management system, the linking of 3D models with excavation data, and the use of 3D models as a scientific tool, demonstrate the huge potential of 3D data for spatio-temporal research. The presented applications can easily be implemented to historical-geographical applications, like retrospectively urban development modelling using scanned historical imagery.

Based on a compilation of previous research results, a new approach for the construction of 3D city models is presented in the last part of this dissertation. ALS point clouds, airborne imagery and digital 2D cadastre data are used in an integrated modelling approach, and validated with high density and high accurate spatial data of the city of Ghent and Geraardsbergen (Belgium). The procedure is supported by widely used geographic and photogrammetric software. Furthermore, a large degree of automation is enabled by the use of scripting tools. The proposed workflow starts with the point cloud processing and the feature detection, where building points and ground points are separated from other points. Thereafter, the detected building features are described by a simplified triangular model and a texture map is generated for the each feature. Each geometric

feature in the models also contains semantics after linking the features with the cadastre data. The results of the presented procedure can be managed and analysed in a CityGML database, and different visualisations can be generated for standard 3D viewers, significantly increasing the range and exchangeability of these 3D city models.

Finally, an overview of the conclusions of this dissertation is recapitulated. These conclusions focus on the different topics mentioned earlier in this summary, and aim to give specific answers to the following research questions:

- Which data acquisition platforms and methods are able to acquire spatial data for the construction of 3D models?
- What geometric accuracies and precisions can be reached using the different data acquisition methods and what are the performances of these methods in view of further data processing?
- Under the assumption that point clouds are used for 3D city modelling, how can information be extracted from these point clouds?
- How can 3D data be managed, more specifically in a spatio-temporal database with multiple data sources and in accordance with a certain data model?
- How can spatial data be used for the construction of 3D city models, using an integrated and semi-automatic procedure?
- What are the potential applications of the modelling of environments, cities or other objects in 3D, and how can these models contribute to multidisciplinary research?

In order to emphasize the wide range of this work, the most important findings are put in a broad context. Moreover, the strengths and opportunities for further research are elaborated. Although the different topics in this dissertation still offer many opportunities for further research, it can be concluded that this work significantly contributes to the research on data acquisition, processing, management and analysis for 3D modelling.

Contents

List of abbreviations and symbols

AGIV	Agentschap voor Geografische Informatie Vlaanderen
AGL	Above Ground Level
ALB	Airborne Laser Bathymetry
ALS	Airborne Laser Scanning
ANOVA	Analysis of Variance
ASPRS	American Socienty of Photogrammetry and Remote Sensing
ASTER	Advanced Spaceborne Therman Emission and Reflection
BLR	Binomial Logistic Regression
B-REP	Boundary Representation
CCD	Charge-Coupled Device
CIR	Colour InfraRed
CityGML	Geographic Markup Language for Cities
CMOS	Complementary Metal Oxide Semconductor
CSG	Consecutive Solid Geometry
DEM	Digital Elevation Model
DSM	Digital Surface Model
DTM	Digital Terrain Model
eATE	enhanced Automatic Terrain Extraction
EDM	Electromagnetic Distance Measurement
FLEPOS	Flemish Positioning System
GCP	Ground Control Point
GDEM	Global Digital Elevation Model
GIS	Geographic Information System
GML	Geographic Markup Language
GNSS	Global Navigation Satellite System
GRB	Grootschalig Referentie Bestand
GSD	Ground Sampling Distance or Ground Space Distance
h	Ellipsoidal height
H	Orthometric height
ICP	Iterative Closest Point
IDW	Inverse Distance Weight
INS	Inertial Navigation System
inSAR	Interferometric Syntetic Aperture Radar
INSPIRE	Infrastructure for Spatial Information in the European Community
IQR	Inter Quartile Range
KML	Keyhole Markup Language
LAS	LASer scanning file format
LiDAR	Light Detection And Ranging
LoD	Level of Detail
LPS	Leica Photogrammetric Suite
LSM	Least-Squares Matching
MAE	Mean Absolute Error
MBES	Multi-Beam Echo Sounder

MPG	Multi-Photo Geometrically
MS	Mean Square
MTLS	Mobile Terrestrial Laser Scanning
MVS	Multi-View Stereo
NDVI	Normalized Difference Vegetation Index
NGI	Nationaal Geografisch Instituut
OBIA	Object Based Image Analysis
OGC	Open Geospatial Consortium
P2M	Point to Mesh
P2P	Point to Point
POS	Positioning and Orientation System
RMSE	Root Mean Square Error
RTK	Real Time Kinematic
SD, StDev, STD	Standard Deviation
SDI	Spatial Data Infrastructure
SfM	Structure from Motion
SRTM	Shuttle Radar Topography Mission
STLS	Static Terrestrial Laser Scanning
TEN	Tetrahedronized Irregular Network
TIF	Tagged Image Format File
TIN	Triangular Irregular Network
TOF	Time Of Flight
UAV	Unmanned Aerial Vehicle
UTM	Universal Transversal Mercator
VHR	Very High Resolution (satellite imagery context)
WGS	World Geodetic System
WMS	Web Mapping Service
WRL	Virtual Reality Markup Language (from VRML)
X3D	XML based 3D format
XML	eXchange Markup Language

List of figures

1. General introduction

2. 3D data acquisition

3. Digital representation of historical globes: methods to make 3D and pseudo-3D models of 16th century Mercator globes

4. Comparison of airborne laser scanning and image based modelling techniques

5. Airborne photogrammetry and LiDAR for DSM extraction and 3D change detection over an urban area: a comparative study

9. Discussion and general conclusions

List of tables

8. 3D city mapping and data management using interconnected GI-software and Python

List of equations

2. 3D Data acquisition

4. Comparison of airborne laser scanning and image based modelling techniques

5. Airborne photogrammetry and LiDAR for DSM extraction and 3D change detection over an urban area: a comparative study

6. Classification of airborne laser scanning point clouds based on binomial logistic regression analysis

Chapter 1

General introduction

1. General introduction

1.1. *Research context*

During the last century, our environment has changed dramatically. The booming population, increasing prosperity and improving mobility are just a few reasons for the significant growth of cities and for the urbanization of open spaces in Europe. Social dynamics and technological developments have increased the number of activities in both urban and rural spaces (Vos and Meekes, 1999). Moreover, the number of functions assigned to space has improved significantly. Especially in urban spaces, the environment itself is becoming more and more complex and activities in these areas are intensified. Moreover, the pressure on rural areas as urban spheres of influence and as intermediate between urban areas is enormous (Antrop, 2000). The growth of urban areas does not seem to temper in the near future and the pressure on rural and open spaces will increase even more. Without smart policy and governing, these developments have a negative influence on the environment as a whole. Hence, the need for sustainable management of space emerges (Naess, 2001). Various aspects were discussed in literature, like the relation between spatial planning and the conservation (or the improvement) of biodiversity (Sandström et al., 2006) and the link with water management (Niemczynowicz, 1999).

A thorough understanding of these phenomena in a geographical context is required to facilitate spatial development, environmental management and protective planning. Thus, planning and management of the environment are based on conceptual models and high quality spatial data (Antrop, 2004). Spatial data are defined as data that identify the location, geometry and semantic attributes of any object or feature in space. The spatial component is supplied with a coordinate reference system and, optionally, with topology or with appearance rules. Geographic Information Systems (GIS) play an important role in acquiring, analysing, manipulating, managing, presenting and storing spatial data. Crisis management (Vakalis et al., 2004), cadastre mapping (Bartoněk et al., 2011) or pollution modelling (Merbitz et al., 2012) are just a few examples of issues that find a solution or at least a support in the use of GIS. Unfortunately, the ability to perform environmental analysis and to support various discussion making processes is limited by the dimension of the data, where a single attribute is assigned to a planimetric shape (point, line, polygon or raster cell).

Most spatial data, as well as the analysis, data formats, processing platforms, et cetera are traditionally in 2D. If the elevation of a terrain or surface is assigned to a planimetric feature as an attribute, one will speak of a Digital Elevation Model (DEM). In this case, one and only one elevation is assigned to a geometric feature, which is mostly either a (raster) cell in a grid or a point in a Triangular Irregular Network (TIN) (De Wulf et al., 2012). A transitional dimension of 2.5D is assigned to these features (Axelsson, 2000). This means that a planimetric point has only one elevation value assigned to it, so $f(x,y) = h$ (ellipsoidal height) or H (orthometric height) (Gruen and Akca, 2005). In this context, a measured point cloud in 3D may be converted to a 2.5D grid, describing elevations as a series of bivariate functions within a horizontal plane (Pfeifer, 2002). The resulting DEM may consist of features covering the Earth's ground surface and objects on this surface, like vegetation, buildings ... In this case, the model is called a Digital

Surface Model (DSM). When a ground point filtering or feature classifier has been applied on the DEM, a Digital Terrain Model (DTM) can be constructed, representing the earth topography (Pfeifer and Mandlburger, 2008). It is essential to use appropriate filters or classifiers, taking specific data properties into account like the point density, terrain roughness or the covered environment. If an object can be modelled as a closed and bounded geometry, Constructive Solid Geometries (CSG) (Over et al., 2010), boundary representations (B-REP) or Tetrahedonized Irregular Network (TEN) (Penninga et al., 2006) can be used. These types of geometries enable to define a feature as a volume, possibly combined with attributes or appearance properties. All these 2.5D geometric models can be extended to full 3D, but the data storage and analytical complexity increases considerably. However, for most spatial applications and environmental applications in particular, 2.5D DEMs are used, (Tack et al., 2012a; Werbrouck et al., 2011).

Since a few years, full 3D spatial data play an essential role in environmental research and even in society as a whole. It was only since recently that 2.5D and 3D spatial data were acquired and used by a limited number of companies and institutions. The larger availability of data acquisition sensors, the increasing capacities of PCs and improved methods to exchange data between users have caused an immense need for more spatial data and applications (Horne et al., 2007). On the data supply side, recent developments in airborne and terrestrial laser scanning, conventional and close-range photogrammetry, satellite remote sensing or Global Navigation Satellite Systems (GNSS) have resulted in new methods for fast and accurate data acquisition (Molina et al., 2014). On the data demand side, ‘open’ initiatives like community based mapping (OpenStreetMap) and 3D modelling (Google Earth and Google/Trimble SketchUp, Figure 1-1) have seeded a public conscience on the need for spatial data and for 3D spatial data in particular. The absence of a quality control system for these open data (the community controls its own data) is one of the reasons that the use of open spatial data is limited to virtual tourism or some experimental scientific projects (Jacob et al., 2009; Schilling et al., 2009). Although the open initiatives lack legal responsibility on the data quality, the projects were probably a motivation for governmental institutions to make their data available for the public. New ‘official’ data sources are now made available with various levels of accessibility (EC, 2007; US, 1994). In most cases, professionally acquired data are preferred, in correspondence with predefined and well-documented protocols. Governmental organizations unambiguously define these quality criteria in public tenders (Swart, 2010).

Figure 1-1: Screenshot from *Google Earth*, containing 3D buildings in the Damrak area in Amsterdam (the Netherlands)

On the hardware and software side, it is obvious that recent developments in Graphics Processing Units (GPU) and powerful 3D renderers have increased the accessibility of 3D city models for a large non-expert public. Whereas widely used software packages like *Google Earth* are frequently used for visualization only, computer games allow sweeping interaction between the user (gamer) and the 3D model (game). In order to illustrate the popularity of these games, two examples can be given: *Assassin's Creed III*, with 12 million distributed units sold in 2012 (Figure 1-2, left, www.ubisoftgroup.com) or *Grand Theft Auto V*, with even 29 million units sold in 2013, after the release in September 2013 (Figure 1-2, right, www.rockstargames.com). Among others, these two examples are well known for their pleasant graphics, generated by powerful graphic engines. Mentioning computer games may sound casual in this context, but game development is very interesting for 3D environmental modelling in applied sciences (Anderson et al., 2010). Many topics that are covered in this domain also have great relevance in city modelling, like the concepts of optimized geometric modelling, Levels of Detail (LoD) or texture mapping (Ahearn, 2008). Moreover, the design process of 3D games highly corresponds with the city modelling process (Fritsch and Kada, 2004). However, real-world structures of cities are not accurately modelled in 3D games and much repetition of geometrical shapes is performed. Accurate 3D models with a high LoD representing real-world objects require a lot of manual processing (Tack et al., 2012b). Moreover, the local accuracy of the models in 3D games does not mean that a geographic framework is defined and that coordinate systems are absent.

Figure 1-2: Computer games as interface between 3D models and non-expert users in *Assassin's Creed III* (Venice, left, *Ubisoft* ®) and *Grant Theft Auto V* (Los Angeles, right, *Rockstar* ®)

The developments of environmental models, of 3D city models but also of 3D models of small objects are driven by various scientific disciplines, like computer sciences, geographic information sciences or remote sensing. The construction and use of 3D models implies some important facets in these disciplines: data acquisition using different sensors and techniques (Baltsavias, 1999; Beccari et al., 2010), data processing and feature modelling using various algorithms (Benner et al., 2005; Sampath and Shan, 2010), the management and exchange of the models (Kolbe et al., 2005; Pauwels et al., 2011), but also the visualization and analysis of the city models (Manferdini and Remondino, 2010; Mendes et al., 2012). Most of these aspects are covered individually in literature. The fragmentation of the various acquisition, processing and finalization approaches hampers the development of an integrated solution for the construction of 3D city models. Such an integrated procedure would facilitate the integration of various concepts and methods in the different steps of the modelling process. Data fusion plays an important role in this process and can be defined as the framework in which the means and tools are expressed for the conflation of different data sources or sensors into one single data set (Wald, 1999). Much research has already been done on the fusion of spatial data, focusing on raw data, processed data or analysed data. In a virtual model, 3D spatial data should be structured in accordance with a predefined conceptual data model. This conceptual data model describes the requirements of the data and the formal rules of these data. CityGML is such a model and enables to describe urban features by a predefined ontology in terms of geometry, semantics, appearance and topology (Gröger et al., 2008; Kolbe, 2009). The question now arises how to process, reformulate or transform the large amount of different data sets towards these sets of rules, in order to generate city models and to facilitate the management and planning of urban and rural spaces.

1.2. ***Research questions***

As discussed above, city modelling covers a long chain of various steps. The entire process contains an interconnected chain of steps, where the results of one phase have an explicit

influence on the quality of the following phases. Moreover, different aspects of the city modelling process suffer from various difficulties that have to be identified. Döllner et al. (2006) focus on the lack of automation in the production process and the weak integration of data sets. These bottlenecks are related to the following aspects of 3D modelling:

- The data acquisition using different sensors and techniques;
- The data processing and feature modelling using various algorithms;
- The data management;
- The data exchange of the final city models.

Thus, a thorough knowledge of the different spatial data acquisition, data processing and data conceptualization steps is indispensable. Gathering and compiling this knowledge in the broad context of city modelling and substantiated by some interesting applications are the main objectives of this dissertation. This objective can be re-formulated with the following central research question:

"Which aspects have to be taken into account for 3D feature modelling, when dealing with the acquisition, processing, management and analysis of spatial data?"

An exploration of this central research question is represented in our cognitive model in Figure 1-3, covering different aspects of 3D modelling. Based on this schema, six more specific research questions are formulated:

RQ1: Which data acquisition platforms and methods are able to acquire spatial data for the construction of 3D models?

RQ2: What geometric accuracies and precisions can be reached using the different data acquisition methods and what are the performances of these methods in view of further data processing?

RQ3: Under the assumption that point clouds are used for 3D city modelling, how can information be extracted from these point clouds?

RQ4: How can 3D data be managed, more specifically in a spatio-temporal database with multiple data sources and in accordance with a certain data model?

RQ5: How can spatial data be used for the construction of 3D city models, using an integrated and semi-automatic procedure?

RQ6: What are the potential applications of the modelling of environments, cities or other objects in 3D, and how can these models contribute to multidisciplinary research?

The core of the schema in Figure 1-3 deals with aspects of spatial data acquisition, data conceptualization and data processing. Spatial data acquisition is subdivided in different platforms

and acquisition methods and is covered by research question 1 and 2, aiming at the theoretical elaboration of 3D data acquisition sensors and methods, as well as on the quality assessment of the resulting models. Among others, data processing for 3D modelling consists of point cloud classification, which is covered by research question 3. This processing aspect also regards feature reconstruction and appearance reconstruction, which is a part of research question 5. This question, together with research question 4, is part of the discussion on data conceptualization. The geometrical representation is described by this element, focussing on the dimensional complexity of the data, the LoD, the conceptual data model and the physical data model. The last element of this schema, dealing with 3D modelling applications, is purposefully positioned in the centre. Different applications are presented when discussing research question 6. The modelling applications are heavily related with other elements (acquisition, processing and conceptualization) and vice versa. In the rest of this section, the different research questions will be discussed in more detail, making links between the questions and different chapters of this dissertation.

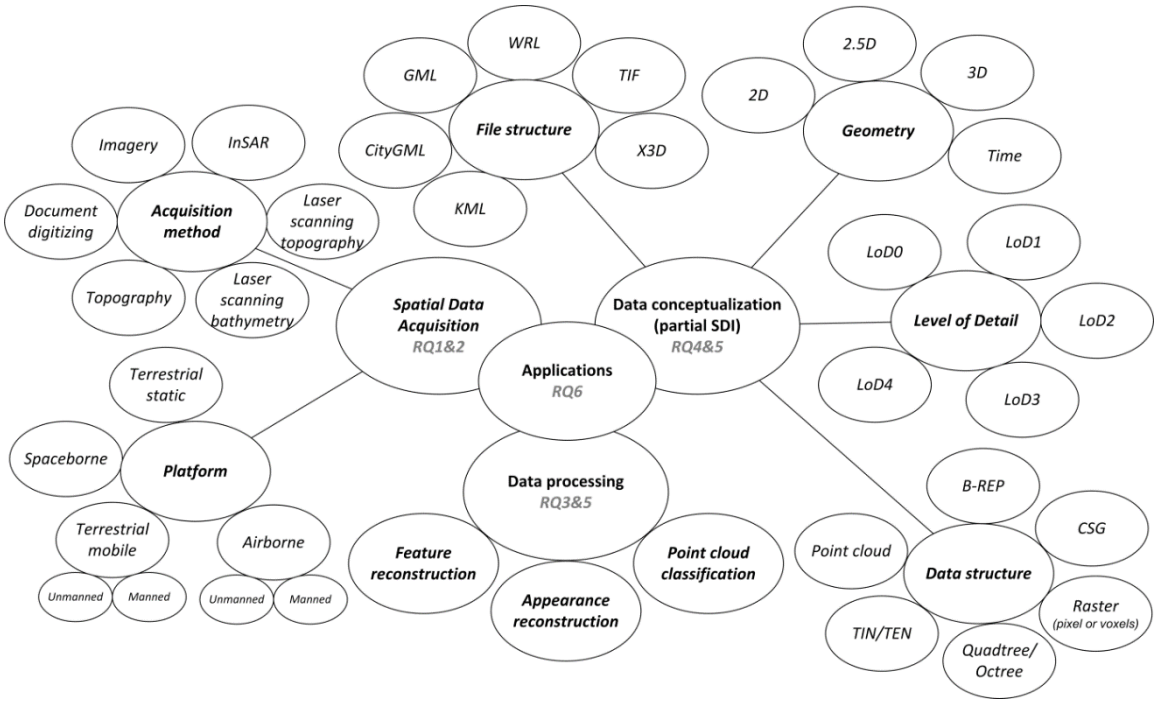

Figure 1-3: Cognitive model of the different aspects of the research questions

RQ1: Which data acquisition platforms and methods are able to acquire spatial data for the construction of 3D models?

The data acquisition platforms and methods are important for a full comprehension of the spatial data itself as well as for the selection of appropriate methods for the data processing. Moreover, the evaluation of platforms and sensors enable to perform an a-priori data quality assessment and also allows the evaluation of the project feasibility. A theoretical elaboration of the different data acquisition platforms and methods is therefore presented in chapter 2. For 3D modelling using airborne and spaceborne platforms, the use of Airborne Laser Scanning (ALS) (Doneus et al., 2008; Oude Elberink and Vosselman, 2011), Interferometric Synthetic Aperture Radar (InSAR) (Simarda et al., 2008) and image based modelling (Frankl et al., 2008; Tack et al., 2012a) are

well-known in literature. Besides, conventional photogrammetry and Structure from Motion and MultiView Stereo (SfM-MVS) are frequently used as image based techniques for environmental modelling. Furthermore, combinations of different systems (Haala and Kada, 2010; Rottensteiner et al., 2007) are well-known for airborne applications. For terrestrial application, mobile (or kinematic) and static platforms can be distinct. Both Mobile Terrestrial Laser Scanning (MTLS) and Static Terrestrial Laser Scanning (STLS) (Jaboyedoff et al., 2009), image based modelling (Tack et al., 2005) and integrated systems are currently in use (Briese et al., 2012; Remondino, 2011) and can be seen in similarity with airborne techniques. Notwithstanding the correspondence between airborne and terrestrial techniques, a theoretical research is required to support further qualitative studies on the geometric accuracy and feasibility of the techniques for environmental modelling and city modelling.

RQ2: What geometric accuracies and precisions can be reached using the different data acquisition methods and what are the performances of these methods in view of further data processing?

In this dissertation, the following definition for accuracy and precision are respected (OGC, 2013): *"The degree to which information on a map or in a digital database matches true or accepted values. Accuracy pertains to the quality of data and the number of errors contained in a dataset or map. In discussing a GIS database, it is possible to consider horizontal and vertical accuracy with respect to geographic position, as well as attribute, conceptual, and logical accuracy. The effect of inaccuracy and error on a GIS solution is the subject of sensitivity analysis. Accuracy, or error, is distinguished from precision, which concerns the level of measurement or detail of data in a database."* Describing geometric accuracy is thus a matter of comparing a spatial data set with a ground truth or reference data set (Hyyppä et al., 2005). From a more statistical point of view, accuracy can be defined as the 'correctness' of data, frequently measured by the mean deviation from a ground truth (Stal et al., 2011). In this context, precision is defined by the noise of the data, measured by the standard deviation and designated by the LoD. In many cases, spatial data and the resulting 3D models have to be in conformity with predefined geometric accuracy requirements or directives. These definitions are formalized in international standards for environmental modelling using CityGML (Fan and Meng, 2009) and for laser scanning in general (APSRS, 2004), but also for bathymetric applications (Mills, 1998). The discussions about the formulation of standards for bathymetric modelling and quality assessment of the resulting data even date back to 1957 (IHO, 2008). For CityGML, the classes of accuracy are constrained for each of the five LoDs (Gröger et al., 2008). Qualifying the geometric accuracy of spatial data sets enables to evaluate the correspondence of the modelling results with the requirements and directives. Clear procedures for accuracy assessments are therefore indispensable. The data quality of terrestrial 3D models and modelling performance are discussed in chapter 3. For airborne applications, accuracy and performance are the main topics of the comparative studies presented in chapter 4 and 5. In chapter 4, the analysis will result in the selection of the most optimal airborne 3D data acquisition methodology, whereas in chapter 5, the models from two techniques are used for automated change detection.

RQ3: Under the assumption that point clouds are used for 3D city modelling, how can information be extracted from these point clouds?

Frequently, ALS point clouds are just a large series of points with (*x*,*y*,*z*)-coordinates, possibly accompanied with other measured parameters like the colour or intensity value. When using the standardized LAS-format, these values are stored in accordance with a specific record format (ASPRS, 2013). A point classification value is also allowed, but the possibility to define real-time classes to points during the data acquisition is very limited. Therefore, point cloud classification or filtering is required within an information extraction process using post-processing software (Chen, 2007). On the one hand, classification is the process where points are assigned to a specific class based on certain properties (Xu et al., 2012). On the other hand, filtering will also use these properties, but will remove points that do not meet these similar properties. Thus, point cloud filtering is mainly used for the derivation of DTMs after separating ground-points and non-ground-points (Li, 2013; Podobnikar and Vrecko, 2012). Different ground extraction algorithms and classification procedures are discussed and compared by Sithole and Vosselman (2004), distinguishing different methods by the way these classifiers make assumptions about a point and its neighbourhood. Some techniques are based on mathematical morphology (Chen et al., 2007; Mongus and Žalik, 2012), surface roughness analysis (Höfle et al., 2009), local slope analysis using distance thresholds (Meng et al., 2009) or surface based robust interpolation (Briese et al., 2002). Another possibility for the classification of point clouds is the use of geometrical clustering analysis using feature spaces. This classification technique evaluates the correspondence of the feature space of a point with its neighbourhood properties (Bartels and Wei, 2010) or with a best fitting plane (Dorninger and Pfeifer, 2008). A variant of such a neighbourhood-based classification procedure is presented in chapter 6.

RQ4: How can 3D data be managed, more specifically in a spatio-temporal database with multiple data sources and in accordance with a certain data model?

A solid data management is indispensable for the proper use of large spatial data sets. The rules that define all aspects of spatial data in a project are embodied in a Spatial Data Infrastructure (SDI), dealing with the geographical data, but also with standards, metadata, tools, technical aspects of the data and different systems, as well as the policy and legal context (Steiniger and Hunter, 2011). Besides the knowledge of origin of different data sources for spatial data, data fusion and data standardization are also very important and need to be elaborated. This becomes clear with the research in chapter 5, 7 and 8, where different data sources are used in an integrated way for the construction of one final model or series of models. Wald (1999) defines data fusion as the framework on which the means and tools are expressed for the conflation of different data sources or sensors into one single data set. Much research has already been done on the fusion of spatial data, focusing at the acquisition level (sensor fusion), the processing level or the level of the final results (Becker, 2009; Vaaja et al., 2011; Würländer and Wenger-Oehn, 2007). These levels of data fusion are related to the information content and the degree of complexity of the different described features or phenomena in the data (Zhang, 2010). A data model is an abstraction of the real world, functioning as an intermediate between real world objects and phenomena on the one hand and the data structure (logic model) and file structure (physical model) on the other hand (Peuquet, 1984). The data structure defines how spatial data are stored in a database (TIN, point cloud, BREP), whereas the file structure is defined by file definition

standards, like the Geographic Markup Language (GML, extended by the previously mentioned CityGML), Web Mapping Service (WMS) or Keyhole Markup Language (KML) (Chen and Xie, 2008).

RQ5: How can spatial data be used for the construction of 3D city models, using an integrated and semi-automatic procedure?

When it is known how to prepare spatial data in accordance with a SDI, the final question is how to generate 3D city models out of these data. Referring to the concept of LoDs, buildings in 3D city models may be represented as flat surfaces in a DEM (LoD0), vertical extruded bodies (LoD1), generalized geometries (LoD2) or exact geometries (LoD3 and LoD4) (Löwner et al., 2013). LoD3 and LoD4 cover fully 3D building modelling, including façade modelling and indoor modelling respectively (Isikdag and Zlatanova, 2009). The concept of LoD is illustrated in Figure 1-4. In this dissertation, procedures for the (semi-) automated construction of 3D city models with LoD1 and LoD2 are elaborated, and presented in chapter 8. CityGML has already been implemented in different 3D cadastres in Europe (Over et al., 2010; van den Brink et al., 2013). The interoperability of Belgian spatial data and 3D city modelling using CityGML is intensively discussed by De Cubber and Van Orshoven (2012). These authors mainly focus on the different approaches for defining relations between features and on the rather diverging ontology of the standard.

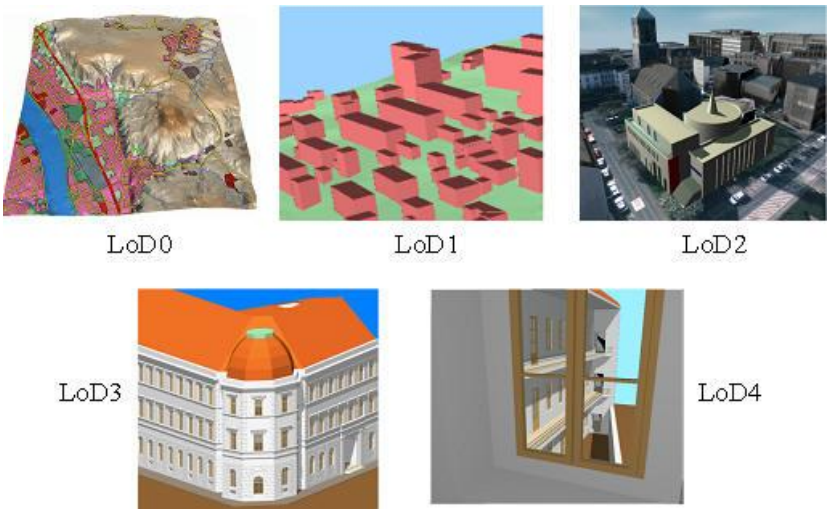

Figure 1-4: Different Levels of Detail (LoD) in CityGML (Gröger et al., 2008)

RQ6: What are the potential applications of the modelling of environments, cities or other objects in 3D, and how can these models contribute to multidisciplinary research?

The necessity of acquiring, processing and analysing high quality 2.5D and 3D spatial data has already been discussed above. Indeed, these spatial data are essential for a various range of scientific disciplines and even more applications. DEMs or 3D city models play an indisputable role in environmental research (Dubovyk et al., 2011; Hape and Purps, 1999), spatial planning and management (Kolbe et al., 2005; Smart et al., 2011; Stoter et al., 2008), as well as architectural design (Becker, 2009) or archaeology and cultural heritage (Hendrickx et al., 2011; Koller et al., 2009; Remondino, 2011) to mention a few. Giving a full list of applications for 3D

spatial data would be an impossible task, but a short overview of some projects is presented in this section. The author of this dissertation contributed significantly to all projects presented here. One or two references at each topic can be used for further readings, but many of the topics are also integrated in the different chapters of this dissertation.

RQ6-1: Physical geography

A rapid and detailed approach to quantifying gully morphology by using image-based 3D modelling (Stal et al., 2014): the modelling and monitoring of gully erosion is very important to comprehend the morphological processes that occur at gullies. Understanding these processes enable to master the resulting issues and to minimize the difficulties and cost that are entailed. Gully erosion occurs on a large scale in both developed and less-developed countries. Especially the latter are very vulnerable for this environmental problem. In both situations, the need for a fast, cheap and flexible 3D modelling technique emerges. In this study, the image based 3D modelling technique was applied to quantify the morphology of some gullies in Belgium and Ethiopia. Images were taken and GNSS measurements were performed during field campaigns. These data are processed in a SfM-MVS workflow, resulting in highly detailed and highly accurate 3D models (Figure 1-5). Moreover, derivative products, like DEMs and cross-sections, are generated using these models. When consecutive models are placed in a time series, volume changes and differences on shape and pipe inlets are modelled.

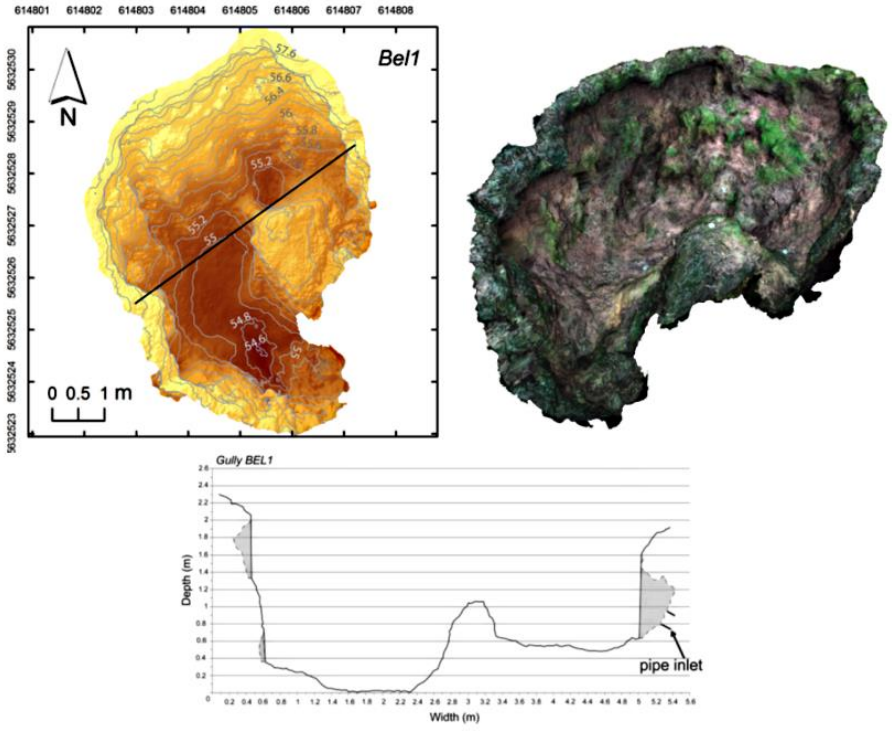

Figure 1-5: DEM with contour lines and cross section situation (upper-left), top view on the 3D model (upper-right) and the actual cross section (below)

RQ6-2: Bathymetric mapping

Accuracy aspects of processing and filtering of multibeam data: grid modelling versus TIN based modelling (De Wulf et al., 2012): in this study, the accuracy of volume computations in a TIN and

in a grid are mathematically derived on a statistical basis. Both modelling techniques (TIN and grid) yield their own advantages and drawbacks. In many bathymetric applications, multibeam echosounder measurements serve to make DEMs of underwater surfaces. The results of this study are used by the author of this dissertation for the 3D modelling of an artificial lake in France (Lake of Vassivière, Figure 1-6). The Delaunay triangulation is a widely appreciated and investigated mathematical model to represent the seabottom topography and is highly efficient for building TINs (Triangular Irregular Networks) out of non-homogeneous data such as raw multibeam data. Obtaining an accurate model of underwater surfaces is a major concern in dredging works, offshore mining or reservoir management. Contemporary hydrographical surveying tools, especially the multibeam echosounder, yield a very dense point sampling of the underwater surface. Subsequently, this immense amount of data needs to be processed in order to generate an accurate terrain model. Modelling can be carried out in post-processing or in real-time. Performing a real-time accountability keeps track of the cut- or fill volume changes realized at that moment. Most multibeam systems deliver equidistant interpolated data, allowing faster processing to be achieved using equidistant grid-based modelling. It goes without saying that these concepts can easily be applied for topographic applications.

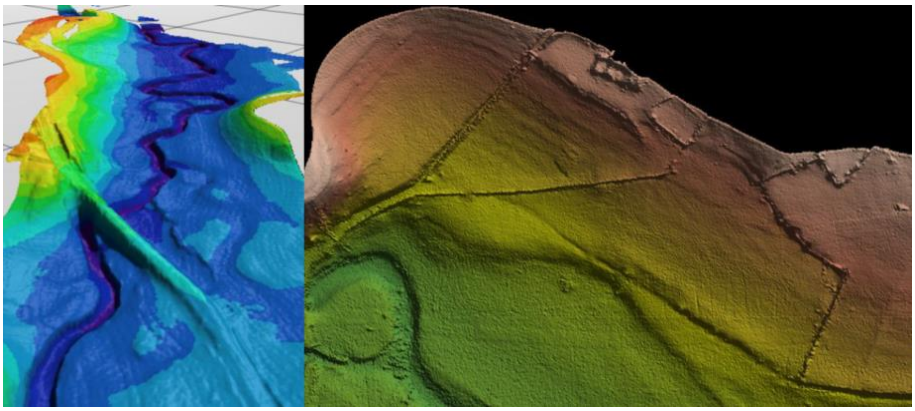

Figure 1-6: Birds-eye view (left) and vertical view (right) of the bottom of the Lake of Vassivière (France), generated using bathymetric sensors for the volume calculation of the lake (unscaled, unreferenced)

RQ6-3: Coastal mapping

Feasibility study of the use of bathymetric surface modelling techniques for intertidal zones of beaches (De Wulf et al., 2014): this study elaborates on the use of different 3D data acquisition techniques for the construction of DSMs of intertidal zones of beaches and for the detection of archaeological relicts (Figure 1-7). DSMs are an indispensable tool for the development and sustainable management of cultural heritage and archaeological relicts. In many applications, these models are used for the analysis of known archaeological features or for the detection of new features. This is also the case in the presented project on archaeological research in the Belgian North Sea (SeARCH). Obtaining a sufficient resolution and accuracy for these models is a challenging task, especially for intertidal zones of beaches. Specific difficulties in these transitional areas require a thorough study of available spatial data acquisition techniques, focussing on the various system properties and measurement methods. In general, bathymetric techniques make use of different approaches compared with topographic techniques, like the use of acoustic versus electromagnetic signals for distance measurements. The limited draft in

intertidal zones, as well as the turbidity and tempestuous weather conditions are additional limiting factors for the Belgian North Sea coast. Based on a field survey, the use of MTLS appears to be very useful for the construction of the required DSMs. This study is performed by the author of this dissertation in collaboration with scientists of the *École Nationale Supérieure de Techniques Avancées Bretagne* (Brest, France).

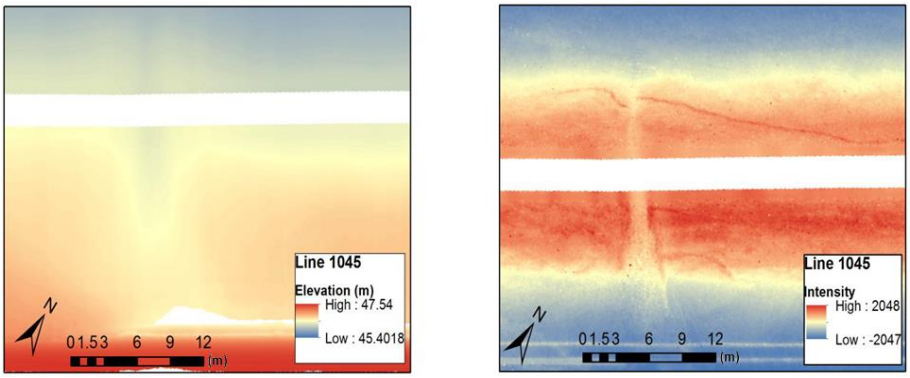

Figure 1-7: DEM of a small part of an intertidal beach (left) and the same area with return intensity values (right)

RQ6-4: Historical geography

A 3D model and orthophoto of the Ethiopian Highlands in 1935 (Frankl et al., 2014) and *Kemmelberg (Belgium) case study - comparison of DTM analysis methods for the detection of relicts from the First World War* (Stal et al., 2010): both projects concern the use of modern 3D reconstruction techniques for historical geography. On the one hand, ancient airborne images, like Italian war images of Ethiopia (1930s) or German and English images of WWI (1914-1918) can be very suitable for 3D modelling (Figure 1-8, left). The Kemmelberg (Belgium) was heavily bombed and photographed during the First World War. Italian images are the oldest data source for the documentation of land use, land cover and geomorphology of Ethiopia. In both cases, unique airborne imagery allows the construction of 3D models of the past. These models enable to describe environmental changes in land use and coverage, geomorphology or land degradation. On the other hand, DTMs based on ALS data can be used for the detection of small relicts in the landscape, like trenches, artillery emplacements ... (Figure 1-8, right). A common method to detect these large scale and small scale changes in the environment is the use of historical aerial photographs. The interpretation of historical photographs requires thorough and specialized knowledge of the elements on these pictures. Moreover, analogue stereoscopic analysis of randomly taken airborne imagery is very time consuming. Thus, these research projects focus on different filter techniques to enhance the detection of these objects, using SfM-MVS for the image series and convolution matrices for the ALS-based DTMs. For both the Belgian and Ethiopian case study, the author of this dissertation has contributed by organizing the actual 3D reconstruction. For the Kemmelberg study, image enhancement techniques have also been applied on the models by the author. The resulting data are important research tools for historical geographic research, archaeology and landscape analysis.

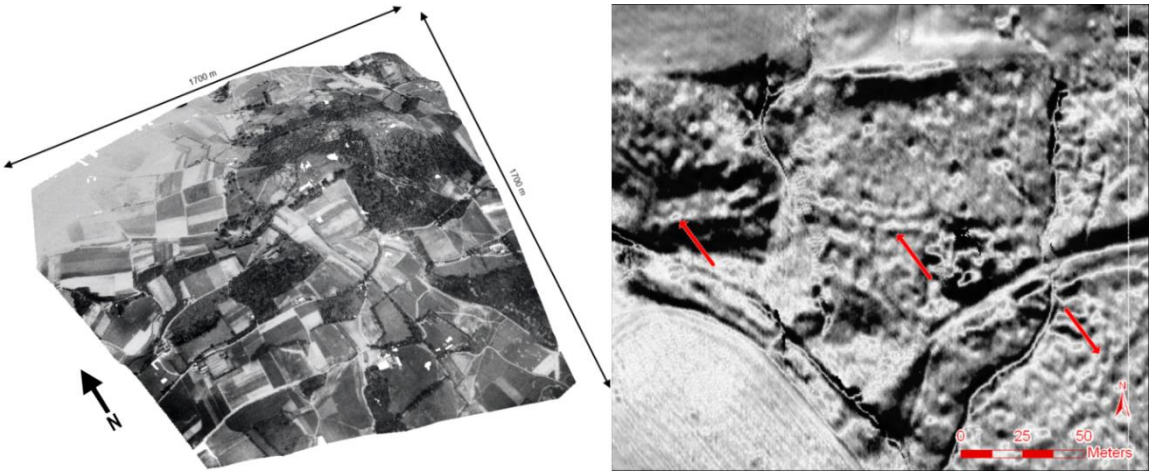

Figure 1-8: Birds-eye view of the Kemmelberg (Belgium) using airborne images of 1913 (left) and elevation enhancement for the detection of WWI relicts (right)

RQ6-5: Landscape research

Digital elevation model generation for historical landscape analysis based on LiDAR data: a case study in Flanders (Belgium) (Werbrouck et al., 2011): This project is part of a larger project entitled: "Prehistoric settlement and land-use systems in Sandy Flanders (NW Belgium)". The main objective is to create a detailed topographical surface free of artificial features and topographical artefacts, in the form of a DEM based on high density ALS. This model should allow the visualization of natural and current topography through the sole implementation of true ground points, which can be used for a landscape-archaeological study. Based on topographical vector data, visual interpretations and slope analysis, a semi-automatically removal of the artificial features and topographical artefacts is aimed at. The first resulting model is a TIN, whereby the inherent large file format restricts the usability for a large spatial extend. The second model is an equidistant grid model which can be used for small-, medium- and large-scale applications. Both data sets were generated and processed by the author of this dissertation and were used as an image which could be interpreted using ancillary data from historical sources. Starting from this DEM, the approach of a landscape historical study is mainly retrogressive, i.e. starting from the landscape structures and elements that are still present in the contemporary landscape and moving into the past.

RQ6-6: Civil engineering

Methodology for the ovalisation monitoring of newly built circular train tunnels based on laser scan measurements: Liefkenshoek Rail Link (Belgium) (Nuttens et al., 2014) and *Automatic filtering of terrestrial laser scanner data from cylindrical tunnels* (Stal et al., 2012b): two tunnel monitoring projects on which this research is based are the first projects in Belgium in which STLS is used to systematically monitor the ovalisation of multiple tunnel sections under construction. The methodology focuses on a clear processing workflow and easily interpretable deliverables, minimizing the use of high-end 3D processing or visualization software. Moreover, simultaneous data sets of both laser scanning and strain gauge measurements open important opportunities to improve the knowledge of tunnel behaviour in in-situ conditions. The extensive and systematic monitoring coverage from the time of assembly of a circular tunnel structure until several months after placement delivers an important contribution to the understanding of the

behaviour of the tunnel constructions between the construction phase and the final stabilized shape. Conventional monitoring techniques result in a limited number of measurements to evaluate the performance and accuracy of the tunnelling process in comparison with design-models at an early stage. The results of such the presented systematic monitoring program allow the contractors or engineers involved to validate the theoretical models and to compare with the actual behaviour of large diameter shield tunnelling in soft soil. Therefore, this study focuses on optimized data acquisition, data processing and point filtering, as well as on quality assessment. The author of this dissertation has significantly contributed to the automation of the data processing, by developing various on-demand workflows and point cloud filtering procedures.

RQ6-7: Cultural heritage and architecture
Evaluation of the accuracy of 3D data acquisition techniques for the documentation of cultural heritage (Stal et al., 2012a): different cultural heritage sites in the city of Ghent (Belgium, Figure 1-9), but also at various sites in the rest of Belgium, Greece, Mexico, France, … are used as test cases for the development and accuracy assessment of 3D data acquisition techniques. These projects mainly involve the use of terrestrial techniques, like STLS and terrestrial close range photogrammetry for façade modelling in LoD3. Since recently, Unmanned Aerial Vehicles (UAV) are also deployed in image based modelling reconstruction workflow for the full 3D modelling of cultural heritage. In most cases, the resulting 3D models are used by local cultural heritage directors for the management and preservation of the patrimony. The deployment of these sensors and platforms, as well as the 3D data acquisition and processing lay within the expertise of the author of this dissertation. The author already has been able to participate in very interesting projects.

Figure 1-9: 3D representation of the northern part of the cloister of the Sint-Baafs abbey (Ghent, Belgium)

1.3. *Dissertation outline*

This dissertation is structured as follows:

In chapter 2 (3D data acquisition), different 3D data acquisition techniques, which can be used for the construction of DEMs or environmental models and 3D city models are elaborated. The presented list is a sample of the large number of available sensors and techniques, but a selection was made based on prevalence in literature, giving an insight on RQ1. Different types of laser scanning, image based modelling and conventional topographic measurement techniques are covered and analysed. The research is mainly focussed on the first technique, covering some fundamental topics on the theory of laser scanning, as well as different types of airborne and

terrestrial laser scanning applications. However, the use of GNSS, total station measurements, conventional photogrammetry and Structure from Motion and Multi-View Stereo (SfM-MVS) are also described. This chapter ends with an overview of theoretical data resolutions and accuracies. ALS-based point clouds are intensively used in chapter 4, 5, 6 and 8. Images are used as a data source for geometric reconstructions in chapter 3, 4, 5 and 7. In chapter 8, airborne images are solely used to perform the texture mapping of the geometric models of buildings.

The following three chapters aim to clarify RQ2: in chapter 3 (*Digital representation of historical globes: methods to make 3D and pseudo-3D models of sixteenth century Mercator globes*), a feasibility and comparative study for the documentation of small scale cultural heritage is presented. In this case, two 16th century globes, made by Gerardus Mercator, were used in a test case. As with the study on ancient manuscripts and books, the use of digital versions of globes was preferred above the use of the original work for intensive content analysis. Moreover, virtual globes can easily be distributed over the internet, increasing the scope of this patrimony. This study aimed at selecting the most optimal 3D reconstruction methodology for this kind of features as an extension of the previously mentioned modelling applications. The 3D modelling of spheres was a challenging task, since a very high precision is required, but the quality of the texture must be high as well for these small objects. Consequently, the same modelling techniques were used here, but on a total different scale: laser scanning and image based modelling. SfM-MVS, dynamic imaging and the georeferening of images are presented in this chapter as applications of image based modelling. The results of the different modelling techniques are evaluated by the performance and especially by the quality of the model appearance, rather than the geometric quality.

In chapter 4 (Comparison of airborne laser scanning and image based modelling techniques), a quality assessment on the use of the previously presented airborne techniques is elaborated. In this case, it is assumed that the time gap between the two data sets will not result in significant aberrations. The first model is generated in accordance with a conventional photogrammetric workflow, whereas the second model was generated using new SfM-MVS techniques. Two ALS data sets of an urban area and a rural area in Belgium are postulated as reference data for a qualitative comparison of two image based DEMs. Furthermore, the performance of a standard point cloud filtering procedure is assessed for the image based models in comparison with filtered ALS data. In this comparison, a statistical analysis on the classified ground-points and non-ground points is performed. The idea behind this research is to evaluate the ability to use relatively fast and low-cost SfM-MVS processing techniques with airborne imagery as an alternative for ALS data and conventional photogrammetry. The fact is that ALS data are relatively expensive and sometimes even unavailable for very remote areas, whereas DEM construction from conventional photogrammetry is a very time consuming process.

Chapter 5 (Airborne photogrammetry and LiDAR for DSM extraction and 3D change detection over an urban area: a comparative study) also covers the statistical comparison of two DEMs, as required in RQ2, but also covers some elements of RQ4. In this case, an ALS-based DEM and a DEM based on conventional photogrammetry are evaluated for an urban area. In contrast with the previous chapter, the time interval between the ALS point cloud and the airborne images is

assumed to be significant. An automated change detection procedure is presented based on this assumption. Significant differences of the elevations between the two acquisition moments indicate changes of the urban morphology, whereas smaller changes are indicators for the geometric quality of the models. The difference between significant and non-significant changes will be evaluated using image-based enhancement techniques and elevation thresholds. This is useful for monitoring the evolution of built-up areas and possibly for the detection of violations of urban development regulations.

RQ3 is fully covered in chapter 6 (Classification of airborne laser scanning point clouds based on binomial logistic regression analysis), where a new classification procedure is presented for point clouds. In order to use ALS point clouds for the construction of environmental models and 3D city models, ground points, building points, vegetation points ... must be distinct. The proposed classification algorithm makes use of Binominal Logistic Regression (BLR) analysis on a training sample. For each point in this sample, a feature space is defined by a large number of geometric properties. All significant properties are used to define a logistic response function, which estimates the probability that a point with a given feature space can be assigned to a certain class. The accuracy of the proposed classification procedure is assessed by the comparison with a reference classification tool and a reference filtering algorithm.

In chapter 7 (Integrating geomatics in archaeological research at the site of Thorikos (Greece)), the importance of an efficient data management system for a large series of 3D models is emphasized, in correspondence with RQ4. These 3D models were generated using image based modelling on a daily base during an archaeological excavation campaign at the site of Thorikos, Greece. Each model is connected with other consecutive 3D models using a Harris matrix. This topological model functions as an interface between each 3D model, dynamic map series and a databank with metadata in an interactive and digital environment. The implementation allows to manage, analyse and visualize data in accordance with the temporal evolution of the excavation. Next to this application, which can easily be adjusted for 3D city modelling in a historical context, additive advantages of virtual 3D modelling in archaeology are discussed.

In chapter 8 (3D city mapping and data management using interconnected GI-software and Python), a complete workflow for 3D city modelling is presented using ALS data, cadastre data and airborne imagery. Consequently, this chapter is fully dedicated to RQ5, but also covers some aspects of RQ3 and RQ4. Various widely used geographic information software packages are used for this workflow, allowing the implementation of the procedure by a wide range of spatial scientists without a thorough knowledge of programming. A common scripting language (*Python*) was selected to allow a large degree of automation. Point classification, feature modelling, texture mapping and spatial data management are covered in this chapter. Thus, the various city modelling steps which are also elaborated in previous chapters are further developed and automated in an interconnected and practical way.

The subject of this dissertation is 3D modelling sensu lato. The decision to add research papers about cultural heritage modelling and archaeological 3D modelling is motivated by the broad applicability of the elaborated sensors and techniques. For example, the management system used

for the archaeological time series in chapter 7 is an extension of the dual time series analysis presented in chapter 5. Furthermore, the developed extensions are already implemented for the analysis of multiple time series of urban areas (Stal et al., 2014). The different projects discussed in this dissertation indicate the interdisciplinary of the challenge of 3D modelling. As a result, it becomes clear that RQ6 is covered by all chapters of this dissertation, because of the pragmatic approach of the presented work. A large number of different applications are illustrated in various chapters and in a multidisciplinary context. Finally, a discussion and general conclusions are presented in chapter 9.

1.4. *City modelling and data management as part of a larger project*

The research presented in this PhD dissertation is part of a larger project entitled “3D CAD-modelling of spatial architectural volumes using terrestrial and airborne laser scanning”. This project is funded by the Fund for Scientific Research Flanders (FWO, G082309N) and promoted by Prof. Dr. Ir. A. De Wulf, Prof. Dr. Ph. De Maeyer, Prof. Dr. N. Van De Weghe, Prof. Dr. ir. S. Gautama, Prof. Dr. R. De Meyer and Arch. M. Mattys. The presented dissertation covers a range of subjects of this project and thus provides a significant contribution to this interesting subject.

References

Ahearn, L., 2008. 3D game environmnents: create professional 3D game worlds. Focal Press, Burlington, MA, USA.

Anderson, E., McLoughlin, L., Liarokapis, F., Peters, C., Petridis, P., de Freitas, S., 2010. Developing serious games for cultural heritage: a state-of-the-art review. Virtual Reality 14 (4), 255-275.

Antrop, M., 2000. Background concepts for integrated landscape analysis. Agriculture, Ecosystems & Environment 77 (1-2), 17-28.

Antrop, M., 2004. Landscape change and the urbanization process in Europe. Landscape and Urban Planning 67 (1-4), 9-26.

APSRS, 2004. ASPRS Guidelines Vertical accuracy reporting for LiDAR data. American Socienty of Photogrammetry and Remote Sensing, Betesda, MA, USA, p. 20

ASPRS, 2013. LAS specification. American Socienty of Photogrammetry and Remote Sensing, Bethesda, MA, USA, p. 28

Axelsson, P., 2000. DEM generation from laser scanner data using adaptive TIN models. International Archives of Photogrammetry and Remote Sensing 33 (B4), 111-118.

Baltsavias, E., 1999. Airborne laser scanning: basic relations and formulas. ISPRS Journal of Photogrammetry and Remote Sensing 54 (2-3), 199-214.

Bartels, M., Wei, H., 2010. Threshold-free object and ground point separation in LiDAR data. Pattern Recognition Letters 31 (10), 1089-1099.

Bartoněk, D., Bureš, J., Dráb, A., 2011. Usage of GIS technology in civil engineering. Journal of Environmental Science and Engineering 5 (2), 177-183.

Beccari, C., Farella, E., Liverani, A., Morigi, S., Rucci, M., 2010. A fast interactive reverse-engineering system. Computer-Aided Design 42 (10), 860-873.

Becker, S., 2009. Generation and application of rules for quality dependent façade reconstruction. ISPRS Journal of Photogrammetry and Remote Sensing 64 (6), 640-653.

Benner, J., Geiger, A., Leinemann, K., 2005. Flexible generation of semantic 3D building models, in: Gröger, G., Kolbe, T. (Eds.), 1st International ISPRS/EuroSDR/DGPFWorkshop on Next Generation 3D City Models, Bonn, Germany

Briese, C., Pfeifer, N., Dorninger, P., 2002. Applications of the robust interpolation for DTM determination. International Archives of Photogrammetry and Remote Sensing 34 (Part A), 55-61.

Briese, C., Zach, G., Verhoeven, G., Ressl, C., Ullrich, A., Studnicka, N., Doneus, M., 2012. Analysis of mobile laser scanning data and multi-view image reconstruction. International Archives of Photogrammetry and Remote Sensing 39 (B5), 163-168.

Chen, Q., 2007. Airborne LiDAR data processing and information extraction. Photogrammetric Engeneering and Remote Sensing 73 (2), 109-112.

Chen, Q., Gong, P., Baldocchi, D., Xie, G., 2007. Filtering airborne laser scanning data with morphological methods. Photogrammetric Engeneering and Remote Sensing 73 (2), 175-185.

Chen, R., Xie, J., 2008. Open source databases and their spatial extensions, in: Hall, G., Leahy, M. (Eds.), Open Source Approaches in Spatial Data Handling, Heidelberg, Germany, pp. 105-129.

De Cubber, I., Van Orshoven, J., 2012. Towards an internationally more accessible data model for the GRB, the 2D-large scale topographic inventory of Flanders, in: Billen, R.E., Binard, M. (Ed.), Hallot, P. (Ed.), Donnay, J. (Ed.), (Ed.), USB-Proceedings of the Spatial Analysis and Geomatics, Liège, Belgium, pp. 145-157

De Wulf, A., Constales, D., Stal, C., Nuttens, T., 2012. Accuracy aspects of processing and filtering of multibeam data: grid modeling versus TIN based modeling, FIG Working Week, Rome, Italy, pp. 6 (on CD-ROM)

De Wulf, A., De Maeyer, P., Incoul, A., Nuttens, T., Stal, C., 2014. Feasibility study of the use of bathymetric surface modelling techniques for intertidal zones of beaches, FIG Working Week, Kuala Lumpur, Malaysia, pp. 8 (on CD-ROM)

Döllner, J., Kolbe, T., Liecke, F., Sgouros, T., Teichmann, K., 2006. The virtual 3D city model of Berlin: managing, integrating, and communicating complex urban information, Urban Data Management Symposium (UDMS), Aalborg, Denemark, 15-17 May, pp. 12 (on CD-ROM)

Doneus, M., Briese, C., Fera, M., Janner, M., 2008. Archaeological prospection of forested areas using full-waveform airborne laser scanning. Journal of Archaeological Science 35 (4), 882-893.

Dorninger, P., Pfeifer, N., 2008. A comprehensive automated 3D approach for building extraction, reconstruction and regularization from airborne laser scanning point clouds. Sensors 8 (11), 7323-7343.

Dubovyk, O., Sliuzas, R., Flacke, J., 2011. Spatio-temporal modelling of informal settlement development in Sancaktepe district, Istanbul, Turkey. ISPRS Journal of Photogrammetry and Remote Sensing 66 (2), 235-246.

EC, E.C., 2007. Establishment of an Infrastructure for Spatial Information in the European Community (INSPIRE) in: Council, E.P.a.o.t. (Ed.), 108, Brussels, Belgium, pp. 1-14

Fan, H., Meng, L., 2009. Automatic derivation of different levels of detail for 3D buildings modeled by CityGML, 24th International Cartography Conference, Santiago, Chile, pp. 10 (on CD-ROM)

Frankl, A., Meire, E., de Mûelenaere, S., De Dapper, M., Poesen, J., Haile, M., De Wulf, A., Deckers, J., Nyssen, J., 2008. Analyzing gully erosion in its relation to land use changes in the North Ethiopian Highlands using terrestrial photographs, aerial photographs and satellite images, GAPSYM2: Mobilities in Africa - Africa in Mobility (book of abstracts), pp. 38-38

Frankl, A., Nyssen, J., Seghers, V., Stal, C., 2014. A 3D model and orthophoto of the Ethiopian Highlands in 1935. Journal of Maps (under review), 8.

Fritsch, D., Kada, M., 2004. Visualisation using game engines. International Archives of Photogrammetry, Remote Sensing and Spatial Information Sciences 35 (B5), 621–625.

Gröger, G., Kolbe, T.H., Czerwinski, A., Nager, C., 2008. Open City Geography Markup Language (CityGML) encoding standard, Open GIS Encoding Standard. Open Geospatial Consortium Inc., p. 234

Gruen, A., Akca, D., 2005. Least squares 3D surface and curve matching. ISPRS Journal of Photogrammetry and Remote Sensing 59 (3), 151-174.

Haala, N., Kada, M., 2010. An update on automatic 3D building reconstruction. ISPRS Journal of Photogrammetry and Remote Sensing 65 (6), 570-580.

Hape, M., Purps, J., 1999. Digitale Geländemodelle als Grundlage für stationäre und instationäre Überflutungssimulationen, Fachtagung Elbe, Dynamik und Interaktion von Fluß und Aue. Elbe-Ökologie & BMBF, Berlin, Germany, Wittenberge, Germany, pp. 152-155

Hendrickx, M., Gheyle, W., Bonne, J., Bourgeois, J., De Wulf, A., Goossens, R., 2011. The use of stereoscopic images taken from a microdrone for the documentation of heritage - An example from the Tuekta burial mounds in the Russian Altay. Journal of Archaeological Science 38 (11), 2968-2978.

Höfle, B., Mücke, W., Dutter, M., Rutzinger, M., Dorninger, P., 2009. Detection of building regions using airborne LiDAR: a new combination of raster and point cloud based GIS methods, GI-Forum 2009 - International Conference on Applied Geoinformatics, Salzburg, Austria, pp. 66-75

Horne, M., Thompson, E., Podevyn, M., 2007. An overview of virtual city modelling: emerging organisational issues, CUPUM07 10th International Conference on Computers in Urban Planning and Urban Management, Iguassu Falls, Brazil, pp. 11-13

Hyyppä, H., Yu, X., Hyyppä, J., Kaartinen, H., Kaasalainen, S., Honkavaara, E., Rönnholm, P., 2005. Factors affecting the quality of DTM generation in forested areas. International Archives of Photogrammetry, Remote Sensing and Spatial Information Sciences 36 (3/W19), 85-90.

IHO, 2008. IHO standards for hydrographic surveys. International Hydrographic Bureau.

Isikdag, U., Zlatanova, S., 2009. Towards defining a framework for automatic generation of buildings in CityGML using Building Information Models, in: Lee, J., Zlatanova, S. (Eds.), 3D Geo-Information Sciences. Springer-Verlag, Berlin, Germany, pp. 79-96.

Jaboyedoff, M., Demers, D., Locat, J., Locat, A., Locat, P., Oppikofer, T., Robitaille, D., Turmel, D., 2009. Use of terrestrial laser scanning for the characterization of retrogressive landslides in sensitive clay and rotational landslides in river banks. Canadian Geotechnical Journal 46 (12), 1379-1390.

Jacob, R., Zheng, J., Ciepłuch, B., Mooney, P., Winstanley, A., 2009. Campus guidance system for international conferences based on openstreetmap, in: Carswell, J., Fotheringham, S., McArdle, G. (Eds.), Web and Wireless Geographical Information Systems. Springer, Heidelberg, Germany, pp. 187-198.

Kolbe, T., 2009. Representing and exchanging 3D city models with CityGML, in: Lee, J., Zlatanova, S. (Eds.), 3D Geo-Information Sciences. Springer-Verlag, Berlin, Germany.

Kolbe, T.H., Gröger, G., Plümer, L., 2005. CityGML: interoperable access to 3D city models, First International Symposium in Geo-Information for Disaster Management. Springer Verlag, Delft, the Netherlands, pp. 883–899

Koller, D., Frischer, B., Humphreys, G., 2009. Research challanges for digital archives of 3D cultural heritage models. Journal on Computing and Cultural Heritage 2 (3), 1-17.

Li, Y., 2013. Filtering airborne LiDAR data by in improved morphological method based on multi-gradient analysis. International Archives of Photogrammetry and Remote Sensing and Spatial Information Sciences 40 (1), 191-194.

Löwner, M., Benner, J., Gröger, G., Häfele, K., 2013. New concepts for structuring 3D city models, an extended level of detail concept for CityGML buildings, in: Murgante, B., et, a. (Eds.), Lecture Notes on Computer Sciences. Springer, Heidelberg, Germany, pp. 466-480.

Manferdini, A., Remondino, F., 2010. Reality-based 3D modeling, segmentation and web-based visualization, in: Ioannides, M. (Ed.), Lecture Notes in Computer Sciences. Springer, Heidelberg, Germany, pp. 110-124.

Mendes, C., Silva, L., Bellon, O., 2012. IMAGO Visualization System: an interactive web-based 3D visualization system for cultural heritage applications. Journal of Multimedia 7 (2), 205-210.

Meng, X., Wang, L., Silván-Gárdenas, J., Currit, N., 2009. A multi-directional ground filtering algorithm for airborne LiDAR. ISPRS Journal of Photogrammetry and Remote Sensing 64 (1), 117-124.

Merbitz, H., Buttstädt, M., Michael, S., Dott, W., Schneider, C., 2012. GIS-based identification of spatial variables enhancing heat and poor air quality in urban areas. Applied Geography 33 (3), 94-106.

Mills, G., 1998. International hydrographic survey standards. International Hydrographic Review 75, 79-86.

Molina, J., Rodríguez-Gonzálvez, P., Molina, M., González-Aguilera, D., 2014. Geomatic methods at the service of water resource modelling. Journal of Hydrology 509 (February), 150-162.

Mongus, D., Žalik, B., 2012. Parameter-free ground filtering of LiDAR data for automatic DTM generation. ISPRS Journal of Photogrammetry and Remote Sensing 67 (1), 1-12.

Naess, P., 2001. Urban planning and sustainable development. European Planning Studies 9 (4), 503-524.

Niemczynowicz, J., 1999. Urban hydrology and water management: present and future challenges. Urban Water 1 (1), 1-14.

Nuttens, T., Stal, C., De Backer, H., Schotte, K., Van Bogaert, P., De Wulf, A., 2014. Methodology for the ovalisation monitoring of newly built circular train tunnels based on laser scan measurements: Liefkenshoek Rail Link (Belgium). NDT&E International (under review), 24.

OGC, 2013. Open Geospatial Consortium, http://www.opengeospatial.org

Oude Elberink, S., Vosselman, G., 2011. Quality analysis on 3D building models reconstructed from airborne laser scanning data. ISPRS Journal of Photogrammetry and Remote Sensing 66 (2), 157-165.

Over, M., Schilling, A., Neubauer, S., Zipf, A., 2010. Generating web-based 3D city models from OpenStreeMap: the current situation in Germany. Computers, Environment and Urban Systems 34 (6), 496-507.

Pauwels, P., Van Deursen, D., De Roo, J., Van Ackere, T., De Meyer, R., Van De Walle, R., Van Campenhout, J., 2011. Three-dimensional information exchange over the semantic web for the domain of architecture, engineering, and construction. Artificial Intelligence for Engineering Design, Analysis and Manufacturing 25 (4), 317-332.

Penninga, F., van Oosterom, P., Kazar, B., 2006. A tetrahedronized irregular network based dbms approach for 3D topographic data modeling, in: Riedl, A., Kainz, W., Elmes, G. (Eds.), Progress in Spatial Data Handling. Springer, Heidelberg, Germany, pp. 581-598.

Peuquet, D., 1984. A conceptual framework and comparison of spatial data models. Cartographica 21 (4), 66-113.

Pfeifer, N., 2002. 3D Terrain models on the basis of a triangulation. Institute für Photogrammetie und Fernkundung, Vienna, Austria.

Pfeifer, N., Mandlburger, G., 2008. LiDAR data filtering and DTM generation, in: Shan, J., Toth, C. (Eds.), Topographic laser ranging and scanning: principles and processing. CRC Press, Boca Raton, Fl, USA, pp. 307-333.

Podobnikar, T., Vrecko, A., 2012. Digital elevation model from the best results of different filtering of a LiDAR point cloud. Transactions in GIS 16 (5), 603-617.

Remondino, F., 2011. Heritage recording and 3D modeling with photogrammetry and 3D scanning. Remote Sensing 3 (6), 1104-1138.

Rottensteiner, F., Trinder, J., Clode, S., Kubik, K., 2007. Building detection by fusion of airborne laser scanner data and multi-spectral images: performance, evaluation and sensitivity analysis. ISPRS Journal of Photogrammetry and Remote Sensing 62 (2), 135-149.

Sampath, A., Shan, J., 2010. Segmentation and reconstruction of polyhedral building roofs from aerial LiDAR point clouds. IEEE Transactions on Geoscience and Remote Sensing 48 (3), 1554-1567.

Sandström, U., Angelstam, P., Khakee, A., 2006. Urban comprehensive planning: identifying barriers for the maintenance of functional habitat networks. Landscape and Urban Planning 75 (1-2), 43-57.

Schilling, A., Lanig, S., Neis, P., Zipf, A., 2009. Integrating terrain surface and street network for 3D routing, in: Lee, J., Zlatanova, S. (Eds.), 3D Geo-Information Sciences. Springer, Heidelberg, Germany, pp. 109-126.

Simarda, M., Rivera-Monroyb, V., Mancera-Pinedac, J., Castañeda-Moyab, E., Twilleyb, R., 2008. A systematic method for 3D mapping of mangrove forests based on Shuttle Radar Topography Mission elevation data, ICEsat/GLAS waveforms and field data: Application to Ciénaga Grande de Santa Marta, Colombia. Remote Sensing of Environment 112 (5), 2131-2144.

Sithole, G., Vosselman, G., 2004. Experimental comparison of filter algorithms for bare-Earth extraction from airborne laser scanning point clouds. ISPRS Journal of Photogrammetry and Remote Sensing 59 (1-2), 85-101.

Smart, P., Quinn, J., Jones, C., 2011. City model enrichment. ISPRS Journal of Photogrammetry and Remote Sensing 66 (2), 223-234.

Stal, C., Bourgeois, J., De Maeyer, P., De Mulder, G., De Wulf, A., Goossens, R., Nuttens, T., Stichelbaut, B., 2010. Kemmelberg (Belgium) case study - comparison of DTM analysis methods for the detection of relicts from the First World War, 30th Annual EARSeL Symposium, Paris, France, pp. 66-72

Stal, C., De Wulf, A., De Maeyer, P., Goossens, R., Nuttens, T., 2012a. Evaluation of the accuracy of 3D data acquisition techniques for the documentation of cultural heritage, 3rd EARSeL Workshop on Remote Sensing for Archaeology, Ghent, Belgium, pp. 8 (on CD-ROM)

Stal, C., Frankl, A., Abraha, A., Nyssen, J., Rieke-Zapp, D., De Wulf, A., Poesen, J., 2014. A rapid and detailed approach to quantifying gully morphology by using image-based 3D modelling. Catena (under review), 18.

Stal, C., Nuttens, T., Bourgeois, J., Carlier, L., De Maeyer, P., De Wulf, A., 2011. Accuracy assessment of a LiDAR digital terrain model by using RTK GPS and total station. EARSeL eProceedings 10 (1), 1-8.

Stal, C., Nuttens, T., Constales, D., Schotte, K., De Backer, H., De Wulf, A., 2012b. Automatic filtering of terrestrial laser scanner data from cylindrical tunnels, FIG Working Week, Rome, Italy, pp. 12 (on CD-ROM)

Stal, C., De Wulf, A., De Maeyer, P., Goossens, R., Nuttens, T., Tack, F., Hendrickx, M., 2014. Quantitative modelling of urban changes using digital elevation models in a time series. EARSeL eProceedings, submitted.

Steiniger, S., Hunter, A., 2011. Free and open source GIS software for building a spatial data infrastructure, in: Bocher, E., Neteler, M. (Eds.), Building, pp. 1-13.

Stoter, J., de Kluijver, H., Kurakula, V., 2008. 3D noise mapping in urban areas. International Journal of Geographic Information Science 22 (8), 907-924.

Swart, L., 2010. How the up-to-date height model of the Netherlands (AHN) bacame a massive point data cloud, in: van Oosterom, P., Vosselman, G., van Dijk, T., Uitentuis, M. (Eds.), Management of Massive Point Cloud Data: Wet and Dry. NCG-KNAW, Delft, the Netherlands.

Tack, F., Buyuksalih, G., Goossens, R., 2012a. 3D building reconstruction improvement based on given ground plan information and surface models extracted from spaceborne imagery. ISPRS Journal of Photogrammetry and Remote Sensing 67 (1), 52-64.

Tack, F., Buyuksalih, G., Goossens, R., 2012b. A mixed spaceborne sensor approach for surface modelling of an urban scene. International Journal of Remote Sensing 33 (19), 6035-6059.

Tack, F., Debie, J., Goossens, R., De Meulemeester, J., Devriendt, D., 2005. A feasible methodology for the use of close range photogrammetry for the recording of archaeological excavations, Proceedings of the CIPA 2005 XX International Symposium, Torino, Italy, pp. 561-565

US, P., 1994. Coordinating geographic data acquisition and access: the national spatial data infrastructure, in: House, t.W. (Ed.), 12906, Washington D.C., USA, p. 4

Vaaja, M., Hyyppa, J., Kukko, A., Kaartinnen, H., Hyyppa, H., Alho, P., 2011. Mapping topography changes and elevation accuracies using mobile laser scanner. Remote Sensing 3 (3), 587-600.

Vakalis, D., Sarimveis, H., Kiranoudis, C., Alexandridis, A., Bafas, G., 2004. A GIS based operational system for wildland fire crisis management II. System architecture and case studies, Applied Mathematical Modelling 28 (4), 411-425.

van den Brink, L., Stoter, J., Zlatanova, S., 2013. Establishing a national standard for 3D topographic data compliant to CityGML. International Journal of Geographic Information Science 27 (1), 92-113.

Vos, W., Meekes, H., 1999. Trends in European cultural landscape development: perspectives for a sustainable future. Landscape and Urban Planning 46 (1-3), 3-14.

Wald, L., 1999. Some terms of reference in data fusion. IEEE Transactions on Geoscience and Remote Sensing 37 (3), 1190-1193.

Werbrouck, I., Antrop, M., Van Eetvelde, V., Stal, C., De Maeyer, P., Bats, M., Bourgeois, J., Court-Picon, M., Crombé, P., De Reu, J., De Smedt, P., Finke, P., Van Meirvenne, M., Verniers, J., Zwertvaegher, A., 2011. Digital elevation model generation for historical landscape analysis based on LiDAR data: a case study in Flanders (Belgium). Expert Systems With Applications 38 (7), 8178-8185.

Würländer, R., Wenger-Oehn, K., 2007. Die verfeinerte Georeferenzierung von ALS-Daten - Methodik und praktische Erfahrungen. Angewandte Geoinformatik 19, 885-890.

Xu, S., Oude Elberink, S., Vosselman, G., 2012. Entities and features for classification of airborne laser scanning data in urban area. ISPRS Annals of the Photogrammetry, Remote Sensing and Spatial Information Sciences 1 (4), 257-262.

Zhang, J., 2010. Multi-source remote sensing data fusion: status and trends. International Journal of Image and Data Fusion 1 (1), 5-24.

Chapter 2

3D data acquisition

2. 3D data acquisition

In this chapter, different 3D data acquisition techniques are elaborated. A special focus is set on the theory of laser scanning, since this technique is currently used in many applications of 3D environmental modelling. Furthermore, conventional topographic surveying techniques, conventional photogrammetry and image based modelling are also discussed in this chapter. The knowledge of these measurement techniques is required for a better understanding of the following chapters in this dissertation. It must be mentioned that although spaceborne techniques can also be used for environmental modelling, these techniques will not be discussed here. Notwithstanding this absence, it is worth mentioning that in the past Digital Elevation Models (DEM) were generated for city modelling using VHR imagery (sub meter) from spaceborne sensors like *Ikonos* or *QuickBird* (Kocaman et al., 2006; Tack et al., 2012). Coarser resolutions are achieved for the GDEM (Global Digital Elevation Model), derived from *ASTER* imagery (*Advanced Spaceborne Thermal Emission and Reflection Radiometer*, 30 meter), or InSAR-based (Interferometric Synthetic Aperture Radar) DEMs, like *SRTM* data (*Shuttle Radar Topography Mission*, 30 meter in the USA, 90 meter worldwide) (Frey and Paul, 2012; Grus et al., 2010) or *TerraSAR-X* (1 meter) (Bamler et al., 2009).

2.1. ***Laser scanning***

2.1.1. Introduction

LiDAR is an acronym that stands for 'Light Detection And Ranging' and is a generic term for all techniques where (laser) light is used to derive the distance between a sensor and an object or surface (Wehr and Lohr, 1999). All types of laser scanning systems are optical, reflection based and contact free 3D scanning methods (Galantucci *et al.*, 2006). The used electromagnetic signal is situated in the visible, near- and short-wave infrared range (500-1600 nm). In addition to this distance measurement, a horizontal and vertical angle is also recorded. By transmitting signals from a measuring instrument, of which the orientation and the coordinates are known in 3D, polar coordinates can be calculated based on the measurements of angles and a distance. Using this technique, also called the 'Electromagnetic Distance Measurement' (EDM), a distance is derived by means of counting the duration of a pulse or the phase difference of a continuous wave. Next to these two techniques, the distance between the scanner and the object can be calculated by laser triangulation. Pulse-based systems are most common in airborne laser scanning applications, whereas phase-based systems may be implemented in faster and more accurate terrestrial laser scanners. Polar coordinates are usually directly converted to Cartesian coordinates. The signals are broadcasted over different known angles, using rotating mirrors. The pulse frequency varies with different airborne units from 20 to 500 kHz (pulse frequency, sampling interval per pulse), where between 5 to more than 400 scan lines per second (scan frequency) can be recorded. For terrestrial applications, these values may increase strongly up to 1 GHz, when a phase-based laser scanner is deployed. Laser triangulation scanners are used to measure very short distances and small objects, with a much lower scanning speed of around 10 kHz. In addition to the measurement of a single echo or a series of discrete echoes per pulse, it is also possible to register the entire backscatter of the returned signal. Full-waveform laser scanning allows to describe the

physical properties of the reflecting object and facilitates point cloud classification and feature detection (Briese et al., 2008; Mallet and Bretar, 2009). This type of laser scanning is not used in this dissertation and will not be discussed in this chapter.

2.1.1.1. *Light Amplification by Stimulated Emission of Radiation*

The main element of a laser scanning system, whatever the application or measuring technique may be, is the laser signal generator. This device is able to generate a monochromatic (constant wavelength), collimated (parallel) and coherent (in phase) electromagnetic signal (Thomas and Isaacs, 2011). The system contains three main components (Figure 2-1): an energy source, an optical resonator and a laser medium inside the resonator. The energy source generates a huge amount of photons, which are beamed inside the optical resonator. Inside this resonator, the atoms of the medium absorb these photons, resulting in excited atomic states. In order to get back to its ground state, excited atoms will spontaneously emit the photon in a random direction. If the photon is reflected by the mirror on one side of the resonator, the photon will return in the medium and an exited atom may absorb this photon. This over-exited atom results in the stimulated emission of two photons and a ground state atom (Stoker, 2005). A high energetic bundle of these photons form the actual laser beam.

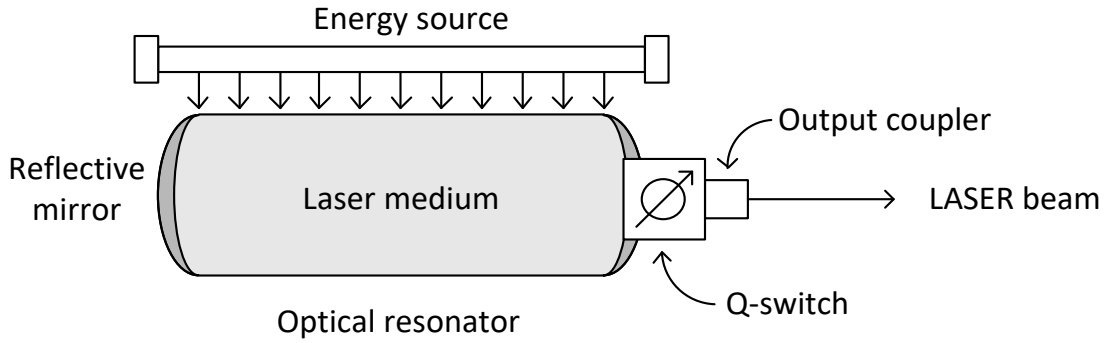

Figure 2-1: Construction of a laser system

In case of continuous wave lasers, the photons are directly released through the output coupler, which is a partially reflective mirror. For pulse based scanners, a Q-switch is used, containing an attenuator or photon absorbing crystal. If the energy of the laser medium has reached a certain threshold, the switch will open and an energy pulse is transmitted. The amount of energy in this pulse, with a typical duration of 10 ns for airborne laser scanners (Baltsavias, 1999a), is much higher than the amount of energy of a continuous wave with the same duration. This explains the significant longer ranges of pulse-based laser scanners in comparison with phase-based laser scanners. However, the range of phase-based laser scanners is also more limited by the longest possible phase shift, as discussed below (Delaloye et al., 2014).

2.1.1.2. *Behaviour of the signal*

The shape of a laser scanning beam can be defined as a Gaussian beam, where the wave front radius ω increases in function of the propagation distance d, which is the distance between the laser sensor and the reflecting object, along the directional axis of the signal. This property is the

same for both conventional and laser beams and will cause a Gaussian spread of the energy of the beam in a perpendicular direction of the propagation axis. In contrast with conventional light beams, laser beams do not diverge entirely linear, but a cone is approached in the far-field, while the divergence in the near field is very small (Weichel, 1990). As a result, a laser beam can be described by an asymptotic cone. The shape of the beam is defined by an $1/e^2$ irradiance surface. The value of e^2 defines a circle, where 86% of the laser beam energy is situated, according to a Gaussian distribution. It will be clear that this divergence has a major impact on the resolution of the point cloud, the accuracy and precision (Lichti and Gordon, 2004). The d_R or the 'Rayleigh range' defines the distance where the beam radius has been spread by a factor $\sqrt{2}$. At this distance, the $1/e^2$ irradiance surface has its maximal curvature. The value of the Rayleigh range is used to distinguish near-field divergence and far-field divergence. Besides, the distance between the $1/e^2$ irradiance surface and the main axis equals the wavefront radius in the far-field. The divergence, given in a laser scanner specification, is usually defined as the divergence of ten times the Rayleigh range. For the measurement of short range distance using a terrestrial laser scanner, the beam waist ω_0 and wavelength λ are smaller than for the measurement of long distances using airborne laser scanners.

In order to calculate the beam width ω for a given distance d, or the impact of the beam waist ω_0 (minimum spot size) on the radius of the beam width for a given distance d and beam wavelength λ, Equation 2-1 is used for a vacuum (Self, 1983):

$$\omega^2(d) = \omega_0^2 \left[1 + \left(\frac{\lambda d}{\pi \omega_0^2}\right)^2\right]$$

Equation 2-1: Wavefront radius or beamwidth in function of the beam waist and distance

Since the beamer in the laser scanner has a certain sensitivity and only measures a certain part of the entire returning laser beam, the relation between the beam width and the measured distance is very important. The normalized distribution of the total beam power I can be formulated as (Self, 1983):

$$I(r, \omega) = \left(\frac{2}{\pi \omega^2}\right) e^{-2\left(\frac{r}{\omega}\right)^2}$$

Equation 2-2: Normalized intensity of the total beam power

ω is described as the wavefront radius in Equation 2-1 and r is the perpendicular distance from a given point to the main axis. The geometry of a Gaussian laser beam is presented in Figure 2-2, demonstrating different characteristics of the signal. The above states the hypothesis that the returning energy that can be detected is strongly related to the wavelength, the distance of the measured object and the size and sensitivity of the detector. These parameters are limited by physical factors: increasing the wavelength requires more sophisticated power boosters. Moreover, as demonstrated above, a higher wavelength increases the beam spot radius, which implies lower point accuracy. This limits the maximum distance to the measured object as well. Finally, the size and sensitivity of the detector are limited, because of physical restrictions on the one hand and

noise sensitivity on the other hand. Because of the wide range of distances to measure for terrestrial laser scanning and airborne laser scanning (sub-centimetre to a few kilometre), the physical properties of the laser beam are determined for both techniques in terms of the wavelength, spot radius and the related beam intensity and accuracy.

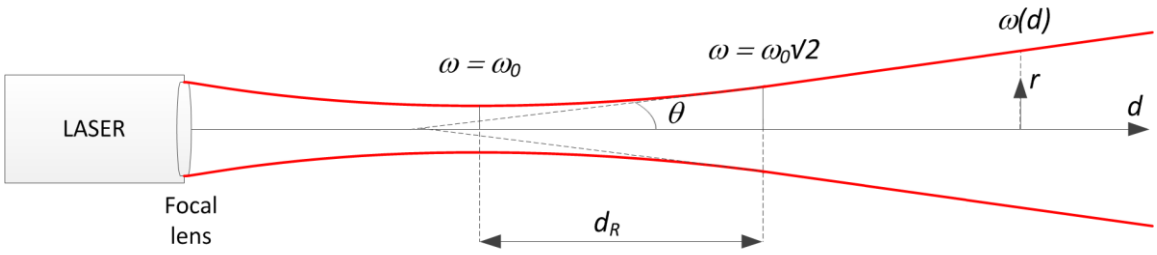

Figure 2-2: Along geometry of a Gaussian beam width *ω(d)* as a function of the axial distance *d*

The presented model for the normalized intensity in Equation 2-2 is a generalization of the so called 'laser equation', which is related to microwave radar distance measurements and clearly explained by Wagner, et al. (2006):

$$P_r = \frac{P_t}{4\pi d^2} \cdot \frac{4\pi}{\theta_t^2} \cdot \frac{\sigma}{4\pi d^2} \cdot \frac{\pi \omega_0^2}{4} \cdot \eta_{atm} \cdot \eta_{sys} + P_{bk}$$

Equation 2-3: Laser equation

This equation defines the relation between the transmitted power (P_t) and the received power (P_r), taking the beam width opening angle θ_t, the propagation distance d and the properties of the of the reflecting surface or 'backscatter cross-section' σ into account. Finally, some error terms related to the atmosphere (η_{atm}), system losses (η_{sys}) and background radiations (P_{bk}) are added.

2.1.1.3. *Distance measurement*

The acquisition of a point cloud by laser scanning is based on the registration of horizontal angles, vertical angles and on the (direct or indirect) measurement of distances. Absolute coordinates *r* (X_R, Y_R, Z_R) of an object R are determined in relation to the position *p* (X_P, Y_P, Z_P) of sensor P and the distance and direction of vector *a* from the sensor P to the object R (Katzenbeisser, 2003). The object R can be any properly reflecting object within the range of the sensor (Figure 2-3).

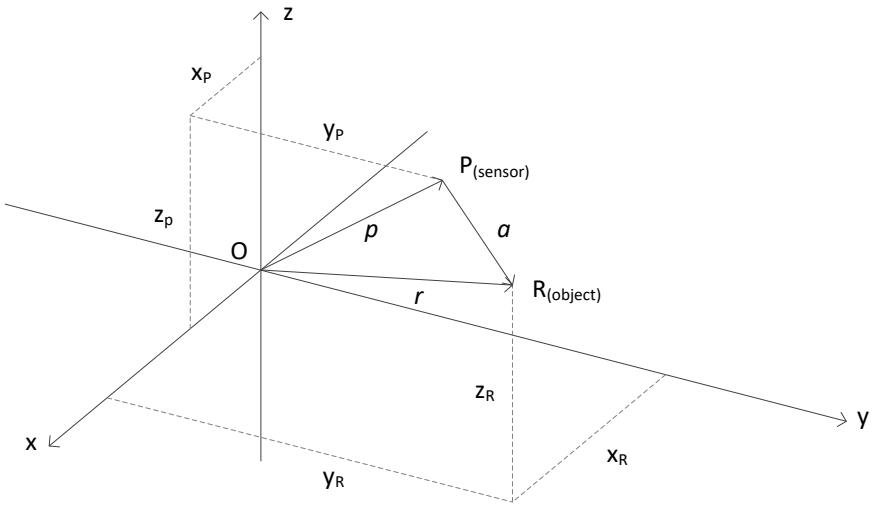

Figure 2-3: Determination of the coordinates of object R (Katzenbeisser, 2003)

The position *p* of sensor P is measured by the combined use of Global Navigation Satellite System (GNSS) and INS (Inertial Navigation System) in mobile applications, or by point cloud registration in static applications. The actual angular and distance measurements of vector *a* are performed by the laser scanner. The angle, from which this distance is measured, is determined by the registration of the rotation of a rotating mirror. This mirror must be perfectly aligned and calibrated with respect to a reference orientation. Pulse-based and phase-based laser scanning are the most common techniques for the distance measurement (Baltsavias, 1999a) and will be discussed in more detail. For the sake of completeness, laser triangulation is also briefly discussed, which is mainly applied for short range and reverse-engineering applications. However, this technique is not applied for environmental modelling.

Pulse-based measurement

Pulse-based laser scanning systems, also called Time-Of-Flight (TOF) scanning systems, are frequently used for airborne applications (Hug et al., 2004) and terrestrial applications with relatively long ranges. Using this technique, the distance between the sensor P and the reflecting object R are directly calculated by counting the time delay *t* between an emitted and received pulse. This delay is multiplied by the speed of light *c* and divided by two (Baltsavias, 1999a):

$$d = \frac{1}{2} c \cdot t$$

Equation 2-4: Pulse-based distance measurement

with

$$\Delta d = \frac{1}{2} c \cdot \Delta t$$

Equation 2-5: Resolution of a pulse-based distance measurement

The time of flight of the signal is registered by a counter, which multiplies the number of cycles *n* by a given frequency *f*. The resolution of the counter has a linear relation with the range resolution of the measurement system (Wehr and Lohr, 1999). A constant time factor should compensate the time delays, inherent to the electronics of the system and should be carefully calibrated.

Phase based measurement

Most short range terrestrial laser scanners make use of phase-based distance measurements. These types of laser scanners are known for their high scanning speed and accuracy, in comparison with pulse-based laser scanners (Nuttens et al., 2010b). Instead of measuring the time interval between the emission and reception of a pulse, a continuous electromagnetic wave is propagated. The total number of elapsed waves, combined with the rest fraction of the last wave is used (Baltsavias, 1999a):

$$d = \frac{1}{2} c \left(\frac{1}{2\pi} \frac{1}{f} \varphi \right) = \frac{1}{4\pi} \frac{c}{f} \varphi$$

Equation 2-6: Phase-based distance measurement

with

$$\Delta d = \frac{1}{4\pi} \frac{c}{f} \Delta\varphi$$

Equation 2-7: Resolution of a phase-based distance measurement

As demonstrated in Equation 2-4, the calculated distance *d* is also related to the time of flight of the signal. However, this travelling time is calculated as a function of the frequency *f* of the signal and the phase shift φ. The limiting effect of the phase shift φ was already mentioned above and is found by the maximal detectable proportion of this value (Delaloye et al., 2014). The resolution of the system is then limited by the extent to which this phase shift can be measured (Wehr and Lohr, 1999).

Laser triangulation

Triangulation based laser scanning is not used for 3D city modelling, but will be mentioned briefly for the sake of completeness. This acquisition technique is frequently used to model objects with a limited size and with a limited distance between the object and the scanner (Pieraccini *et al.*, 2001). Current systems in the field of reverse engineering, where the distance between the scanner and the surface is limited (e.g. from 1 cm to 1 m) and where resolutions of 0.005 mm with a standard deviation of 0.02 mm can be reached (Vukašinović et al., 2010). As with pulse-based and phase-based systems, triangulation systems are also based on the projection of a laser beam to a surface. Caused by the local normal of the surface, the beam will reflect over a certain angle in the direction of a camera, and will be registered by an (CCD or CMOS) image sensor (Figure 2-4, left).

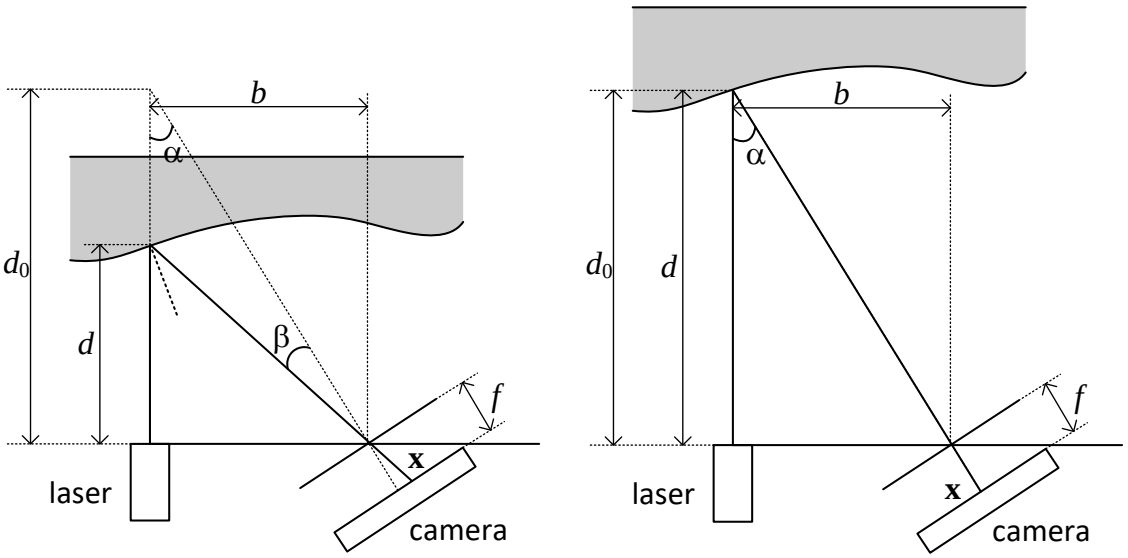

Figure 2-4: Laser triangulation-based distance measurement (left) and system calibration (right)

Since the 3D coordinates of the laser and the camera, the distance between the laser and the focal point of the camera (*b*), the focal length (*f*) and pixel size of the camera and the 2D coordinates of the received signal on the sensor (**x**) are known, the 3D coordinates of the reflective surface point can be calculated, using the following known parameters:

- 3D coordinates of the laser and the camera;
- The distance between the laser and the focal point of the camera (*b*);
- The focal length (*f*);
- The pixel size of the camera;
- The 2D coordinates of the received signal on the sensor (**x**).

These parameters used to derive the following distance Equation 2-8 (Peiravi and Taabbodi, 2010):

$$d = b\cot(\alpha + \beta)$$

Equation 2-8: Laser triangulation based distance measurement

Based on the rather simple Equation 2-8, it becomes clear that the system requires calibration in order to measure angles (α and β) and to start measurements (Fontana et al., 2002). Since the 2D coordinates of the received signal on the sensor (**x**) is directly related to angle β, the system calibration can be performed by creating a fixed distance between the system and the surface so that $d = d_0$.The reflected laser beam will be detected by the central pixel of the sensor, with $\beta = 0$. Under these conditions, angle α can be calculated and fixed for the entire measurement. The short working range of this type of scanners can be explained by the linear relation between the distance measurement and the baseline.

2.1.2. Applications of laser scanning

2.1.2.1. *Airborne Laser Scanning*

Airborne Laser Scanning (ALS) is a relatively new technique in surveying and engineering for topographic surface modelling, but also the oldest 3D data acquisition technique where laser scanning is used in civil applications. Although the acquisition technique itself is known for several decades, much research is still performed on different applications, accuracy improvement and processing performance. Especially in geo-sciences and engineering, ALS is frequently used to generate 2.5D and 3D models. The main advantages of ALS are the fast and relatively accurate acquisition of topographic point clouds, with a wide range of possible point densities. Among others, this density is related to the flying height. Besides, recent research on processing ALS data enabled a reliable and straightforward workflow for the generation of Digital Terrain Models (DTM) and Digital Surface Models (DSM) (Podobnikar and Vrecko, 2012).

The ALS systems deflect the laser beam across a flight path in order to acquire a certain field of view (Figure 2-5). Each separate distance and angle measurement is combined with synchronized observations of a Position and Orientation measurement System (POS). This enables the direct georeferencing of the measured points in a common coordinate frame. The POS typically consists of a GNSS and an INS (Mallet and Bretar, 2009). As with all other mobile and integrated spatial measurement systems, the calibration of these different sensors is very important. This calibration consists of the determination of the lever-arm and bore-sight parameters, representing positional and angular offsets of the different local coordinate systems of the sensors (Skaloud and Lichti, 2006).

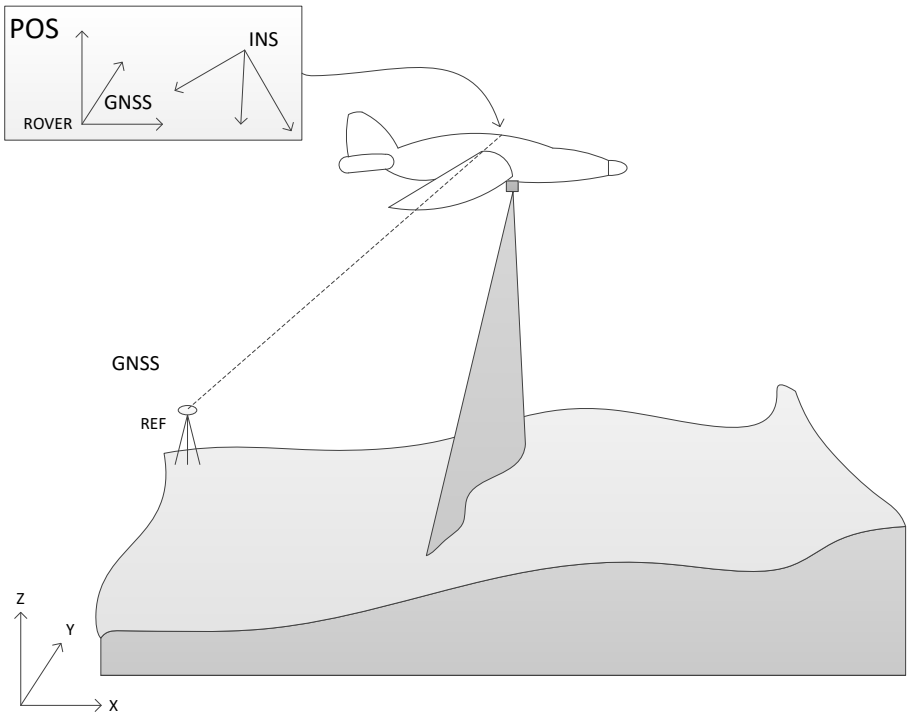

Figure 2-5: General operation principle of an ALS-system

For the last decennium, ALS is applied on a large scale for the generation of country-covering digital elevation models. Different public and private institutions and companies have seen the usefulness of this technique and offer (filtered) point sets or rasterized elevation models to their customers.

Platform

The acquisition of ALS data is performed using different flying platforms. In most cases, a helicopter of airplane is deployed with at least a scanner, inertial measurement unit and a global navigation system, as described in the following paragraph. A helicopter is frequently deployed when the area to be covered is relatively small in relation to the required point density, e.g. in urban areas or archaeological sites, or when the flight plan is rather irregular, e.g. in mountainous areas. Recent developments with Unmanned Aerial Vehicles (UAVs) also enabled the deployment of laser scanning with these flying platforms, allowing very limited elevations (Lin et al., 2011). These systems are mainly used to fully cover buildings or cultural heritage structures with very dense point clouds. However, most institutions and companies in the Northern European lowland plain are using airplanes, since bigger areas can be covered in a smaller time frame. The internal configuration of the equipment on airplanes and helicopters are largely identical. Typical flying heights of the platform vary between 20 and 6000 meter above the ground. For example, the first (2003) ALS data of the Flemish Agency for Geo-Information (AGIV, Agentschap voor GeoInformatie Vlaanderen) were acquired by an airplane at an average flying height of 3000 meter above the ground, resulting in a point density of one point per 2-4 m^2 (Kellens, 2006). In 2012, the AGIV has acquired a new point cloud using ALS, at an average flying height of 400 meters above the ground, resulting in a much higher point density of 27 points per m^2. In general, the maximal flying height of the platform relies on the energy of the laser pulse, the sensitivity of the receiver and the maximal range of the signal counter (Baltsavias, 1999b). The first two factors are related to distortions that occur during the on-going of the emitted and returned signal. The usable energy of the signal is limited by technical reasons and by security regulations. Signal noise is the addition of false information, in form of net energy. Since the sensor should only recognize and process its own signal, the noise on the reflected signal should be as low as possible or at least easily deductible from the true signal. However, a loss of energy of the original signal will occur, caused by cushion by molecules in the atmosphere, loss by divergence of the pulse and signal turning off by refraction of different aerial layers. These limiting factors are already mentioned above in Equation 2-3. Based on this equation, it is obvious that the impact of the parameters can be dwindled by reducing the flying height, increasing the transmitted power …. By reducing the flying height, the point density and distance accuracy will increase, but the flying time and acquisition cost will increase as well. Another solution is the discernment of multiple simultaneous pulses on the fly within a single profile by assigning unique signatures to these pulses. In this case, the next pulse can be emitted before the echo of previous pulse is received by the sensor. Riegl, Leica and Optech have implemented this principle by their "Multiple Time Around" (MTA), "Multiple-Pulses-in-the-Air" (MPiA) and "Continuous MultiPulse" (CMP) respectively (Petrie, 2011).

Components of the system

The ALS measuring system contains at least three components (Würländer, 2007). Studying these three components enables the analysis of possible errors and their sources, which can occur during the acquisition and processing of the point sets:

- Global Navigation Satellite System (GNSS) in differential mode with real time processing (Skaloud et al., 2010) or without real time positioning, e.g. fast static in post processing (Katzenbeisser, 2003). The system will be equipped with a code- and L1/L2 phase compatible GNSS receiver and data will be post processed using data from one or more reference stations in the area of interest. This will typically result in positioning data with a frequency of up to 10 points per second and an overall accuracy of 10 cm or better;
- INS, complementing the trajectory measurement of the system between two consecutive GNSS measurements. The system contains a series of gyroscopes and accelerometers in order to continuously measure respectively the velocity and acceleration of the platform (Woodman, 2007). 'Tactical grade' INSs are currently used in ALS-systems, with an acquisition speed of 400 Hz and a drift of approximately 1^{o} per hour (Skaloud and Viret, 2004);
- The ALS itself, containing four sub-components: the laser generator, the counter, the signal emitter and the signal detector. The ALS sensor is placed at the bottom of the aircraft, preferably aligned with the vertical axis, beneath the point of intersection of this axis with the longitudinal and transverse axis of the aircraft. This is to reduce the possible presence of tilt during the measurements.

Furthermore, the platform could be equipped with a video camera or medium digital camera (Baltsavias, 1999b). The resulting images can be used for easier point processing and logging, but also for point colouring or model texturing. A more frequently used approach for colouring (airborne) laser scanning point clouds is based on the alignment of orthoimages (Gerke and Xiao, 2014).

2.1.2.2. *Airborne Laser Bathymetry*

Airborne Laser Bathymetry (ALB) is a new remote sensing technique that has known a very fast development over the last few years. In most aspects, ALB is very similar with regular ALS systems. However, a common ALB system is equipped with a pulse-based dual wavelength signal emitter and receptor, typically with wavelengths of 1064 nm (near infrared, like in ALS) and 532 nm (green) (Long et al., 2011). The first signal is reflected by the dry ground and the water surface; the second signal penetrates into the water and is reflected on the sea bottom (Figure 2-6). Modern ALB systems, like the Riegl VQ-820-G, solely make use of a green signal (i.e. with a single wavelength of 532 nm) with a very short and narrow pulse (Steinbacher et al., 2012).

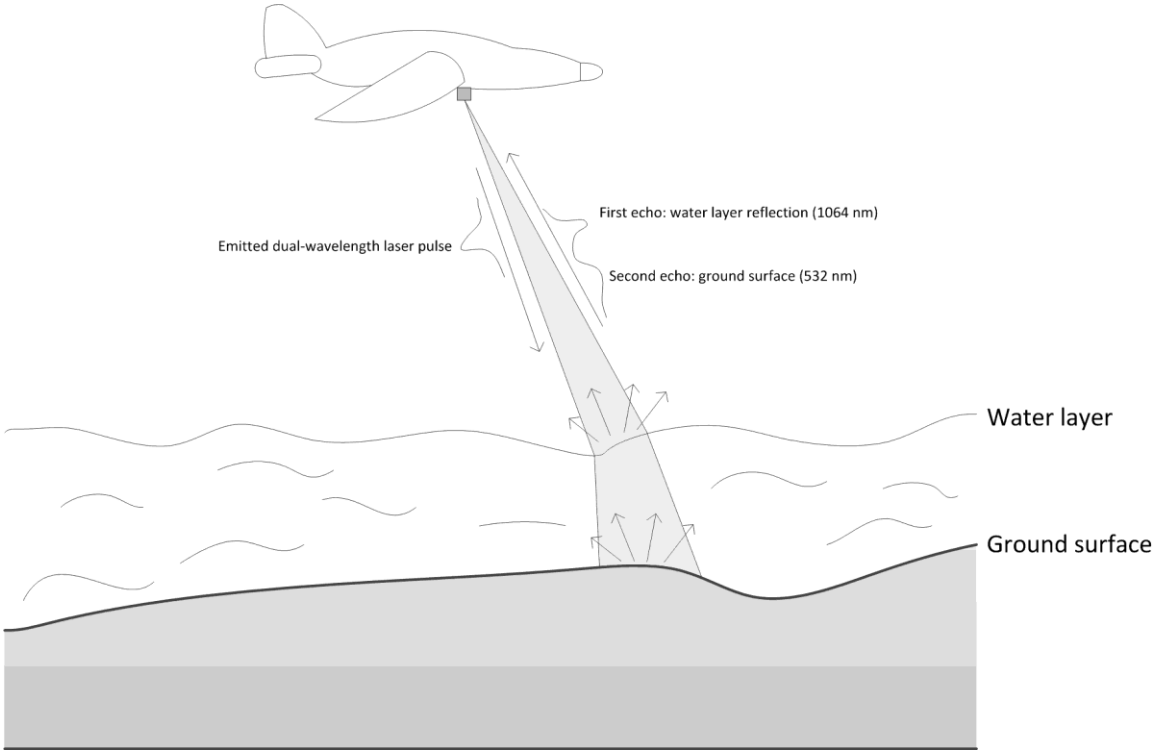

Figure 2-6: Operational principle of Airborne Laser Bathymetry (ALB)

The technique is used for bathymetric surveying of shallow coastal waters and in the right environmental conditions, it will provide significant efficiency advantages over survey by regular survey vessels. The most recent advances have enabled the recovery of reflectivity information from the seabed footprint, leading the way to seabed classification and advanced feature detection. This technique is very similar to full-waveform analysis with ALS. Earlier research has demonstrated the potential of ALB in areas with water turbidity of 2-3 secchi depths (Pastol, 2011; Pe'eri et al., 2011). In clear water, this corresponds with approximately 50 m. Due to the active billow and strong tidal current in the near shore North Sea coast, high water turbidity occurs, limiting this secchi requirement to only a few decimetres. Using ALB, it is possible to cover both the dry beach, as well as the sea bottom. The technique does not necessarily provide a full coverage of the area, because of interference of the two signals in very shallow waters (approximately 20 cm). The automatic detection of the current shoreline will be hampered and additional campaigns have to be performed to overcome this problem (Pe'eri et al., 2011). Multiple scan campaigns during different tidal situations could solve this data gap issue as well.

In contrast with the high pulse frequency of ALS systems, ALB systems operate with a frequency of only 1 kHz. However, the previously mentioned ALB system has a pulse repetition rate of 250 kHz (Steinbacher et al, 2012). In order to penetrate a water column with the green signal, a significantly longer and more powerful laser pulse is required. Complex interactions occur between the emitted laser signal and the environment. After emission, attenuation takes place on the beam by absorption and scattering. Signal losses, caused by diffuse reflection, occur on the water layer, but also the influence of refraction is very important to mention and has to be taken into account. The green signal will penetrate the water layer until it is fully absorbed or until it reaches the ground surface, where a second diffuse reflection takes place. During the return of the

signal, the same phenomenon occurs, but in the opposite direction (Mitchell, 2008). Increasing the emitted energy of the signal will clearly increase the penetrating capacity and thus the maximal depth of the water layer. The signal-to-noise ratio will also increase with higher power levels. Nevertheless, this power level is limited by legal void for security reasons: high energetic green light may cause irrevocable eye damage. Besides, officially preparatory permission is required to perform the flight, reducing the flexibility of measuring the intertidal zones under acceptable weather and tidal conditions. Based on this theoretical comparison of ALS and ALB, it becomes clear that under typical conditions, ALB campaigns will result in coarser digital surface models with lower accuracies, than an ALS acquisition campaign under the same acquisition circumstances. However, recent developments have made clear that point densities of 20-50 points per m^2 can be reached with ALB when the flying height is limited (Doneus et al., 2013). Moreover, the quality of the ALB data could be comparable with Multi-Beam Echo Sounder (MBES) data in near shore areas (Pastol, 2011). Besides, the acquisition time and cost of ALB are lower in comparison with conventional bathymetric acquisition techniques, when very large surfaces are covered (Lam and Yip, 2008).

2.1.2.3. *Static Terrestrial Laser Scanning*

Static Terrestrial Laser Scanning (STLS) is a variant of the above mentioned laser scanning techniques, where a huge amount of accurate detail points is acquired from a fixed laser scanner position. STLS is frequently used to model objects of a limited size or at a limited distance from the scanner (Pieraccini et al., 2001). The type of application and the range is in this context mainly related to the type of distance measurement (i.e. phase-based with a range up to 100 m or pulse-based with a range up to 6 km) (Pertrie and Toth, 2009; Laefer et al., 2014). High resolution STLS is more and more being applied for measuring and monitoring geometric deformations of civil technical constructions (Nuttens et al., 2010a), but also in cultural heritage (Pesci et al., 2012; Stal et al., 2012) or earth sciences (Brodu and Lague, 2012; Jaboyedoff et al., 2012). STLS offers a non-invasive solution for the need for 3D data in a short time frame and in difficult field conditions.

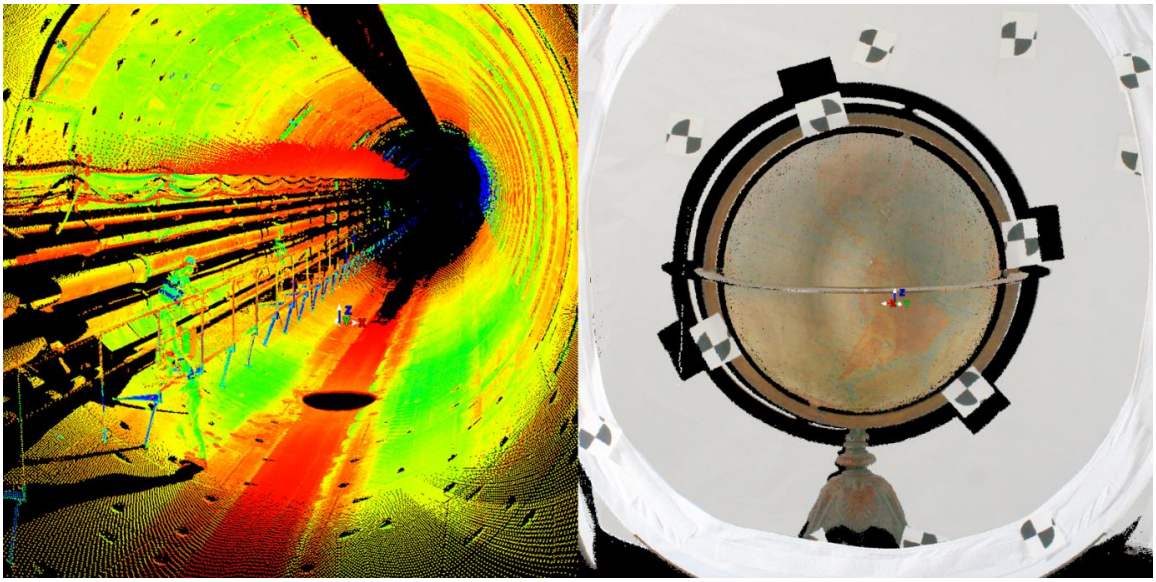

Figure 2-7: Two applications of STLS: deformation measurements in tunnels (left, Ø7.3 m, Nuttens et al. (2012)) and the modelling of ancient globes (right, Ø0.4 m)

The technique can be used for topographic surface modelling (Slob and Hack, 2004), but it is obvious that STLS suffers from some important drawbacks for topographic mapping. The number of scans is related with the size of the area that has to be scanned. Because of the lack of topographic variability of the terrain, a target based registration is required (González-Aguilera et al., 2009). Since each target, or materialised reference point, has to be positioned in a coordinate system, the campaign can be very time consuming. An even more important drawback of static measurements is the fact that on flat terrain, the angle of incidence will be very large. A scanner is often placed on a tripod, meaning that the scanning height is around 1.5 to 2.0 m. Even with a range of 8.5 m, there will be an incidence angle of 80°, resulting in large beam spots or radiation angles. Thereupon, lower signal to noise ratios will occur and lower point accuracies will be reached (Soudarissanane et al., 2011). Summarizing, it can be concluded that STLS will be very useful for the detailed modelling of small surfaces and vertical structures, but attention on the speed and accuracy has to be paid for the mapping of larger areas.

2.1.2.4. *Mobile Terrestrial Laser Scanning*

With Mobile Terrestrial Laser Scanning (MTLS), the system configuration is very similar to an airborne setup. A laser scanner, GNSS and INS are the main components, mounted on a driving platform. As in airborne applications, the combination of GNSS and INS (or IMU) measurements from the POS provide highly accurate positioning, whilst the laser scanner produces a very precise point cloud. The accurate determination of the calibration parameters is also essential for the correct use of MTLS. However, the required power level for the laser scanners is much lower in comparison with airborne sensors, reducing the dimensions of the system and therefore improving the usability on compact platforms. This is mainly due to the more limited distances to measure in terrestrial applications.

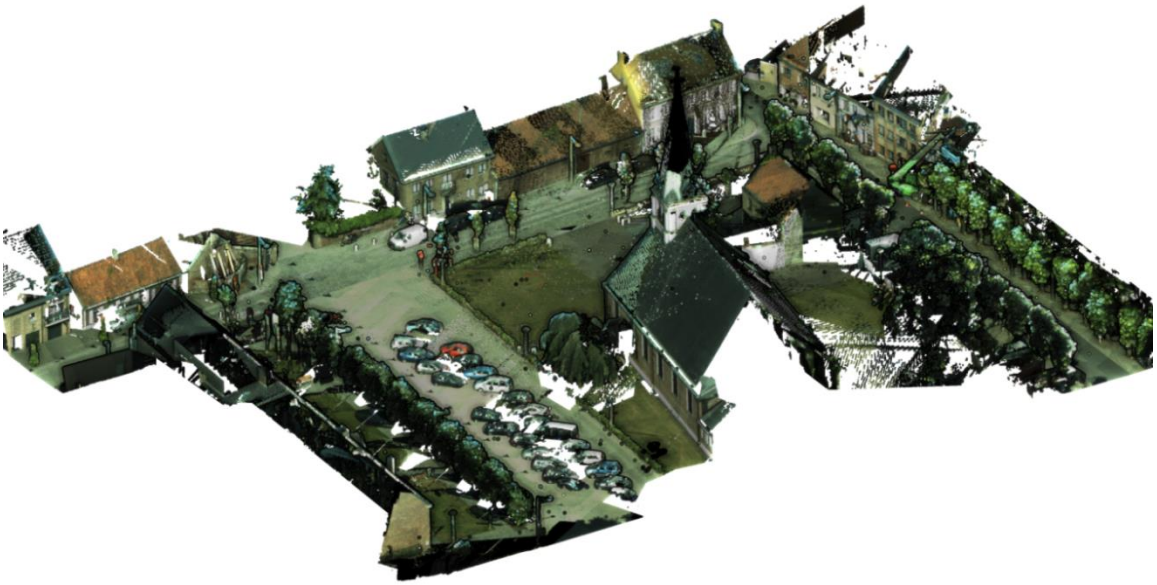

Figure 2-8: MTLS point cloud of an urban area (source: *Teccon*)

MTLS is frequently used for fast topographic mapping (Figure 2-8), but it has also been applied for river bed mapping (Vaaja et al., 2011) and on beaches for coastal protection applications (Bitenc et al., 2011). Under regular topographic campaigns, the MTLS configuration is mounted on a van or normal car with imperial. For intertidal beach modelling, the driving platform needs to perform in very shallow water, but also in shifting sand. An amphibious vehicle, like the ARGO (Figure 2-9) is then an obvious choice. Although 2D profile scanners can be used for MTLS, it is also possible to deploy regular STLS systems configured as a profiler. Nevertheless, the centimetre accuracy of both systems is comparable. STLS has the advantage of generating point clouds of the surface in a strip-wise manner as with airborne scanning. Using the ARGO, the scanning height will be more or less equal to the height of a scanner on a tripod. The previously mentioned issue concerning the large incidence angles can be reduced by limiting the scanning range and allowing enough overlap between subsequent strips (Vosselman and Maas, 2001).

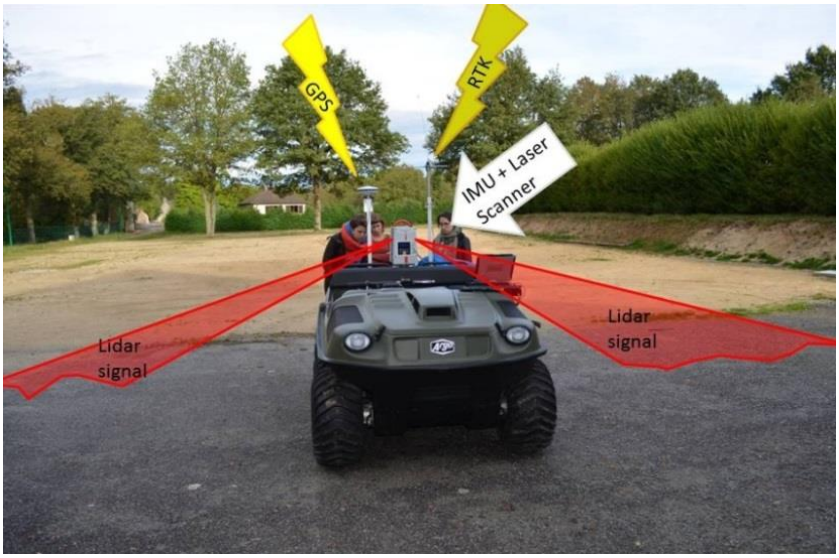

Figure 2-9: Main components of a mobile laser scanning system, mounted on the ARGO

2.1.3. Error sources in laser scanning

Much is already written about errors and error sources for laser scanning (Huising and Gomes Pereira, 1998; Nuttens et al., 2009; Soudarissanane et al., 2008; Soudarissanane et al., 2011). A thorough synthesis of these contributions is beyond the scope of this chapter, but a short summary is required for a better understanding of the following chapters. Since terrestrial laser scanning and airborne laser scanning are very similar data acquisition techniques, some important possible error sources on both techniques can be studied together. All kinematic laser scanning techniques suffer from the following error sources:

- Errors related to the scanner and its mechanisms, like the offsets of the axes, offset of the mirror, time delays or errors in the rotating mechanism;
- Furthermore errors are related to the signal and its detection. A pulse for laser scanning applications has a typical duration of 10 ns (Baltsavias, 1999b). Within this pulse, a specific time range is required to reach a maximum energy value. The energy of a pulse is mathematically not defined as a discrete boost, but rather as a Gaussian bell shape distribution. In this form, the energy value of the pulse increases in accordance with a particular function up to a maximum, after which it gradually decreases again. Therefore, the transmitted signal needs to reach a certain energy level, in order to be detected by the receiver (Baltsavias, 1999a);
- Errors related to the positioning and orientation of the laser scanner, which can be minimized by a thorough determination of bore side angles and lever arm offsets of the scanner, INS (or IMU) and GNSS (Skaloud and Lichti, 2006). For STLS, georeferencing or point cloud registration is performed by a target based registration (Nuttens et al., 2010a) or by running an Iterative Closest Point (ICP) algorithm (Figure 2-10);
- Errors related to the surface to be scanned, like its colour, material, roughness or humidity. In Equation 2-3, this error source is described by the parameter σ;
- Errors related to the environment, like the air temperature and air humidity or the light conditions. In Equation 2-3, this error source is described by η_{atm};
- Errors related to the relation between the position of the scanner and the object to be scanned, in terms of the distance and the incidence angle (Würländer, 2007). This error has been mentioned explicitly during the discussion on the use of STLS for topographic surface modelling.

A detailed description of these error sources is also presented by Delaloye et al. (2014), where an error budget is discusses for the different sources. Moreover, multiple approaches and methodologies for the documentation of these errors in spatial data are presented in the next chapters of this dissertation (e.g. in chapter 4).

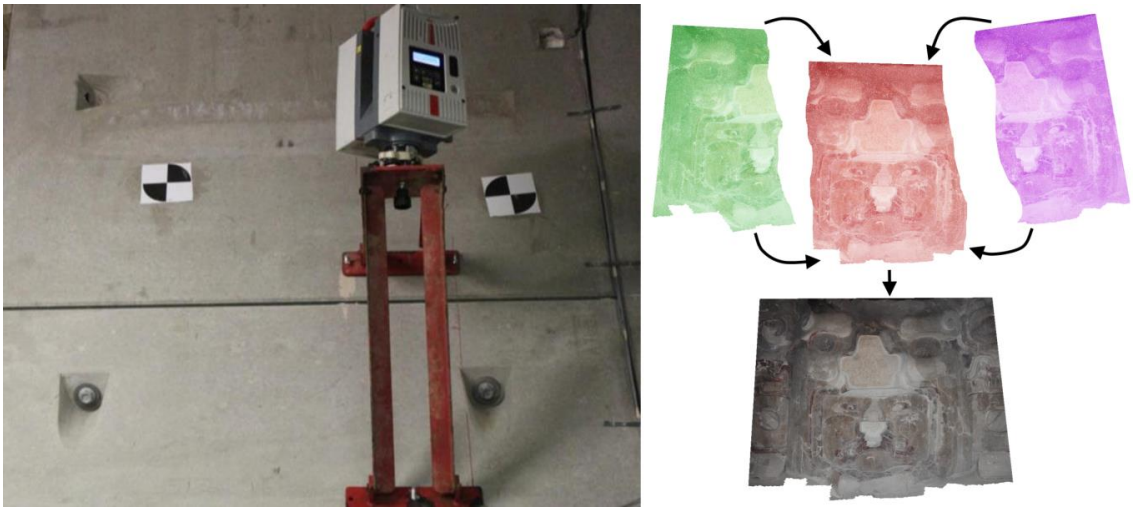

Figure 2-10: Point cloud registration using a target based registration (left, (Nuttens et al., 2010a)) or by performing an ICP algorithm (right)

Some of these errors can be eliminated (partially) by performing a careful system calibration (Katzenbeisser, 2003) or by applying some error model on the raw data. Another procedure to reduce errors of airborne data is strip adjustment (Attwenger and Briese, 2003). In spite of these efforts, the data may still contain outliers or noise, but these points can be filtered using different algorithms.

2.2. ***Photogrammetry or image based modelling***

In contrast with the discussion on laser scanning, image based modelling techniques can be distinguished by processing algorithms, rather than by the used acquisition techniques and platforms. Photographs can be taken during an airborne or terrestrial campaign or on a mobile or static platform. In all cases, the initial data for the surface reconstruction are two or more digital images. As with ALS, airborne photogrammetric campaigns also require predatory permission, and in Belgium the number of optimal flying days is very limited as a result of seasons (vegetation) and weather (clouds). The use of an UAV, like a drone or kite, could be an alternative, notwithstanding the fact that favourable weather conditions are also required and the use is restricted by legal regulations as well. On terrestrial images, it is very difficult to define corresponding points between different images for topographic surface modelling. Large incidence angles away from the acquisition point of an image result in very large Ground Sampling Distance (GSD), so terrestrial photogrammetry and image based modelling is only advisable for very small and characteristic areas.

2.2.1. Conventional photogrammetry

A conventional photogrammetric workflow can be subdivided into two main processes. The chain starts with the aerial triangulation for which aerial images, camera details, orientation files and Ground Control Points (GCP) are required. If this process is successful, the triangulated images and generated tie-points make it possible to extract detailed and accurate DSMs. Conventional

digital photogrammetric software packages process stereo couples one by one. This means that different images are aligned with each other in a pair-wise way. Although recent software may merge different stereo-based DSMs in the last step of the processing workflow, the calculated elevations are only a function of single image pairs, averaged over all available stereo couples. Since this technique is also very well documented, (Kraus, 2007) or (McGlone et al., 2004) can be used for further readings.

2.2.2. Image based modelling

New 3D photo modelling software is able to generate 3D models based on a large series of images using Structure from Motion and MultiView Stereo (SfM-MVS). SfM-MVS is a technique to reconstruct the camera acquisition parameters and a sparse point set of the scene using multi stereo matching (SfM), as well as a technique to acquire the 3D geometry of an object, or a series of objects (MVS), using a series of 2D images (Lourakis and Argyros, 2009). The projection of a real 3D object on a 2D image plane and the inverse transformation of the resulting 2D image coordinates into a virtual model in a 3D space, result in the determination of the extrinsic parameters and require the intrinsic camera parameters for the initial step of the iterative refinement (Robertson and Cipolla, 2009). This is also applied in conventional photogrammetry, but in this case, multiple images can be used instantly. The intrinsic parameters, like the image format, the principal point and the focal length of the images are extracted from the metadata of the images. The extrinsic parameters are calculated by the projection of the images in the 3D space. Characteristic points or feature points are detected on different images and matched with each other. In order to recover the position and orientation of the different camera positions, a system of geometrical projective matrices, based on the 3D coordinates of the features points, has to be solved (Pollefeys et al., 2000). The first step in this process is the (automatic) detection of these feature points. After initialization, both the intrinsic and extrinsic parameters are iteratively adjusted, until a best fitting solution is achieved. This solution is evaluated using least squares adjustment, which is implemented in an Expectation-Maximization (EM) algorithm. Using the final parameters, the extrinsic transformation parameters of the images in a virtual 3D space are calculated. The result of the SfM is a sparse point cloud and aligned images in a 3D space (Verhoeven, 2011).

For the absolute orientation of the images, the derived feature points and the 3D model, GCPs or a-priori known acquisition coordinates are required. GCPs are frequently measured using conventional topographic techniques. As with conventional photogrammetry, these points must be unambiguously detectable. An example of the temporal scene structure, the orientation and position of the images are demonstrated in Figure 2-11. The numbered rectangles, representing the images, their recording positions and the feature points, give an indication of the correctness of the image alignment. This first scene visualization also enables the selection of a part of the study area for further processing by defining a bounding box around this area. In Figure 2-11, the GCPs measured by RTK GNSS are visualized as flags with numbers. The rather equal spatial distribution of the GCPs becomes clear in this figure.

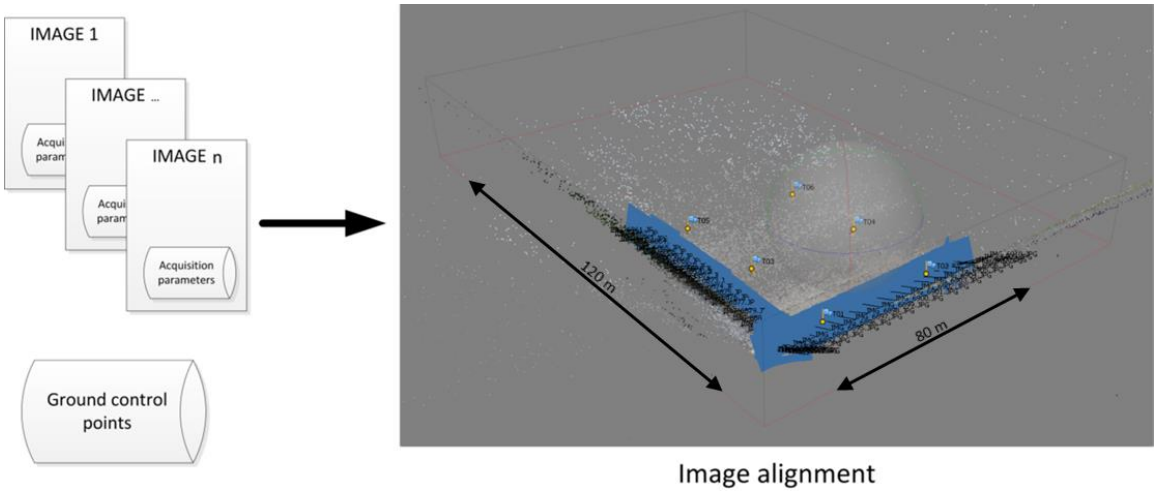

Figure 2-11: Scene structure with matched feature points (sparse point cloud) and positioned and oriented images of a part of the beach of Raversijde (Belgium)

Instead of using the 3D feature points or sparse point cloud, the positioned and oriented images are used for the actual 3D reconstruction after the image alignment. A 3D mesh is generated based on the intersection of perspective pixel rays (MVS). The linear projection parameters of these 2D image pixels in a 3D space are defined by the focal length of the used camera. This results in a series of depth maps, representing the distance between the intersection of perspective rays and the focal centre of the camera. Combining these depth maps from differently oriented positions enables the creation of a dense point cloud (Figure 2-12).

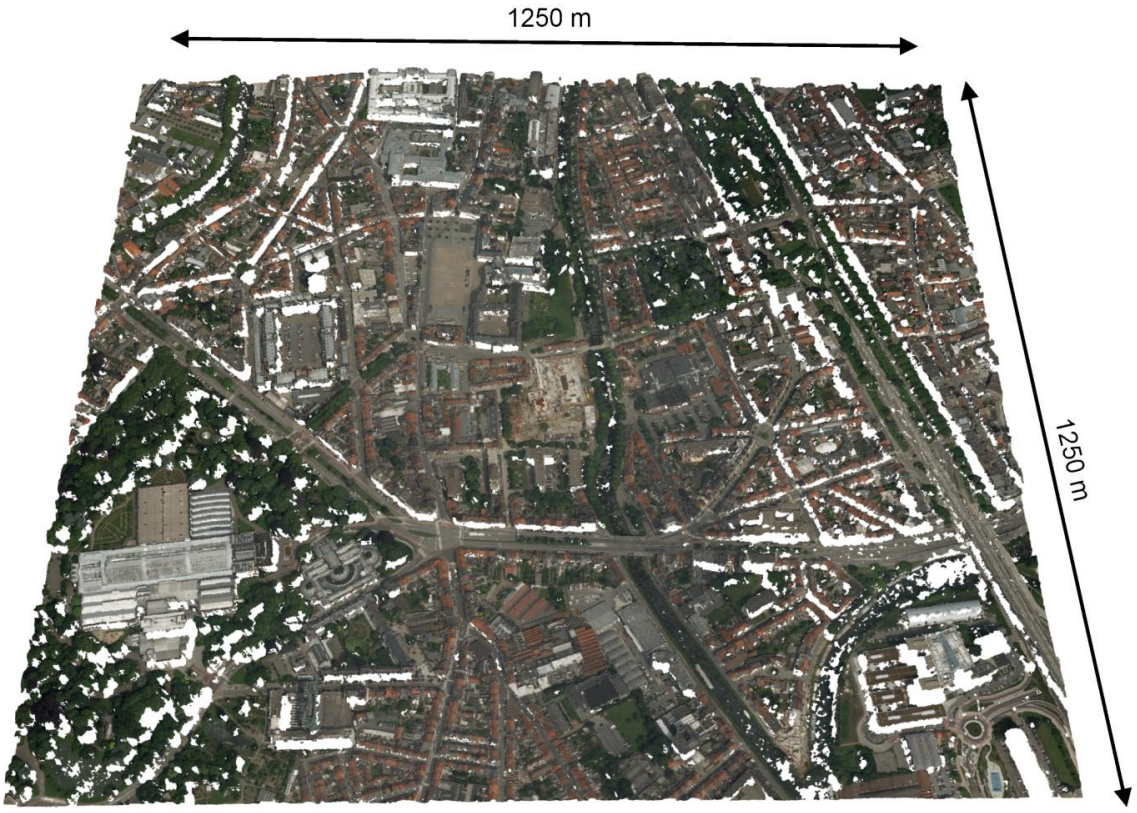

Figure 2-12: Birds-eye view on the dense point cloud of the Overpoort area in Ghent (Belgium)

The dense point cloud set is hereafter triangulated into a mesh, as illustrated in Figure 2-13. In this case, a 2.5D triangulation is performed, corresponding with a Triangular Irregular Network (TIN) (De Wulf et al., 2012). For more complex scenes, full 3D meshing is obviously possible. However, since façades are frequently not properly covered by airborne data, a 2.5D reconstruction is sufficient. Thus, it is obvious that the point cloud suffers from data holes. These holes are mainly caused by (cast) shadows and vegetation. This limitation is typical for photogrammetric data, since many features cannot be determined in 3D by their lack of unambiguous appearance in sequential images. These TINs can also be interpolated for the construction of equidistant DSMs.

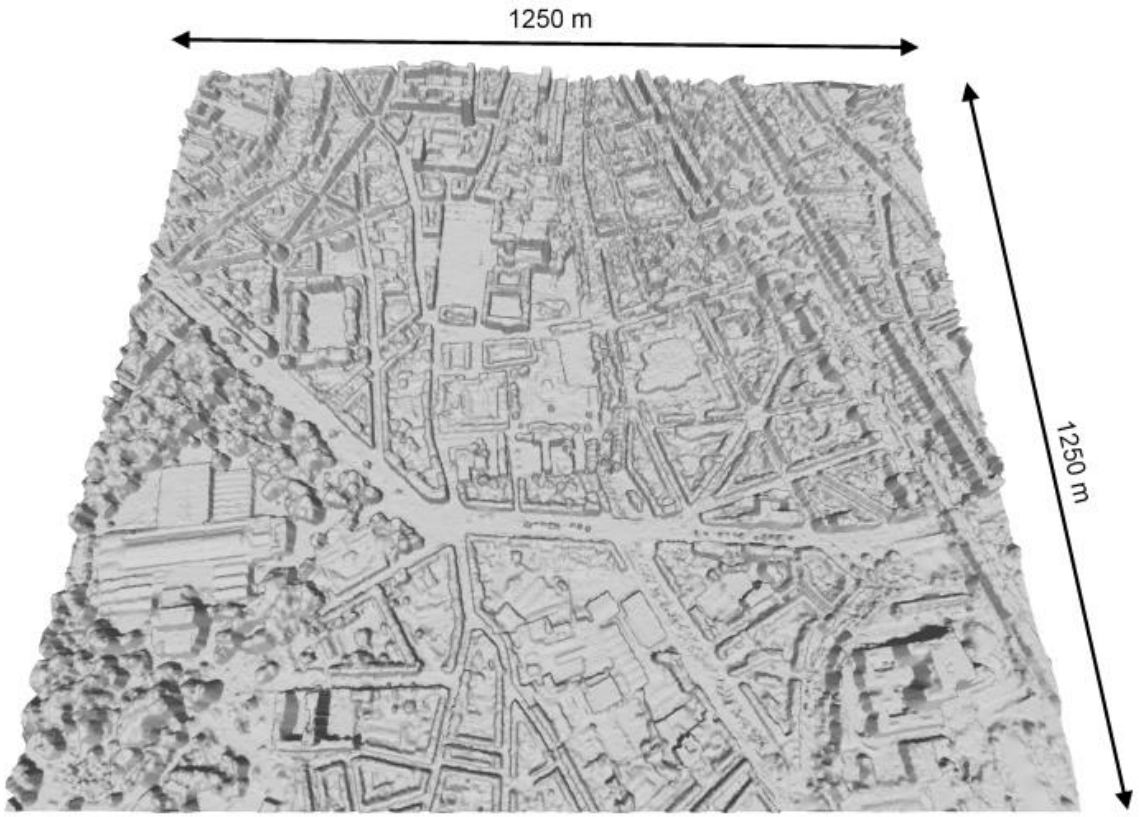

Figure 2-13: Birds-eye view on the triangular model of the Overpoort area in Ghent (Belgium)

After reconstructing the geometry of the scene, it is possible to assign a single colour value to each separate geometric primitive or face. This colour may be chosen arbitrary as a function of the feature type (e.g. roof, wall …) or based on semantic attributes. This procedure also allows the visualization of the results of certain analysis. Photorealistic model appearance can be achieved by image based texturing, also called projective texture mapping (Rüther et al., 2012). In most cases, a 3D vertex (*x*,*y*,*z*) in the model is assigned to the 2D coordinate (u, v) of a texture map. A series of vertices are part of a face, corresponding with a polygon on the texture. This polygon is draped on the area of the face between the vertices. This procedure, uv-mapping, is frequently used for photorealistic modelling (Hülksen et al., 2007). For the extraction of a single texture map from a large series of images, the most appropriate combination of image information is required. Besides, the correct position and orientation of each camera in a 3D space, as well as the focal length and image distortions should be known for an accurate texture mapping. Radial distortions,

heterogeneous feature geometry or unequal lighting and focussing conditions are just a few examples of issues that may occur with texture mapping (Bannai et al., 2007). These issues are the most obvious using colour interpolation, using bi-cubic convolution with a fixed projection space kernel. Better results can be achieved using a weight image blending, optionally combined with colour outlier elimination or with the statistical analysis of a depth map for each image (Grammatikopoulos et al., 2007). A weight can be assigned to each pixel as a function of a series of parameters, derived from the geometry of the projection, like the incidence angle and the image resolution. In this case, the estimation of weights with spatial variance is preferred above the calculation of a global weight function (Wang et al., 2001). The entire 3D reconstruction technique (SfM-MVS) is extensively discussed by Robertson and Cipolla (2009) or Seitz et al. (2006). An example of the final textured 3D model is illustrated in Figure 2-14, where all colours in the model facilitate the generation of this photo-realistic representation.

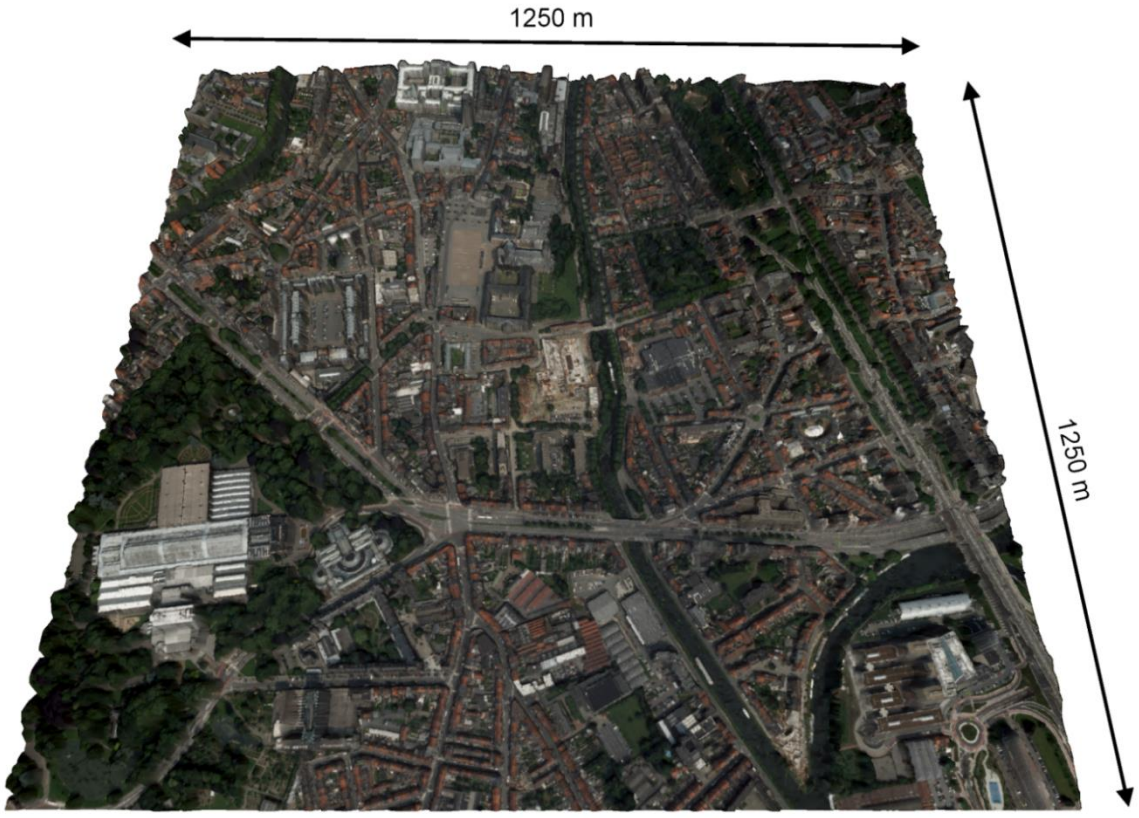

Figure 2-14: Birds-eye view on the textured 3D model of the Overpoort area in Ghent (Belgium)

2.3. *Conventional topographic measurements*

GNSS measurements or measurements with a total station are probably the most well-known conventional techniques for topographic surface modelling. In contrast with the mentioned laser scanning techniques and image based modelling, which have been discussed in the previous section, the measurements for a DSM are a mainly manual process. The theoretically possible point density of conventional topography is equal to the other techniques, but this is hardly feasible for practical reasons. Consequently, these techniques are mainly applied for low

resolution surface modelling with high accuracy, e.g. for the calculation of reference surfaces which can be used for quality evaluation of DSMs acquired by more automated techniques. Besides, conventional topography is frequently applied for the measurement of GCPs or reference points as input for the georeferencing of laser scan or image based modelling DEMs.

2.3.1. GNSS

Until a few years ago, it was very difficult and expensive to measure single points with centimetre accuracy. Moreover, these measurements were extremely time-consuming. The ability to use data connections over mobile networks has speeded up the development of Real Time Kinematic (RTK) GNSS measurements with centimetre accuracy. The Flemish Positioning Service (FLEPOS) is the implementation of such a system in Flanders, consisting of a network of 40 permanent reference stations. Users can use this FLEPOS by downloading real time correction messages for their own GNSS measurements (De Wulf et al., 2006). By using FLEPOS, point precisions between 1 and 4 cm (67% or 1 sigma) can be reached for planimetry and altimetry (AGIV, 2008). Other examples of RTK networks in Europe are 06-GPS in the Netherlands, OsNet in the United Kindom or Teria in France. This easy access to very accurate GNSS measurements has opened a lot of possibilities to use GNSS for the fast and accurate generation of DSMs. However, the technique is still limited by the achievable point density of the measurements.

2.3.2. Total station measurements

Recent developments towards robotic total stations make it possible to perform reflector-less distance measurements using EDM by only one operator, significantly increasing the performance of total station measurements. The use of such a total station for surface mapping may result in an accuracy of 1 or 2 cm, although sub-centimetre single point precisions can be reached. Another interesting development is the integration of total stations with imaging sensors (Sakimura and Maruyama, 2007). Nevertheless, the same remarks have to be made as with the GNSS measurements regarding the slow and manual surface modelling. Due to the slower measurement speed (in comparison with e.g. laser scanners) and the higher degree of manual intervention by the operator, only a lower point density is achievable.

2.4. ***Comparative analysis of the different techniques and recommendations***

With the knowledge of the above mentioned surface modelling techniques and the comparative study, it is possible to select the most suitable methodology for surface modelling for the benefit of environmental modelling and 3D city modelling in particular. Especially when the 3D models of these areas are used for spatial management with legal implications or life-saving applications, the suggested technique or series of integrated techniques must result in high resolution data with a sufficient accuracy. Furthermore, the complexity and size of built-up areas, and especially the dynamics and fast changeability of cities require the usage of relatively fast and cheap 3D reconstruction techniques. It is well known that these four parameters (resolution, accuracy, price

and speed) mostly contradict each other, but an equilibrium between them is necessary. Achievable GSD and vertical accuracies of DSMs are presented in Table 2-1, assuming typical acquisition conditions. Experimental values may vary because of the many parameters determining the final quality of the data. For example, many photogrammetric projects using UAVs will reach a much higher GSD and vertical accuracy. For the sake of completeness, ALB and spaceborne techniques are also included in the table.

Table 2-1: Overview of different surface generating techniques under typical conditions

Acquisition technique	GSD	Vertical accuracy	Reference
Airborne Laser Scanning (ALS)	10 cm	5 cm	(Stal et al., 2013)
Airborne Laser Bathymetry (ALB)	1 m	25 cm	(Doneus et al., 2013)
Mobile Terrestrial Laser Scanning (MTLS)	10 cm	5 cm	(Bitenc et al., 2011)
Static Terrestrial Laser Scanning (STLS)	2 cm	2 - 5 cm	(Pertrie and Toth, 2009)
Airborne photogrammetry	9 cm	9 cm	(Rottensteiner et al, 2013)
Image based using SfM-MVS	2-5 cm	2 - 15 cm	(Ortiz et al., 2013)
Global Navigation Satellite System (GNSS)	-	2 - 4 cm	(Taaouati et al., 2011)
Total station	-	1 - 2 cm	
VHR satellite imagery	05 – 2.0 m	2.0 m	(Tack et al., 2012)
InSAR	1.5 m	1.5 m	(Bamler et al., 2009)

Another interesting comparison between ALS and airborne photogrammetry is presented by Baltsavias (1999b). Although this publication dates back 15 years ago, the conclusions of this comparison are still highly relevant and resumed in Table 2-2. It is obvious that this comparison can easily be extended to terrestrial applications.

Table 2-2: Comparison of Airborne Laser Scanning (ALS) and airborne photogrammetry (after: Baltsavias, 1999b)

Airborne Laser Scanning	Airborne Photogrammetry
Active	Passive
Point sensor with polar geometry	Frame or linear sensor with perspective geometry
Point wise sampling	Full area coverage
Direct 3D point measurement	Indirect point measurement
Limited imaging capabilities	High quality geometric and radiometric imaging
Object smaller than laser footprint detectable	Level of Detail limited by sensor resolution

The sole use of conventional topographic measurements is thus impossible. However, these techniques can be used for the construction of supplementary data sets for the referencing and quality analysis of other data sets. Notwithstanding the low point density of conventional topography, it delivers the highest possible accuracy in comparison with the other surface modelling techniques presented in this chapter. STLS also results in point clouds with high accuracies and has the additional advantage of generating dense point clouds as well. However, for the coverage of large areas, a kinematic platform is advisable, like manned airborne platforms or MTLS. Companies like *Google* or *TeleAtlas* are organizing large data acquisition campaigns using mobile mapping vans. The resulting data are used for traffic sign detection, road facility

management and of course building modelling. Obviously, it is only possible to cover and to model objects that are visible from public areas. Building modelling using MTLS is therefore mostly limited to architectural façade mapping. UAVs are able to fully cover architectural features and thus generate 3D models of entire structures. Especially the low flying height and flexible deployment are big advantages of these systems. However, the biggest problem with UAVs is their lesser technical reliability, range and durability than regular airplanes or helicopters. The light-weight of the platform makes it more sensitive for rapidly changing wind conditions. This aspect is very obvious in urban canyons or at the corners of large structures. The environmental conditions or privacy and safety regulations are just some examples for limiting the uses of UAVs (especially low-cost systems) to rural areas. In case of limited risks, the use of this system is very profitable.

As a result, ALS and SfM-MVS seems to be the most appropriate techniques to generate 3D environmental models using airborne platforms from a practical point of view. The image and point cloud data acquisition is traditionally performed on a predefined time base by national mapping agencies. Moreover, no physical contact with the area to be modelled is required and large areas can be covered in a limited time frame. Thus, environmental modelling and 3D city modelling using these data can be seen as a valuable extension of the current spatial data applications, organized by these agencies. A quality assessment of ALS data and airborne imagery is presented in the following chapter.

References

AGIV, 2008. Uitvoeren van GPS-metingen met behulp van Flemish Positioning Service (FLEPOS). www.agiv.be/flepos, 34.

Attwenger, M., Briese, C., 2003. Vergleich digitaler Geländemodelle aus Photogrammetrie und Laserscanning. Österreichische Zeitschrift für Vermessung und Geoinformation 91 (4), 271–280.

Baltsavias, E., 1999a. Airborne laser scanning: basic relations and formulas. ISPRS Journal of Photogrammetry and Remote Sensing 54 (2-3), 199-214.

Baltsavias, E., 1999b. A comparision between photogrammetry and laser scanning. ISPRS Journal of Photogrammetry and Remote Sensing 54 (2-3), 83-94.

Bamler, R., Eineder, M., Adam, N., Zhu, X., Gernhardt, S., 2009. Interferometric potential of high resolution spaceborne SAR. Photogrammetrie-Fernerkundung-Geoinformation 2009 (5), 407-419.

Bannai, N., Fisher, R., Agathos, A., 2007. Multiple color texture map fusion for 3D models. Pattern Recognition Letters 28 (6), 748-758.

Bitenc, M., Lindenbergh, R., Khoshelham, K., Van Waarden, P., 2011. Evaluation of a LiDAR land-based mobile mapping system for monitoring sandy coasts. Remote Sensing 3 (7), 1472-1491.

Briese, C., Höfle, B., Lehner, H., Wagner, W., Pfennigbauer, M., Ullrich, A., 2008. Calibration of full-waveform airborne laser scanning data for object classification, SPIE: Laser Radar Technology and Applications XIII, Orlando, FL, USA, pp. 8 (on CD-ROM)
Brodu, N., Lague, D., 2012. 3D terrestrial LiDAR data classification of complex natural scenes using a multi-scale dimensionality criterion: applications in geomorphology. ISPRS Journal of Photogrammetry and Remote Sensing 68 (1), 121-134.

Delaloye, D., Diederichs, M., Walton, G., Hutchinson, J. (2014), Sensitivity testing of the newly developed elliptical fitting method for the measurement of convergence in tunnels and shafts. Rock Mechanics and Rock Engineering 2014 (March), 1-17.

De Wulf, A., Brondeel, M., Willems, T., Neutens, T., 2006. GPS Work of Ghent University. Bulletin de la Société Géographique de Liège 47, 57-72.

De Wulf, A., Constales, D., Stal, C., Nuttens, T., 2012. Accuracy aspects of processing and filtering of multibeam data: grid modeling versus TIN based modeling, FIG Working Week, Rome, Italy, pp. 6 (on CD-ROM)

Doneus, M., Doneus, N., Briese, C., Pregesbauer, M., Mandlburger, G., Verhoeven, G., 2013. Airborne laser bathymetry: detecting and recording submerged archaeolgical sites from the air. Journal of Archaeological Science 40 (4), 2136-2151.

Fontana, R., Greco, M., Materazzi, M., Pampaloni, E., Pezzati, L., Rocchini, C., Scopigno, R., 2002. Three-dimensional modelling of statues: the Minerva of Arezzo. Journal of Cultural Heritage 3 (4), 325-331.

Frey, H., Paul, F., 2012. On the suitability of the SRTM DEM and ASTER GDEM for the compilation of topographic parameters in glacier inventories. International Journal of Applied Earth Observation and Geoinformation 18 (2012), 480-490.

Galantucci, L., Percoco, G., Angelelli, G., Lopez, C., Introna, F., Liuzzi, C., De Donno, A., 2006. Reverse engineering techniques applied to a human skull, for CAD 3D reconstruction and physical replication by rapid prototyping. Journal of Medical Engineering & Technology 30 (2), 102-111.

Gerke, M., Xiao, J. (2014), Fusion of airborne laserscanning point clouds and images for supervised and unsupervised scene classification. ISPRS Journal of Photogrammetry and Remote Sensing 87 (January), 78–92.

González-Aguilera, D., Rodríguez-Gonzálvez, P., Gómez-Lahoz, J., 2009. An automatic procedure for co-registration of terrestrial laser scanners and digital cameras. ISPRS Journal of Photogrammetry and Remote Sensing 64 (3), 308-316.

Grammatikopoulos, L., Kalisperakis, I., Karras, G., Petsa, E., 2007. Automatic multi-view texture mapping of 3D surface projections. International Archives of Photogrammetry and Remote Sensing and Spatial Information Sciences 36 (5), 6.

Grus, L., Cartelein, W., Crompvoets, J., Overduin, T., Van Loenen, B., Van Groenestijn, A., Rajabifard, A., Bregt, A., 2010. An Assessment View to Evaluate Whether Spatial Data Infrastructures Meet Their Goal. Computers, Environment and Urban Systems 35 (3), 217-229.

Hug, C., Ullrich, A., Grimm, A., 2004. Litemapper 5600 - A waveform digitizing LiDAR terrain and vegetation mapping system. International Archives of Photogrammetry and Remote Sensing 36 (3), 24-29.

Huising, E., Gomes Pereira, L., 1998. Errors and accuracy estimates of laser data acquired by various laser scanning systems for topographic applications. ISPRS Journal for Photogrammetry and Remote Sensing 53 (5), 245-261.

Hülksen, F., Eckes, C., Kuck, R., Unterberg, J., Jörg, S., 2007. Modeling and animating virtual humans for real-time applications. International Journal of Virtual Reality 6 (4), 11-20.

Jaboyedoff, M., Oppikofer, T., Abellán, A., Derron, M., Loye, A., Metzger, R., Pedrazzini, A., 2012. Use of LiDAR in landslide investigation: a review. Natural Hazards 61 (1), 5-28.

Katzenbeisser, R., 2003. About the calibration of LiDAR sensors. International Archives of Photogrammetry and Remote Sensing 34 (3), 6 (on CD-ROM).

Kellens, W., 2006. Het Digitaal Hoogtemodel Vlaanderen als basis voor hydrografisch onderzoek (thesis). Universiteit Gent, Gent, België.

Kocaman, S., Zhang, L., Gruen, A., Poli, D., February). . In Proceedings of ISPRS Workshop on Topographic Mapping from Space 2006, Proceedings in CD-ROM., 2006. 3D city modeling from high-resolution satellite images. International Archives of Photogrammetry, Remote Sensing and Spatial Information Sciences 36 (41), 6 (on CD-ROM).

Kraus, K., 2007. Photogrammetry: geometry from images and laser scans, 2nd ed. Walter de Gruyter, Berlin, Germany.

Laefer, D., Truong-Hong, L., Carr, H., Singh, M. (2014), Crack detection limits in unit based masonry with terrestrial laser scanning. NDT&E International 62 (March), 66–76.

Lam, S., Yip, T., 2008. The role of geomatics engineering in establishing the marine information system of maritime management. Maritime Policy and Management 35 (1), 53-60.

Lemmers, M., 2007. Airborne LiDAR sensors. GIM International 21 (2), pp. 3 (on CD-ROM).

Lichti, D., Gordon, S., 2004. Error propagation in directly georeferenced terrestrial laser scanner point clouds for cultural heritage recording, FIG Working Week, Athens, Greece, p. 16 (On CD-ROM).

Lin, Y., Hyyppa, J., Jaakkola, A., 2011. Mini-UAV-borne LIDAR for fine-scale mapping. IEEE Geoscience and Remote Sensing Letters 8 (3), 426-430.

Lourakis, M., Argyros, A., 2009. SBA: A software package for generic sparse bundle adjustment. ACM Transactions on Mathematical Software 36 (1), 1-30.

Long, B., Aucoin, F., Montreuil, S., Robitaille, V., Xhardé, R. (2011), Airborne LiDAR bathymetry applied to coastal hydrodynamic processes. Coastal Engineering Proceedings, 1 (32), 1-26.

Mallet, C., Bretar, F., 2009. Full-waveform topographic LiDAR: state-of-the-art. ISPRS Journal of Photogrammetry and Remote Sensing 64 (1), 1-16.

McGlone, J., Mikhail, E., Bethel, J., Mullen, R., 2004. Manual of Photogrammetry. American Society for Photogrammetry and Remote Sensing, Bethesda, MA, USA.

Mitchell, S., 2008. Electromagnetic wave propagation: theory and application to bathymetric LiDAR simulation. University of Colorado, Boulder, CO, USA.

Nuttens, T., De Wulf, A., Bral, L., De Wit, B., Carlier, L., De Ryck, M., De Backer, H., 2009. Tunnel deformation measurements with high resolution laser scanning, in: De Maeyer, P., Neutens, T., De Ryck, M. (Eds.), Proceedings of the 4th International Workshop on 3D Geo-Information. DCL Print&Sign, Ghent, Belgium, pp. 167-181

Nuttens, T., De Wulf, A., Bral, L., De Wit, B., Carlier, L., De Ryck, M., Stal, C., Constales, D., De Backer, H., 2010a. High resolution terrestrial laser scanning for tunnel deformation measurements, XXIV FIG International Congress, Sydney, Australia (on CD ROM).

Nuttens, T., De Wulf, A., Bral, L., De Wit, B., Carlier, L., De Ryck, M., Stal, C., Constales, D., De Backer, H., 2010b. High resolution terrestrial laser scanning for tunnel deformation measurements, FIG Congress, Sydney, Australia

Nuttens, T., De Wulf, A., Deruyter, G., Stal, C., De Backer, H., Schotte, K., 2012. Application of laser scanning for deformation measurements: a comparison between different types of scanning instruments, FIG Working Week, Rome, Italy, pp. 13 (on CD-ROM)

Ortiz, J., Gil, M., Martínez, S., Rego, T., Meijide, G., 2013. Three-dimensional modelling of archaeological sites using close-range automatic correlation photogrammetry and low-altitude imagery. Archaeological Prospection 20 (2).

Pastol, Y., 2011. Use of airborne LiDAR bathymetry for coastal hydrographic surveying: the French experience. Journal of Coastal Research Special Issue (62), 6-18.

Pe'eri, S., Morgan, L., Philpot, W., Armstrong, A., 2011. Land-water interface resolved from Airborne LiDAR Bathymetry (ALB) waveforms. Journal of Coastal Research 62 (SI), 75-85.

Peiravi, A., Taabbodi, B., 2010. A reliable 3D laser triangulation-based scanner with a new simple but accurate procedure for finding scanner parameters. Journal of American Science 6 (5), 80-85.

Pertrie, G., Toth, C., 2009. Terrestrial laser scanners, in: Shan, J., Toth, C. (Eds.), Topographic laser ranging and scanning: principles and processing. CRC Press, Boca Raton, Fl, USA, pp. 87-128.

Petrie, G., 2011. Airborne topographic laser scanners. GEO Informatics, (January/Februari), 34-44.

Pesci, A., Bonali, E., Galli, C., Boschi, E., 2012. Laser scanning and digital imaging for the investigation of an ancient building: Palazzo d'Accursio study case (Bologna, Italy). Journal of Cultural Heritage 13 (2), 215-220.

Pieraccini, M., Guidi, G., Atzeni, C., 2001. 3D digitizing of cultural heritage. Journal of Cultural Heritage 2 (1), 63-70.

Podobnikar, T., Vrecko, A., 2012. Digital elevation model from the best results of different filtering of a LiDAR point cloud. Transactions in GIS 16 (5), 603-617.

Pollefeys, M., Koch, R., Vergauwen, M., Van Gool, L., 2000. Automated reconstruction of 3D scenes from sequences of images. ISPRS Journal of Photogrammetry and Remote Sensing 55 (4), 251-267.

Robertson, D., Cipolla, R., 2009. Structure from motion, in: Varga, M. (Ed.), Practical image processing and computer vision. John Wiley, Hoboken, NJ, USA., p. 49.

Rottensteiner, F., Sohn, G., Gerke, M., Wegner, J., (2013). ISPRS test project on urban classification and 3D building reconstruction. Photogrammetric Computer Vision and Image Analysis, Working Group 3 (4), 1-17.

Rüther, H., Held, C., Bhurtha, R., Schroeder, R., Wessels, S., 2012. From point cloud to textured model, the Zamani laser scanning pipeline in heritage documentation. South African Journal of Geomatics 1 (1), 44-59.

Sakimura, R., Maruyama, K., 2007. Development of a new generation imaging total station system. Journal of Surveying Engineering 133 (1), 14-22.

Seitz, S., Curless, B., Diebel, J., Scharstein, D., Szeliski, R., 2006. A comparison and evaluation of multi-view stereo reconstruction algorithms, IEEE Computer Society Conference on Computer Vision and Pattern Recognition, New York, NY, USA, 17-22 June, pp. 519-528

Self, S., 1983. Focusing of Spherical Gaussian Beams. Applied Optics 22 (5), 658-661.

Skaloud, J., Lichti, D., 2006. Rigorous approach to bore-sight self-calibration in airborne laser scanning. ISPRS Journal of Photogrammetry and Remote Sensing 61 (1), 47-59.

Skaloud, J., Schaer, P., Stebler, Y., Tomé, P., 2010. Real-time registration of airborne laser data with sub-decimeter accuracy. ISPRS Journal of Photogrammetry and Remote Sensing 65 (2), 208-217.

Skaloud, J., Viret, P., 2004. GPS/INS integration. European Journal of Navigation 2 (4), 40-44.

Slob, S., Hack, H., 2004. 3D terrestrial laser scanning as a new field measurement and monitoring technique, in: Hack, R., Azzam, R., Charlier, R. (Eds.), Engineering geology for infrastructure planning in Europe. Springer, Berlin, Germany, pp. 179-189.

Soudarissanane, S., Lindenbergh, R., Gorte, B., 2008. Reducing the error in terrestrial laser scanning by optimizing the measurement set-up. International Archives of Photogrammetry, Remote Sensing and Spatial Information Sciences 37 (5), 615-620.

Soudarissanane, S., Lindenbergh, R., Menenti, M., Teunissen, P., 2011. Scanning geometry: influencing factor on the quality of terrestrial laser scanning points. ISPRS Journal for Photogrammetry and Remote Sensing 66 (4), 389-399.

Stal, C., De Wulf, A., De Maeyer, P., Goossens, R., Nuttens, T., 2012. Evaluation of the accuracy of 3D data acquisition techniques for the documentation of cultural heritage, 3rd EARSeL Workshop on Remote Sensing for Archaeology, Ghent, Belgium, pp. 8 (on CD-ROM)

Stal, C., Tack, F., De Maeyer, P., De Wulf, A., Goossens, R., 2013. Airborne photogrammetry and LiDAR for DSM extraction and 3D change detection over an urban area: a comparative study. International Journal of Remote Sensing 34 (4), 1087-1110.

Steinbacher, F., Pfennigbauer, M., Aufleger, M., Ullrich, A. (2012), High resolution airborne shallow water mapping. International Archives of the Photogrammetry, Remote Sensing and Spatial Information Sciences 39 (B1), 55-60.

Stoker, M., 2005. Basic principles of lasers. Aneasthesia and Intensive Care Medicine 6 (12), 402-404.

Taaouati, M., El Mrini, A., Nachite, D., 2011. Beach morphology and sediment budget variability based on high quality digital elevation models derived from field data sets. International Journal of Geosciences 2 (2), 111-119.

Tack, F., Goossens, R., Buyuksalih, G., 2012. Assessment of a photogrammetric approach for urban DSM extraction from tri-stereoscopic satellite imagery. The Photogrammetric Record 27 (139), 293-310.

Thomas, G., Isaacs, R., 2011. Basic principles of lasers. Aneasthesia and Intensive Care Medicine 12 (12), 574-577.

Vaaja, M., Hyyppa, J., Kukko, A., Kaartinnen, H., Hyyppa, H., Alho, P., 2011. Mapping topography changes and elevation accuracies using mobile laser scanner. Remote Sensing 3 (3), 587-600.

Verhoeven, G., 2011. Taking computer vision aloft - archaeological three-dimensional reconstruction from aerial photographs with PhotoScan. Archaeological Prospection 18 (1), 67-73.

Vosselman, G., Maas, H., 2001. Adjustment and filtering of raw laser altimetry data, OEEPE workshop on Airborne Laserscanning and Interferometric SAR for Detailed Digital Elevation Models, 1-3 March, 40, Stockholm, Sweden, pp. 11 p. (on CD-ROM)

Vukašinović, N., Korošec, M., Duhovnik, J., 2010. The influence of surface topology on the accuracy of laser triangulation scanning results. Journal of Mechanical Engineering 56 (1), 23-30.

Wagner, W., Ullrich, A., Ducic, V., Melzer, T., Studnicka, N., 2006. Gaussian decomposition and calibration of a novel small-footprint full-waveform digitising airborne laser scanner. ISPRS Journal of Photogrammetry and Remote Sensing 60 (12), 100-112.

Wang, L., Kang, S., Szeliski, R., Shum, H., 2001. Optimal texture map reconstruction from multiple views. IEEE Computer Vision and Pattern Recognition 1 (1), 1-8.

Wehr, A., Lohr, U., 1999. Airborne laser scanning - an introduction and overview. ISPRS Journal of Photogrammetry and Remote Sensing 54 (2-3), 68-82.

Weichel, H., 1990. Laser Beam Propagation in the Atmosphere, Bellingham, WA, USA.

Woodman, O., 2007. An introduction to inertial nagivation. University of Cambridge, Computer Laboratory, Cambridge, UK

Würländer, R., & Wenger-Oehn, K., 2007. Die verfeinerte Georeferenzierung von ALS-Daten - Methodik und praktische Erfahrungen. Angewandte Geoinformatik, XIX, Wichmann.

Chapter 3

Digital representation of historical globes: methods to make 3D and pseudo-3D models of 16th century Mercator globes

3. Digital representation of historical globes: methods to make 3D and pseudo-3D models of 16th century Mercator globes[3]

Abstract

In this paper, the construction of digital representations of a terrestrial and celestial globe will be discussed. Virtual digital (3D) models play an important role in recent research and publications on cultural heritage. The globes discussed in this paper were made by Gerardus Mercator (1512 – 1594) in 1541 and 1551. Four techniques for the digital representation are discussed and analysed, all using high resolution photographs of the globes. These photographs were taken under studio conditions in order to get equal lighting and to avoid unwanted light spots. These lighting conditions are important, since the globes have a highly reflective varnish covering. Processing these images using structure from motion, georeferencing of separate scenes and the combination of the photographs with terrestrial laser scanning data results in true 3D representations of the globes. Besides, pseudo-3D models of these globes were generated using dynamic imaging, which is an extensively used technique for visualisations over the Internet. The four techniques and the consequent results are compared on geometric and radiometric quality, with a special focus on their usefulness for distribution and visualisation during an exhibition in honour of the 500th birthday of Gerardus Mercator.

Keywords: Globes, Mercator, 3D modelling, virtual reality, comparison

3.1. *Introduction*

In 2012, the celebration of the 500th birthday of Gerardus Mercator will take place. In honour of this special occasion, 3D models were generated of two of his famous globes for visualisation purposes. It concerns a terrestrial globe, constructed in 1541 (Figure 3-1), and a celestial globe of 1551. Both globes are on display at the Mercator Museum in the city of Sint-Niklaas near Antwerp, Belgium.

The importance of virtual representations of globes has been discussed by different authors, such as Adami (2009), Gede (2009a, b) or Hruby et al. (2005, 2006). These authors mainly focus on the data acquisition of the virtual representations of the globes. Adami (2009) discusses the use of 3D scanners or range cameras in order to generate triangulated models of globes that can be used to investigate the real shape of the sphere. Based on his work, it becomes clear that the use of 3D scanners is suitable for deformation measurements and supplements the research on the internal structure of the globe. Furthermore, he analyses the projective representation of the map content by using specialised software. Image-based representations of historical globes by projecting image parts on a sphere are also discussed (Dorffner, 1996; Hruby et al., 2006), as well as possible digital formats and viewers for these globes (Gede, 2009a, b; Hruby et al., 2005). An

[3] Modified from: Stal, C., De Wulf, A., De Coene, K., De Maeyer, P., Nuttens, T., & Ongena, T. (2012). Digital representation of historical globes : methods to make 3D and pseudo-3D models of sixteenth century Mercator globes. *Cartographic Journal*, *49*(2), 107–117.

earlier example of such image based visualisation can be found on www.hcl.harvard.edu. Hruby et al. (2005, 2006) combine coloured images of the globe with black and white scans of the reprinted gores, in order to improve the readability of the textures. For the virtual representations of the globes used in this article, only the two globes were used as data source. The research of these authors will be used for a comparative study in this paper, complemented with the structure from motion modelling technique and dynamic imaging. The focus of this paper is on the 3D representation of globes for visualisation purposes, using the different implementations of the authors mentioned above.

After a brief presentation of the globes in section 3.2, the acquisition of the photographs in terms of studio configuration, camera configuration and image pre-processing is the topic of section 0. Four modelling and visualisation techniques are discussed: dynamic images for the pseudo-3D model (paragraph 3.4.1), laser scanning and image draping (paragraph 3.4.2), structure from motion (paragraph 3.4.3) and georeferencing and merging fragments of the globe (paragraph 3.4.4). Section 3.5 considers the use of different software packages to visualise 3D models. Digital images of the globe were used for all modelling techniques. While the dynamic images do not result in a 3D-model, the others do. In the case of laser scanning and image draping the images are supplemented with a point set, generated by a 3D laser scanner. By scrutinising the advantages and disadvantages of each technique, summarised in section 3.6, the optimal workflow for the construction of virtual globe representations will become clear.

Figure 3-1: Terrestrial globe in the Mercator Museum, Sint-Niklaas, Belgium (source: Paul Hermans, www.wikipedia.org)

3.2. ***Mercator Globes***

Gerardus Mercator (Gerard De Cremer, °1512, Rupelmonde, Belgium; †1594, Duisburg, Germany) is one of the most important 16th century cartographers in the Low Countries. Even to

this day global navigation makes use of his major achievement. His cylindrical map projection represents lines of constant course (i.e. rhumb lines or loxodromes) as straight segments (*Nova et aucta orbis terrae descriptio ad usum navigantium emendate accommodata*, 1569). Besides, Mercator created a large set of cartographic products. His map of Palestine (*Amplissima terrae sanctae descriptio*, 1537) still fits in the medieval tradition of maps with biblical interpretation. With the heart-shaped projection on his *Orbis imago* (1538), Mercator sought to represent the globe on a plane surface. In Duisburg he realised his map of Europe (1554) and most of his later maps. In 1578 he released Ptolemaeus' *Geographia* with the intention to correct the maps according to the author's mind (Watelet, 1994). The originally three independent volumes *Galliae tabulae geographicae*, *Belgii inferioris geographicae tabulae* and *Germaniae tabulae geographicae* were combined in Mercator's atlas and later completed by his son (*Atlas sive cosmographicae meditationes de fabrica mundi et fabrica figura*, 1585).

Although maps received ample treatment in his oeuvre, Mercator decided in around 1541 to prefer the construction of globes for commercial and financial reasons. Columbus' discovery of America enlarged political life with a lot of new territorial disputes. The Treaties of Tordesillas (1494) and Zaragoza (1529) defined a border meridian between Portuguese and Spanish foreign trade territories. Globes were especially suited for the representation of an overview of the whole world. They were excellent representations of territorial claims and were therefore favoured and patronised by the rulers. Both Gemma Frisius and Mercator dedicated their globes to Charles V or his entourage and in return received exclusive rights on the reproduction of their globes (Brotton, 2003). Mercator's terrestrial globe from 1541, the first globe dealt with in this paper, includes corrections on Gemma Frisius' globe (1535), while combining the antique worldviews of Ptolemaeus and Strabo with the works of Marco Polo and more of his contemporary cartographers such as Jacob Ziegler (1470-1549), Olaus Magnus (1490-1557) and Martin Waldseemüller (1470-1520). The result is a globe with a diameter of 41.5 cm of which the map image contains twelve north-south oriented ribbons. The second globe we will discuss is a celestial globe constructed in 1551 with approximately the same dimensions as the terrestrial globe (Blondeau, 1993). While the Discoveries changed the image of the world, the celestial representation remained largely based on Ptolemaeus' Almagest. But instead of the common ecliptic coordinates, Mercator used equatorial coordinates for the constellations of the stars. In spite of the differences, both the terrestrial- and celestial globes were sold together. That is probably why they have been mounted in a black-painted wooden construction with four bases and a circular frame along the ecliptic plane. Furthermore, a copper circular ring is mounted on this wooden frame with a longitudinal direction (Watelet, 1994).

3.3. ***Image acquisition and pre-processing***

All images were taken with a Canon EOS 60D digital camera. However, the aperture, exposure time, film exposure and focal length varied during different acquisition steps, in order to acquire optimal images (Table 1). Both globes are varnished, which results in highly reflective areas on the surface of the globes. Therefore, all photographs were taken using a polarised filter. Furthermore, light sources around the globes needed to be controlled. In order to do so, a 'light

tent' (www.lighttent.eu) was used to generate diffuse lighting and thereby avoid or minimise direct light beams on the globes. This 'light tent' has a cubed shape with an opening in one of the six sides. The other sides are covered with a white synthetic textile. A light spot is placed in the front left and front right side of the tent, accompanied with a frontal soft box. A synthetic textile sheet was placed in front of this soft box, to make this light even more diffuse. During the entire acquisition process of the images, the configuration of the constant beaming lights and semi-opaque sheets was not changed. Only the rotation angle of the globes was altered during the acquisition of the images. The centres of all light beams were aligned with the ecliptic plane of the globe. This configuration is illustrated in Figure 3-2.

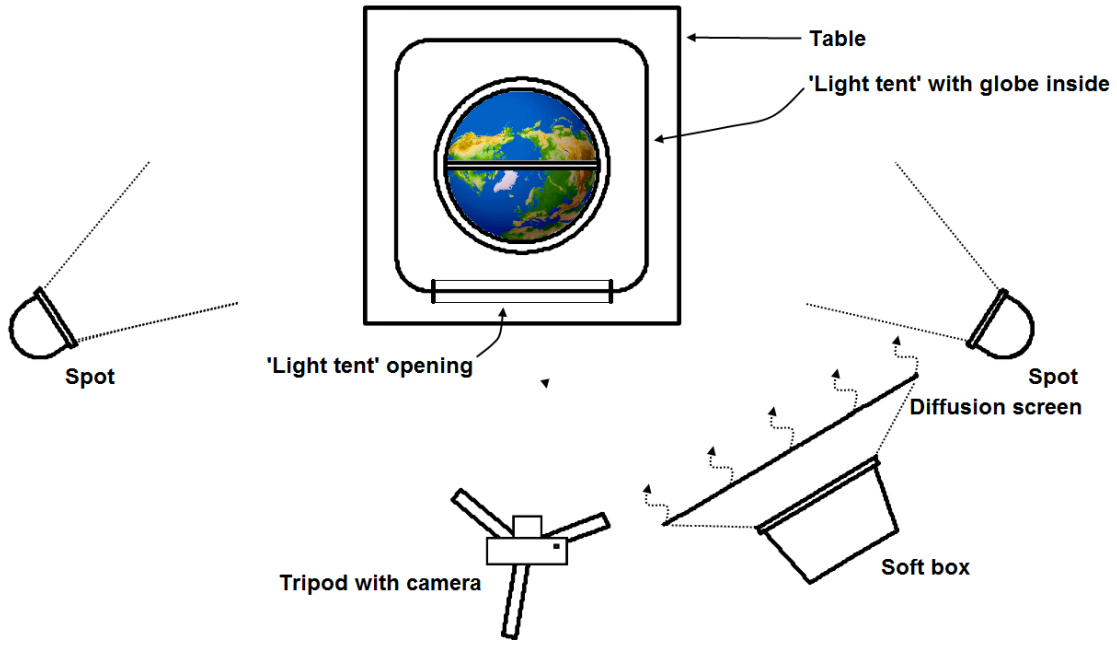

Figure 3-2: Configuration of the spots, camera and globe (top view)

The Canon EOS 60D single lens reflex digital camera contains an 18 MP CMOS sensor, with a size of 22.3 x 14.9 mm and each colour capturing cell has a size of 4.4 μm. To achieve an optimal overall sharpness of the images, each photograph of the ecliptic plane was focused on approximately 1/3 of the sphere, north or south of the ecliptic plane. A tripod was used to keep a constant distance between the camera and the globe. Polar zones were photographed by hand, using variable camera parameters as a function of the illumination of the photographed area. These parameters are shown in Table 3-1.

Table 3-1: Camera parameters during the image acquisition

	Ecliptic plane	**Polar area**
Lens	50/1.8 mm	35/2.0 mm and 24/2.8 mm
Aperture	f/8	f/5.6 and f/2.8
Film speed	ISO 200	ISO 1600
Exposure time	0.6 - 1.0 sec	0.067 - 0.008 sec

The lens used for the ecliptic plane images is included in a database of Adobe's Lightroom and Photoshop image processing software. Therefore a correction of the geometric aberration on all images of the ecliptic plane was possible (Ojanen, 1999). The images of the series of both the terrestrial and celestial globe contain a grey value scale and a standard GretagMacBeth colour checker (www.xrite.com). Based on the grey scale, the colour temperatures of the terrestrial and celestial globes were set to respectively 5100 Kelvin and 5000 Kelvin, in order to get neutral grey values. The colour checker was used to set the colour balance correctly. On top of that, a set of filtering procedures was executed on all images to improve the contrast, sharpness and clarity of the images. The results of these procedures enable better image matching during the structure from motion modelling, as well as a better and sharper approximation of the real colours of the globes by the images. To compare the results of these procedures with the original images, a fragment of the celestial globe is shown in Figure 3-3.

Figure 3-3: Fragment of the celestial globe before (left) and after (right) image correction

3.4. ***Image Processing***

3.4.1. Dynamic images

For the generation of dynamic images, the Object2VR software package of Garden Gnome was used (www.gardengnomesoftware.com). This software package requires a series of images of the object and uses each image as a video frame for a movie of the object (Collmann, 2011). In this case, both the position of the camera and the orientation of the frame of the globe were kept static, in order to generate a single row moving image on the ecliptic plane. During the acquisition of the different images, the sphere of the globe itself was rotated with a step size of approximately 10°.

After each rotation, an image of the globe was taken in the ecliptic plane. No supplementary images of the polar areas were included in this process. The resulting 36 images were organised chronologically and converted to either a QTVR or Flash file format. These formats can easily be embedded in an internet page using a Java script, calling the involved model file and appropriate viewer. Many interactive model viewers are available for this purpose. On the one hand, the possibility to generate animations in these formats is a big advantage when the model is placed on the internet as it increases the accessibility of the globe for the public. On the other hand, the generated files are quite large to download (85 Mb for the QTVR and 82 Mb for the Flash, with a frame size of 3456 by 5184 pixels), but these sizes could be reduced by using a lower resolution. However, there is no relation between the different images other than their sequence. This means that the resulting products do not contain real 3D information, although it visually looks like a 3D model, hence the term pseudo-3D model. A set of samples of the results are presented in Figure 3-4, demonstrating three neighbouring frames of a dynamic image.

Figure 3-4: Screenshots of a dynamic image in a QuickTime environment

3.4.2. Laser scanning and image draping

3D scanning was used as modelling technique for globe representation, as a variant of the use of 3D range cameras (Adami, 2009). The technique is mainly applied in research about the real shape of the globe, e.g. aberrations from a hypothetic sphere. However, the results can be used for visualisation purposes as well, when the point set is coloured by image draping. A dense point set of the globes was acquired with a Leica HDS 6100 laser scanner. Using this phase-based terrestrial laser scanner (TLS), it is possible to acquire approximately 80 million points within 3.5 minutes. This type of scanner is very useful for applications in civil engineering (Nuttens et al., 2010) and cultural heritage (Stal et al., 2011), wherein high accuracy is indispensable and in which the distance between the scanner and the object to measure is confined. Corresponding with a mean distance between the scanner and the globes of 1.75 meter, an absolute single point accuracy of a few millimetres can be reached. The final data set contains an (x,y,z)-coordinate and an intensity value of the reflected signal for each point. The point set was acquired with a horizontal and vertical angular incremental α of 0.018°. With an average distance between the scanner and the globe of 1.75 m, a minimum point spacing of 0.5 mm can be calculated ($s*\tan(\alpha)$).

The point set, acquired by the terrestrial laser scanner, can be combined with a photograph taken with a Canon EOS 60D DSLR camera in combination with a 50/1.8 mm lens. The acquisition of a

single point set by TLS will result in occlusion zones. In order to have the same perspective geometry of the point set and the images, resulting in the same occlusion zones, both the point set and the image have to be acquired from the same position. In other words, the centre of the laser scanner and the optical centre of the camera - the so called 'no-parallax point' (NPP) - should coincide, as demonstrated in Figure 3-5 (Littlefield, 2006). To determine the NPP of a specific camera and lens in relation to the centre of the laser scanner, two parameters have to be determined in the horizontal plane. The horizontal offset is shown in Figure 3-5. As demonstrated in this figure, it will become clear that rotating the camera around the z-axis will keep the NNP on the same position.

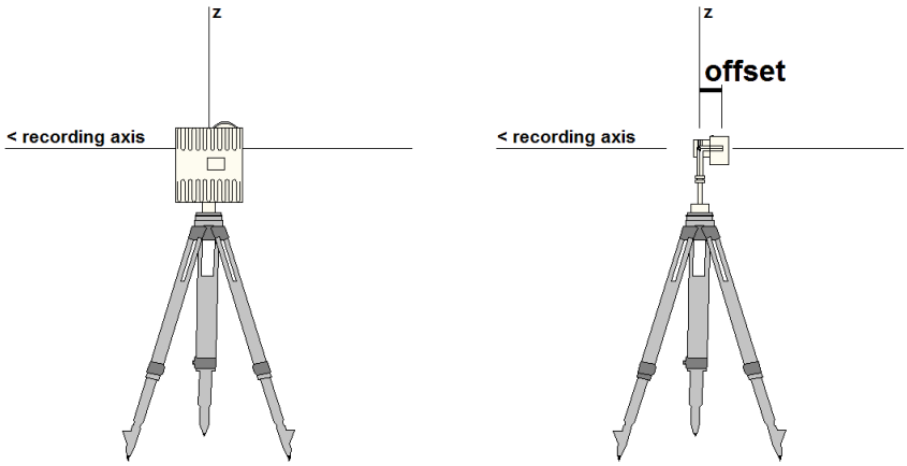

Figure 3-5: TLS set-up and corresponding camera offset

The placement of the NPP of a camera on the same location as the optical midpoint of the scanner can be obtained using the Nodal Ninja 3II camera bracket (Figure 3-6). This bracket contains two measuring rods to perform an axis setup and is used for panoramic photographing as well (Lee et al., 2010).

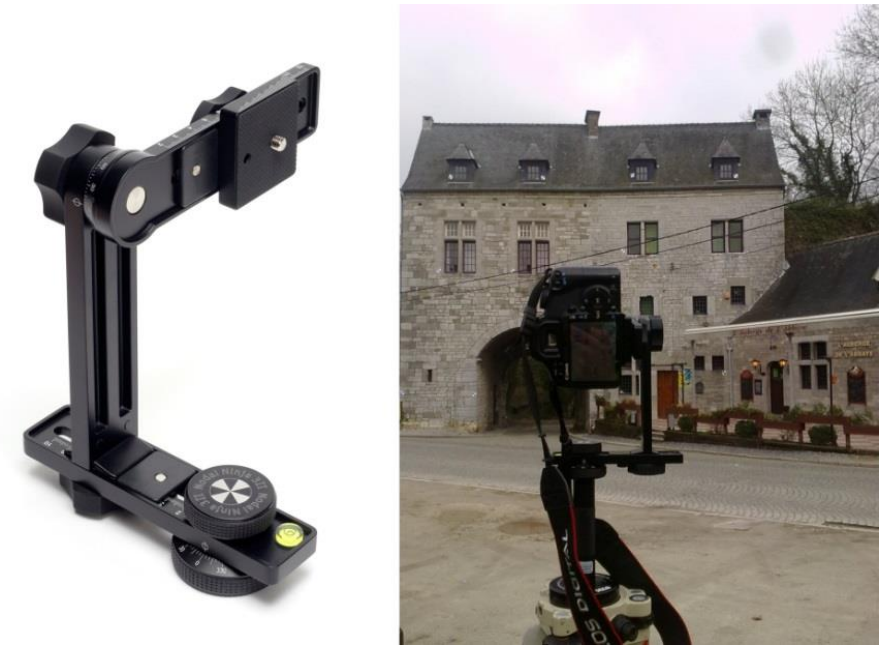

Figure 3-6: Camera bracket (Nodal Ninja 3 II, www.nodalninja.com)

The horizontal offset contains:

- The tripod mount length, which is camera dependent (L1) (Figure 3-7, left);
- The entrance pupil length, which is lens dependent (L2) (Figure 3-7, right).

In this case, a tripod mount length of 42 mm(L1) and an entrance pupil length of 17.5 mm (L2) have been used for the combination of the Canon EOS 60D camera and the 50 mm lens. This resulted in a final horizontal offset of 38.5 mm, but this value will differ for each camera and lens combination. The correct parameters can be calculated by manual offset determination, but online databases, like PanoTools Wiki (http://wiki.panotools.org, 2011), are available with these parameters for widely used camera and lens combinations.

Figure 3-7: Tripod mount length (L1, left) and entrance pupil length (L2, right) (Source: (http://wiki.panotools.org, 2011)

Texturing the point set is done by creating a set of corresponding points, which are points that are unambiguously recognisable in the point set and on the image (Nuttens et al., 2010). During the preparation of this campaign, nine circular black and white targets with a radius of 1.5 cm were glued on different places of the light tent and the frame of the globe as illustrated in Figure 3-8 and Figure 3-9. During the target placement, an equal spread in the x-, y- and z-direction was taken into account. Therefore, targets were placed on the copper ring (Figure 3-8), the wooden frame and the back and front of the light tent (Figure 3-9). Linking points in the point set with pixels in the images follows the same procedure as the registration of multiple point sets after a regular TLS campaign, where recognition of the targets is made possible by the big contrast of the intensity values of these targets.

The acquired point set is textured using Leica's Cyclone point processing software. The 'Texture Mapping' tool in this software package enables the draping of a photograph on a point set, using a minimum of 4 points for orthorectified photos and a minimum of 7 points for perspective photos. In both cases, the photo will be referenced on the point set, based on unambiguous matching points. These points will be selected in both the point set as on the image, as demonstrated in Figure 3-8.

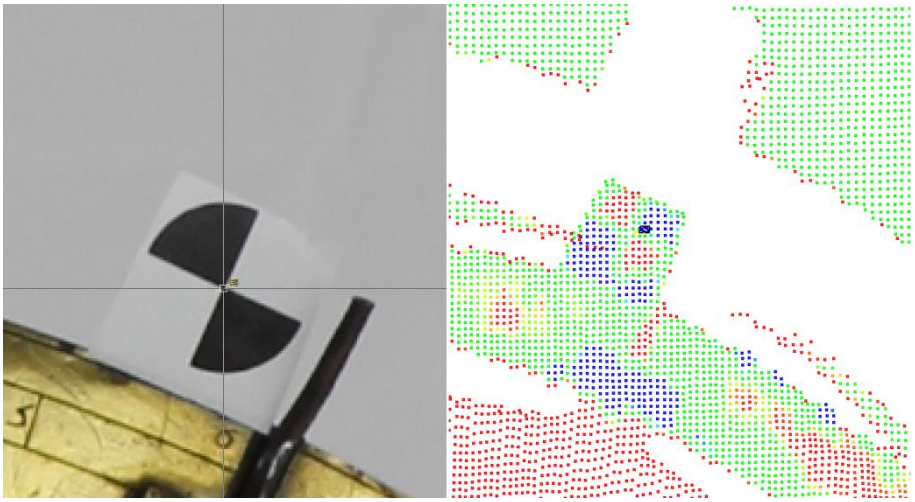

Figure 3-8: Registration point in the photo (left) and the point set (right). Illustrated target has a size of 2.5 x 2.5 cm

The selected pairs of points are used to calculate the translation, rotation and scaling parameters, using a Direct Linear Transformation (Abdel-Aziz and Karara, 1971). The system of linear equations is solved in order to obtain the internal and external image parameters. Optionally, lens distortion parameters are determined using iterative collinear equations (Hu et al., 2008; Ming and Armenakis, 2010). User-defined threshold criteria are used by the algorithm, in order to accept or reject the result. These threshold criteria are based on the Root Mean Square Error (RMSE).

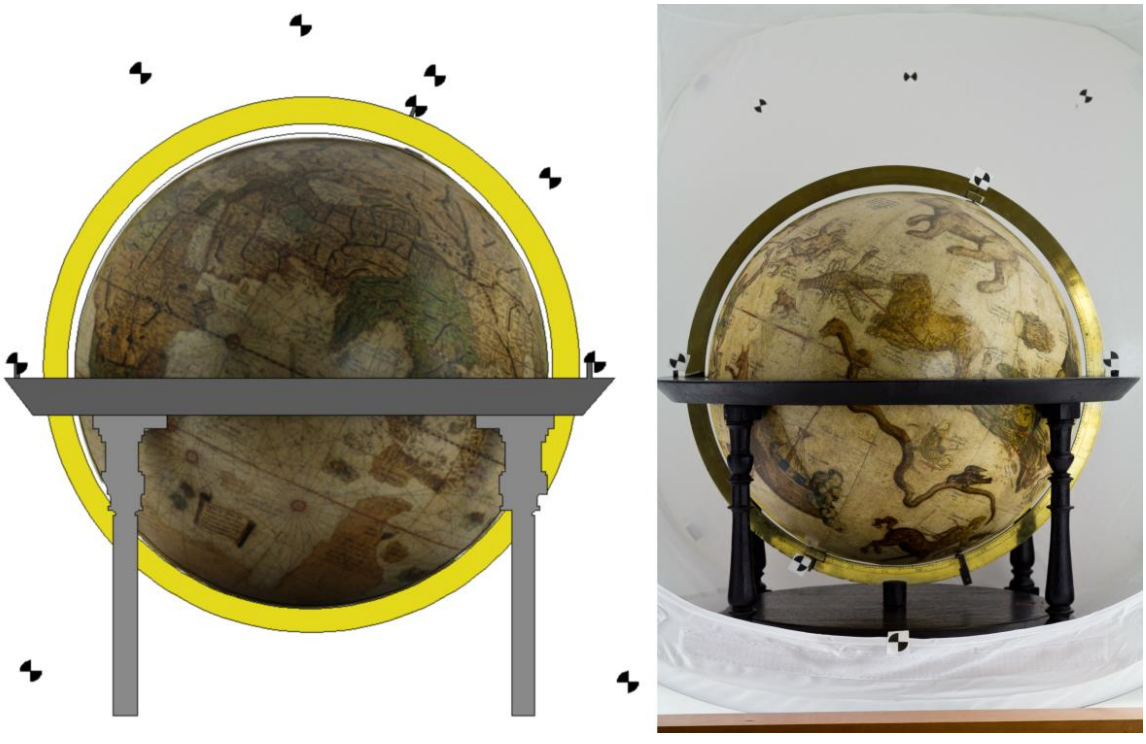

Figure 3-9: Target placement on the wooden frame, copper ring and the light tent

After linking all required targets in the point set and onto the images, the RMSE is calculated. If a registration is performed using the targets as unambiguous points, an RMSE value between 0.50 and 1.00 pixels can be obtained. The registration of the point set and the image, based on other recognisable features in the data, will result in a RMSE value of one pixel (Stal et al., 2011). The

final result, after texturing, is a new point set, containing the measured (x,y,z)-coordinate, the intensity of the reflected signal and the RGB-value of the corresponding pixel of a photo for each scanned point. Figure 3-10 demonstrates a screenshot of the textured point set based on the perspective photo. In the left figure, the intensity is visualised by a colour value, going from low (red) to high (blue). The right image demonstrates the textured point set with RGB-values.

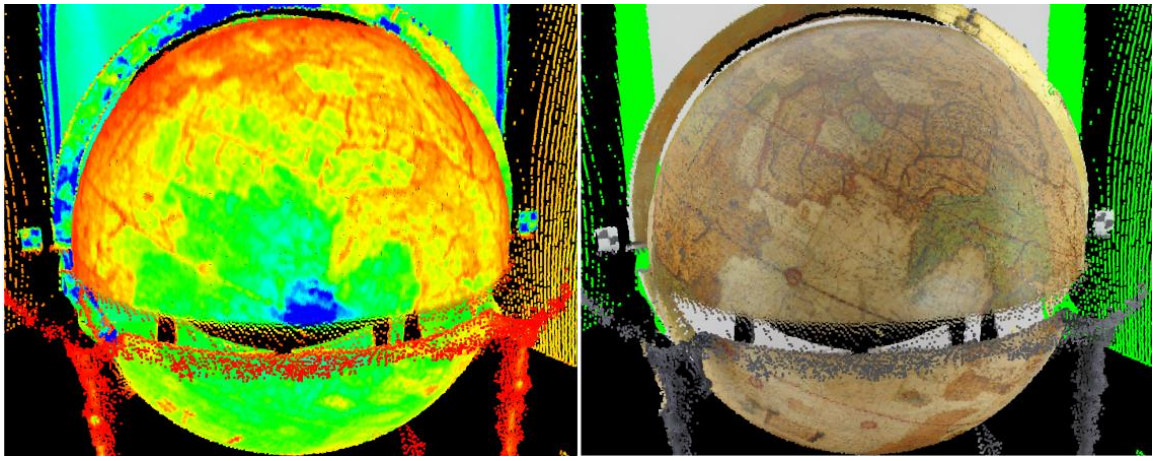

Figure 3-10: TLS point set with intensity (left) and RGB-values (right)

3.4.3. Structure from motion

Structure from motion is a technique in computer vision to acquire 3D geometry from 2D images (Pollefeys et al., 2000; Robertson and Cipolla, 2009). Assuming a set of images, where each point of the study object is projected on a minimum of three images, the 3D positions of these points can be calculated by solving a system of geometrical matrices. If the geometric properties of an image are known, the use of two images is sufficient for the reconstruction of a 3D point. In most situations, an uncalibrated camera is used and the true position and orientation of the camera are unknown. In these cases, the projection of a 3D object on a 2D image plane and the inverse transformation of 2D image coordinates to 3D modelling object coordinates, requires the extrinsic and intrinsic camera parameters and the focal length (Robertson and Cipolla, 2009). The intrinsic parameters and the focal length will be taken from the metadata of each image (EXchange Image Format, EXIF). The extrinsic transformation parameters will be calculated via the detection of matching points on the images. Different automatic matching techniques have been developed over the last decades (Chen et al., 1999; Heipke et al., 1992) and implemented in (commercial) software (Zhang et al., 1996). While digital photogrammetry strongly relies on the presence of camera calibration files for the orientation of the images, structure from motion software, like AutoDesk PhotoFly (www.labs.autodesk.com) or Agisoft PhotoScan (www.agisoft.ru), use series of images and the software automatically calculates the position of the camera, camera calibration parameters and relative scaling factors. This entire process can be split up into three steps (Verhoeven, 2011), which will be further discussed.

The alignment process consists of three steps. First, a set of characteristic points is automatically generated on each image. In the second step, these points are matched with characteristic points of other images. Finally, the scene structure is estimated based on this image matching. The result of

this processing step is a 3D point set of matching points and a graphic representation of the image position. In preparation for the globe reconstruction, the globe's frame has been masked in the software and only the map-image is used for the alignment. In reality, the globe has been rotated during the acquisition of the photographs, but by masking the frame, the photographs appear to have been taken "around the globe". The software interprets this situation as if the globe was in a static situation and the images were taken around the globe, without presence of the wooden frame and copper ring.

Based on the aligned set of photographs, a 3D mesh is constructed. This mesh is calculated by reconstructing the local depths of each photograph. Based on the 3D matching points set, the local depth maps are merged into an overall 3D mesh. After this, the 3D mesh is refined by projecting pixels of different neighbouring images on the overall mesh. More information about the mathematical background of this modelling step is given by Robertson & Cipola (2009) and Seitz et al. (2006). A screenshot of the result of the photo alignment and geometry building step is given in Figure 3-11.

To texture the generated 3D mesh, all images need to be draped onto this mesh. Before starting this process, the dimensions of the texture images will be defined. In combination with the projection parameters of each image, the final texture map is blended. This blending process is performed by taking the maximum or minimum value of all corresponding pixels, or by taking the average of these pixel values. After creating the textured 3D mesh and possible alignment of different sub-meshes (elliptic and polar meshes), the software Agisoft enables the export of the model to different file formats. Based on the requirements of the final product, the texture map can be ignored (e.g. export to Autodesk Exchange Format (dxf)) or included in the model (e.g. Wavefront object file (obj), Stanford polygon file (ply), Collada file (dae)). With these data formats, it is possible to assign a colour to each face in the mesh, or to generate a separate image file, containing the texture of the mesh. In general, the resolution of textures in separate files is higher than the assigned colours of faces.

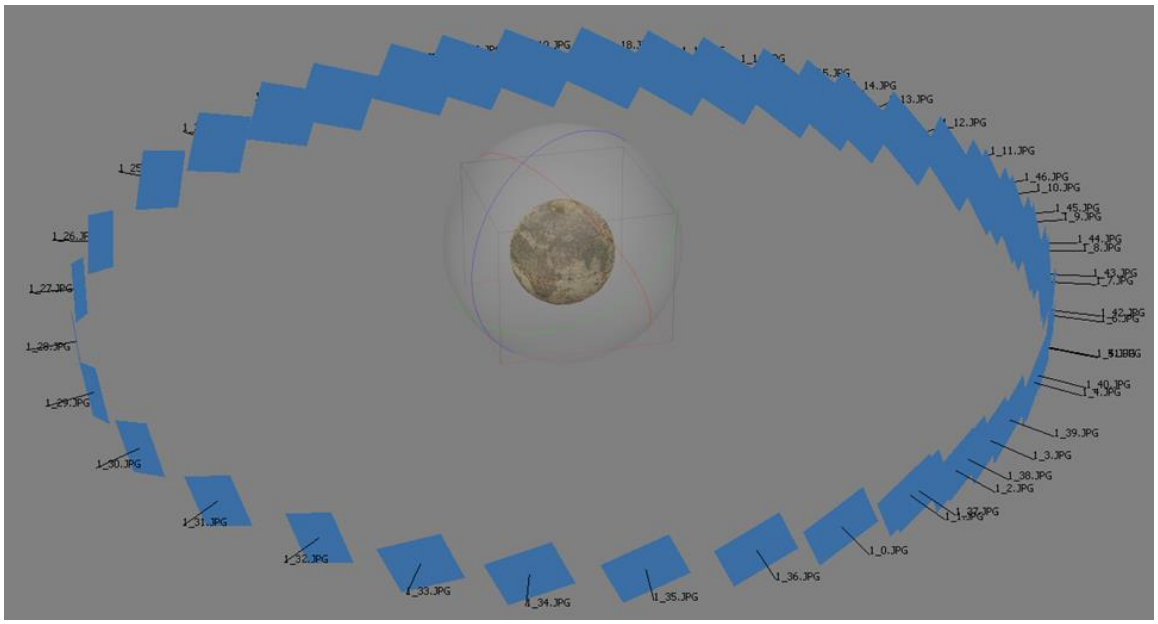

Figure 3-11: Reconstruction of the camera positions and 3D representation of the terrestrial globe

3.4.4. Georeferencing and merging fragments

The last technique with which to make a 3D model of the globe is by georeferencing fragments of images of the globe (Figure 3-12), as presented by Dorffner (1996) and Hruby et al. (2005, 2006). An absolute coordinate system will be used in order to generate a virtual representation. It is thus important to discuss some theory of map projections, in order to be able to predict and describe distortions (Gede, 2009a). During the acquisition and processing of the images of the globes, these globes are assumed to be spherical and the centre of this sphere is supposed to be on the central optical axis of the camera. According to these properties, the globe is projected on the camera sensor, using the vertical perspective projection (Snyder, 1987). If the centre of the sphere and the optical axis do not coincide, a more complex tiled perspective projection is used. Next to the focal length of the camera, the distance between the camera and the globe determines the position of the horizon and the size of the error on the (pseudo) parallels. The area, length and angular errors on the (pseudo) meridians and (pseudo) parallels will increase for increasing distances from the centre of projection. As a result, it is essential to take map fragments from the images as near to the centre of the projection as possible. The terrestrial globe has a grid painted on it, with meridians each 15° and parallels each 10°. This grid is digitalised in a GIS (Geographic Information System) and the resulting grid is georeferenced within a world-wide reference system (WGS 84). The image fragments were chosen from different images, but only one single central fragment was chosen from one single image. To cover the entire earth's surface, a total of 432 fragments were selected, and the corners of each fragment were linked to the digital grid.

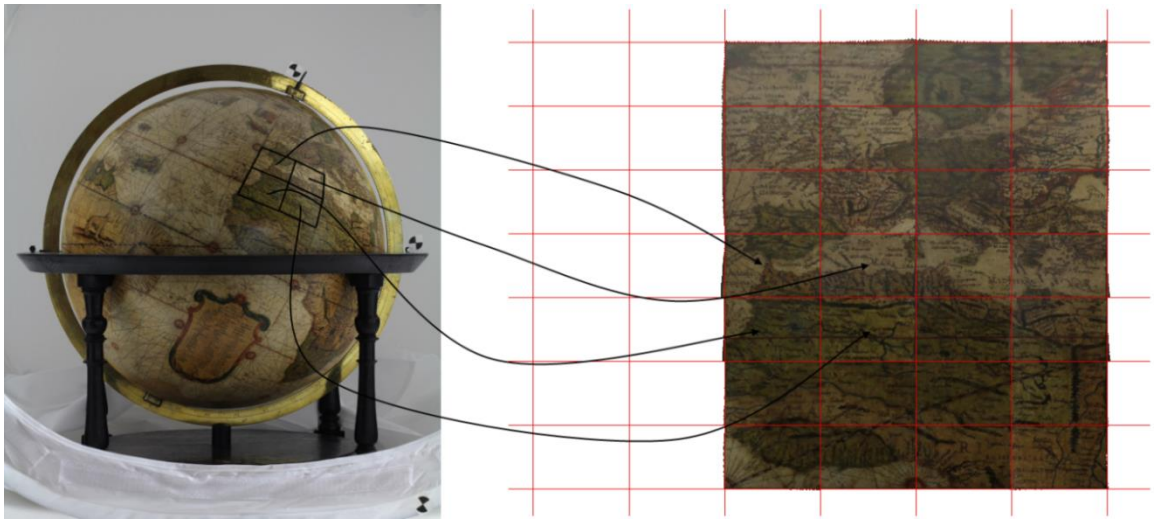

Figure 3-12: Reconstruction of the globe by georeferencing

The technique of generating 3D models by georeferencing fragments of the images has some drawbacks. First of all, the procedure has a relatively time consuming workflow. To cover the entire earth's surface, 432 fragments have to be cut from a selected photograph. After this, all four corners of the 432 fragments have to be aligned with the digital grid. Another drawback is the fact that only four points on the edges of a fragment will be used as unambiguous reference points. In the centre of a cell, the deformations will be maximal and the error vector points to the centre of the globe. This is caused by the non-spherical interpolation of the fragments, and the flat projection of a flat image on a small part of the sphere. Moreover, erroneous geographic

placement of objects on the map of the globe in relation to the used grid will result in geometric displacements as well (Hruby et al., 2006). This displacement will occur in all discussed methods in this article, but with the explicit use of an absolute reference system for the model, and a grid with a user defined resolution, the error will occur most prominently.

3.5. *Visualising the results*

The results of this research can be consulted in different commercial and non-commercial viewers. A very useful software package for 3D mesh visualisation, analysis and modification is MeshLab (www.meshlab.sourceforge.net). All file types mentioned in this article can be handled in this open source software, along with many other file types. For the visualisation of wrl files in an internet browser, Cortona 3D (www.cortona3d.com) could be used, but we experienced better performance with stand-alone software. The consultation of the dynamic images in a browser requires a Flash- or QuickTime plug-in. The digital models of the Mercator globes will be presented within the framework of the 'Mercator Digital' exhibition (www.kokw.be).

3.6. *Discussion*

The generation of 3D models of globes is a challenging task and the presented approaches all have different advantages and drawbacks, depending on the desired quality, processing speed and more importantly: the purpose of the modelling. Within the context of the case study used in this article, the main purpose of the 3D models was to present the globes to the public during the Mercator exposition. The first discussed technique (dynamic imaging) is useful for both visualisation purposes and the research on the cartographic content of the globes. During the reconstruction of the globe, which is solely based on images, no further deformations occurred after the acquisition of the images. Actually, the result can be seen as a dynamic database, enabling fast scrolling through a set of original high resolution images. However, neither 3D visualisation, nor geometrical analysis can be performed with these results, but the results are easily publishable on the internet. This in contrast to the 3D scanning technique, whereby deformation measurements of the globes are possible, as discussed in Adami (2009). In the configuration employed using the light tent, a full coverage by the scanner was not possible, since the main purpose of this project was visualisation and the quality of the images was not satisfactory outside this light tent. A full coverage would require targets around the globe and a free field of view. Another option is the use of a handheld laser scanner (e.g. Creaform HandyScan) or a laser scanning arm (e.g. Faro ScanArm). However, a 3D analysis would still be possible for the measured part of the globe, but the image draping technique, as discussed in this article, does not seem to be suitable for visualisation purposes of detailed textures. The georeferencing of images or image parts is the most common technique for globe visualisation in literature. The method of Dorffner (1996) was used to perform the referencing of the images in a GIS based environment. The method is very straightforward on the one hand, but time consuming on the other hand. Since no sphere was used but rather a rectangular grid as a framework for the georeferencing, the number of images had to be substantial in order to keep the geometrical deformation limited.

Based on the results of this article, the most promising technique for 3D modelling of the globes is structure from motion. Although the processing of the images requires a high performance computer, the results are satisfactory from both a visualisation and a geometric point of view. Before the final presentation of the structure from motion results, the models required some post-processing near the North Pole and South Pole. Both the terrestrial- and the celestial globe will be presented in 3D during the Mercator-exhibition. The models were highly appreciated by the public and further 3D modelling projects are on-going with two historical globes made by Blaeu (Hendrik Concience Library, Antwerp, Belgium) and another Blaeu and Seuter globe (Charles University, Prague, Czech Republic). Moreover, a digital globe library is foreseen, allowing the consultation of digital globes using a combination of GIS and 3D WebGL (e.g. using Google Earth) or 2D WMS (e.g. using QGIS).

3.7. ***Conclusion***

In this article, an overview has been provided of modelling techniques for the virtual representation of two historical globes, focussing on visualisation purposes. Images of two historical globes, constructed by Mercator, are taken under studio conditions and pre-processed in order to have an improved approximation of the real colours of the globes by the images. Thereafter, the images are used for different processing techniques. It has become apparent that all four techniques – dynamic imaging, laser scanning, structure from motion and image georeferencing – have different advantages and drawbacks. After analysing and performing all four techniques, the following statements are formulated in Table 3-2.

Table 3-2: Advantages and disadvantages of the used reconstruction techniques

Dynamic imaging (Obj2VR)	
Advantage	*Drawback*
Easy to use and no high performance hardware required	No true 3D results
Good exchangeability and accessibility via the internet	Geometric quality analysis impossible
Terrestrial laser scanning and image draping (Leica HDS 6100 and Leica Cyclone)	
Advantage	*Drawback*
High accuracy geometric model	Expensive acquisition hardware
Quality of point set independent of environmental light sources	Full coverage of both laser scanner and camera not possible
Structure from motion (Agisoft PhotoScan)	
Advantage	*Drawback*
Straightforward 3D model generation	High performance computer required
Flexibility in resulting digital formats	Black-box processing
Georeferencing and merging images (ESRI ArcGIS)	
Advantage	*Drawback*
User controlled processing	Time consuming
	High geometric distortion in the centre of unit cells

The discussed methods using terrestrial laser scanning and manual georeferencing are not very suitable for 3D globe representation in this context. The laser scanning method can be used for geometric analysis rather than texture analysis of the globes, but this is beyond the scope of this paper. The results generated by georeferencing are acquired in a time consuming process and are of much lower quality than the results generated by dynamic imaging and structure from motion.

Based on these statements and experiences, we conclude that for the particular case of mid-sized historical globes, the dynamic imaging and photogrammetric modelling (in this case: structure from motion modelling) techniques are the most suitable for the generation of virtual globes aimed at public exhibitions. The results from the dynamic imaging are very useful for further semantic and historical research of the globes. Globe details, like compass cards, cartouches and text in general, are clearly represented in the model. The resolution of the original images is retained and the constant angular increment of the globe still results in a 3D impression. Some of the image resolution will be lost by structure from motion processing, but this reduction is mainly manageable by using the correct processing parameters. However, the improvement of the geometric accuracy of the products from the structure from motion technique requires further research. Nevertheless, this 3D modelling technique already offers very satisfactory visual results.

Acknowledgement

The authors would like to express their gratitude to the 'Koninklijke Oudheidkundige Kring van het Land van Waas' (KOKW) for their permission and opportunity to take images of the two historical globes and the ability to present the results of this research during the Mercator's exposition.

References

Abdel-Aziz, Y., Karara, H., 1971. Direct linear transformation into object space coordinates in close-range photogrammetry, Close-range Photogrammetry, Urbana, IL, USA, pp. 1-18.

Adami, A., 2009. From real to virtual globe: new technologies for digital cartographic representation. E-Perimetron 4 (3), 144-160.

Blondeau, R., 1993. Mercator van Rupelmonde. Lannoo, Tielt, Belgium.

Brotton, J., 2003. Trading territories mapping the early modern world. The University of Chicago Press, Chicaco, IL, USA.

Chen, L., Lo, C., Liu, C., Chen, A., 1999. Orientation modeling by matching image templates of a GCP database, 28th Asian Conference on Remote Sensing, Kuala Lumpur, Malaysia, pp. 6 (on CD-ROM)

Collmann, R., 2011. Developments in virtual 3D imaging of cultural artefacts. Ariadne 66, 10 (on CD-ROM).

Dorffner, L., 1996. Der digitale Behaim-Globus: Visualisierung und Vermessung des historisch wertvollen Originals. Cartographica Helvetica 14, 20-24.

Gede, M., 2009a. The projection aspects of digitizing globes, 14th ICA Cartographic Conference, Santiago, Chile, pp. 10 (on CD-ROM)

Gede, M., 2009b. Publishing globes on the internet. Acta Geodetica Geographica Hungaria 44 (1), 114-148.

Heipke, C., Kornus, W., Strunz, G., Thiemann, R., Colomina, I., 1992. Automatic photogrammetric processing of Spot imagery for point determination, DTM generation and orthoprojection. International Archives of Photogrammetry and Remote Sensing 29 (4), 465-471.

Hruby, F., Plank, I., Riedl, A., 2005. Potential of virtual 3D-facsimiles: exemplified by the Earth globe of Gerard Mercator (1541), 22nd ICA Cartographic Conference. Spain, La Coruña, pp. 9 (on CD-ROM)

Hruby, F., Plank, I., Riedl, A., 2006. Cartographic heritage as shared experience in virtual space: a digital representation of the earth globe of Gerard Mercator (1541). e-Perimetron 1 (2), 88-98.

http://wiki.panotools.org, 2011. PanoTools Wiki (Accessed 24 March 2011).

Hu, C., Wang, Y., Yu, W., 2008. Mapping digital image texture onto 3D model from LiDAR data. International Archives of Photogrammetry, Remote Sensing and Spatial Information Sciences 37 (5), 611-614.

Lee, H., Tateyama, Y., Ogi, T., 2010. Realistic visual environments for immersive projection display system, 16th International Conference on Virtual Systems and Multimedia (VSMM), Seoul, Korea, pp. 128-132

Littlefield, R., 2006. Theory of the No-Parallax Points, www.janrik.net/PanoPostings/NoParallaxPoint/TheoryOfTheNoParallaxPoint.pdf (Accessed 23 March 2011)

Ming, J., Armenakis, C., 2010. Fusion of optical and terrestrial laser scanner data. International Archives of Photogrammetry, Remote Sensing and Spatial Information Sciences 38 (1), 156-161.

Nuttens, T., De Wulf, A., Bral, L., De Wit, B., Carlier, L., De Ryck, M., Stal, C., Constales, D., De Backer, H., 2010. High resolution terrestrial laser scanning for tunnel deformation measurements, XXIV FIG International Congress, Sydney, Australia (on CD ROM).

Ojanen, H., 1999. Automatic correction of lens distortion by using digital image processing, Technical report. Rutgers University, New Brunswick, NJ, USA, pp. 5 (on CD-ROM).

Pollefeys, M., Koch, R., Vergauwen, M., Van Gool, L., 2000. Automated reconstruction of 3D scenes from sequences of images. ISPRS Journal of Photogrammetry and Remote Sensing 55 (4), 251-267.

Robertson, D., Cipolla, R., 2009. Structure from motion, in: Varga, M. (Ed.), Practical image processing and computer vision. John Wiley, Hoboken, NJ, USA., p. 49.

Seitz, S., Curless, B., Diebel, J., Scharstein, D., Szeliski, R., 2006. A comparison and evaluation of multi-view stereo reconstruction algorithms, IEEE Computer Society Conference on Computer Vision and Pattern Recognition, New York, NY, USA, 17-22 June, pp. 519-528

Snyder, J., 1987. General perspective projection, in: Snyder, J. (Ed.), Map Projections: a Working Manual. USGS Professional Papers, Washington, USA, pp. 169-181.

Stal, C., De Wulf, A., Nuttens, T., De Maeyer, P., Goossens, R.o.C.-R., 2011. Reconstruction of a midieval wall: photogrammetric mapping and quality analysis by terrestrial laser scanning, in: Halounová, L. (Ed.), 31th EARSeL Symposium. 12 (on CD-ROM), Prague, Czech Republic

Verhoeven, G., 2011. Taking computer vision aloft - archaeological three-dimensional reconstruction from aerial photographs with PhotoScan. Archaeological Prospection 18 (1), 67-73.

Watelet, M., 1994. Gerardus Mercator Rupelmundanus. Mercatorfonds, Antwerp, Belgium.

Zhang, J., Zhang, Z., Shen, W., Wang, Z., 1996. VirtuoZo digital photogrammetry system: its theoretical foundation and key algorithms. International Archives of Photogrammetry and Remote Sensing 31 (2), 424-429.

Chapter 4

Comparison of airborne laser scanning and image based modelling techniques

4. Comparison of airborne laser scanning and image based modelling techniques[4]

Abstract

Airborne laser scanning (ALS) and conventional photogrammetry are currently the most common techniques for the generation of digital elevation models (DEMs). Next to conventional stereoscopic image processing, an image-based reconstruction workflow, using a combination of Structure from Motion and Multi-View Stereo (SfM-MVS) algorithms, has recently been introduced for topographic surface modelling. The use of ALS as an automated data acquisition technique resulted in thorough research on the geometric quality of ALS point clouds and the ensuing products in comparison to the products derived from conventional photogrammetric methods. Such research is mostly absent for SfM-MVS based generated DEMs.

In this article, DEMs based on ALS data, conventional photogrammetry and SfM-MVS algorithms are evaluated for both an urban and a rural study area. The different reconstruction techniques are explained, followed by a statistical analysis of the resulting point clouds using a point-to-point comparison and a point-to-mesh comparison. Furthermore, the ability to use image based techniques for the construction of Digital Terrain Models (DTMs) will be elaborated. The pairwise comparison of the two image based reconstruction techniques with the ALS based DEMs makes clear that the results are different for an urban area and a rural area. The 3D error is between 30 cm and 50 cm for both image based reconstruction techniques, corresponding with approximately three times the pixel size of the images covering the urban area and one or two times the pixel size of the rural area. Regardless of the used processing technique, the geometric quality of the final DEM is mainly related to the terrain. However, the results of the point cloud classification clearly indicate that the SfM-MVS results are significantly better than conventionally photogrammetric point clouds, especially for the rural area. Based on this research, it becomes clear that both conventional photogrammetry and SfM-MVS are very useful to calculate DEMs. If the consequent point clouds are used for the construction of a DTM, the use of SfM-MVS is clearly preferred. This obviously states the high potential of this image based technique for the modelling of areas where airborne images are available and ALS data are absent.

Keywords: airborne laser scanning, photogrammetry, structure from motion and multi-view stereo, digital elevation model, quality assessment

4.1. *Introduction*

High quality spatial data with a 2.5D or 3D geometry are essential for a various range of disciplines. The models that can be generated by these data play an important role in environmental research (Dubovyk et al., 2011; Hape and Purps, 1999), in spatial planning and management (Kolbe et al., 2005; Smart et al., 2011; Stoter et al., 2008), as well as in architectural

[4] Modified from: Stal, C., Briese, C., De Maeyer, P., Goossens, R., Hendrickx, M., Nuttens, T., Pfeifer, N. & De Wulf, A. (2013), Comparison of airborne laser scanning and image based modelling technique. *Expert Systems with Applications, Under review.*

design (Becker, 2009) and in archaeology and cultural heritage (Hendrickx et al., 2011; Koller et al., 2009; Remondino, 2011). The acquisition of 3D data for the construction of these models varies as a function of its applications. For urban and rural environmental modelling, the use of laser scanning (Doneus et al., 2008; Oude Elberink and Vosselman, 2011) and image based modelling (Rottensteiner et al., 2007; Tack et al., 2012) or combinations of different systems (Briese et al., 2012; Haala and Kada, 2010) are well known in literature. With the increasing knowledge about these techniques and the growing number of applications using these techniques, the question arises what technique to use under which circumstances. In many cases, no ALS data is available or it is out of the scoop of the project to invest in such expensive data sets, while series of airborne images are available. An a-priori quality estimation of the DEMs that can be generated using these data is frequently required.

In this paper, quality of the Digital Elevation Models (DEMs) is evaluated by the comparison of the different elevation values, derived from all three techniques for a certain planimetric position. The analysis is performed for a comparison of the different techniques and enables the selection of an appropriate modelling technique under specific circumstances. Within this context, the focus is on different environmental parameters (urban and rural environment) as a result of a given point density and resolution of the data. The quality assessment of DEMs by conventional photogrammetry and SfM-MVS in airborne applications is based on a very dense airborne laser scanning (ALS) reference point set. This data set, with an irregular spatial distribution, is already pre-processed (e.g. strip adjustment, data cleaning, ..) and is supposed to represent the earth topography and non-ground objects with a sub decimetre accuracy. The airborne images were processed in photogrammetric workstations, using camera (calibration) parameters and ground control points (GCPs) for relative and absolute orientation, through current workstations mainly process stereo couples one by one, and are frequently limited to a 2.5D approach. *Leica Photogrammetry Suite* (LPS) was used for a conventional photogrammetric processing in combination with the *enhanced Automatic Terrain Extraction* (eATE, http://geospatial.intergraph.com). Besides, SfM-MVS-based models were generated for this project using aerial images processed in *Agisoft PhotoScan* (www.agisoft.ru). This software has already been used for the construction of very short range archaeological 3D models (Doneus et al., 2011; Plets et al., 2012) and virtual building colouring techniques (Bartie et al., 2011). In correspondence to the current tendency in literature, the ALS data are used as a reference for the analysis of these image based models. For this analysis, the open source point and mesh processing software *CloudCompare* (www.danielgm.net/cc) was used.

Next to the calculation of DEM using the three mentioned surface modelling techniques, the derived point clouds can be filtered for the construction of a DTM. The accurate and efficient point classification of filtering is frequently one of the main requirements when dealing with point clouds (Briese, 2010; Pfeifer and Mandlburger, 2008). Since point sets are frequently just a large list of point coordinates without further attributes, most classification algorithms are typically based on geometrical properties. In most cases, it is obvious to take the configuration of a local neighbourhood around a point into account. Using ALS sensors, the transmitted signal may return a single echo on either ground or non-ground surfaces, or it may return multiple echoes when the signal is partially reflected by the canopy of a tree and the underlying ground surface. Using

image data, the value of a pixel is defined by either the radiometric properties of the object covering that pixel, or by a mixture of radiometric properties of multiple objects within that pixel. As a result, it will be difficult to construct DTMs of vegetated areas. In order to assess the feasibility of using image based surface modelling techniques for the calculation of DTMs, a classification is performed on the two image based point clouds and evaluated against the ALS based classified point cloud. The classification is performed using *LASTools* (Isenburg and Shewchuk, 2013). Although a large number of classification algorithms are presented and evaluated in literature (Chen et al., 2013; Sithole and Vosselman, 2004), the algorithms behind the classification modules of *LASTOOLS* are not known (Podobnikar and Vrecko, 2012).

4.2. ***Study areas***

Two study areas were selected for this comparison: one urban area in the city of Ghent (Belgium) and one rural area in the municipality of Kooigem (Belgium), respectively in the provinces of East- and West Flanders (Figure 4-1).

Figure 4-1: Overview of the study areas (www.answers.com)

The study area in Ghent is selected for its variability of building types, roughly divided over three zones (Figure 4-2, left). On the east side of the Scheldt River, the area is characterized by a large number of three floor residential buildings. Most of these buildings are surrounded by trees and contain a small garden at the back. Large deciduous trees are located along the river and along most of the streets. The southern area contains some large buildings, such as the Saint Peter's abbey and the faculty of Economics of Ghent University. Besides, a big square is located in the middle of this area with four floor buildings opposite of the abbey. The northern part of the second area contains a compact series of four and five floor residential buildings and university

buildings with a large variability of heights. In contrast to the first region, the area west of the Scheldt River does not contain gardens and large trees. This study area is also discussed by Stal et al. (2012), where the authors did a pairwise comparative study on airborne laser scanning and conventional photogrammetry, in favour of change detection in urban areas.

The second study area is situated between Kortrijk, Tournai and Oudenaarde, on a hill top of the forest of 'Kooigem' (in Dutch: 'Kooigembos'), just a few kilometres from the Scheldt river (Figure 4-2, right). The dominance of the hill offers a good visual coverage over the river Scheldt valley in the south and the old road between Kortrijk and Tournai in the east. The flanks of the hill are covered by mixed farmland and the top of the hill is covered by deciduous forest.

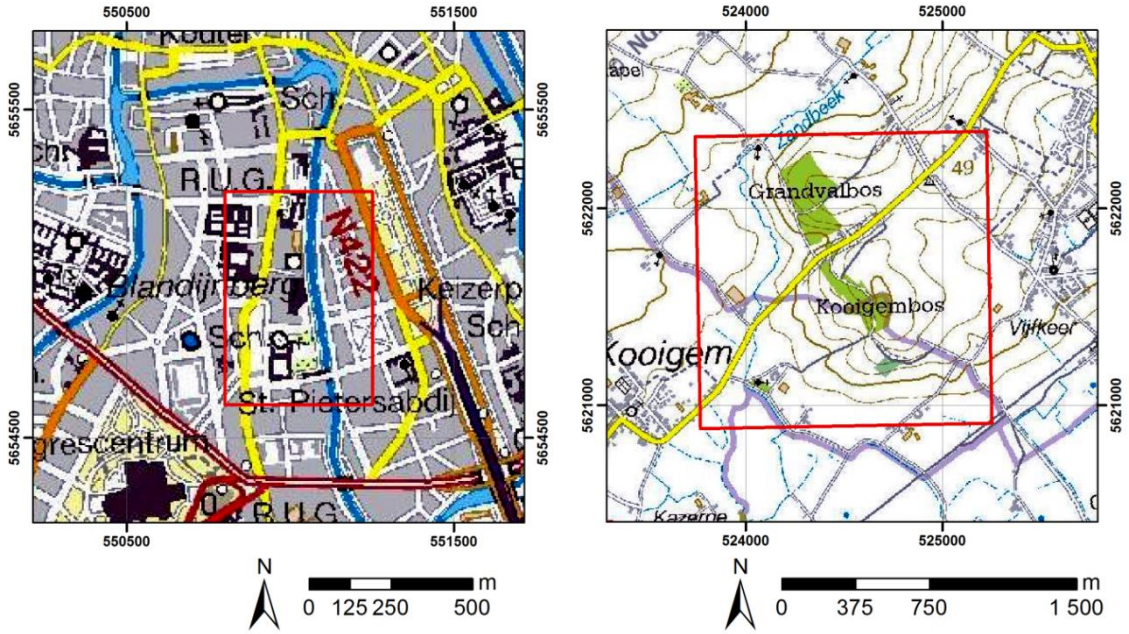

Figure 4-2: Study area in Ghent (left) and Kooigem (right) (units in meter, UTM 31-N, source: NGI, www.ngi.be)

4.3. ***Data sets***

From the three DEMs that are compared in this study, two DEMs were derived from digital aerial images. The metadata and the relevant acquisition parameters of the used aerial images of the Ghent study area and the Kooigem study area are summarized in Table 4-1.

The study area of Kooigem was also measured during a larger ALS campaign on the area of Spiere-Helkijn and the Kemmelberg in 2008. This campaign was ordered by the province of West Flanders for archaeological research by Ghent University (Stal et al., 2011). The used ALS data of the Ghent study area were commissioned by the city of Ghent and by the *AGIV* (Flemish Agency for Geographical Information). Further metadata about these two data sets are presented in Table 4-2.

Table 4-1: Properties of the used panchromatic camera and the study area

Metadata - Aerial image campaign					
Study area		Ghent (Belgium)		Kooigem (Belgium)	
Flight date		April 1st 2008, noon		April 9th 2012, noon	
Measuring system		*Microsoft UltraCamX*		*ZI-Imaging*	
Altitude (above ground) [m]		2250		3000	
Image format	long track [mm][pixel]	67.8	9420	92.2	7680
	cross track [mm][pixel]	103.9	14430	165.9	13824
Pixel size [µm]		7.2 x 7.2		12.0 x 12.0	
GSD [m]		0.15		0.30	
Focal length [mm]		100.5		120.0	
Scale		1/22 500		1/25 000	

Table 4-2: Properties of the used airborne laser scanner and the acquisition project

Metadata - LiDAR campaign		
Study area	Ghent (Belgium)	Kooigem (Belgium)
Flight period	July 2009	April 2008
Measuring system	*FUGRO Fli-Map 1000*	*IGI LiteMapper 5600*
Altitude (above ground) [m]	290	400
Measuring frequency [Hz]	250 000	200 000
Laser wavelength [nm]	1500	1550
Pulse length [ns]	4.0	3.5
Range accuracy [m] = 1 sigma	0.01	0.02
Strip width [m]	320	462
Strip overlap [%]	77	10
Average point density [P/m²]	20	4.5

In order to allow the absolute orientation of the image based models, a series of anchor points or GCPs were defined. The selection of these points is performed by manual identification of unambiguously features on the images. The resulting 25 and 48 points in the Ghent study area and the Kooigem study area respectively were measured with GNSS (both GPS and GLONASS). The GCPs are equally distributed over the entire study area and its surroundings where overlap between consecutive images occurs. Fieldwork is needed to measure the GCPs with a sufficient accuracy corresponding with the GSD of 0.15 and 0.30 m respectively (Vassilopoulou et al., 2002). Using the Flemish FLEPOS RTK system in the Kooigem study area, with a baseline of 10-15 km, an accuracy better than 1.1 cm in planimetry and 2.5 cm in altimetry (67% or 1σ) was achieved (AGIV, 2008).

4.4. ***Image processing***

4.4.1. Stereo photogrammetry

The complete conventional photogrammetric workflow was performed in *Leica Photogrammetric Suite* (*LPS*) and its *enhanced Automatic Terrain Extraction* (*eATE*) module.

This workflow is subdivided into two main processes. It starts with the aerial triangulation for which aerial images, camera details, orientation files and GCPs are required. If this process is successful, the triangulated images and generated tie-points make it possible to extract detailed and accurate terrain information.

eATE creates a point cloud, which is derived from a series of matching points. Only the irregular matching point sets will be used for further geometrical evaluation, in order to minimize interpolation errors. After evaluation of the error reports, the triangulation and the terrain extraction can be refined to get the best results. This means that during the modelling process, the eATE-data iterates towards the most optimal results and the best solution is selected, according to the error reports.

4.4.2. Structure from motion and multi-view stereo software

Agisoft PhotoScan is used for the construction of the SfM-MVS-based DEM. This software uses images for the 3D reconstruction. The entire process from original images to fully textured 3D meshes is covered. SfM-MVS is a technique to reconstruct the camera acquisition parameters and a sparse point set of the scene (SfM), as well as a technique to acquire the 3D geometry of an object, or a series of objects (MVS), using a series of 2D images (Lourakis and Argyros, 2009). The intrinsic parameters, like the image format, the principal point and the focal length of the images are extracted from the metadata of the images to initialize the SfM parameters. These parameters are iteratively adjusted in order to get the best fitting reconstruction solution. The extrinsic parameters are calculated by the projection of the images in the 3D space. Characteristic points or feature points have to be detected on different images and matched with each other. For the recovering the position and orientation of the different camera positions, a system of geometrical projective matrices, based on the 3D coordinates of these points, has to be solved (Pollefeys et al., 2000).

The final scene structure, the orientation and position of the images used for the Kooigem study area are illustrated in Figure 2-11. The numbered rectangles, representing the images, their recording positions and the feature points, give an impression about the correctness of the image alignment. This first scene visualization also enables the selection of the study area by defining a bounding box around this area. In Figure 2-11, the GCPs measured by RTK GNSS are visualized as flags with numbers. The rather equal spatial distribution of the GCPs becomes clear in this figure.

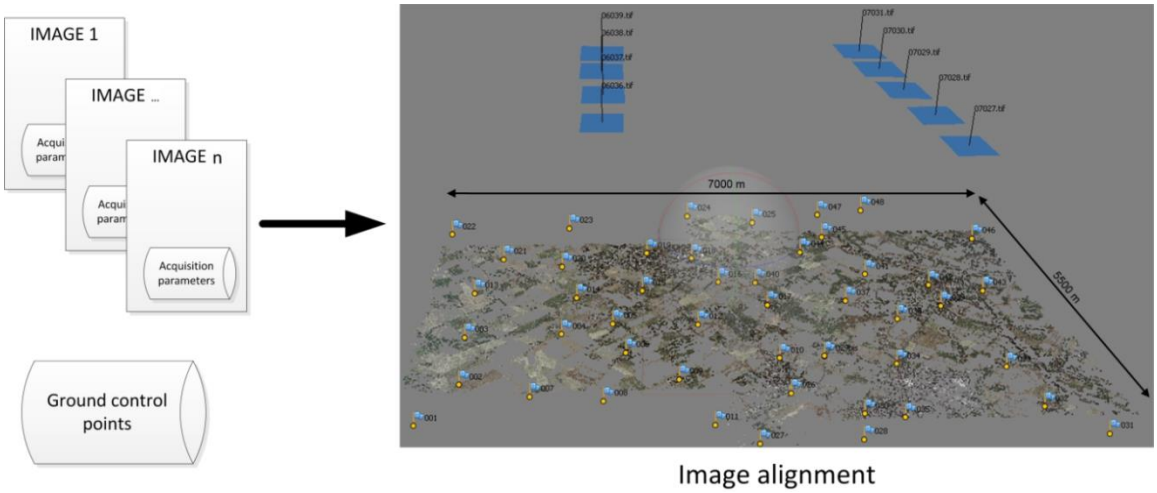

Figure 4-3: Scene structure with matched feature points and positioned and oriented images

Instead of using the 3D feature points or sparse point cloud, the positioned and oriented images are used for the actual 3D reconstruction after the image alignment. A 3D mesh is generated based on the intersection of perspective pixel rays. The linear projection parameters of these 2D image pixels in a 3D space are defined by the focal length of the used camera. This results in a series of depth maps, representing the distance between the intersection of perspective rays and the focal centre of the camera. Combining these depth maps from differently oriented positions enables the creation of a dense point set. This point set is hereafter triangulated into a mesh. This 3D reconstruction technique is extensively discussed by Robertson and Cipolla (2009) and Seitz et al. (2006). The results of the reconstruction of the Kooigem study area are illustrated in Figure 2-13, where for example some farms, the forest, but also the micro topography are clearly visible.

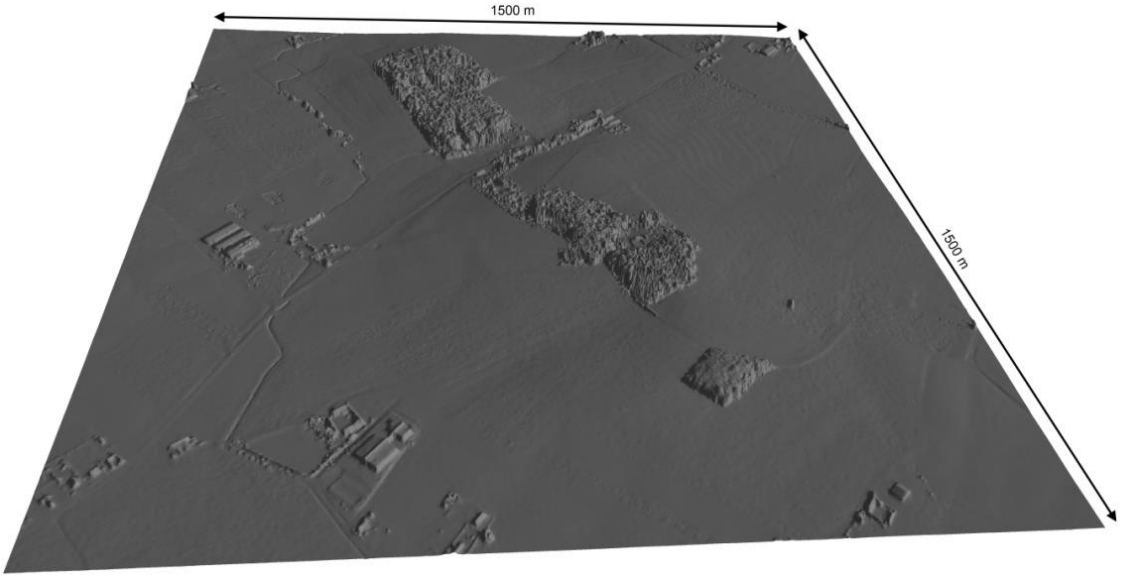

Figure 4-4: Visualization of the DEM of the Kooigem study area

4.5. ***Quality analysis***

4.5.1. Methodology

For this research, a mesh is generated by triangulation of the ALS-based point cloud, resulting in a Triangulated Irregular Network (TIN). The deviation between the ALS based point cloud and the image based point clouds are defined by the vertical distance between each point in the eATE-based point cloud or the SfM-MVS-based point cloud and the intersecting ALS-based face in the mesh (point to mesh comparison). This quality analysis method is limited to the evaluation of elevation data, or the z-component of vertices. It will be clear that this procedure requires some interpolation of at least one of the data sets, which is a simple linear interpolation of the ALS point cloud in this case. This interpolation results in a significant smoothing effect and thus a less accurate quality assessment.

Another approach for the qualitative analysis of point clouds is a closest point matching, or point to point comparison. For each point in one of the image based point clouds, the closest point is found in the ALS based point cloud. Deviations between separate pairs of points are used in this case and enable the comparison in all directions. The presented analysis consists of these two different approaches, as illustrated in Figure 4-5. It is obvious that the point to point comparison suffers from irregular point densities. Therefore, the two approaches will give different results, but the combination of both will be used to describe the quality of the data.

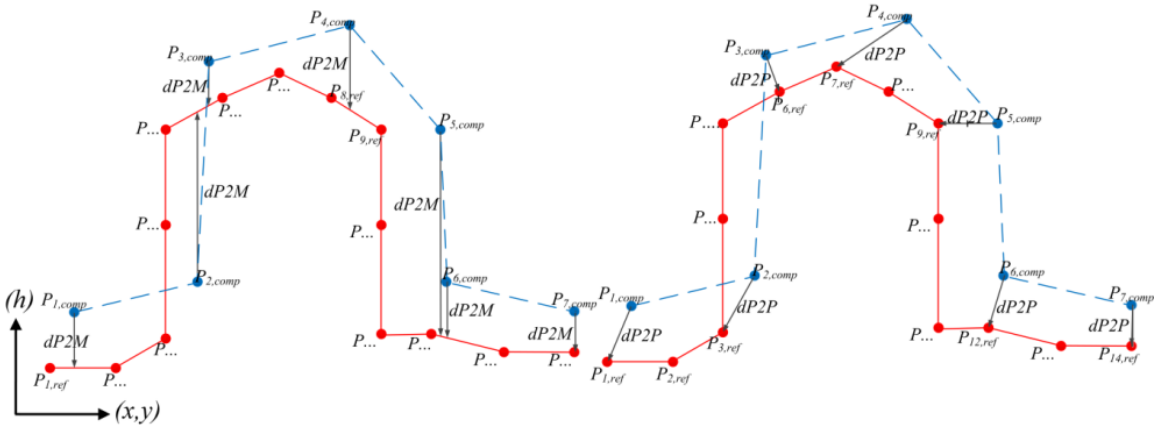

Figure 4-5: Vertical projection of a point cloud on reference mesh (P2M, left) and nearest point comparison (P2P, right)

In this approach, it is important to identify outliers in the data set and to describe the influence of outliers to the comparison. An outlier can be detected when a value is smaller than the lower limit of the first quartile (Q1) minus 1.5 times the Interquartile Range (IQR), or bigger than the upper limit of the third quartile (Q3) plus 1.5 times the IQR (Dawson, 2011). Using this threshold criterion and under the assumption of normality or, alternatively, the assumption of a large positive kurtosis or leptokurtic distribution, it is important to mention that the values must be equally distributed around the mean (Moore et al., 2009). Even without the use of more complex tests of normality, it is clear that the total data set does not have a normal distribution. However, the data set has a large positive kurtosis. This can be motivated by the fact that the theoretical Q1

and Q3 values are much higher than the experimental Q1 and Q3 values, calculated by $2\Phi^{-1}(25\%)$ and $2\Phi^{-1}(75\%)$ of the distribution, which represents the 50 confidence interval.

4.5.2. Data comments

It is important to assess the quality of a point cloud as a function of the data's predefined requirements, rather than by the identification of all error sources during the acquisition and pre-processing steps (Vosselman, 2012). In this case, it is chosen to define the requirements as a function of the GSD of the data. Inversely, it is assumed that the acquisition parameters of the aerial images are taken as such, that the models would fulfil predefined requirements, as formulated by the commissioning institute. Notwithstanding these requirements, some additional issues influencing the data quality must be kept in mind.

The quality of the two image based modelling techniques is assessed using two image series and an ALS point cloud of an urban study area and a rural study area. Per study area, the same image series is used, eliminating the influence on temporal changes between the image-based models. The time differences between the ALS campaign and the image acquisition of the urban study area and rural area are fifteen months and four years respectively. Such a time difference will irrevocably lead to topographical differences and misalignments between the models. This error source may be eliminated by analytical change detection algorithms (Koutsoudis et al., 2013). A more important aspect to keep in mind is the fundamental difference between the acquisition geometry of ALS data and images. An ALS campaign results in a series of scanning lines, which are perpendicular to the directional vector of the sensor. The footprint elongation is a function of the incidence angle and the normal vector of the laser beam (Soudarissanane et al., 2011). The central projection of an image implies that the resolution of an uncorrected image is variable as a function of the distance to the central point of the image. A more detailed discussion about the differences between ALS and photogrammetry is presented by Baltsavias (1999).

The selection of two different study areas is motivated by the significantly different degrees of roughness of the terrain. Steep or abrupt slopes and urban canyons are characteristics of urban areas and they are very hard to eliminate by conventional photogrammetric processing, especially when only one stereo couple is processed. A certain smoothing effect cannot be avoided in this case. Therefore, it was chosen to use the raw processing data, resulting in irregular point clouds. The influence of data interpolation is known to be significant, and a function of the used interpolator (Höhle and Höhle, 2009). As a result, point to point comparison and point to mesh comparison are implemented without gridding the data. Next to the impact of a certain interpolator, the influence of irregular point densities is thus minimized. This irregularity is clearly visible for the urban study area in Figure 4-6. The dense SfM-MVS-based point cloud is the result of the pixel ray projection, whereas the eATE-based point cloud corresponds with the sparse point cloud after feature point extraction. This explains the difference in point densities.

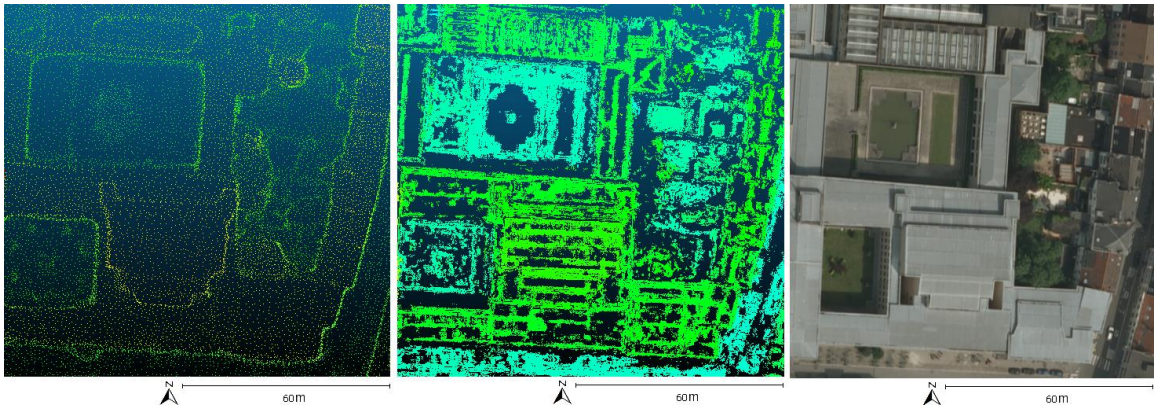

Figure 4-6: Indication of the distribution of the SfM-MVS-based point set (left), the eATE-based point set (middle) and the corresponding airborne image (right)

4.5.3. Results

4.5.3.1. *Point to mesh comparison*

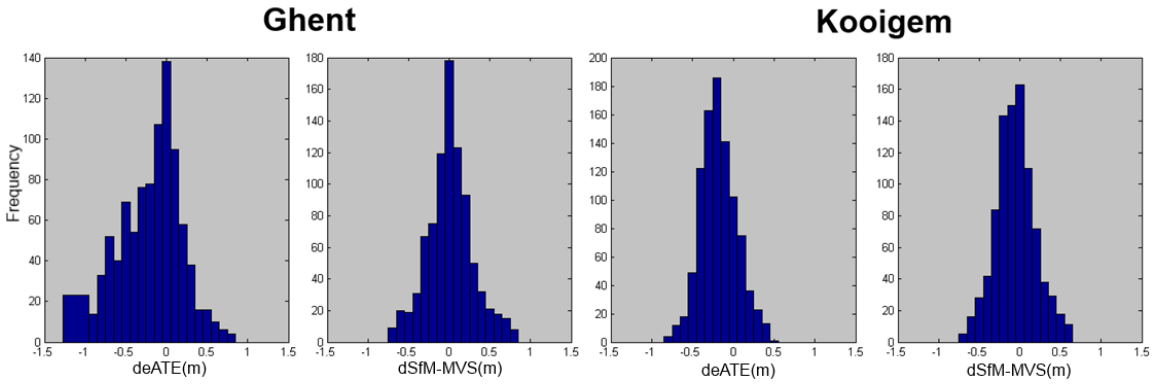

Figure 4-7: Distribution of the point to mesh deviations after outlier removal for the Ghent study area (left) and the Kooigem study area (right)

The point to mesh comparison is performed in CloudCompare and the accompanying distributions are demonstrated in Figure 4-7. These histograms suggest normal distributions of the differences. Some statistics of the data set are presented in Table 4-3. The mean absolute error (MAE, Equation 4-1) and root mean square error (RMSE, Equation 4-2) are calculated as discussed in Tack et al. (2012), with:

$$\mathrm{MAE} = {}^{1}/_{n} \sum_{i=1}^{n} \left| \Delta h_i - \overline{\Delta h} \right|$$

Equation 4-1: Mean absolute error (MAE)

$$\mathrm{RMSE} = \sqrt{{}^{1}/_{n} \sum_{i=1}^{n} \left(\Delta h_i - \overline{\Delta h} \right)^2}$$

Equation 4-2: Root mean square error (RMSE)

Here, n is the number of points, Δh_i is the elevation difference of point i, $\overline{\Delta h}$ is the averaged elevation difference over all n points and $s_{\Delta h}$ is the standard deviation of the all differences.

Table 4-3: Statistics of the point to mesh deviations (units in meter)

			Count	Min	Max	Mean	MAE	RMSE	Kurtosis
Ghent	with outliers	deATE	1000	-10.827	19.976	-0.138	0.566	1.490	73.433
		dSfM-MVS	1000	-9.365	12.195	0.088	0.468	1.209	41.019
	without outliers	deATE	927	-1.268	0.810	-0.184	0.315	0.372	-0.028
		dSfM-MVS	878	-0.740	0.789	0.011	0.213	0.282	0.415
Kooigem	with outliers	deATE	1000	-5.253	3.639	-0.161	0.281	0.398	46.403
		dSfM-MVS	1000	-2.805	2.402	-0.026	0.285	0.473	8.059
	without outliers	deATE	945	-0.769	0.451	-0.177	0.237	0.221	0.057
		dSfM-MVS	909	-0.730	0.637	-0.054	0.196	0.244	0.166

Based on these results, important differences between the urban study area and the rural study area can be noticed. The impact of outliers on the data set becomes clear by the different kurtoses, indicating shifts from leptokurtic (large kurtosis) to normal distributions (zero kurtosis).

Using the differences from vertical point projection (point to mesh) of the urban area of Ghent with the outliers included, the mean deviations are more different from zero for the eATE-based deviations than for the SfM-MVS-based deviations (respectively -0.138 m 0.088 m). Moreover, the RMSE of the eATE-based deviations and the SfM-MVS-based deviations are also different after outlier removal (respectively 1.490 m and 1.209 m). The same holds for the mean deviations and RMSE, when outliers are excluded (respectively -0.184 m and 0.372 m for the eATE-based deviations and 0.011 m and 0.282 m for the SfM-MVS-based deviations). Concerning the rural study area of Kooigem, the mean deviations and MAE are slightly higher for the eATE-based deviations (respectively -0.177 m and 0.237 m) than for the SfM-MVS-based deviations (respectively -0.054 m and 0.196 m) after outlier removal. However, the RMSE of the eATE-based deviations and the SfM-MVS-based deviations are more or less the same after outlier removal (respectively 0.221 m and 0.244 m). These values indicate that SfM-MVS is more suitable for both urban modelling and rural modelling. Therewithal, the eATE-based model of the urban area has a larger MAE than the rural area (respectively 0.315 m and 0.237 m), caused by the stereo-processing workflow of images, and the fact that results are only merged in the last processing stage. This will cause bell-shaped building blocks in dense areas. Although the mean, RMSE and MAE of the two study areas are comparable with each other for the same processing techniques and after outlier removal, the correlation with the original GSD (see Table 4-3) is higher for the rural study area (0.30 m, with RMSE values of 0.244 m and 0.221 m) than the urban study area (0.15 m, with RMSE values of 0.372 m and 0.282 m).

Based on the point to mesh comparison, it can be concluded that the outlier removal results in significantly improved results, for both data sets. Since a reference data set is often not available, it could be important to mention the results without outlier removal combined with the results with outlier removal, as presented in the point to mesh comparison. Plotting the outliers on an orthoimages, as presented in Figure 4-8, indicates some interesting reasons for the outliers. Based on this visual analysis, it becomes clear that outliers occur:

(1) Near façades and steep roofs;
(2) In densely vegetated areas with trees;
(3) On water surfaces;
(4) On newly built, modified or destroyed structures (Stal et al., 2013).

These object types can easily be identified and masked on both images based models, and ALS based models. Therefore, the outliers are ignored in the point to point comparison.

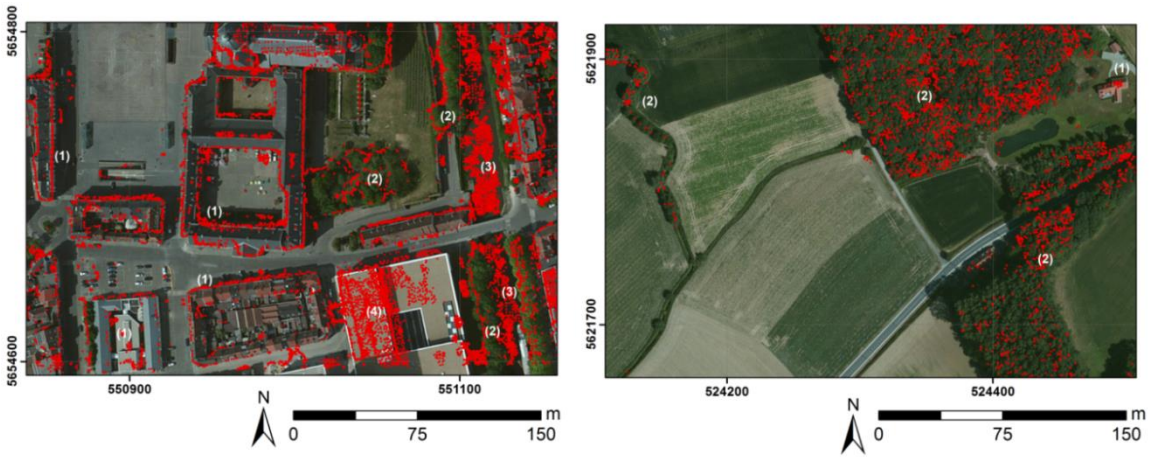

Figure 4-8: Screenshot of outliers plotted on an orthoimage of the urban study area (left) and the rural area (right) (units in meters, UTM 31N)

4.5.3.2. *Point to point comparison*

The results of the point to point comparison are based on closest point analysis and presented in Table 4-4. An outlier removal is also performed on this data set, as discussed above. However, only the values without outliers are presented. Based on the geometric properties of the measured points, it is clear that only the altimetric error (abbreviated as dZ in the table) may have negative values with a normal distribution, and that the 2D and 3D deviations are positive. As a result, the mean differences and the MAE of the derived deviations are equal for the 2D and 3D deviations.

Table 4-4: Statistics of the point to point comparison after closest point analysis (units in meters)

			Count	Min	Max	Mean	MAE	RMSE	Kurtosis
Ghent	eATE	dZ	952	-1.235	0.785	-0.218	0.722	0.375	-0.026
		2D	903	0.008	0.603	0.191	0.191	0.125	0.953
		3D	936	0.036	1.361	0.445	0.445	0.282	0.271
	SfM-MVS	dZ	909	-0.946	0.969	-0.011	0.024	0.357	0.106
		2D	898	0.008	1.202	0.316	0.316	0.260	1.203
		3D	902	0.016	1.691	0.505	0.505	0.357	1.088
Kooigem	eATE	dZ	953	-0.772	0.428	-0.171	0.203	0.220	0.073
		2D	979	0.008	0.399	0.174	0.174	0.078	-0.404
		3D	956	0.017	0.710	0.312	0.312	0.135	-0.129
	SfM-MVS	dZ	917	-0.768	0.656	-0.075	0.065	0.264	0.121
		2D	857	0.008	0.642	0.217	0.217	0.127	1.381
		3D	912	0.040	1.153	0.385	0.385	0.239	0.854

It goes without saying that the altimetric errors, thus elevation component of the nearest neighbour analysis, are strongly correlated with the vertically projected point deviations. As a result, the conclusions from the vertical quality assessment, stating comparable or better modelling results with SfM-MVS in comparison with eATE, also hold when it concerns the differences in elevation in a point to point analysis. The eATE-based modelling technique performs better on the planimetric correlation between the reference data set than its SfM-MVS-based counterparts. This statement holds for both the urban study area (with mean deviations of respectively 0.191 m and 0.316 m), as well as the rural study area (with mean deviations of respectively 0.174 m and 0.217 m). However, the values make clear that for both processing techniques, the rural study area is modelled with a higher accuracy, since the planimetric averaged deviations are lower than the GSD of 0.30 m.

Based on these findings, it can be concluded that for modelling of rural areas, the new SfM-MVS-based modelling technique is definitely comparable with the more time consuming and conventional photogrammetric eATE workflow. The differences between the two processing techniques do not differ very much. The differences are larger for the urban study area, where the planimetric errors of the eATE processing technique are lower and the altimetric errors are higher than its SfM-MVS-based counterpart. For both techniques, the errors are larger than the GSD of 0.15 m.

4.6. ***Point cloud filtering***

In order to derive DTMs from the ALS point cloud and the image based point clouds, a ground filtering is performed using *LAStools*. Although this software can be used for a much further classification of point clouds (vegetation, buildings, ground and undefined classes), only the performance of the ground filtering will be tested for the image-based surface reconstruction techniques. In order to enable the comparison, the processing parameters are kept equal for all three data sets. After classifying the data, each point in the image based point cloud is compared to its nearest neighbour in the ALS point cloud. The results of these comparisons are summarized in the crosstabs in Table 4-5 for Ghent and in Table 4-6 for Kooigem. True and false positives and negatives for the ground classification.

Table 4-5: Crosstab of the classification for the urban study area of Ghent

		eATE					SfM		
		ground	n-ground	Σ			ground	n-ground	Σ
ALS	ground	1383301	1228942	2612243	ALS	ground	67361	34860	102221
	n-ground	127066	3463980	3591046		n-ground	13985	354248	368233
	Σ	1510367	4692922	6203289		Σ	81346	389108	470454

Table 4-6: Crosstab of the classification for the rural study area of Kooigem

		eATE					SfM		
		ground	n-ground	Σ			ground	n-ground	Σ
ALS	ground	8406854	2214058	10620912	ALS	ground	116756	28450	145206
	n-ground	32669	324092	356761		n-ground	752	85023	85775
	Σ	8439523	2538150	10977673		Σ	117508	113473	230981

In order to assess the inter-rater reliability of the image based results in comparison to the ALS data, the Cohen's kappa can be calculated. This value is considered to be an improvement over using the proportional agreement of the data by taking random variability into account. In order to calculate the kappa value, the categories of the nominal scale have to be independent, mutually exclusive, and exhaustive (Cohen 1960). This is obviously the case here, since the different data sets are processed independently. Initially, the proportions are determined for the overall agreement (p_a) and calculated using the tabulation diagonals. Then, the proportional expectations to agree by change (p_e) are calculated using the subtotals. Finally, the kappa-value is defined by:

$$\kappa = \frac{p_a - p_e}{1 - p_e}$$

Equation 4-3: Cohen's kappa-value

A kappa-value of one indicates a perfect correspondence between the image-based models and the ALS-based models, whereas a kappa-value of zero indicates a purely random correspondence between the data sets.

Table 4-7: Overall agreement (p_a), change agreement (p_e) and resulting kappa-value's

		p_a (%)	p_e (%)	k
Ghent	eATE	0.78	0.54	0.52
	SfM	0.90	0.68	0.67
Kooigem	eATE	0.80	0.75	0.18
	SfM	0.87	0.50	0.75

The calculated overall agreements and change agreements, as well as the kappa-value are presented in Table 4-7, indicating a clear difference between the two study areas. This large difference is mainly caused by the irregular spatial distribution of the point cloud covering the rural area and generated with conventional photogrammetry. The number of used feature points in this area is limited for the eATE-based reconstruction, because of the lack of characteristic features in large open fields. The SfM-MVS-based reconstruction uses a pixel based image matching instead of an object based matching, resulting in an equal distribution of the points. This issue has a lesser relevance for the urban study area, where the textural complexity of the images is very large. Based on these results, it is obvious that both image-based reconstruction techniques give reasonable classification results for the urban test area. For the rural area, the eATE-based classification results in a very low agreement with the ALS-based data, whereas the SfM-based classification has a very high correspondence with the reference data.

4.7. *Conclusion*

In this article the quality assessment of DEMs derived from ALS, conventional photogrammetry and SfM-MVS was discussed. Two different study areas, one covering a heavily built-up area in the city of Ghent and one a rural area in the municipality of Kooigem (both in Belgium), were processed using these three techniques. The resulting DEMs are geometrically compared in this study. Based on the results of this comparison, it can be concluded that conventional photogrammetric modelling will result in lower planimetric errors than using the SfM-MVS-based workflow for both urban study areas and rural study areas. However, the differences between the altimetric errors are not appreciable. Notwithstanding the similarity of altimetric deviations, the larger planimetric errors in SfM-MVS based models may require a thorough quality control after generating the models, especially in urban applications. The analysis also made clear that the geometric quality of the urban area is much lower (two or three times the pixel size, ~0.30-0.45 m) than of the rural area (around one time the pixel size, ~0.20-0.40m). This is mainly due to the topographic complexity of urban areas in comparison with rural areas. Hence, the geometric deviations between the techniques for the different areas are not very large, although the influence of outliers is significant. It has been demonstrated that outliers may occur on facades, steep slopes, vegetation, water and large modified structures (either constructed or destroyed). These object types can easily be identified in the data, and eventually be eliminated in order to increase the accuracy of the model. Especially for the conventional photogrammetric workflow the number of outliers seems rather large, based on the different kurtosis of the error distribution before and after outlier removal. Finally, this study made clear that issues concerning surface roughness and complex topography in urban area modelling are more prominent when using conventional photogrammetry, since a stereo-matching reconstruction is used instead of a multi-stereo based reconstruction as with SfM-MVS. Apparently, this does not affect the overall accuracy of the model.

Next to the geometrical comparison of the DEMs, the resulting point clouds were filtered in order to generate DTMs. The pairwise comparison of the resulting number of ground points and non-ground points enabled the calculation of a series of kappa-values. For the urban study area, the difference between the conventional photogrammetric DTM and the SfM-MVS-based DTM is not large. For the rural area, the filtering of the SfM-MVS-based point cloud is significantly better than its counterpart. Therefore, it can be stated that the new SfM-MVS-based reconstruction techniques do not only result in attractive visualizations of a scene, but the technique can also be applied for 3D reconstructions with a high geometric quality for both urban areas and rural areas in a limited time frame. As such, the technique is a reliable alternative for conventional photogrammetry.

Acknowledgement

This research is part of the research project “3D CAD modelling of spatial architectural volumes, using terrestrial laser scanning and LiDAR”, supported by the Research Foundation Flanders (FWO). The authors would like to express their gratitude to the Flemish Geographical Information Agency (AGIV) for providing the airborne image data and the City of Ghent for the airborne LiDAR data. Besides, the NGI (Belgian National Mapping Agency) and the Provence of West Flanders are respectively acknowledged for the provision of the airborne images and airborne LiDAR data. The Ludwig Boltzmann Institute for Archaeological Prospection and Virtual Archaeology is based on an international cooperation of the Ludwig Boltzmann Gesellschaft (Austria), the University of Vienna (Austria), the Vienna University of Technology (Austria), the Austrian Central Institute for Meteorology and Geodynamics, the office of the provincial government of Lower Austria, Airborne Technologies GmbH (Austria), RGZM (Roman-Germanic Central Museum Mainz, Germany), RA (Swedish National Heritage Board), VISTA (Visual and Spatial Technology Centre, University of Birmingham, UK) and NIKU (Norwegian Institute for Cultural Heritage Research).

References

AGIV, 2008. Uitvoeren van GPS-metingen met behulp van Flemish Positioning Service (FLEPOS). www.agiv.be/flepos, 34.

Baltsavias, E., 1999. A comparision between photogrammetry and laser scanning. ISPRS Journal of Photogrammetry and Remote Sensing 54 (2-3), 83-94.

Bartie, P., Reitsma, F., Mills, S., 2011. A combined GIS and stereo vision approach to identify pixels in images and determine appropriate color terms. Journal of Spatial Information Science 2 (6), 59-83.

Becker, S., 2009. Generation and application of rules for quality dependent façade reconstruction. ISPRS Journal of Photogrammetry and Remote Sensing 64 (6), 640-653.

Briese, C., 2010. Extraction of digital terrain models, in: Vosselman, G., Maas, H. (Eds.), Airborne and terrestrial laser scanning. Whittles Publishing, Dunbeath, UK, pp. 135-167.

Briese, C., Zach, G., Verhoeven, G., Ressl, C., Ullrich, A., Studnicka, N., Doneus, M., 2012. Analysis of mobile laser scanning data and multi-view image reconstruction. International Archives of Photogrammetry and Remote Sensing 39 (B5), 163-168.

Chen, C., Li, C., Li, W., Dai, H., 2013. A multiresolution classification algorithm for filtering airborne LiDAR data. ISPRS Journal for Photogrammetry and Remote Sensing 82 (1), 1-9.

Dawson, R., 2011. How significant is a boxplot outlier? Journal of Statistics Education 19 (2), 1-12.

Doneus, M., Briese, C., Fera, M., Janner, M., 2008. Archaeological prospection of forested areas using full-waveform airborne laser scanning. Journal of Archaeological Science 35 (4), 882-893.

Doneus, M., Verhoeven, G., Fera, M., Briese, C., Kucera, M., Neubauer, W., 2011. From deposit to point cloud: a study of low-cost computer vision approaches for the straightforward documentation of archaeological excavations, 22th CIPA Symposium, Prague, Czech Republic, pp. 8 (on CD-ROM)

Dubovyk, O., Sliuzas, R., Flacke, J., 2011. Spatio-temporal modelling of informal settlement development in Sancaktepe district, Istanbul, Turkey. ISPRS Journal of Photogrammetry and Remote Sensing 66 (2), 235-246.

Haala, N., Kada, M., 2010. An update on automatic 3D building reconstruction. ISPRS Journal of Photogrammetry and Remote Sensing 65 (6), 570-580.

Hape, M., Purps, J., 1999. Digitale Geländemodelle als Grundlage für stationäre und instationäre Überflutungssimulationen, Fachtagung Elbe, Dynamik und Interaktion von Fluß und Aue. Elbe-Ökologie & BMBF, Berlin, Germany, Wittenberge, Germany, pp. 152-155

Hendrickx, M., Gheyle, W., Bonne, J., Bourgeois, J., De Wulf, A., Goossens, R., 2011. The use of stereoscopic images taken from a microdrone for the documentation of heritage - An example from the Tuekta burial mounds in the Russian Altay. Journal of Archaeological Science 38 (11), 2968-2978.

Höhle, J., Höhle, M., 2009. Accuracy assessment of digital elevation models by means of robust statistical methods. ISPRS International Journal of Photogrammetry and Remote Sensing 64 (4), 398-406.

Isenburg, M., Shewchuk, J., 2013. LAStools, 1.2 ed, http://lastools.org, pp. Converting, viewing and compressing LIDAR data in LAS format

Kolbe, T.H., Gröger, G., Plümer, L., 2005. CityGML: interoperable access to 3D city models, First International Symposium in Geo-Information for Disaster Management. Springer Verlag, Delft, the Netherlands, pp. 883–899

Koller, D., Frisscher, B., Humphreys, G., 2009. Research challanges for digital archives of 3D cultural heritage models. Journal on Computing and Cultural Heritage 2 (3), 1-17.

Koutsoudis, A., Stravroglou, K., Pavlidis, G., Chamzas, C., 2013. 3DSSE: A 3D scene search engine, exploring 3D scenes using keywords. Journal of Cultural Heritage 13 (2), 187-194.

Lourakis, M., Argyros, A., 2009. SBA: A software package for generic sparse bundle adjustment. ACM Transactions on Mathematical Software 36 (1), 1-30.

Moore, D., McCabe, G., Craig, B., 2009. Introduction to the practice of statistics, 6 ed. W.H. Freeman, New York, NY, USA.

Oude Elberink, S., Vosselman, G., 2011. Quality analysis on 3D building models reconstructed from airborne laser scanning data. ISPRS Journal of Photogrammetry and Remote Sensing 66 (2), 157-165.

Pfeifer, N., Mandlburger, G., 2008. LiDAR data filtering and DTM generation, in: Shan, J., Toth, C. (Eds.), Topographic laser ranging and scanning: principles and processing. CRC Press, Boca Raton, Fl, USA, pp. 307-333.

Plets, G., Gheyle, W., Verhoeven, G., De Reu, J., Bourgeois, J., Verhegge, J., Stichelbaut, B., 2012. Three-dimensional recording of archaeological remains in the Altai Mountains. Antiquity 86 (333), 1-14.

Podobnikar, T., Vrecko, A., 2012. Digital elevation model from the best results of different filtering of a LiDAR point cloud. Transactions in GIS 16 (5), 603-617.

Pollefeys, M., Koch, R., Vergauwen, M., Van Gool, L., 2000. Automated reconstruction of 3D scenes from sequences of images. ISPRS Journal of Photogrammetry and Remote Sensing 55 (4), 251-267.

Remondino, F., 2011. Heritage recording and 3D modeling with photogrammetry and 3D scanning. Remote Sensing 3 (6), 1104-1138.

Robertson, D., Cipolla, R., 2009. Structure from motion, in: Varga, M. (Ed.), Practical image processing and computer vision. John Wiley, Hoboken, NJ, USA., p. 49.

Rottensteiner, F., Trinder, J., Clode, S., Kubik, K., 2007. Building detection by fusion of airborne laser scanner data and multi-spectral images: performance, evaluation and sensitivity analysis. ISPRS Journal of Photogrammetry and Remote Sensing 62 (2), 135-149.

Seitz, S., Curless, B., Diebel, J., Scharstein, D., Szeliski, R., 2006. A comparison and evaluation of multi-view stereo reconstruction algorithms, IEEE Computer Society Conference on Computer Vision and Pattern Recognition, New York, NY, USA, 17-22 June, pp. 519-528

Sithole, G., Vosselman, G., 2004. Experimental comparison of filter algorithms for bare-Earth extraction from airborne laser scanning point clouds. ISPRS Journal of Photogrammetry and Remote Sensing 59 (1-2), 85-101.

Smart, P., Quinn, J., Jones, C., 2011. City model enrichment. ISPRS Journal of Photogrammetry and Remote Sensing 66 (2), 223-234.

Soudarissanane, S., Lindenbergh, R., Menenti, M., Teunissen, P., 2011. Scanning geometry: influencing factor on the quality of terrestrial laser scanning points. ISPRS Journal for Photogrammetry and Remote Sensing 66 (4), 389-399.

Stal, C., De Wulf, A., De Maeyer, P., Goossens, R., Nuttens, T., Tack, F., 2012. Statistical comparison of urban 3D models from photo modeling and airborne laser scanning, SGEM, Albena, Bulgaria, pp. 8 (on CD-ROM)

Stal, C., Nuttens, T., Bourgeois, J., Carlier, L., De Maeyer, P., De Wulf, A., 2011. Accuracy assessment of a LiDAR digital terrain model by using RTK GPS and total station. EARSeL eProceedings 10 (1), 1-8.

Stal, C., Tack, F., De Maeyer, P., De Wulf, A., Goossens, R., 2013. Airborne photogrammetry and LiDAR for DSM extraction and 3D change detection over an urban area: a comparative study. International Journal of Remote Sensing 34 (4), 1087-1110.

Stoter, J., de Kluijver, H., Kurakula, V., 2008. 3D noise mapping in urban areas. International Journal of Geographic Information Science 22 (8), 907-924.

Tack, F., Buyuksalih, G., Goossens, R., 2012. 3D building reconstruction improvement based on given ground plan information and surface models extracted from spaceborne imagery. ISPRS Journal of Photogrammetry and Remote Sensing 67 (1), 52-64.

Vassilopoulou, S., Hurni, L., Dietrich, V., Baltsavias, E., Pateraki, M., Lagios, E., Parcharidis, I., 2002. Orthophoto Generation Using IKONOS Imagery and High-Resolution DEM: a Case Study on Vulcanic Hazard Monitoring of Nisyros Islang (Greece). ISPRS Journal of Photogrammetry & Remote Sensing 56 (3), 24-38.

Vosselman, G., 2012. Automated planimetric quality control in high accuracy airborne laser scanning surveys. ISPRS Journal for Photogrammetry and Remote Sensing 74, 90-100.

Chapter 5

Airborne photogrammetry and LiDAR for DSM extraction and 3D change detection over an urban area: a comparative study

5. Airborne photogrammetry and LiDAR for DSM extraction and 3D change detection over an urban area: a comparative study[5]

Abstract

A digital surface model (DSM) extracted from stereoscopic aerial images, acquired in March 2000, is compared with a DSM derived from airborne Light Detection And Ranging (LiDAR) data collected in July 2009. Three densely built-up study areas in the city centre of Ghent, Belgium, are selected, each covering approximately 0.4 km^2. The surface models, generated from the two different 3D acquisition methods, are compared qualitatively and quantitatively as to what extent they are suitable in modelling an urban environment, in particular for the 3D reconstruction of buildings. Then the data sets, which are acquired at two different epochs t_1 and t_2, are investigated as to what extent 3D (building) changes can be detected and modelled over the time interval. A difference model, generated by pixel-wise subtracting of both DSMs, indicates changes in elevation. Filters are proposed to differentiate 'real' building changes from false alarms provoked by model noise, outliers, vegetation or temporal features like cars. A final 3D building change model maps all destructed and newly constructed buildings within the time interval t_2 - t_1. Based on the change model, the surface and volume of the building changes can be quantified.

5.1. *Introduction*

City monitoring and 3D modelling of continuously and rapidly changing urban environments have become an important study field. Digital surface models (DSMs) and their derivatives are increasingly used in Earth science and the demand for DSMs has matured from a narrow research niche into an expanding market of applications (Baltsavias and Gruen, 2003), going from (3D) urban planning and city management (Kolbe et al., 2005) through architectural design (Haala and Kada, 2010) to microclimate studies (Rigo and Parlow, 2007). At present, many different techniques exist to model the ground surface in three dimensions, such as optical (aerial and space) photogrammetry, Airborne Laser Scanning (ALS), also called airborne light detection and ranging (LiDAR), interferometric synthetic aperture radar (InSAR), and land surveying. The first two acquisition methods are compared in this work.

3D modelling of built-up areas or man-made structures is a hard problem though, due to the structural complexity, great diversity, and high degree of detail of the urban nature. The most prominent distortions that hamper 3D reconstruction are geometrical displacement of features with a certain height above the surface, occlusion, and steep changes in slope and shadow. In the case of LiDAR acquisition in urban areas, the quality of the measurements suffers

[5] Modified from: Stal, C., Tack, F., De Maeyer, P., De Wulf, A., & Goossens, R. (2013). Airborne photogrammetry and LIDAR for DSM extraction and 3D change detection over an urban area : a comparative study. *International Journal of Remote Sensing*, *34*(4), 1087–1110.

heterogeneously from the different types of reflecting surfaces, caused by the variety of roof materials and corresponding albedos (Böhler et al., 2003). The urban issue has been extensively researched for many decades and reported thoroughly in Berthod et al. (1995), Weidner and Förstner (1995), Gabet, et al. (1997), Förstner (1999), Jacobsen (2006), and Tack et al. (2012). Fundamentally, the DSM generation techniques by photogrammetry and by LiDAR are different (Asal et al., 2000). Baltsavias (1999) describes an extensive comparison between data acquisition and processing from passive optical sensors and LiDAR. According to Baltsavias (1999), the main differences are, respectively: passive versus active; generally frame or linear sensors with perspective geometry versus generally point sensors with polar geometry; indirect versus direct acquisition of 3D coordinates; and geometric and radiometric high-quality images versus limited image quality. For extraction of a DSM, the acquisition time and cost for LiDAR is generally much higher than for systematically acquired stereoscopic images; however, in general, the computation cost is lower (Gehrke et al., 2010). According to Baltsavias and Gruen (2003), LiDAR systems are active, are not influenced by shadows, can be employed at night, preserve surface discontinuities, allow high automation of data processing, and have relatively short production times. As such, they provide dense and accurate urban measurements. However, Baltsavias and Gruen (2003) state that they also have some disadvantages, including errors of secondary reflections close to vertical structures, a narrow flight swath, longer flight time, and more complex flight plan compared to aerial image acquisition. Identification and classification of objects based on LiDAR data, without any additional optical sensors or neighbourhood algorithms, is very difficult or even impossible, since the sensor only acquires a point set.

In this article, a surface model extracted from stereoscopic aerial images, acquired in 2000, is compared with a DSM derived from airborne LiDAR data collected in 2009. The DSMs, derived from the aerial imagery at epoch t_1 and the LiDAR acquisition at epoch t_2, are further addressed in this work, respectively, as DSM_{PHG} and DSM_{LiDAR}. Three adjacent densely built-up areas in the city centre of Ghent, Belgium, are selected as a study area, each covering approximately 0.4 km^2. The three areas are characterized by a high diversity in urban morphology and by some significant changed areas in terms of destructed and constructed buildings over the time interval $t_2 - t_1$.

Theoretically seen, the high resolution of the aerial images and the high point density of the LiDAR data set should allow 3D reconstruction of the study area at the object level, i.e. building level. The surface models, generated from the two different 3D acquisition methods, are compared qualitatively and quantitatively as to what extent they are suitable in modelling the urban environment. Moreover, an effective 3D building change detection approach is introduced. The multi-temporal data sets are investigated as to what extent 3D changes can be detected and modelled over the time interval $t_2 - t_1$. Height information appears to be the only true invariant to detect whether there is a 3D change (Jung 2004). In the executed research, exclusively 3D building changes are treated. The presented automatic 3D extraction approach can drastically reduce the amount of human interaction for applications such as the updating of (3D) building databases (Breunig and Zlatanova, 2011) or the modelling and study of urban dynamics, e.g. expansion and densification. The objectives of this study are:

1) to compare the use, performance, and feasibility of aerial photogrammetry and airborne LiDAR in 3D surface modelling or DSM generation of a densely built-up environment, especially in the reconstruction of buildings; and
2) to detect and extract 3D building changes in a highly automated way by comparison of the multi-temporal data sets.

Section 2 describes the LiDAR and aerial image data set as well as the urban area, which is the subject of this research. Section 3 describes the DSM extraction methodology from both data sets, the post-processing and visual-qualitative analysis of the results. In Section 4, statistics are calculated for both DSMs and their comparability is discussed. Section 5 discusses an effective 3D building change detection approach. The article concludes with a brief summary and discussion of the findings. ERDAS LPS is used for the photogrammetric processing, whereas ESRI ArcGIS and PASW SPSS are used for the statistical analysis of the DSMs.

5.2. ***Data sets and study area***

5.2.1. LiDAR data set

The used LiDAR data were acquired by Fugro N.V. (Leidschendam, The Netherlands) and were commissioned by the city of Ghent and the AGIV (Flemish Agency for Geographical Information), Belgium. The used Fugro Fli-Map 1000 was mounted on a helicopter and the entire campaign was executed at an average flight height of 290 m Above Ground Level (AGL). The relatively low flight height was necessary to get an average point density of 125 points m^{-2}, under the condition that each object is measured with a minimal scan angle of 7.5°. Additional metadata is provided in Table 5-1.

Table 5-1: Properties of the used airborne laser scanner and the acquisition project

Metadata - LiDAR campaign	
Flight period	July 2009
Measuring system	*Fugro Fli-Map 1000*
Flight height [m]	290
Measuring frequency [Hz]	250 000
Scan frequency [Hz]	150 - 250
Range accuracy [m] = 1 sigma	0.01
Strip width [m]	320
Strip overlap [%]	77
Point density	
Min [P/m²]	35
Max [P/m²]	140
Average [P/m²]	125

5.2.2. Stereoscopic aerial image data set

The stereoscopic aerial flight has been conducted over the city centre of Ghent on 22 March 2000 at noon with a Wild RC20 photogrammetric aerial frame camera, equipped with a 30/4 NATA-F lens (f = 303 mm). The images are acquired at a flight height of approximately 1200 m, yielding a photo scale of 1:4000 and a resolution of 0.09 m Gound Space Distance (GSD). Each image covers approximately 0.7 km^2 and has a longitudinal overlap between adjacent acquisitions of 60%. The lateral side overlap between the successive flight strips is small and not usable for stereo extraction. Three stereo pairs are selected from the data set. The covered areas are selected based on a differentiated morphology and the occurrence of remarkable construction works during the acquisition of the multi-temporal data sets.

5.2.3. Study area

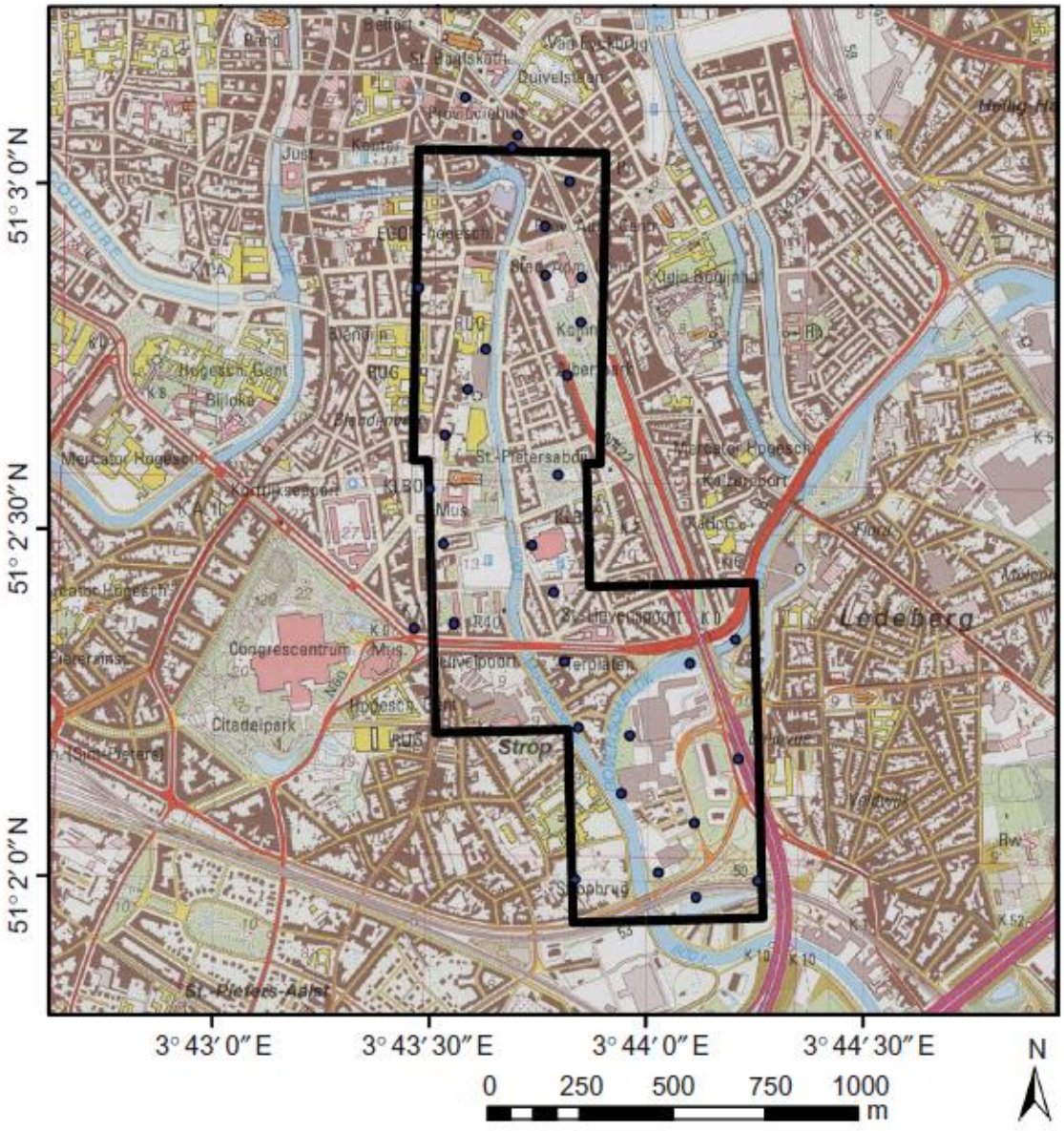

Figure 5-1: Overview map of the three overlapping parts of the study area. In addition, the measured GPS points used for triangulation of the aerial imagery are illustrated as blue dots (1:20,000 topographic map, NGI, 1999)

Three neighbouring study areas were selected in the inner city of Ghent, Belgium, all with a specific urban morphology and a total surface of 1.2 km^2 (see Figure 5-1). It is well known that urban areas are very complex to model by both LiDAR and photogrammetry since steep slopes of the buildings within the area will increase the occurrence of both occlusion zones and shadow. Although this issue can be solved by acquiring data from multiple angles, it remains an important issue when the building density is high in both planimetric and altimetric directions.

The three selected areas are characterized by a different urban morphology and contain different building configurations. The first and most southern area is located around the 'Zuiderpoort' and consists of a widespread commercial area with some 15- to 20-floor buildings. The second area is located around the 'Sint-Pietersplein', a big square in front of the abbey of Saint Peter. Around this old abbey, some other squares and a park are located as well. The most complex area is the 'Rectorate' area in the north, where the Ghent University administration, the university library, and some campuses are located. This dense urban area is characterized by a high diversity in building height and size and buildings are separated by narrow streets and alleys.

The urban diversity of the study area is illustrated by a topographic map (see Figure 5-1). The entire area is dominated by the Upperscheldt River in the south and the Muinkscheldt River from the south to the north. The east flank of the latter is characterized by three- and four-floor townhouses, two parks, and a commercial and administrative centre in the northeast. The areas are not only selected because of their diversity of urban morphology, but also because of the fact that some important changes have taken place between the acquisition of the aerial photos in 2000 and the LiDAR campaign in 2009. The knowledge about these changes enables the creation of a control data set that contains newly constructed buildings. The four most prominent changes in the areas are a new office building in the south ('Zuiderpoort'), a student flat and college building in the centre ('Diamond tower'), and two new university buildings (Faculty of Economics and the Universiteitsforum or 'UFO') in the centre and the north.

5.2.4. Morphological descriptor of the study areas

To quantify the diversity of the three study areas, some metrics are calculated on the DSMs extracted from the LiDAR data. To describe the three data sets, a convolution filter is constructed based on a morphological filter. This concept is well known for the analysis of DSMs and digital terrain models (DTMs) in terms of edge enhancement, followed by object detection (Stal et al., 2010). A new cell value Δh is obtained by taking a kernel w around pixel p in column c and row r (c_p , r_p) and by calculating the difference between the local minimum and maximum of all height values within this kernel (z_p , w):

$$\Delta h = \max_{(c_p, r_p \in w)} (z_p) - \min_{(c_p, r_p \in w)} (z_p)$$

Equation 5-1: Height difference Δh calculated for a given pixel p with a kernel w

This concept is based on, respectively, the dilation and erosion component of a morphological filter (Zhang et al. 2003). The strength of the filter, in contrast with, for example, a high pass filter,

is the preservation of the metric unit in the results. A given cell value defines the real height difference between the maximal height value and the minimal height value for the neighbourhood in the kernel. A high-pass filter, on the other hand, accentuates the edges of an object as well, but normalizes the values. The results of the filter, applied on the three research areas, are summarized in Table 5-2. A sample of the results is illustrated in Figure 5-2. The DSMs have a cell size of 0.50 by 0.50 m and for the neighbourhood data analysis, a kernel size of 3 × 3 pixels is chosen.

Table 5-2: Statistics of the neighbourhood data analysis with a kernel size of 3 × 3 pixels

	Focal analysis				
	Columns	*Rows*	*Max (m)*	*Mean (m)*	*St.Dev. (m)*
Rectorate	1108	1769	63.410	2.312	4.137
Sint-Pietersplein	1030	1833	51.000	2.019	3.583
Zuiderpoort	1204	1933	48.730	1.814	3.772
Total study area	2030	4226	63.410	2.051	3.878

Note: Maximum refers to maximal height difference and minimum refers to mean height difference.

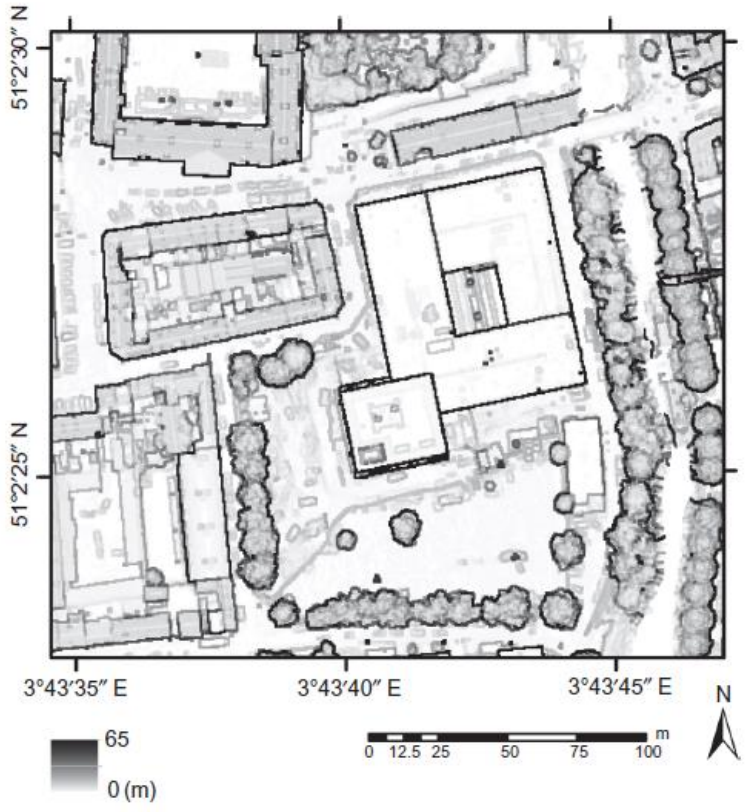

Figure 5-2: Sample of the morphological descriptor applied on the study area

As demonstrated in Table 5-2, the highest maximal height differences are located in the ‘Rectorate’ area. The lowest maximal height differences are located in the ‘Zuiderpoort’ area. These statements are based on the values of the maximal and mean height difference per kernel. This seems to correspond with the observation that the three areas differ from each other from an

urban morphological point of view. Besides, the geometrical properties are statistically different. The ratio F_s between the standard deviations of each separated area, calculated over all local kernels $(c_p , r_p \in w)$ per area, and the total study area has a maximum of 1.546, which is higher than the corresponding theoretical *F*-value $(F_s > F_{\infty,\infty} = 1)$. The fact that the experimental *F*-value is higher than the theoretical *F*-value states the inequality of variance of the study areas. Since the above statistics are calculated for the entire data sets, the degrees of freedom are taken at infinity and the standard deviations should be exactly equal to each other.

5.3. ***DSM extraction methodology***

5.3.1. DSMs generated from LiDAR data set

5.3.1.1. *Quality assessment of the LiDAR point set*

The quality of the LiDAR data has been checked by the AGIV. Important checks are executed by the creation of point density plots, as described by Kraus et al. (2006). Based on these plots, the average point density of 125 points m^{-2} has been calculated. The combination of perpendicular flight strips and an overlap of 77% made it possible to measure each object approximately four times and resulted in the absence of major occlusion zones on and near building façades. The altimetric and planimetric quality assessment of the point set is determined by defining a set of reference areas. In these areas, sets of 25 checkpoints are measured using the Real-Time Kinematic Global Navigation Satellite System (RTK GNSS). Predefined quality criteria were determined by the client concerning the mean error, standard deviation, Root Mean Square Error (RMSE), and skewness of the distribution of the difference between the LiDAR and RTK GNSS data. The criteria were set at a mean error of 0.06 m and an altimetric standard deviation of 0.09 m, including the accuracy of the RTK GNSS measurements of 0.03 m. Since the same RTK network solution calculation is used for the absolute referencing of the aerial images, an accuracy of these measurements of 0.03 m will be taken into account here. Experimental values of the mean altimetric error and altimetric standard deviation are, respectively, −0.02 and 0.03 m. Low values of the skewness of the distribution of residuals are noted for every reference area, indicating no significant errors.

For this research, the quality assessment of the vendor is complemented by an additional comparison of the LiDAR data with a set of secondary reference points (compaction points of the Flemish differential GNSS network). The resulting altimetric deviation between these reference points and the corresponding nearest LiDAR points equals −0.024 m, which is very low in comparison with the given range accuracy of 0.01 m and the RTK GNSS accuracy of 0.03 m. On behalf of these measurements, a Trimble R6 GPS system was used.

5.3.1.2. *DSM and DTM generation*

Methods to filter ground points and non-ground points from a point set acquired by airborne LiDAR are numerous. Many of these methods make use of the irregular – and possibly original – vector point set, where filtering is performed using a slope-based algorithm: by morphologic operators (Vosselman, 2000; Vosselman and Maas, 2001), by the analysis of a triangular irregular

network (TIN)(Krzystek, 2003), by point segmentation and region growing (Sithole and Vosselman, 2005), or by multiple-pass filtering (Bretar et al., 2004). It is also possible to generate a bare Earth model, based on rasterized point sets. Filtering ground and non-ground points on rasterized data sets can be performed by gross error analysis (Briese et al., 2002) or by analysing the difference between first and last pulse heights (Alharthy and Bethel, 2002). In this research, the LiDAR data were processed using Terrasolid software (www.terrasolid.fi), where Axelsson's TIN-based filtering is implemented (Axelsson, 2000; Coluzzi et al., 2011). The algorithm classifies ground and non-ground points using an iterative densification of a TIN and distance criteria.

The two surface models, based on photogrammetry and LiDAR, are compared to each other according to a pixel-based approach. This requires an interpolation of the LiDAR point data set to generate, respectively, a DSM and DTM for each zone. The Inverse Distance Weight (IDW) interpolator is applied for this purpose (Prathumchai and Samarakoon, 2006; Shephard, 1968). Especially when the point density is high in relation to the required resolution of the model, IDW is a proper method (Chaplot et al., 2006). The function for the interpolated elevation *h* of the cell in the c^{th} column and the r^{th} row in the model has the following form:

$$h_{cr} = \sum_{i=0}^{n} \frac{w_i h_i}{\sum_{i=0}^{n} w_i}$$

Equation 5-2: Calculation of the elevation *h* in cell *cr* using IDW

with h_i as the elevation value of the i^{th} point of a total set of points within a given distance d around the centre of the cell in the c^{th} column and the rth row, and with w_i as a weight for this point. In this research, a distance threshold of 2.5 m is used and the weight function is defined as the inverse of the square of the distance between this point and the centre of the cell (Chaplot et al., 2006). DSM and DTM are processed at a grid size of 0.5 m in the UTM system, using the WGS84 ellipsoid. The density of the original LiDAR point set becomes very clear after interpolation. The high point density and the angular configuration of the acquisition sensor result in a detailed representation of both the roofs and façades of buildings; in most cases, occluded areas, which are typical for conventional photogrammetry, are lacking. However, the point set only contains coordinates without information about the intensity of reflected light for the measured point.

5.3.2. DSMs generated from aerial photography

The DSM extraction process from aerial frame camera imagery is relatively well established and the core processing steps consist of the image orientation and image matching process. First, to improve the radiometry of the images, in particular texture in shadowed areas, a Wallis filter is applied (Wallis, 1976). The filter performs a non-linear, locally adaptive contrast enhancement, providing good local contrast on both ends of the dynamic range of grey values.

The aerial triangulation or bundle block adjustment process determines the mathematical relationship between the camera, 2D images, and 3D object space. The interior orientation, involving the relationship between camera and 2D image, is determined by the measurement of the fiducial marks on each image. The exterior orientation, involving the relationship between 2D image and 3D terrain, is established based on a set of ground control points (GCPs). The 3D GCPs are measured with a Trimble R6 GPS system in RTK mode with an accuracy of 0.03 m. Manhole covers are mainly chosen as GCPs as these are stable features over time and as their radiometry contrasts well with the surroundings. A homogeneous distribution of the GCPs over each study part is pursued (see Figure 5-1). However, this is not a straightforward task in a dense urban environment. Positions where a workable satellite constellation can be received and that are not located in an occluded area on both images of the stereo pair are rather rare due to the narrow streets and high-rise buildings, i.e. the so-called urban canyon problem (Cui and Ge, 2003). In Table 5-3, the accuracy of the image orientation process is tabulated. The residuals between an accurately measured position and a calculated position in the surface model are summarized for all GCPs in terms of an RMSE, for each of the three directions *x*, *y*, and *z*, planimetric Circular Error at 90% probability (CE90), and altimetric Linear Error at 90% probability (LE90).

Table 5-3: Geometric accuracy of the image orientation

		Ground control point residuals (m)				
	No. of GCP	*RMSX*	*RMSY*	*RMSZ*	*CE90*	*LE90*
Rectorate	8	0.031	0.033	0.106	0.074	0.186
Sint-Pietersplein	9	0.034	0.064	0.254	0.112	0.442
Zuiderpoort	11	0.032	0.040	0.114	0.082	0.196

The extracted orientation parameters allow us to calculate the position of the camera (X_0 , Y_0 , Z_0) and the rotation along each of the three main axes (ω, ϕ, κ) during image acquisition for each image individually, as well as the 3D ground coordinates for each image feature. Prior to surface model generation, the original images are resampled and rectified to an epipolar geometry based on the exterior orientation parameters of the block bundle adjustment process. Epipolar resampling or normalized image generation applies an affine transformation and aligns the images by a scaling, rotation, and translation in the *y*-direction, yielding the same geometric properties, enabling stereo vision, and enhancing matching.

The subsequent image matching process implies a description or reconstruction of the 3D environment based on 2D imagery. Image matching algorithms are able to automatically detect conjugate points or features in the images, so these corresponding points are projections of the same physical feature in object space. The surface model can be processed afterwards by calculation of the 3D position based on the measurement of the disparity or height parallax between corresponding pixels or features. The applied image correlation algorithm works according to a coarse-to-fine hierarchical matching strategy, with determination and fine-tuning of matching parameters, following a method proposed by Kanade and Okutomi (1994). The matching algorithm is in essence a combination of feature point, grid point, and 3D edge matching. The geometrically constrained cross-correlation or GC3 method (Zhang and Gruen, 2006), an extension of the standard cross-correlation technique, is used to identify possible

matching candidates. In a final stage, an extended Least-Squares Matching (LSM) method, called modified Multi-Photo Geometrically constrained (MPG) LSM, is performed using the redundant matched features as precise approximations to check consistency, to detect mismatches, and to further refine matching results. The MPGC algorithm combines the matched feature points, grid points, and 3D edges with geometrical constraints, derived from image ray intersection conditions, epipolar constraint, and knowledge about the image orientation. The algorithm is developed by Baltsavias (1991) and based on the LSM method described in Gruen (1985).

Each extracted surface model covers an area of approximately 0.4 km^2 . The DSMs are processed at a grid size of 0.5 m in the UTM system, using the WGS84 ellipsoid. The chosen resolution provides a dense 3D description of the covered surface and leads to the best equilibrium between sufficient detail and reduction of noise or information overload. Water bodies are masked out of the model, due to their complex nature, based on a user-clicked seed point and according to the seeded region growing procedure proposed by Adams and Bischof (1994). No manual correction or editing is applied on the generated DSMs. In Figure 5-3, a merge of the three DSMs is illustrated. Figure 5-4 contains a detailed view on the DSM, draped with the produced orthoimage.

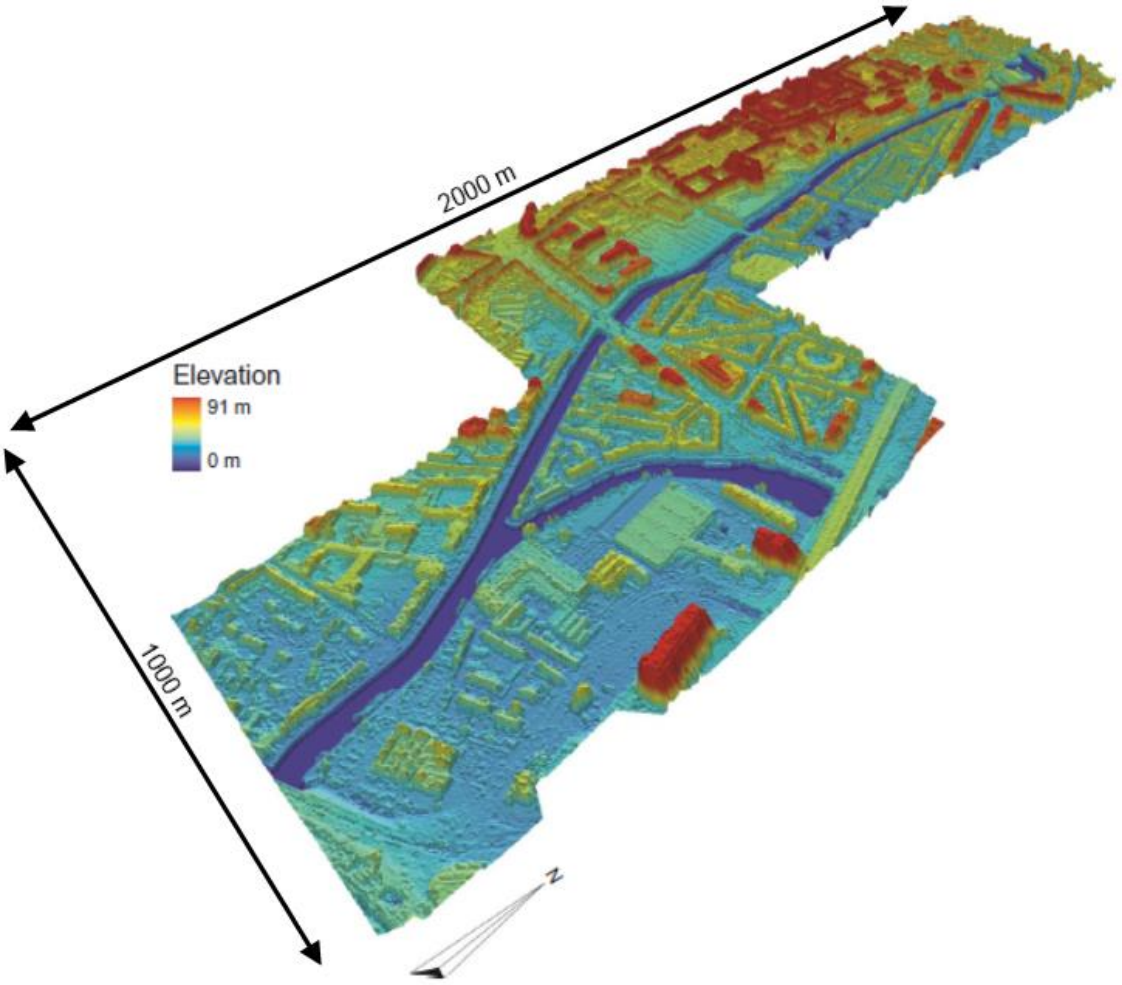

Figure 5-3: Perspective view on the 0.5 m colour-coded DSM extracted from the aerial imagery. The three adjacent test areas are merged

Figure 5-4: Extract of the surface model draped with produced orthoimage for photorealistic visualization (resolution: 0.5 m)

From a qualitative visual analysis, it can be observed that the terrain relief, topography, and street-house pattern are modelled veraciously and detailed. Building walls and roof structures are modelled quite accurately with mostly sharp edges. However, the approach is not robust in the entire data set. Especially in the dense urban core, e.g. the 'Rectorate' area, vertical building walls are curved due to the large presence of occlusion and building shadow. Occluded areas appear predominantly near vertical building walls of high-rise townhouses and apartment or office blocks due to the building displacement in the imagery. The effect of occlusion increases linearly with the building height and with the distance relative to the image acquisition point. Some flaws can be detected in the vicinity of dense vegetation, e.g. city parks. Also, small urban objects such as cars, fences, lamp posts, and other city furniture yield an elevation parallax and are experienced as noise in the model, i.e. a spike or blob.

5.3.3. DSM post-processing

5.3.3.1. *Occlusion modelling*

Occluded or concealed areas are the main source of noise, blunders, and flaws in the models. Photogrammetric theory argues that the projection of a given terrain point must be clearly visible in at least two images in order to extract relevant elevation information. Consequently, occluded areas cannot be matched. Hence, the occlusion phenomenon in the surface models, derived photogrammetrically from aerial imagery, is modelled. Occlusion is also present in but is less pronounced or even negligible due to the many overlapping flight strips in different directions. To quantify the occlusion, a standard ray tracing algorithm is applied on the three extracted models. The position of the camera (X_0 , Y_0 , Z_0) and the rotation along each of the three main axes $(\omega, \phi,$

κ) during image acquisition for each image individually is already calculated by the image orientation process. In zone 'Rectorate', 15.79% of the ground surface is occluded by buildings and other man-made features. Occlusion is, respectively, 12.54% and 11.31% for zone 'Sint-Pietersplein' and 'Zuiderpoort'. Occluded areas can be filtered from the models based on the generated occlusion mask.

5.3.3.2. *DSM noise reduction*

An edge-preserving smoothing filter is used to remove noise and unwanted local relief from the generated surface models, while preserving building discontinuities (Jacobsen, 2006). More specific, a small 5 x 5 median box filter is applied on the models. The filter changes the value of each pixel by looking at the surrounding pixels within the 5 x 5 moving window and by arranging all values in sequential order. Next, the 50th percentile value is assigned to the centre pixel. As the median value is assigned, the influence of unrepresentative pixels or outliers within the kernel will not affect the new pixel value significantly.

5.4. ***DSM comparability analysis***

5.4.1. Overall comparability of the DSMs

Before analysing the DSMs for each study area separately, the comparability between the photogrammetric model DSM_{PHG} and the LiDAR model DSM_{LiDAR} will be examined for the entire study area. The models are compared relatively to each other by pixel-wise differencing of the DSM values. The difference digital surface model (DSM_D) is the result of subtraction of the photogrammetric model from the LiDAR model and the pixel values represent differences in height between DSM_{LiDAR} and DSM_{PHG}.

First, the differences between both models are investigated for zones that are deemed not to have changed over the time interval t_2 - t_1 . Under ideal circumstances, the difference in height between the DSM generated by the photogrammetric process and by the LiDAR data processing should be zero for the non-changed areas. However, this is not the case for several reasons, such as modelling errors, occlusion, local relief induced by cars and other moving objects, changes in phenological state of vegetation, smoothing as a consequence of DSM interpolation, etc. Two point sets of each 100 samples are selected on the street level and roof level, respectively. The point samples are randomly distributed over exclusively unchanged zones. Statistical parameters for the height differences, extracted from DSM_D based on the point samples, are given in Table 5-4.

Table 5-4: Statistical measures for height differences extracted from DSM_{LiDAR} minus DSM_{PHG} based on a set of 100 points on street and roof levels, respectively. The point samples are randomly distributed over exclusively unchanged parts of the study area

	Descriptive statistics for a random set of points (m)					
	Min	*Max*	*Mean*	*St. Dev.*	*MAE*	*RMSE*
Street level	-0.221	0.974	0.195	0.252	0.199	0.318
Roof level	-0.924	0.809	0.146	0.320	0.293	0.351

Based on the calculated statistics, it appears that the elevation differences between both models do not significantly differ from zero in unchanged areas. The results indicate the comparability of the two produced DSMs. Then, descriptive statistics are calculated for the entire study area or for all pixels of DSM_D. Results are summarized in Table 5-5. Different thresholds, defined by a given maximal tolerated difference between the DSM_{PHG} and DSM_{LiDAR} , are applied to cut off the height differences. To interpret the statistical values, it is assumed that both DSMs are parallel and that also the height values in DSM_D are perpendicular to the reference plane.

Table 5-5: Statistical measures for DSM_{LiDAR} minus DSM_{PHG}

	Descriptive statistics for DSM_D (m)					
Threshold	*Min*	*Max*	*Mean*	*St. Dev.*	*MAE*	*RMSE*
no threshold	-43.2	58.3	1.199	5.777	2.722	5.901
25	-25.0	25.0	0.906	4.608	2.409	4.696
10	-10.0	10.0	0.242	2.631	1.504	2.642
5	-5.0	5.0	0.117	1.438	0.911	1.442
2.5	-2.5	2.5	0.121	0.823	0.580	0.832
2	-2.0	2.0	0.119	0.689	0.502	0.699
1.5	-1.5	1.5	0.111	0.547	0.416	0.558
1	-1.0	1.0	0.098	0.396	0.319	0.408
0.5	-0.5	0.5	0.076	0.233	0.204	0.245

The calculated standard deviation, Mean Absolute Error (MAE), and RMSE behave more or less linearly with respect to the threshold value. This is to be expected since higher thresholds enclose more noise and outliers. The statistics, especially at higher thresholds, show evidence of changes that have occurred during the time interval t_2 - t_1 , e.g. destructed and constructed objects. Based on Table 5-5, the mean and standard deviation are plotted against a given threshold value and illustrated in Figure 5-5. For threshold values lower than approximately 7.5 m, the mean error is not linear but stabilizes around a value of 0.11 m. As the height differences larger than 7.5 m can be considered as mainly multi-temporal changes between both models, a value of 0.11 m can be accepted as the systematic offset between the two models. In this particular case, DSM_{LiDAR} altimetric heights are bigger than DSM_{PHG} heights.

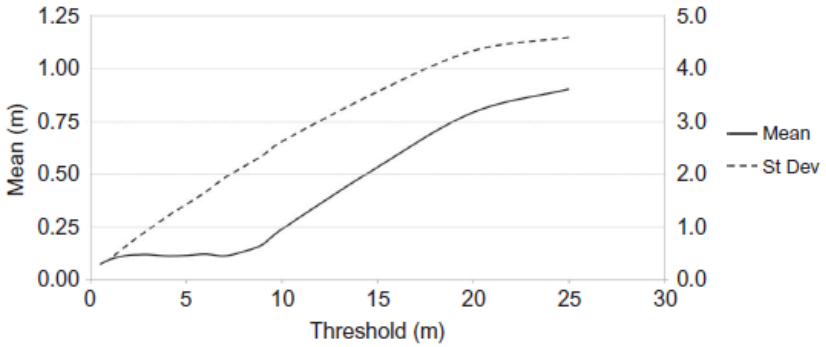

Figure 5-5: Plot of the mean and standard deviation (SD) against different threshold values for the height differences in DSMD

5.4.2. Comparability of the data for the different study areas

The differences between the data sets are evaluated for the three study areas by comparing each set with a random sample of 3D reference points. The 36 reference points are measured using RTK GNSS on the bare Earth at positions where no changes are assumed over the time interval t_2 - t_1 . The accuracy of this control set is 0.03 m, which is theoretically much higher than the accuracy of both photogrammetric and LiDAR data sets. The comparison itself is performed using a one-way ANalysis Of VAriance (ANOVA) (Kutner et al., 2005), where the ideal situation is formulated by the following null hypothesis (H_0), where all population mean elevation values μ of the different data sets are equal. The alternative hypothesis states that at least one population mean elevation is different from another study area:

$$H_0: \mu_{GPS} = \mu_{PHG} = \mu_{LiDAR} \text{ and } H_A: \textit{at least one } \mu \textit{ value is different from the rest}$$

Before performing the ANOVA, a test of homogeneity of variance is performed by calculating the Levene's statistic (Kutner et al., 2005). The corresponding Levene's statistic gives ($0.05 < p < 0.41$), which states the assumption of homogeneity of variance and allows further execution of the ANOVA.

The reference height points are compared with the corresponding height values from the DSM_{LiDAR} and DSM_{PHG} model per study area using ANOVA. The results of the ANOVA are given in Table 5-6. Based on the results in the table, the null hypothesis can be accepted with a 95% level of significance for each study area. The calculated F-values are smaller than the critical F-values, with a 95% confidence interval. This means that no significant difference can be detected between the DSM generated by photogrammetry, the LiDAR DSM, and the GNSS control set ($0.05 < p < 0.95$). In other words, DSM_{LiDAR} and DSM_{PHG} are statistically equal for all study areas.

Table 5-6: Results of the ANOVA, where the three different data sets or groups are compared with each other (SS is the sum of squares; *df* is the number of degrees of freedom; MS is the mean square, *F* is the *F*-value; *p* is the probability value; and *F*-crit is the critical *F*-value)

	ANOVA						
	Source of Variation	*SS*	*df*	*MS*	*F*	*p*	*F crit*
Rectorate	Between groups	11.588	2	5.794	0.080	0.923	4.403
	Within groups	1729.867	24	72.078			
	Total	1741.455	26				
Sint-Pietersplein	Between groups	9.441	2	4.721	0.071	0.931	3.316
	Within groups	1985.679	30	66.189			
	Total	1995.120	32				
Zuiderpoort	Between groups	1.380	2	0.690	0.636	0.537	3.316
	Within groups	32.576	30	1.086			
	Total	33.957	32				

5.5. *3D building change detection*

The multi-temporal data sets are investigated as to what extent 3D changes can be detected and modelled over the time interval t_2 - t_1. The emphasis is exclusively on 3D building changes. A human operator can easily detect and visually interpret the changes from an initial difference change map. However, this is a time-consuming and a not cost-effective task, especially if a big area needs to be analysed. Highly automated 3D building change detection and differentiation from noise, errors, and other off-terrain objects such as trees can be considered as a complex problem. An effective, automated 3D building change detection approach is introduced below. The fundamental steps of the approach are illustrated with a sample of the entire data set, i.e. the area where the new college campus 'Diamond tower' is established.

5.5.1. Thresholding difference map

The two surface models acquired at different instances of time t_1 and t_2 are compared to each other to detect and quantify 3D building changes. The applied change detector is based on a pixel-wise differencing of the DSM values (Lu et al., 2004; Radke et al., 2005):

$$DSM_D(c,r) = DSM_{LiDAR}(c,r) - DSM_{PHG}(c,r)$$

Equation 5-3: Calculation of the difference model by subtracting two DSMs

where DSM_D is the difference surface model, DSM_{LiDAR} is the LiDAR surface model acquired at t_2 , DSM_{PHG} is the photogrammetrically derived surface model acquired at t_1 , and *(c, r)* is the pixel or height value at column *c* and row *r*.

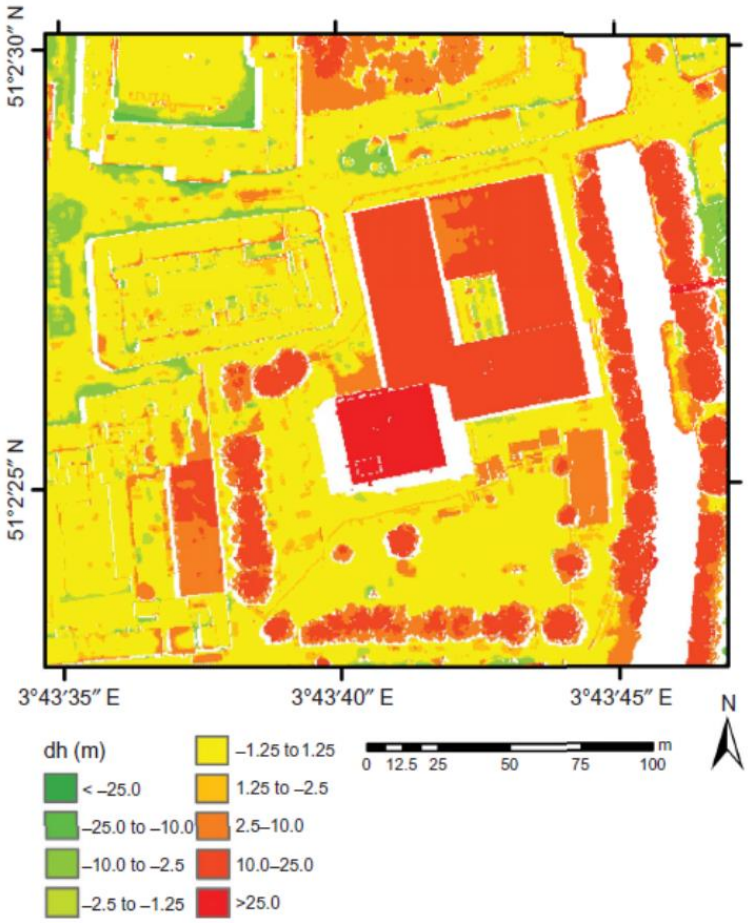

Figure 5-6: Sample of the difference DSMD between the LiDAR and photogrammetric surface models

The difference surface model not only highlights terrain-dependent 'real' changes over time t_2 - t_1, but also noise and modelling errors, as illustrated in Figure 5-6. For example, 3D points collected on cars and city furniture such as fences, lamp posts, and flower boxes induce local relief, spikes and pits, and are modelled differently in both DSMs depending on the characteristics and resolution of the particular acquisition method. Moreover, non-fixed objects such as cars are not located on the same place anymore over the time interval t_2 - t_1.

To differentiate unchanged parts, noise, errors, and 3D modelling deficiencies from real significant changes, DSMD needs to be thresholded. Determination of a suitable threshold to identify a significant real building change is based on the mean difference between DSM_{LiDAR} and DSM_{PHG} for both times and on contextual information, i.e. the legal minimum building floor height in the city of Ghent. Both values correspond with a threshold value T of 2.5 m.

$$DSM_D = \begin{cases} DSM_{D+}(c,r) & if \quad DSM_{LiDAR}(c,r) - DSM_{PHG}(c,r) \geq T \\ DSM_{D0}(c,r) & if \quad |DSM_{LiDAR}(c,r) - DSM_{PHG}(c,r)| < T \\ DSM_{D-}(c,r) & if \quad DSM_{LiDAR}(c,r) - DSM_{PHG}(c,r) \leq -T \end{cases}$$

Equation 5-4: Conditional decision tree for the identification of significant elevation differences

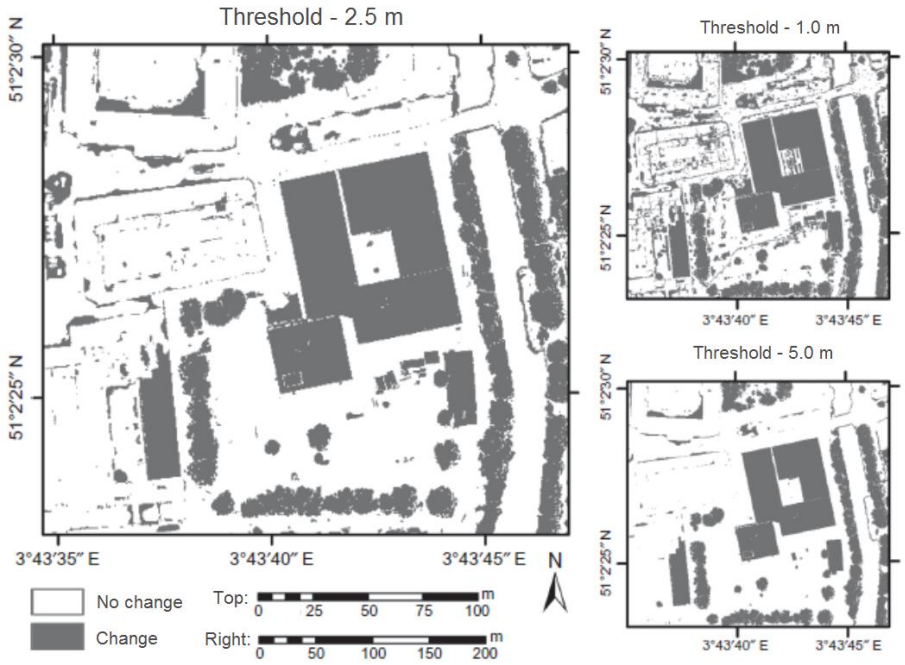

Figure 5-7: Thresholded binary change map. The effect of implementation of different thresholds is illustrated

The thresholded difference surface model DSM_D indicates signed changes in elevation, with positive values (DSM_{D+}) indicating building construction and negative values (DSM_{D-}) pointing at building destruction over time t_2 - t_1. The detected changes for the used threshold value of 2.5 m and the influence of this threshold value are illustrated in Figure 5-7 for the sample data set. In addition to the used threshold of 2.5 m, binary maps are also illustrated for less ideal thresholds. In the case of a low threshold of 1.0 m, too much noise is present in the change map. In the case of a high threshold of 5.0 m (parts of), changed buildings are not detected in the change map.

5.5.2. Building identification and differentiation

However, most model deficiencies and errors are removed, in addition to terrain-dependent changes over the time interval t_2 - t_1, thresholded still contains outliers and anomalies due to noise, model errors, model-specific characteristics, etc. Errors due to presence of vegetation and linear-shaped errors due to the bell-shaped reconstruction of buildings, caused by occlusions, are the most common types of 'false' changes. Below, filters are proposed to differentiate these false alarms from real building changes.

5.5.2.1. *Blunder filter*

Polyline-shaped false alarms and small islands still remain after thresholding the difference surface model DSM_D . The linear-shaped errors mainly occur in the dense urban core, parallel to the street network and the rows of connected houses. These errors are remains of the bell-shaped reconstruction of buildings in the model, caused by geometrical displacement, residual occlusion, height discontinuities, and shadow. To remove most of the linear artefacts and small clusters of pixels, a morphological filtering method can be applied as proposed by Chaabouni-Chouayakh et al. (2010). All filters in mathematical morphology are based on erosion and dilation, which are

performed over a neighbourhood specified by a moving window or structural element (Soille, 2003). Erosion and dilation are defined as follows:

$$[E_S(DSM_D)](c_p, r_p) = min\{w\}$$

Equation 5-5: Erosion filter for a cell *cr* in the difference model

and

$$[D_S(DSM_D)](c_p, r_p) = max\{w\}$$

Equation 5-6: Dilation filter for a cell *cr* in the difference model

where E_S is the erosion operator with the structural element S, D_S is the dilation operator with structural element S, DSM_D is the difference surface model, (c_p , r_p) is the centre pixel of the moving window, and w is the neighbourhood of (c_p , r_p), defined by the structural element.

A morphological opening operation is applied on DSM_D , which is defined by the function $D_S(E_S(DSM_D))$ and executes an erosion followed by dilation. The kernel is parameterized at 10 x 10 pixels, corresponding to 25 m^2 or the minimum area of a living room and kitchen for a household. After morphological filtering, most linear artefacts and insignificant clusters are removed from the change map (see Figure 5-8).

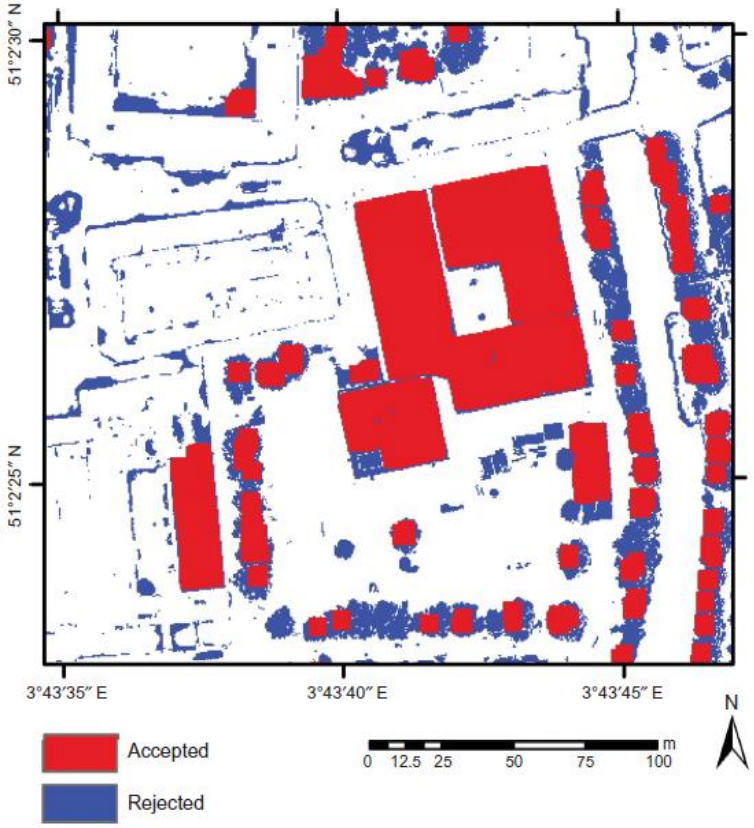

Figure 5-8: Blunder filter, removing linear artefacts, and insignificant clusters from the change map

5.5.2.2. *Vegetation filter*

The vegetation within the study area consists mainly of individual deciduous trees, gardens, and two small parks. Due to the alteration in the phenological state of the present vegetation over time t_2 - t_1 and seasonal effects, vegetation is modelled differently in DSM_{PHG} and DSM_{LiDAR} and results in the detection of 3D changes. The photogrammetrically derived surface model DSM_{PHG} is a winter acquisition, while DSM_{LiDAR} is acquired in the summer season. Mainly the large, freestanding deciduous trees are problematic, as they are not modelled in DSM_{PHG} due to reflectance of the ground surface. However, many 3D points are collected on the trees in DSM_{LiDAR}. To differentiate only the 3D building changes, vegetation needs to be classified and filtered out of the Difference Surface MoDel DSMD . Due to the lack of multispectral image data or Colour InfraRed (CIR) imagery, common vegetation classification based on the normalized difference vegetation index (NDVI) is not feasible (Rottensteiner et al., 2007). Also an Object-Based Image Analysis (OBIA) does not provide satisfying results (Blaschke, 2010). Due to the winter acquisitions of the imagery, most of the individual trees are not identified as vegetation in OBIA since the image pixels mainly contain the radiometry of the ground surface, visible through the tree branches.

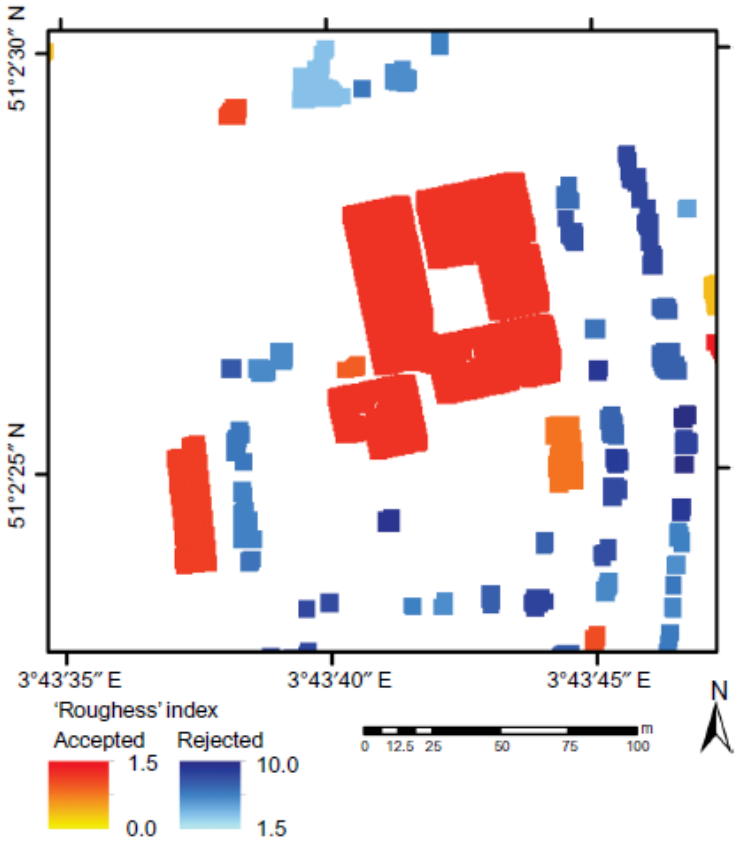

Figure 5-9: Differentiation of artificial objects from natural objects based on a roughness metric

In this research, a variant of a contrast filter is applied to differentiate artificial objects (e.g. buildings) from natural objects (e.g. trees) (Oude Elberink and Maas, 2000). The differences between local height contrast within artificial and natural objects are used to distinguish both, assuming that roofs of buildings mostly consist of planar or at least smooth surfaces. This

'roughness' metric will give irregular patterns for vegetation while measuring sharp shapes for buildings. The morphological or blunder filter, presented in the last paragraph, will result in regions of neighbouring cells, corresponding to changes. Regions will be grouped to clusters of cells, with no connection values between each separated cluster. For each cluster, the 'roughness' is calculated by the mean of all focal height contrasts within the cluster. The outcome of this operation is illustrated in Figure 5-9 for the sample data set, where red-coloured clusters correspond with artificial objects, i.e. buildings, and blue clusters correspond with natural objects, i.e. vegetation. The blue clusters, characterized by high roughness, are removed from the change map.

5.5.3. Polygon vector change map

Filtered DSM_D , indicating whether the elevation value of a pixel is changed over the time interval t_2 - t_1, can be subsequently converted into a polygon vector layer by applying polygon fitting on the different clusters of extracted pixels. Next, the polygons can be simplified according to a method based on Douglas and Peucker (1973). The line simplification method removes small fluctuations, extraneous bends, and redundant vertices from its boundary while preserving the essential shape. The resulting vector map consists of polygons indicating a building construction or destruction.

5.5.4. Final 3D building change model

The polygon vector change map can be applied to extract the height for the detected building changes. Elevation is extracted from DSM_{D+} in the case of construction and from DSM_{D-} in the case of destruction. The resulting 3D building change model is illustrated in Figure 5-10. For reasons of visualization, interpretation, and analysis, the changed buildings are merged with the DSM layer, which is draped with the orthoimage generated from the aerial image data set. Newly constructed buildings are reproduced in red colour, while demolished buildings are represented in blue. Quantification of the surface and volume of destructed and constructed buildings within the global study area is straightforward, based on the planimetric and altimetric dimensions of the detected 3D changes. According to the presented 3D change detection approach, approximately 21,725 m^2 or a volume of 281,504 m^3 is constructed over time interval t_2 - t_1, yet approximately 19,425 m^2 or 141,212 m^3 is destructed.

The resulting 3D building change model, illustrated in Figure 5-10, is assessed by visual analysis and a field comparison. The four most prominent changes within the study area are detected properly, i.e. a new office building in the south ('Zuiderpoort'), a student flat and college building in the centre ('Diamond tower'), and two new university buildings (Faculty of Economics and the Universiteitsforum or 'UFO'), respectively, in the centre and the north. Also smaller changes, such as individual single-family dwellings are detected properly in nearly all cases.

It must be mentioned that buildings need to be changed significantly (in height) to enable their detection. If a building is destructed and a new one is constructed on the same surface without any

change in volume, the building will not be detected by the presented approach. In some cases, an old building has been replaced by a construction covering a bigger surface, but not necessarily a bigger height. In such a case, only the parts of the new building that are raised on the non-built surface will be detected, resulting in sometimes odd-shaped polygons. This is, for example, the case for the 'UFO' building. Destructed buildings, such as a large hangar in the south and some dwellings in the neighbourhood of the Faculty of Economics, are detected and modelled correctly as well. However, there is a slight overestimation of destructed objects, due to remaining occlusion zones and some trees that could not be filtered out. Such false alarms occur, for example, in the patio of Saint Peter's abbey. In this case, the erroneously detected changes fall within the criteria of a height difference of 2.5 m and area difference of 25 m^2.

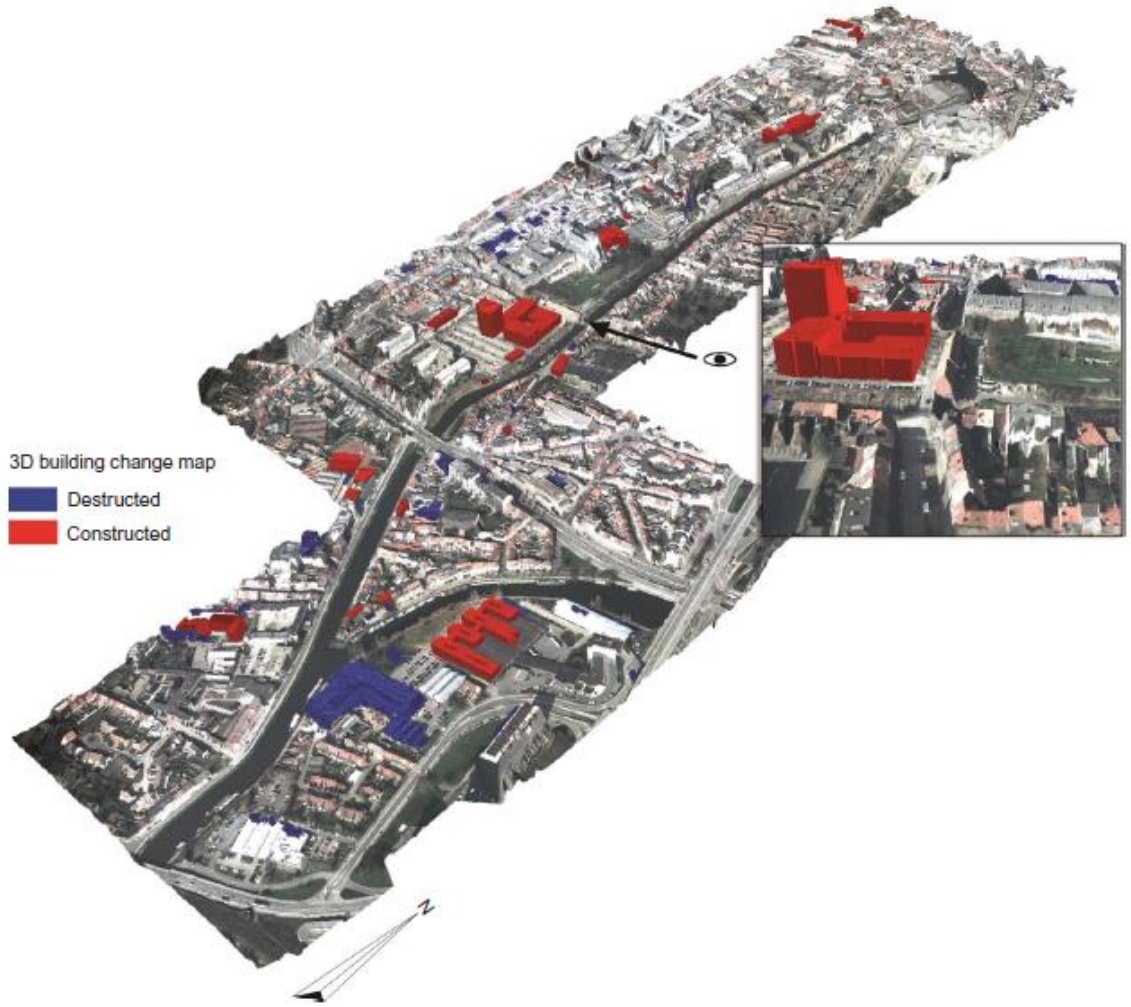

Figure 5-10: Final 3D building change model for the global study area in perspective view with a zoom on the 'Diamond tower' area. The detected building changes are draped on the DSM and orthoimage, generated from the aerial imagery

To illustrate the robustness of the 3D change detection approach, it is interesting to mention that a funfair took place on Saint Peter's square at the moment of the acquisition of the aerial images, while the square was empty during the LiDAR acquisition. As demonstrated in the final 3D change model, many of the fairground attractions are detected as destructed objects.

5.6. *Conclusion and discussion*

In the presented research, DSMs are generated from both stereo aerial imagery and ALS data. This is done for three adjacent areas, characterized by varying urban morphology. Notwithstanding the fundamental differences between the study areas, the resulting surface models of both approaches are highly comparable in a qualitative and quantitative/statistical way for all zones (see Section 5.4, concerning the DSM comparability analysis). Baltsavias (1999) and Asal, et al. (2000) already stated that, although LiDAR and photogrammetry are different measurement systems, results can be strikingly comparable. The techniques have the potential to be highly complementary in terms of degree of detail, coverage size, necessity for spectral information, etc.
The results from both approaches are clearly suitable in terms of quality and accuracy to model an urban environment and for veracious 3D reconstruction of individual buildings or building blocks and other urban features. However, the indirect derivation of elevation data, based on image matching and parallax measurements, usually exhibits more noise and larger blunders than observed in raw LiDAR data. The projection of the three-dimensional urban environment on a 2D image plane invariably causes distortions and information loss, e.g. occlusion, shadow, image displacement, and edge smoothing due to interpolation near discontinuities. This hampers the 3D photogrammetric reconstruction.

Visual analysis of the results from the 3D change detection approach points out that even with the generation of an occlusion mask, a substantial amount of occluded areas is still present in DSM_{PHG}. Occlusion is most present in zone 'Rectorate' due to the high building density, high-rise townhouses, and narrow streets. The effects of occlusion and other distortions, present in DSM_{PHG}, could be reduced in future research by photogrammetric processing of multiple overlapping images instead of processing stereo pairs. A multiscopic approach can drastically reduce the amount of occlusion and subsequent flaws in DSM modelling (Tack et al., 2012). In addition to the comparison of both acquisition techniques, an effective 3D building change detection approach is introduced. The emphasis focuses primarily on 3D building changes. The investigated and described methodology for extracting 3D building changes is highly automated and is able to yield a 3D building change model for any input of two multi-temporal DSMs. The different parameters can be set by an operator, depending on the quality of the DSMs, the type of study area, and the applicable construction permit regulations. The 3D change detection workflow is schematized in Figure 5-11. The semi-automatic approach can drastically reduce the amount of human intervention for applications such as the updating of building databases or the monitoring and modelling of urban growth.

DSM errors, model noise, lack of quality, and insufficient detail or low spatial resolution have a significant impact on the accuracy and performance of the change detection approach. Filtering of the initial difference surface model DSM_D is unavoidable in case of an automatic approach to differentiate 'real' building changes from false alarms. However, if the quality of the input DSMs is low, thresholds for the filters have to be set high to filter out most of the model errors. Consequently, also small 'real' building changes will be rejected from the change model. In the presented case study, this will happen when the height difference of the changed building is

smaller than 2.5 m and the area difference is smaller than 25 m^2. Both models, generated in the context of this research, are of high quality and allowed to set the thresholds relatively low. Small buildings can still be detected, without a large presence of false alarms in the 3D change model. The robustness of the 3D change detection approach is illustrated with the example of the detected fairground attractions on Saint Peter's square. We also expected to detect small structural changes in backyards, such as newly constructed (illegal) barns and garden houses. However, due to the coverage of mostly large trees, this was not the case.

At present, dense LiDAR data sets are scarce and mostly they consist of small coverage. Systematic acquisitions with regional or global coverage, as existing for aerial and satellite image data sets, are not available for LiDAR. However, with technological advances, we can expect an increase of LiDAR acquisitions with higher coverage in the (near) future.

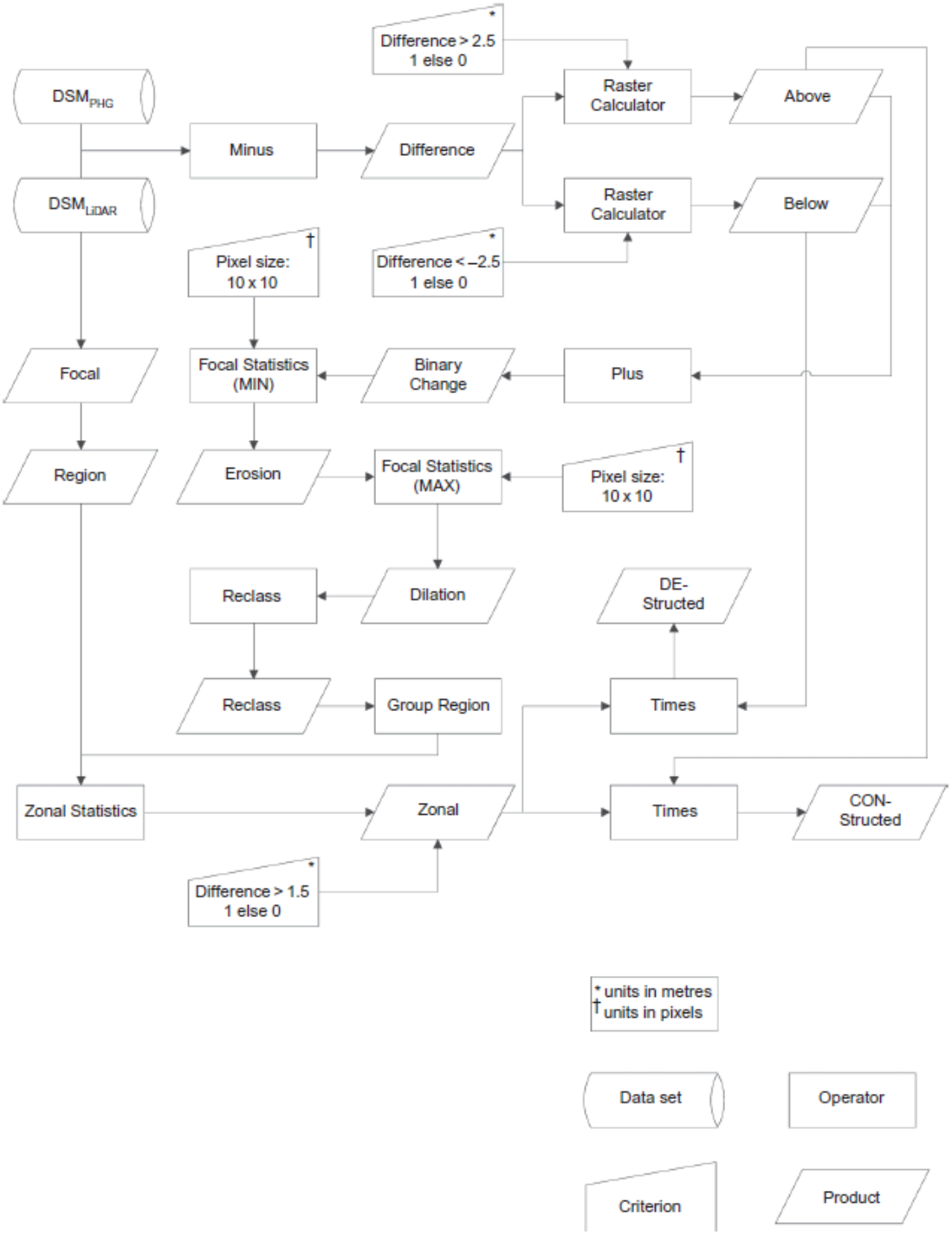

Figure 5-11: 3D change detection workflow

Most likely, this will elevate 3D change detection studies of urban areas to the forefront of research.

Acknowledgements

The Belgian Science Policy Office (BELSPO) and the Research Foundation Flanders (FWO) are gratefully acknowledged for funding the work presented in this article. The authors would like to express their gratitude to the Flemish Geographical Information Agency (AGIV) for providing the aerial image data and the municipality of Ghent for the LiDAR data.

References

Adams, R., Bischof, L., 1994. Seeded region growing. Pattern Analysis and Machine Intelligence 16 (6), 641-647

Alharthy, A., Bethel, J., 2002. Heuristic filtering and 3D feature extraction from LiDAR data. International Archives of Photogrammetry and Remote Sensing 34 (Part A+B3), 29-34.

Asal, F., Smith, M., Priestnall, G., 2000. Combining LiDAR and photogrammetry for urban and rural landscape studies. International Archives of Photogrammetry and Remote Sensing 33 (B3), 44-50.

Axelsson, P., 2000. DEM generation from laser scanner data using adaptive TIN models. International Archives of Photogrammetry and Remote Sensing 33 (B4), 111-118.

Baltsavias, E., 1991. Multiphoto geometrically constrained matching, Institute of Geodesy and Photogrammetry. ETH, Zurich, Switzerland, p. 221

Baltsavias, E., 1999. A comparision between photogrammetry and laser scanning. ISPRS Journal of Photogrammetry and Remote Sensing 54 (2-3), 83-94.

Baltsavias, E., Gruen, A., 2003. Resolution convergence: a comparison of aerial photos, LiDAR and IKONOS for monitoring cities, in: Mesev, V. (Ed.), Remotely-Sensed Cities. Taylor & Francis, London, pp. 47-82.

Berthod, M., Gabet, L., Giraudon, G., Lotti, J., 1995. High-resolution stereo for the detection of buildings, in: Gruen, A., Kuebler, P., Agouris, P. (Eds.), Automatic Extraction of Man-Made Objects from Aerial and Space Images. Birkhäuser Verlag, Basel, Switserland, pp. 135-144.

Blaschke, T., 2010. Object based image analysis for remote sensing. ISPRS Journal of Photogrammetry and Remote Sensing 65 (1), 2-16.

Böhler, W., V., B., Marbs, A., 2003. Investigating laser scanner accuracy. International Archives of Photogrammetry and Remote Sensing 34 (Part 5), 696–701.

Bretar, F., Chesnier, M., Pierrot-Deseilligny, M., 2004. Terrain modeling and airborne laser data classification using multiple pass filtering. International Archives of Photogrammetry and Remote Sensing and Spatial Information Sciences 35 (part B), 314–319.

Breunig, M., Zlatanova, S., 2011. 3D geo-database research: retrospective and future directions. Computers & Geosciences 37 (7), 791-803.

Briese, C., Pfeifer, N., Dorninger, P., 2002. Applications of the robust interpolation for DTM determination. International Archives of Photogrammetry and Remote Sensing 34 (Part A), 55-61.

Chaabouni-Chouayakh, H., Krauss, T., d'Angelo, P., Reinartz, P., 2010. 3D change detection inside urban areas using different digital surface models. International Archives of Photogrammetry, Remote Sensing and Spatial Information Sciences 38 (Part B3), 86-91.

Chaplot, V., Darboux, F., Bourennane, H., Leguédois, S., Silvera, N., Phachomphon, K., 2006. Accuracy of interpolation techniques for the derivation of digital elevation models in relation to landform types and data density. Geomorphology 77 (1-2), 126-144.

Coluzzi, R., Masini, N., Lasaponara, R., 2011. Flights into the past: full-waveform airborne laser scanning data for archaeological investigation. Journal of Archaeological Science 37 (9), 2061-2070.

Cui, Y., Ge, S., 2003. Autonomous Vehicle Positioning with GPS in Urban Canyon Environments. IEEE Transactions on Robotics and Automation 19 (1), 15-25.

Douglas, D., Peucker, T., 1973. Algorithms for the reduction of the number of points required for represent a digitized line or its carricature. Canadian Cartographer 10 (2), 112-122.

Förstner, W., 1999. 3D-city models: automatic and semiautomatic acquisition methods, in: Fritsch, D., Spiller, R. (Eds.), Photogrammetric Week '99. Wichman Verlag, Heidelberg, Germany, pp. 291-303.

Gabet, L., Giraudon, G., Renouard, L., 1997. Automatic generation of high resolution urban zone digital elevation models. ISPRS Journal of Photogrammetry and Remote Sensing 52 (1), 33-47.

Gehrke, S., Morin, K., Downey, M., Boehrer, N., Fuchs, T., 2010. Semi-global matching: an alternative to LiDAR for DSM generation? International Archives of Photogrammetry, Remote Sensing and Spatial Information Sciences 38 (1), 6 (on CD-ROM).

Gruen, A., 1985. Adaptive least squares correlation: a powerful image matching technique. South Africa Journal of Photogrammetry, Remote Sensing and Cartography 14 (3), 175-187.

Haala, N., Kada, M., 2010. An update on automatic 3D building reconstruction. ISPRS Journal of Photogrammetry and Remote Sensing 65 (6), 570-580.

Jacobsen, K., 2006. Digital surface models of city areas by very high resolution space imagery, EARSeL Workshop of the SIG Urban Remote Sensing, Berlin, Germany, pp. 10 (on CD-ROM)

Kanade, T., Okutomi, M., 1994. A stereo matching algorithm with an adaptive window: theory and experiment. Pattern Analysis and Machine Intelligence 16 (9), 920-932.

Kolbe, T.H., Gröger, G., Plümer, L., 2005. CityGML: interoperable access to 3D city models, First International Symposium in Geo-Information for Disaster Management. Springer Verlag, Delft, the Netherlands, pp. 883–899

Kraus, K., Karel, W., Briese, C., Mandlburger, G., 2006. Local accuracy measures for digital terrain models. The Photogrammetric Record 21 (116), 342-354.

Krzystek, P., 2003. Filtering of laser scanning data in forest areas using finite elements. International Archives of Photogrammetry and Remote Sensing 34 (3), 6 (on CD-ROM).

Kutner, M., Nachtsheim, C., Neter, J., Li, W., 2005. Applied linear statistical models. McGray-Hill, New York, NY, USA.

Lu, D., Mausel, P., Brondizio, E., Moran, E., 2004. Change detection techniques. ISPRS Journal of Photogrammetry and Remote Sensing 25 (12), 2365-2401.

Oude Elberink, S., Maas, H., 2000. The use of anisotropic height texture measures for the segmentation of airborne laser scanner data. International Archives of Photogrammetry and Remote Sensing 33 (Part B3), 678-684.

Prathumchai, K., Samarakoon, L., 2006. Elevation surface interpolation of point data using different techniques: a GIS approach, in: Saandar, M. (Ed.), Asian Association on Remote Sensing, Ulaanbataar, Mongolia, p. 6

Radke, R., Andra, S., Al-Kofahi, O., Roysam, B., 2005. Image change detection algorithms: a systematic survey. IEEE Transactions on Image Processing 14 (3), 294-307.

Rigo, G., Parlow, E., 2007. Modelling the ground heat flux of an urban area using remote sensing data. Theoretical and Applied Climatology 90 (3-4), 185-199.

Rottensteiner, F., Trinder, J., Clode, S., Kubik, K., 2007. Building detection by fusion of airborne laser scanner data and multi-spectral images: performance, evaluation and sensitivity analysis. ISPRS Journal of Photogrammetry and Remote Sensing 62 (2), 135-149.

Shephard, D., 1968. A two-dimensional interpolation function for irregular spaced data, ACM National Conference, New York, USA, pp. 517 - 524

Sithole, G., Vosselman, G., 2005. Filtering of airborne laser scanner data based on segmented point clouds. International Archives of Photogrammetry and Remote Sensing 36 (3), 66–71.

Soille, P., 2003. Morphological image analysis: principles and applications, 2nd Edition ed. Springer-Verlag, New York, NY, UAS.

Stal, C., Bourgeois, J., De Maeyer, P., De Mulder, G., De Wulf, A., Goossens, R., Nuttens, T., Stichelbaut, B., 2010. Kemmelberg (Belgium) case study - comparison of DTM analysis methods for the detection of relicts from the First World War, 30th Annual EARSeL Symposium, Paris, France, pp. 66-72

Tack, F., Goossens, R., Buyuksalih, G., 2012. Assessment of a photogrammetric approach for urban DSM extraction from tri-stereoscopic satellite imagery. The Photogrammetric Record 27 (139), 293-310.

Vosselman, G., 2000. Slope based filtering of laser altimetry data. International Archives of Photogrammetry and Remote Sensing 33 (B3), 935-942.

Vosselman, G., Maas, H., 2001. Adjustment and filtering of raw laser altimetry data, OEEPE workshop on Airborne Laserscanning and Interferometric SAR for Detailed Digital Elevation Models, 1-3 March, 40, Stockholm, Sweden, pp. 11 p. (on CD-ROM)

Wallis, R., 1976. An approach to the space variant restoration and enhancement of images, Symposium on Current Mathematical Problems in Image Science, Monterey, California, pp. 641-662

Weidner, U., Förstner, W., 1995. Towards automatic building extraction from high-resolution digital elevation models. ISPRS Journal of Photogrammetry and Remote Sensing 50 (4), 38-49.

Zhang, L., Gruen, A., 2006. Multi-image matching for DSM generation from IKONOS imagery. ISPRS Journal of Photogrammetry and Remote Sensing 60 (3), 195-211.

Chapter 6

Classification of airborne laser scanning point clouds based on binomial logistic regression analysis

6. Classification of airborne laser scanning point clouds based on binomial logistic regression analysis[6]

Abstract

This article presents a newly developed procedure for the classification of airborne laser scanning (ALS) point clouds, based on binomial logistic regression analysis. By using a feature space containing a large number of adaptable geometrical parameters, this new procedure can be applied to point clouds covering different types of topography and variable point densities. Besides, the procedure can be adapted to different user requirements. A binomial logistic model is estimated for all a priori defined classes, using a training set of manually classified points. For each point, a value is calculated defining the probability that this point belongs to a certain class. The class with the highest probability will be used for the final point classification. Besides, the use of statistical methods enables a thorough model evaluation by the implementation of well-founded inference criteria. If necessary, the interpretation of these inference analyses also enables the possible definition of more sub-classes. The use of a large number of geometrical parameters is an important advantage of this procedure in comparison with current classification algorithms. It allows more user modifications for the large variety of types of ALS point clouds, while still achieving comparable classification results. It is indeed possible to evaluate parameters as degrees of freedom and remove or add parameters as a function of the type of study area. The performance of this procedure is successfully demonstrated by classifying two different ALS point sets from an urban and a rural area. Moreover, the potential of the proposed classification procedure is explored for terrestrial data.

6.1. *Introduction*

Airborne laser scanning (ALS) is a popular 3D data acquisition technique for urban and rural environmental modelling (Doneus et al. 2008; Oude Elberink and Vosselman 2011; Stal et al. 2013). It allows the measurement of a 3D point cloud that represents the area of interest, by irradiating it with a laser beam from an airborne platform (Baltsavias 1999). One of the main requirements when dealing with an ALS point cloud is an accurate and efficient point classification or filtering (Briese 2010; Pfeifer and Mandlburger 2008). Classification, on the one hand, is the process where points are assigned to a certain class based on common properties. Filtering, on the other hand, also involves classification of a point cloud, but points that do not meet certain requirements are then removed. Using ALS sensors, the backscatter of the laser signal can occur on either ground or non-ground objects, resulting in a single point per transmitted signal. Moreover, due to the laser beam footprint size, several objects at different distances may contribute to the echo waveform (e.g. by the canopy of a tree and the underlying ground). In this case, it is useful to distinguish first, second, … echoes. Since point sets are frequently simply a large list of point coordinates without further attributes, most classification algorithms are

[6] Modified from: Stal, C., Briese, C., De Maeyer, P., Dorninger, P., Nuttens, T., Pfeifer, N. & De Wulf A. (2013) Classification of airborne laser scanning point clouds based on binomial logistic regression analysis, *International Journal of Remote Sensing*, *35* (9), 3219-3236.

typically based on geometrical properties. However, advanced full-waveform ALS sensors offer the potential to analyse the digitized backscatter signal, taking into account the different backscatter echoes (Wagner et al. 2006). This allows the extraction of further parameters per echo detected. In many cases, only a bare-earth model is required for further analysis, which only requires the separation of terrain and non-terrain points (Kraus and Pfeifer, 1998). After classification of the point cloud into these two classes, the resulting terrain points can be used for construction of a digital terrain model (DTM).

An overview and comparison of different ground point extraction algorithms is presented by Sithole and Vosselman (2004) and Chen et al. (2013). These authors suggest different types of point classification methods, for example based on either the assumptions about a point and its neighbourhood or the used segmentation or clustering procedure. According to the assumptions about a point and its neighbourhood, recent classification algorithms can apply mathematical morphology (Mongus and Žalik 2012; Li 2013), surface roughness analysis (Höfle et al. 2009), local slope analysis using distance thresholds (Meng et al. 2009), or surface-based robust interpolation (Briese, Pfeifer, and Dorninger 2002). Based on the segmentation used or clustering procedure, a distinction can be made between procedures using feature spaces and correspondence with best-fitting planes (Dorninger and Pfeifer 2008) and those using geometrical clustering analysis of neighbourhood properties (Bartels and Wei 2010). Sampath and Shan (2010) distinguish two other types of hierarchical segmentation or clustering, differing in the initial phase of the procedure. The first, agglomerative hierarchical clustering, assigns every point to a separate cluster, and different points or clusters are merged based on common properties. Divisive hierarchical clustering starts with one cluster containing all points and iteratively splits this cluster into smaller clusters.

As mentioned above, most of the classification algorithms discussed here concern the distinction of ground points and non-ground points. Ten years after the publication of Sithole and Vosselman (2004), a large number of bare-earth extraction algorithms have been implemented in freely available software (Podobnikar and Vrečko 2012). Some of these classifiers are also expanded to the extraction of other features from the point cloud. A typical example where point cloud classification is indispensable is in building reconstruction for city modelling (Brenner 2005). For this type of application, the development of reliable classifiers and filtering techniques is an ongoing area of research, especially for the detection of multiple classes (Xu, Oude Elberink, and Vosselman 2012; Chen et al. 2013).

Addressing this need for multiple class detection, this article presents a new classification procedure for ALS data, based on binomial logistic regression (BLR) analysis. Rather than implementing a binary classifier, the probability of a point belonging to different classes is calculated. For each point an extensive feature space is determined, containing a large number of geometrical parameters. Additionally, a training set is defined containing a certain number of manually classified points. This training set is used as a ground truth for the regression analysis, resulting in a logistic model for each class. The estimated regression parameters are thus based on feature space parameters and will determine the probability of a point belonging to a certain class. The procedure can be summarized in the following steps:

(1) Determine the feature space for each point;
(2) Generate a training data set for model learning and ground truth;
(3) Evaluate the multicollinearity of the parameters;
(4) Estimate the model parameters by using BLR;
    (a) Are the separate parameters significant?
    (b) Is the model significant as a whole?
(5) Use the parameters in a logistic model to evaluate the different class probabilities and to classify the points.

The large number of features in the feature space is an important advantage of this classification procedure, since the most distinctive parameters can be selected based on statistical inference. The number of classes and the way these classes are defined depend on the definition of the training set and are therefore user controlled. The size of the feature space is not a significant restriction, bearing in mind the increasing level of performance of processing computers.

The main concepts of BLR, parameter estimation, and prior assumptions for using this statistic analysis are discussed in Section 2. The concepts presented are then applied to two different data sets, as explained in Section 3. Thereafter, the results are illustrated and discussed in Section 4, with a special focus on statistical inference and quality parameters. A performance analysis and comparison between our results and the results of the classifier of LAStools (Isenburg and Shewchuk 2013) and the Multiscale Curvature Classification (MCC (Evans and Hudak 2007)) is also presented here.

6.2. ***Binomial logistic regression***

6.2.1. Principles of binomial logistic regression

The classification of ALS-based point clouds should result in the assignment of a class label for each individual point. Current classification techniques make use of one or a limited number of geometrical neighbourhood parameters and are often limited to a fixed number of defined classes, as with LAStools and MCC. Frequently, ground and non-ground point filtering is performed, followed by further classification of more specific point classes. As a Boolean decision, a point is typically assigned to a specific class if this point fulfils one or more predefined geometrical criteria. This article however, is built upon the idea of the calculation of the probability of membership of a point for all possible classes. Given a point set **P** with each point p_i in 3D space, with $p_i = (x_i, y_i, z_i) \in \mathbf{R}^3$, $i = 1, \ldots, n$, Y_{ij} is the probability that each point i belongs to class j, with $j = 1, \ldots, m$ classes. If this probability, or class membership, can be calculated for each point and every available class, a point will be assigned to a certain class based on the largest significant probability. This classification process is based on and evaluated by the use of statistical inference methods.

The probability that a point belongs to a certain class suggests that the response variable Y_{ij} is binary, following a binomial distribution. The outcome of this variable is an independent Bernoulli random variable with $Yij = E\{Y_{ij}\} + \varepsilon_j = \pi_{ij}$. Here, π_{ij} is the logit of the estimated posterior probability and ε_j is an error term for a given class j. The relation between a point and its

parameters to this probability can be described by a multiple logistic response function (Flury 1997):

$$E\{Y_{ij}\} = \pi_{ij} = \frac{exp(\boldsymbol{X}_i\boldsymbol{\beta}_j)}{1 + exp(\boldsymbol{X}_i\boldsymbol{\beta}_j)}$$

Equation 6-1: Multiple logistic response function

$\boldsymbol{X_i}$ is a known predictor vector for point i, and β_j is the regression coefficient vector of class j. The vector β_j contains p elements β_p, defining the feature space of class j. π_{ij} is thus calculated by a linear function of the regression coefficient vector β_j. Each parameter in this vector corresponds to a feature in the feature space, which is calculated for each point based on the large number of geometrical parameters. Variables in bold type represent vectors, and scalar values are presented in non-bold type.

6.2.2. Feature space definition

As discussed above, the main principle for the use of logistic regression in point classification is the construction of a feature space. For each point in the point set, a feature space is calculated using OPALS (Orientation and Processing of Airborne Laser Scanning, http://www.ipf.tuwien.ac.at/opals). OPALS is a software package providing a complete processing chain for large ALS data sets. It is a series of modules with clearly defined functions using an efficient point manager (ODM, OPALS Data Manager (Mandlburger et al. 2009; Otepka, Mandlburger, and Karel 2012)). Modules that enable the calculation of normal vectors and local neighbourhood descriptors are used. Moreover, manual functions are defined and also echo ratio functions are used. The feature space contains the following parameters:

$$\boldsymbol{p_i} = \textbf{(}\boldsymbol{X,Y,Z}\textbf{, Class, }\boldsymbol{n\sigma 0}\textbf{, n\#ptsG , n\#ptsU, }\boldsymbol{\lambda_1, \lambda_2, \lambda_3, \varphi, \theta, \lambda_n}\textbf{, Range, Mean, Var, RMS, PCount, Rank, EchoRatio}\}_i$$

- X, Y, Z = 3D position of a single point;
- Class = the predefined class assigned to this point, possibly assigned at training set definition stage, otherwise ignored;
- $n\sigma 0$ = standard deviation of the least square fitted local plane;
- n#ptsG = number of points within the neighbourhood;
- n#ptsU = number of points within the neighbourhood used for feature space calculation;
- λ_1, λ_2, λ_3 = eigenvalues of the covariance matrix subscribing the set of points in a neighborhood;
- $\varphi = acos(n_z)$ = arccosine of the z-direction of the normal vector;
- $\theta = atan(n_x / n_y)$ = arctangent of the ratio of the planimetric component of the normal vector (Filin, 2002);
- $\lambda_n = \lambda_1 / (\lambda_1 + \lambda_2 + \lambda_3)$ = normalized eigenvalue or surface curvature;
- Range = $z_{max} - z_{min}$ = difference between minimal and maximal elevation within a neighbourhood;
- Mean = $1/n \, \Sigma_{n,i=1}(z_i)$ = averaged elevation within a neighbourhood;

- Var = $1/n \, \Sigma_{n,i=1}(z_i\text{-}mean)^2$ = variance of the elevation within a neighbourhood;
- RMS = $sqrt(1/n \, \Sigma_{n,i=1}(z_i\text{-}mean)^2)$ = root mean square of the elevation within a neighbourhood;
- PCount = number of valid points within a cell;
- Rank = quartile rank;
- Slope adapted echo ratio (Höfle et al. 2009).

The advantage of the use of the parameters φ, θ, and λ_n is that it enables the delineation of a local surface in 3D (Filin 2002). Many parameters are calculated as a function of a particular neighbourhood definition. The size of this neighbourhood can be defined by a number of points, or an Euclidean metric. In both cases, the point density of the point cloud plays an important role. For most parameters, the neighbourhood is defined as a sphere of radius equal to twice the squared point density. In some cases, the distance to an estimated local tangent plane is taken, rather than the Euclidian distance to a central point. The slope-adaptive neighbourhood definition is important for inter alia normal calculation of rough surfaces with abrupt elevation shifts (Filin and Pfeifer 2005), which is subsequently essential for slope-based building segmentation (Dorninger and Pfeifer 2008).

6.2.3. Underlying assumptions of logistic regression

Before implementing logistic regression analysis for the estimation of class membership probabilities, two assumptions should be considered, namely multivariate normal distribution and multicollinearity of the data. The assumption of a multivariate normal distribution suggests that all separate predictors used for the logistic regression analysis are normally distributed. However, this is not confirmed by the multivariate central limit theorem, since the variables are derived from a point cloud and are not necessarily independent. Although the sample size is fairly large, the distributions of the different predictors are not identical. This is mainly caused by the nature of the predictors, as demonstrated later in this article. The assumption of multivariate normal distribution is therefore not met and the results of the regression will have to be evaluated carefully using the multicollinearity criteria.

In order to meet the assumption of data multicollinearity, a certain predictor should not be a function of one or more other predictors. The assumption deals with variable independence and this could be detected by calculating the 'Variance Inflation Factor' (VIF) for each regression coefficient. The VIF provides a measure for the relation between the variance of an estimated regression coefficient and the degree of collinearity (Stine 1995), and can be calculated by:

$$VIF = \frac{1}{1 - R_p^2}$$

Equation 6-2: VIF for the evaluation of the degree of collinearity

R^2_p is the coefficient of determination of parameter *p* as response variable; all other variables are predictors of the parameter *p* in a linear regression model. A threshold of 10 or 5 is frequently used to determine whether a certain coefficient is causing problematic collinearity in the model, and thus if the coefficient and accompanying parameter will be retained in the analysis. However, dropping a predictor from the model with a high VIF is only possible if it can be theoretically motivated (e.g. removing the variable 'standard deviation' when the variable 'variance' is also present in the data (O'Brien 2007)). In order to minimize the collinearity effect of the parameters in the model, a stepwise coefficient removal is suggested. In each step, a VIF is calculated for each coefficient.

6.2.4. Regression coefficient vector

In contrast with linear regression, the coefficient vector of a logistic response model cannot be found by a closed-form expression that maximizes the likelihood function. The log-likelihood function for logistic regression has the following form (Kutner et al. 2005):

$$\ln L(\boldsymbol{\beta_j}) = \sum_{i=1}^{n} Y_{ij}(\boldsymbol{X_i}\boldsymbol{\beta_j}) - \sum_{i=1}^{n} \ln\left[1 + \exp(\boldsymbol{X_i}\boldsymbol{\beta_j})\right]$$

Equation 6-3: Log-likelihood function for logistic regression

This function can be calculated for each class j over all points *i* in the point cloud. Different methods are available to iteratively derive the coefficient vector. At every iteration step, the vector is estimated by adding a new parameter to the model and by accepting or rejecting this parameter by the statistical evaluation of the model improvement. The degree of model improvement with this extra parameter is then evaluated by the likelihood ratio test. For this test, the following hypothesis, H_0 is tested, assuming that the coefficient vector is equal to zero and that the data cannot be described by a logistic model. On the contrary, H_A assumes that at least one parameter β describes the probability of a point belonging to a certain class:

$$H_0: \beta_1 = \beta_2 = \ldots = \beta_p = \boldsymbol{\beta_j} = 0$$

H_A: at least one of the β parameters is not equal to 0

In order to perform the classification, H_0 must be rejected. Thus, the evaluation of these hypotheses is iteratively performed using a test statistic on the likelihood ratio test, as discussed in the following section.

6.2.5. Parameter contribution and model quality

The contribution of a particular parameter to the model is evaluated by calculation of the maximum likelihood of the pre-existing parameters without the new parameter *L(OLD)*, and by calculation of the maximum likelihood of those parameters including the new parameter *L(NEW)*. The following test statistic is used:

$$G^2 = -2 \ln \left[\frac{L(OLD)}{L(NEW)} \right]$$

Equation 6-4: Measure for the evaluation of the contribution of a new parameter in comparison with the previous log-likelihood

Since the log-likelihood ratio follows a χ^2 distribution, a decision about the above hypothesis is reached as follows (Hosmer and Lemeshow 2004):

$$\begin{cases} G^2 \leq \chi^2_{(1-\alpha,1)} & : \text{accept } H_0 \\ G^2 > \chi^2_{(1-\alpha,1)} & : \text{reject } H_0 \end{cases}$$

If H_0 does not hold, the new parameter is significant and is added to the model. A level of significance of 95% is generally used for the inference. The iterative addition of parameters will consequently result in a model where all parameters are significant. The amount of variance that is explained by the model can be expressed by the coefficient of determination, R^2. This coefficient is calculated as a generalization of the well-known procedure in linear regression (Nagelkerke 1991):

$$R^2 = 1 - \left(\frac{L(0)}{L(\boldsymbol{\beta_j})} \right)^{2/n}$$

Equation 6-5: Coefficient of determination for the explanation of the amount of variance

where $L(0)$ is the likelihood of the interception model, $L(\boldsymbol{\beta_j})$ is the estimated model, and n is the number of elements. The interpretation of this coefficient is equivalent to its linear regression counterpart. It may be interesting to evaluate the contribution of an individual parameter, βp to the final model. As with linear regression, where individual parameter inference is performed using a t-test, the ratio of the parameter and its error is also used for logistic regression inference. The following H0 hypothesis is tested:

$$H_0: \beta_p = 0$$
$$H_A: \beta_p \neq 0$$

This hypothesis is tested using the Wald-statistic (Menard 2010):

$$\text{Wald}_p^2 = \left(\frac{\beta_p}{SE\{\beta_p\}} \right)^2$$

Equation 6-6: Wald-statistic as a variant of the χ^2 distribution

The squared Wald-statistic will also follow a χ^2 distribution. In both situations, a one-sided test is performed with $\alpha = 0.05$. A decision about the hypothesis is then reached by:

$$\begin{cases} \text{Wald}_p^2 \leq \chi^2_{(1-\alpha,1)} & : \text{accept } H_0 \\ \text{Wald}_p^2 > \chi^2_{(1-\alpha,1)} & : \text{reject } H_0 \end{cases}$$

Once all parameters in the model are estimated, the general properties of the model and its parameters are significant, the probability being that a point belonging to a certain class can be derived. The logit of the model is equal to the natural logarithm of the odds, and thus to (Peng, Lee, and Ingersoll 2002):

$$\text{logit}\left(E\left\langle Y_{ij} \middle| \boldsymbol{X}_i \right\rangle\right) = \text{logit}\left(\pi_{ij}\right) = \ln\left(\frac{Y_{ij}}{1 - Y_{ij}}\right) = \boldsymbol{X}_i \boldsymbol{\beta_j}$$

Equation 6-7: Logit of the model in relation with the odds

The odds are defined as the probability that a point belongs to a certain class, in relation to the probability that that point does not belong to a certain class. As a result, the odds ratio is a measure used to describe the effect of a certain parameter for the probability of a point belonging to a certain class (i.e. the strength of a parameter to the decision). This is the exponent of the regression parameter, β_p.

6.3. ***Model estimation and implementation***

6.3.1. Test sites and data

The first test site is located in the city centre of Ghent, Belgium (, Figure 6-1, left). A detailed description of the study area is presented in Stal et al. (2012). The ALS measurement campaign of the Ghent study area was commissioned by the city of Ghent and AGIV (Flemish Agency for Geographical Information) and was acquired by the company FUGRO (www.fugro.com). A FUGRO Fli-Map 1000 airborne laser scanner was mounted on a helicopter platform and the entire campaign was executed at an average altitude of 290 m above ground. The low altitude, in combination with the agile platform and large strip overlaps, resulted in an average point density of 20 m^2.

The second test site covers most of the area of the municipality of Ctiněves, Czech Republic, situated 34 km north of Prague (Figure 6-1, right). The area is situated on the southeastern flank of the Řip Mountain and is mainly represented by farmland and some forest. The village of Ctiněves is situated in the centre of the area, and has approximately one hundred two-storey buildings with gable roofs. The area is traversed by a railway, which is built on an embankment with an elevation of up to 4 m. An IGI LiteMapper 6800 airborne laser scanner was mounted on an aeroplane and used at an altitude of 1200 m above ground, resulting in an average point density of 1.2 m^2. The data were acquired within the context of a mapping project of the entire area of the Czech Republic. Further metadata from these two data sets are presented in Table 6-1 or are available at the Czech Office for Surveying, Mapping and Cadastre (www.cuzk.cz).

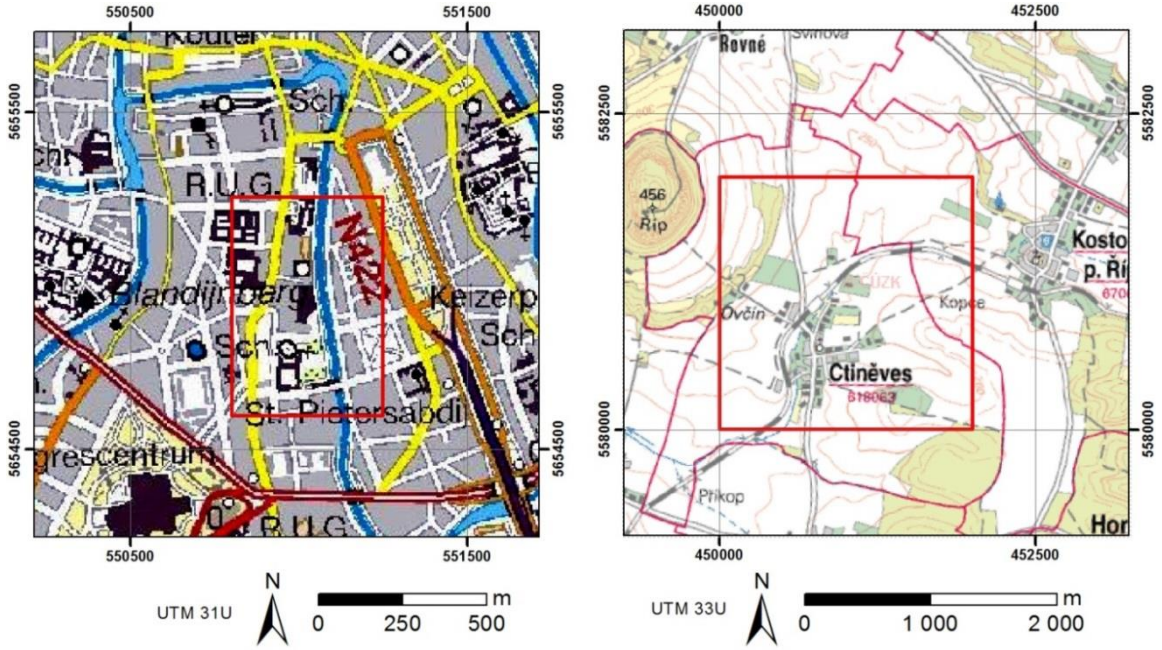

Figure 6-1: Overview of the Ghent test site (left, source: NGI) and the Ctiněves test site (right, source: ÇÚZK)

There is a big difference between the point densities of the two test sites. As discussed earlier, this will have an influence on the neighbourhood size in the analysis. If the neighbourhood parameters, which have to be found experimentally, are set correctly, the point density will not have an impact on the classification results. However, as a result of the low point density at the rural test site of Ctiněves (Czech Republic), and by the fact that buildings in this area are limited in elevation to two storeys, no points on wall surfaces were positively identified. The difference between high and low vegetation, such as trees and bushes, respectively, is not based on statistics but by a clear visual distinction between various vegetation units in the point cloud. The construction of a BLR model requires a training data set, which is generated by the manual classification of points and is also used as a ground truth data set. For each test site, four classes were defined (Table 6-2), and a random classification of points was performed for both test sites.

Table 6-1: Properties of the used airborne laser scanner and the acquisition project

Study area	**Ghent (Belgium)**	**Ctiněves (Czech Republic)**
Flight period	Summer 2009	Summer 2010
Measuring system	*FUGRO Fli-Map 1000*	*IGI LiteMapper 6800*
Altitude (above ground) [m]	290	1200
Measuring frequency [Hz]	250 000	266 000
Laser wavelength [nm]	1500	1550
Pulse length [ns]	4	3
Range accuracy [m] = 1 sigma	0.01	0.18
Strip width [m]	320	715
Strip overlap [%]	77	50
Average point density [P/m²]	20.0	1.2

Table 6-2: Construction of ground truth data set

Study area	Ghent (Belgium)	Ctiněves (Czech Republic)
Number of points	10 085 792	5 155 651
Classes	Ground	Ground
	Roof	Roof
	Wall	High vegetation
	Vegetation	Low vegetation

The training sets were finalized by generating an equal sample of 500 points for each class, using the open-source point and mesh-processing software, CloudCompare (www. danielgm.net/cc). This software has been developed by Daniel Girardeau-Montaut, and contains a powerful engine for visualizing, subsampling, and processing large point sets (Brodu and Lague 2012). The minimal sample size needed for the BLR training set is limited and can be calculated by taking 10 times the number of parameters in the feature space and the proportion of the smallest class to the entire point set (Peduzzi et al. 1996). After the construction of the training sets, each point in the point cloud contains the parameters of the feature space, as mentioned in section 3.1.

6.3.2. Model adjustment

In order to improve the modelling results, some extra constraints were introduced. Based on neighbourhood functions, which are used for the determination of the feature space, a rule-based model adjustment can be performed. This technique is also applied on gridded ALS data (Matikainen et al. 2010), but in this case only a limited number of constraints were required. The adjustment is numerically illustrated for the urban study area, where for each point, a subset of 25 nearest points was selected. Thereafter, the following constraints and accompanying thresholds were found experimentally that yielded optimal results.

- If a point has the class ‘Building’ and fewer than eight points in the subset are also classified as ‘Building’, then assign the class with the highest occurrence in this subset to this point;
- If a point has the class ‘Vegetation’ and fewer than eight points in the subset are also classified as ‘Vegetation’, then assign the class with the highest occurrence in this subset to this point;
- If a point has the class ‘Ground’ and fewer than eight points in the subset are also classified as ‘Ground’ and the majority of all points in the subset are classified as ‘Roof’, then assign the class ‘Roof’ to this point
- Triangulation of all ‘Ground’ points is performed and all ‘Wall’ points closer than 0.10 m to this surface should be classified as ‘Ground’ points.

The above-mentioned constraints are based on the typical characteristics of the test sites and are implemented in a Java application. It will be clear that the number of constraints can easily be adjusted depending on the type of dataset or user requirements, but that is beyond the scope of this work. The final results of this research are based on the combined use of BLR and these proposed adjustment constraints.

6.4. ***Results***

6.4.1. Multicollinearity within the feature space

Model estimation and logistic regression analysis can be performed by well-known statistical software such as R or PASW SPSS. As mentioned in Section 2.3, however, the assumption of multivariate normal distribution is not met by using this type of ALS data. It is well known that, for example, the local slope of a point neighbourhood will have a gamma distribution, while the standard deviation of the fitted plane should have a normal distribution. Besides, many parameters in the feature space are not independent. The assumption of normality is therefore taken for granted, in contrast to the assumption of multicollinearity, which will now be studied in detail. In order to minimize the collinearity effect of the parameters in the model, a stepwise predictor removal is suggested. In each step, the VIF is calculated for each predictor. If the VIF is greater than 10, corresponding to the threshold suggested by Chatterjee and Hadi (2006), this predictor will be removed. The factors are recalculated until there are no longer higher than the threshold. The results of this iterative removal process are presented in Table 6-3. For both test sites, the final factor values are presented for the accepted parameters. Parameters thus removed are shown, with their final VIF before removal as well as the step of removal.

Table 6-3: Checking for multicollinearity using the Variance Inflation Factor (VIF)

	Ghent			**Ctiněves**		
	Rejected		**Accepted**	**Rejected**		**Accepted**
	VIF	**Iteration**	**VIF**	**VIF**	**Iteration**	**VIF**
nσ0	10.061	5	-	11.388	3	-
n#ptsG	15.818	3	-	-	-	6.582
n#ptsU	15.818	2	-	31.541	3	-
λ_1	-	-	4.707	-	-	4.645
λ_2	-	-	2.737	-	-	4.041
λ_3	-	-	1.527	-	-	2.575
φ	-	-	2.377	-	-	1.776
θ	-	-	1.430	-	-	1.082
λ_n	-	-	4.015	-	-	5.630
Range	11.928	4	-	11.163	4	-
Mean	-	-	1.943	-	-	1.878
Var	-	-	2.714	-	-	1.626
RMS	102.538	1	-	85.198	1	-
PCount	-	-	3.118	-	-	1.949
Rank	-	-	1.907	-	-	1.353
EchoRatio	-	-	4.016	-	-	5.145

6.4.2. Model evaluation

The accepted predictors are used for the actual model estimation, as discussed above. The resulting parameters, β and Wald-statistics, will not be described here entirely, but Table 6-4 shows an example of these values for the 'Ground' class of the Ghent test site. With $\chi^2_{0.05,1}$ = 3.841, the Wald statistics indicate the significance of the parameters presented. Parameters not quantified in this table are removed by the multicollinearity test or have a non-significant parameter value ($\beta_i = 0$).

Table 6-4: Example of the estimated model parameters and Wald-statistics

	βi	Wald		βi	Wald
nσ0	-	-	**Range**	-	-
n#ptsG	-	-	**Mean**	0.663	29.085
n#ptsU			**VAR**	-0.194	19.878
ʎ1	-4.924	36.083	**RMS**	-	-
ʎ2	-	-	**PCount**	0.166	34.890
ʎ3	-	-	**Rank**	-0.010	15.080
φ	-6.683	119.468	**EchoRatio**	0.051	56.824
θ	-	-	**Constant**	-7.595	70.957
ʎn	6.873	55.477			

The overall model statistics allow the statistical acceptance of the models, as demonstrated in Table 6-5. With $\chi^2_{0.05,1} = 3.841$, the likelihood ratios G^2 are significant for all classes with a 95% level of significance. The coefficients of determination, R^2, suggest that a sufficient amount of variance is explained by the model. However, the roof classifier of the Ghent study area and the low vegetation classifier of the Ctiněves study area have low R^2 values. As explained below, visualization of these areas will clarify these low values.

Table 6-5: Evaluation of the significance of the entire model

Ghent			
	Iteration	**G²**	**Nagelkerke R²**
Ground	8	972.075	0.699
Roof	6	1608.674	0.406
Vegetation	6	1132.240	0.634
Wall	8	1184.435	0.611

Ctiněves			
	Step	**G²**	**Nagelkerke R²**
Ground	9	759.717	0.778
Roof	9	1489.857	0.468
Low vegetation	6	2015.859	0.163
High vegetation	9	921.049	0.719

The errors in the final models are summarized in terms of both Type I errors (a point is incorrectly categorized as another class) and Type II (a class is incorrectly assigned to a point), as seen in Table 6-6. The same statistics are also presented for comparative filtering using LASTools and MCC. Both classifiers perform ground point and non-ground point filtering, respectively based on the local slope and curvature of a certain neighbourhood. After this filtering, LASTools also enables the classification of roofs and vegetation by the analysis of planarity or irregularity of non-ground points. By using LASTools, it is possible to automatically detect the classes ‘Ground’, ‘Roof’, ‘Vegetation’, and ‘Unknown’. Since MCC detects only ground points, the technique is not described for other classes. These two techniques are selected for comparison because of their availability on the Internet and the fact that they can be used directly using stand-alone applications. In contrast to the classification method presented in this article, detectable classes are fixed for both techniques.

Table 6-6: Comparison between the errors of the BLR method and LASTools and MCC classification method

		Ghent		Ctiněves	
Class	**Algorithm**	**Type I (%)**	**Type II (%)**	**Type I (%)**	**Type II (%)**
Ground	**BLR**	0.42	0.52	7.72	3.82
	LASTOOLS	0.09	7.23	3.34	2.23
	MCC	0.66	0.99	4.04	4.55
Unknown class	**BLR**	3.22	1.72	7.33	5.25
	LASTOOLS	1.62	4.72	3.03	6.48
Building	**BLR**	3.91	2.39	2.01	6.41
	LASTOOLS	5.26	1.07	6.04	0.54
Vegetation	**BLR**	2.31	5.23	1.15	2.73
	LASTOOLS	1.22	1.97	0.58	3.75

For comparison among algorithms, the detected classes based on BLR are translated to standard LAS classes. So ‘Walls’ in the urban area are set to ‘Unknown class’. Notwithstanding the fact that ‘Low vegetation’ is a standard LAS class, it is not explicitly implemented in the LASTools algorithm. ‘Building’ class in LAS is actually a classification of roof points of a point cloud, and therefore the wall points detected by the BLR technique do not fit in this class. This performance comparison with other techniques already indicates one of the main advantages of the newly developed point classification procedure, as it allows enlargement of or changing the range of classes that can potentially be detected. In general, the figures are in line with previously published comparisons of other classifiers (e.g. Chen et al. 2013).

The overall success of the classification method described is obvious for both the urban study area of Ghent and the rural area of Ctiněves. Although the results are not the same for the different classes, the ‘Ground’ classification of the urban area is very good. For all other classes, both the Type I and Type II error of BLR are lower than in the other classification algorithm. The ‘Building’ and ‘Vegetation’ classification of the rural area resulted in a better classified point cloud than the urban point cloud, taking into account both Type I and Type II errors. This classification error in the urban test site is mainly caused by the mixture of classes directly under the tree canopy. Type I error of ‘Ground’ and ‘Other’ classes of the rural area is relatively high. For the rural area point cloud, a manual classification was performed as ground truth for the quality analysis, based on a user interpretation of the relatively low-density point cloud. As a result, this data set is not free from human errors and this has an influence on quality assessment. This becomes clear with the comparison of BLR classification results to an ortho image, as discussed below.

The values shown in Table 6-6 indicate that the results of the classifier depend on the definition of classes and the type of terrain. This can be illustrated with the samples in Figure 6-2 and Figure 6-2. The presented grids in the figure below are generated with a size of 0.5 m for the Ghent test site and 1.5 m for the Ctiněves test site. Each cell represents the class that has the highest occurrence within the neighbourhood of the centre of that cell. The upper left ortho image in this figure, as well as the ortho image in Figure 6-3 are acquired in 2009, thus no significant difference between the data sets and the images is assumed.

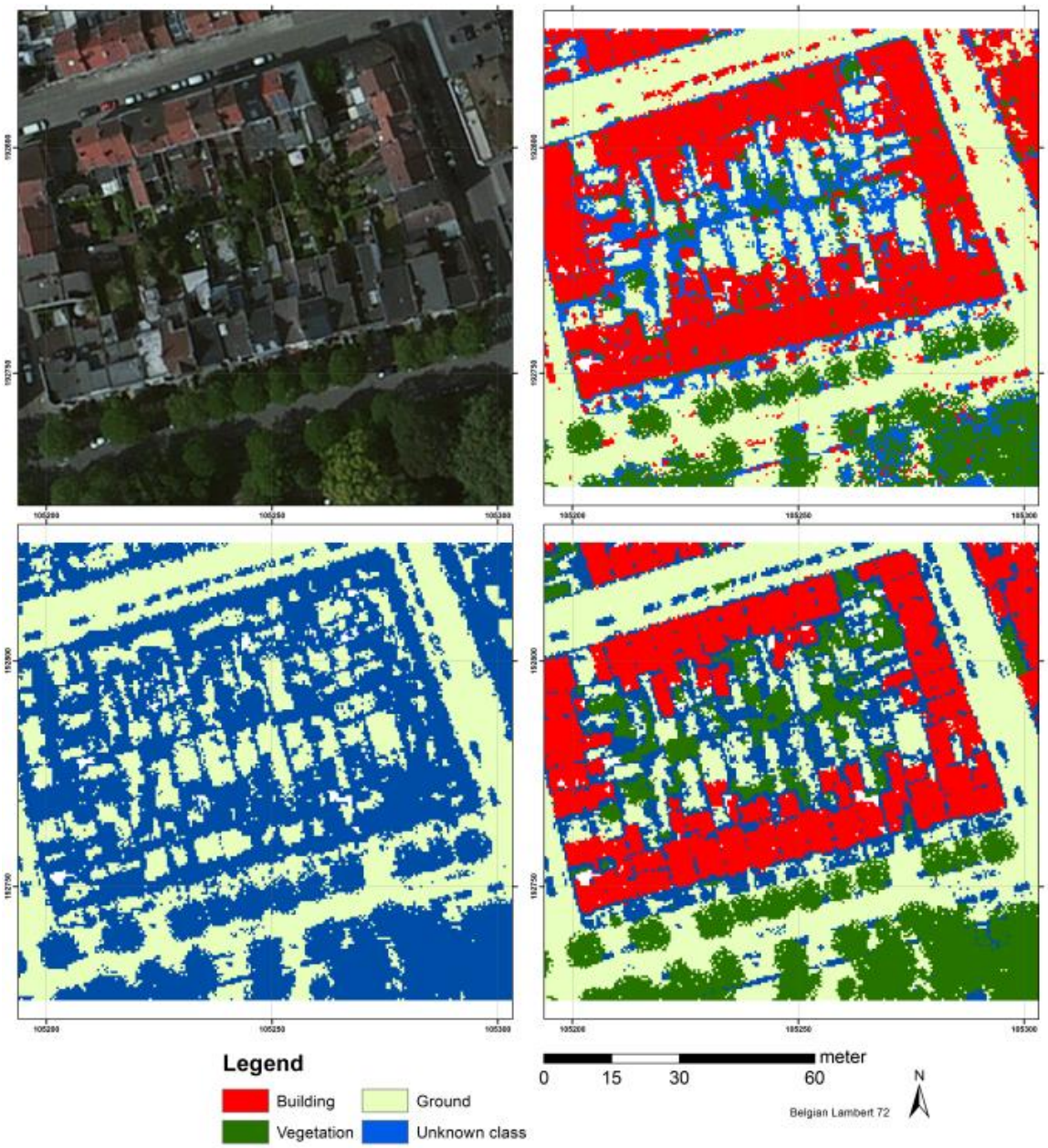

Figure 6-2: Overview of the Ghent test site with ortho image (top left, source: Microsoft), BLR results (top right), MCC (bottom left) and LASTools (bottom right).

Initially, most areas below trees are erroneously classified as wall points using the BLR technique. This error is reduced by the adjusted classifier, where the elevation of two points from different classes is considered. In the Ghent test site (Figure 6-2), the most obvious error in the classification result is in regard to flat roofs, but this issue is also seen in other classification algorithms and requires further research. Using the current parameters, these areas will result in a mixture of roof and ground points. Misclassification of flat roofs generally indicates some terrain dependency of the algorithm. This also caused the classification of cars as 'Building', visible as small red areas around the building block. A new class can easily be defined and implemented for these points, using elevation thresholds. Besides, very good results occur for the backyards of buildings. The introduction of a new class for walls resulted in the allocation of garden fences to

this class. LASTools will misclassify these points as trees or will not allocate any class at all to these points.

In regard to the Ctiněves test site (Figure 6-3), a fence or hedge, which is the line-shaped structure on the south side, is clearly misclassified by LASTools as a roof. Besides, the occurrence of the class 'Low vegetation' is high around roofs, especially on their ridges. It is not possible to use this class in LASTools and most low-vegetation points are therefore classified as 'Unknown class'. LASTools also seems to underestimate buildings, in contrast to the MCC and BLR algorithms. Although MCC does not classify buildings explicitly, their outlines are clearly visible, especially in combination with the orthoimage. The over-estimation of building points, vegetation points, and especially low-vegetation points by BLR in comparison with the manually classified data set can be explained by the orthoimage (Figure 6-3, right). This image shows a large number of complex structures in the backyards of buildings, such as sheds and fences. Much of the vegetation in these areas can indeed be classified as bushes, and thus as low vegetation. Apparently, the manually classified data set was not sufficiently classified to meet the high quality of the BLR classifier. This was probably caused by the relatively low resolution of this data set, and therefore the difficulty in manually determining low vegetation and very small built-up structures. Visual interpretation of the results indeed supports the statistical results, indicating the high suitability and flexibility of the BLR classifier for rural areas.

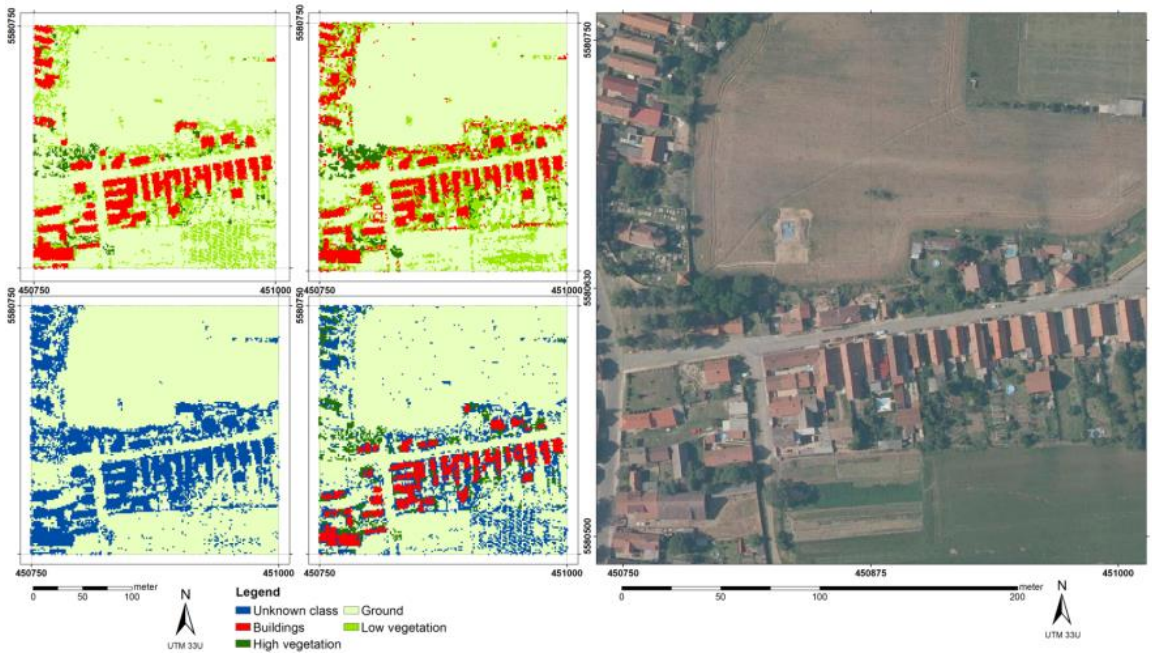

Figure 6-3: Detail of the Ctiněves test site with the reference (top left), BLR results (top middle), MCC (bottom left), LASTools (bottom middle) and ortho image (right, source: ČÚZK)

6.5. *Classification performance*

Obviously, LASTools is targeted towards production workflows and has been optimized after its first release 10 years ago. The efficiency of the current version of the BLR-based prototype is estimated at half that of LASTools. The calculation of feature spaces and accompanying

probabilities per point is reasonably computational intensive. In this context, the processing time increased quadratically for feature space determination and linearly for the probability calculation. However, it is possible to optimize the efficiency of the procedure by implementation of iterative classifiers, tiled processing, or point cloud indexing, etc. It must be emphasized that despite increased processing time, many conventional point classifiers are unable to take generic classes into account. For point cloud classification using regular classes (ground, roofs, and vegetation), conventional classifiers may be more suitable, but for more complex scenes, BLR-based classification is a reliable alternative for user-defined classes. It is also expected that subsequent reuse of the training sets for point cloud filtering of the same scene, or for the filtering of similar areas, would result in considerable time saving.

Supervised classification techniques are well known in regard to image based processing, where the construction of training sets is performed in 2D. The generation of training sets for BLR-based classification is facilitated by 3D software, minimizing the amount of noise in the sets. Moreover, the quality of the training sets can be assessed by evaluating the uniformity of the distributions of all parameters in the feature space. For the classification of very complex features, it can be assumed that an unsupervised point cloud classification can be used. In this case, a cluster analysis on the feature space could enable the automated classification of point clouds, without explicitly assigning semantics to the resulting classes.

6.6. *Conclusion and further work*

In this article, the use of BLR analysis for ALS point set classification is discussed. In contrast to current classification techniques, using one or a limited number of geometric criteria for the assignment of a point to a class, the proposed method makes use of a large feature space, the parameters of which are also based on the geometry of the neighbourhood. Rather than constructing a threshold-based decision tree, the entire feature space is used for the generation of a series of logistic models for each class. These models calculate the probability that a point belongs to a certain class. Since a probability is assigned to each point for each class, the class assignment will be based on the highest probability. The method also enables model evaluation by statistical inference. Nevertheless, using the above classification technique, the use of BLR for ALS point set classification appears promising.

The procedure is explained by the classification of two different ALS data sets. The first is a dense point set of an urban area in the city of Ghent, Belgium. For this area, ground and non-ground filtering with a Type I error of 4% and an overall correctness of 95% was achieved. For the second test site, located around the rural village of Ctiněves (Czech Republic), a Type I error of 8% and an overall correctness of 96% were recorded. These values are in line with other state-of-the-art classification methods for ground point extraction. However, in contrast to most other classification methods, multiple classes can be extracted from an ALS point set.

The potential of the new classification procedure has been demonstrated for ALS data. In contrast to LASTools, the method does not require that the data be acquired from an airborne platform,

and it can also be extended to Static Terrestrial Laser Scanning (STLS) and Mobile Terrestrial Laser Scanning (MTLS). Care needs to be taken with respect to the different properties of ALS on the one hand and STLS and MTLS on the other. For terrestrial scanning, variation in point density (caused by data heterogeneity) and data holes (caused by shadows) must be taken into account. Furthermore, the feature space should not only contain parameters that are dependent of the elevation, such as local mean and standard deviation, but also parameters that take all dimensions into account, such as planimetric distribution descriptors or local eigenvalues. Besides, parameters related to the measured distance or intensity can be used for unprocessed STLS measurements, and colour information can be used for many MTLS point clouds.

The ability to generate a wide range of classes is the greatest strength of the proposed method. This user adaptability of the algorithm, dependent on the type of measurement area and the user's experience, allows a very wide range of applications in the field of point classification supported by a thorough statistical basis for interpretation of the performance of the results. Moreover, not only can the BLR procedure itself be optimized, but also the model adjustment constraints can be fine-tuned depending on the application. If the training sets are defined correctly, the ratio of misclassified points will be around 5–12%. It should be mentioned that parameters other than those mentioned in this article could be taken into account. Besides, the results obtained appear very promising in regard to further improvement in the classification procedure (e.g. by either taking the neighbourhood of the class assignment into account or the use of a rough DTM for the calculation of a preparatory normalized elevation model).

Acknowledgement

The authors would like to express their gratitude to the city of Ghent and to the government of the Czech Republic for the airborne laser scanning data. The Czech data set was classified by Petr Hoffman. The Ludwig Boltzmann Institute for Archaeological Prospection and Virtual Archaeology is based on international cooperation of the Ludwig Boltzmann Gesellschaft (Austria), the University of Vienna (Austria), the Vienna University of Technology (Austria), the Austrian Central Institute for Meteorology and Geodynamics, the office of the provincial government of Lower Austria, Airborne Technologies GmbH (Austria), RGZM (Roman-Germanic Central Museum Mainz, Germany), RA (Swedish National Heritage Board), VISTA (Visual and Spatial Technology Centre, University of Birmingham, UK), and NIKU (Norwegian Institute for Cultural Heritage Research).

References

Baltsavias, E., 1999. Airborne laser scanning: basic relations and formulas. ISPRS Journal of Photogrammetry and Remote Sensing 54 (2-3), 199-214.

Bartels, M., Wei, H., 2010. Threshold-free object and ground point separation in LiDAR data. Pattern Recognition Letters 31 (10), 1089-1099.

Brenner, C., 2005. Building reconstruction from images and laser scanning. International Journal of Applied Earth Observation and Geoinformation 6 (3-4), 187-198.

Briese, C., 2010. Extraction of digital terrain models. In: Airborne and terrestrial laser scanning, Eds. Vosselman, G., Maas, H. Dunbeath, UK: Whittles Publishing, 135-167.

Briese, C., Pfeifer, N., Dorninger, P., 2002. Applications of the Robust Interpolation for DTM Determination. International Archives of Photogrammetry and Remote Sensing 34 (Part A), 55-61.

Brodu, N., Lague, D., 2012. 3D terrestrial LiDAR data classification of complex natural scenes using a multi-scale dimensionality criterion: applications in geomorphology. ISPRS Journal of Photogrammetry and Remote Sensing 68 (1), 121-134.

Chatterjee, S., Prince, B., 1991. Analysis of collinear data. In Regression Diagnostics. Hoboken, NJ, USA: John Wiley, 221-258

Chen, C., Li, C., Li, W., Dai, H., 2013. A multiresolution classification algorithm for filtering airborne LiDAR data. ISPRS Journal for Photogrammetry and Remote Sensing 82 (1), 1-9.

Doneus, M., Briese, C., Fera, M., Janner, M., 2008. Archaeological prospection of forested areas using full-waveform airborne laser scanning. Journal of Archaeological Science 35 (4), 882-893.

Dorninger, P., Pfeifer, N., 2008. A comprehensive automated 3D approach for building extraction, reconstruction and regularization from airborne laser scanning point clouds. Sensors 8 (11), 7323-7343.

Evans, J., Hudak, A., 2007. A multiscale curvature algorithm for classifying discrete return LiDAR in forested environments. IEEE Transactions on Geoscience and Remote Sensing 45 (4), 1029-1038.

Filin, S., 2002. Surface clustering from airborne laser scanning data. International Archives of Photogrammetry and Remote Sensing and Spatial Information Sciences 34 (Part 3), 119-124.

Filin, S., Pfeifer, N., 2005. Neighborhood systems for airborne laser data. Photogrammetric Engeneering and Remote Sensing 71 (6), 743-755.

Flury, B., 1997. A first course in multivariate statistics. New York, NY, USA: Springer.

Höfle, B., Mücke, W., Dutter, M. Rutzinger, M., Dorninger, P., 2009. Detection of building regions using airborne LiDAR: a new combination of raster and point cloud based GIS methods. GI-Forum 2009: International Conference on Applied Geoinformatics, Salzburg, Austria, July 7-10, 2009.

Hosmer, D., Lemeshow, S., 2004. Applied logistic regression. Hoboken, NJ, USA.: John Wiley.

Isenburg, M., Shewchuk, J., 2013. LAStools. In, Converting, viewing and compressing LIDAR data in LAS format. http://www.cs.unc.edu/~isenburg/lastools/.

Kraus, K., Pfeifer, N., 1998. Determination of terrain models in wooded areas with airborne laser scanner data. ISPRS Journal of Photogrammetry and Remote Sensing 53 (8), 193-203.

Kutner, M., Nachtsheim, C., Neter, J., Li, W., 2005. Applied linear statistical models. New York, NY, USA: McGray-Hill, pp. 1396.

Li, Y., 2013. Filtering airborne LiDAR data by in improved morphological method based on multi-gradient analysis. International Archives of Photogrammetry and Remote Sensing and Spatial Information Sciences 40 (1), 191-194.

Mandlburger, G., Otepka, J., Karel, W., Wagner, W., Pfeifer, N., 2009. Orientation and processing of airborne laser scanning data (OPALS): concept and first results of a comprehensive ALS software. International Archives of Photogrammetry and Remote Sensing and Spatial Information Sciences 38 (Part 3), 55-60.

Matikainen, L., Hyyppä, J., Ahokas, E., Markelin, L., Kaartinen, H., 2010. Automatic detection of buildings and changes in buildings for updating of maps. Remote Sensing 2 (5), 1217-1248.

Menard, S. 2010. Logistic regression: from introduction to advanced concepts and applications. Thousand Oaks, CA, USA: Sage Publications, pp. 378.

Meng, X., Wang, L., Silván-Gárdenas, J., Currit, N., 2009. A multi-directional ground filtering algorithm for airborne LiDAR. ISPRS Journal of Photogrammetry and Remote Sensing 64 (1), 117-124.

Mongus, D., Žalik, B., 2012. Parameter-free ground filtering of LiDAR data for automatic DTM generation. ISPRS Journal of Photogrammetry and Remote Sensing 67 (1), 1-12.

Nagelkerke, N., 1991. A note on a general definition of the coefficient of determination. Biometrika 78 (3), 691-692.

O'Brien, R., 2007. "A caution regarding rules of thumb for variance inflation factors." Review of. Quality and Quality 41 (5), 673-690.

Otepka, J., Mandlburger, G., Karel, W,. 2012. The OPALS data manager: efficient data manager for processing large airborne laser scanning projects. International Archives of Photogrammetry and Remote Sensing and Spatial Information Sciences 39 (Part 3), 153-159.

Oude Elberink, S., Vosselman, G., 2011.Quality analysis on 3D building models reconstructed from airborne laser scanning data. ISPRS Journal of Photogrammetry and Remote Sensing 66 (2), 157-165.

Peduzzi, P., Concato, J., Kemper, E., Holford, T, Feinstein, A., 1996. A simulation study of the number of events per variable in logistic regression analysis. Journal of Clinical Epidemiology 49 (12), 1373-1379.

Peng, C., Lee, K., Ingersoll, G., 2002. An introduction to logistic regression analysis and reporting. Journal of Educational Research 96 (1), 3-14.

Pfeifer, N., Mandlburger, G,. 2008. LiDAR data filtering and DTM generation. In: Topographic laser ranging and scanning: principles and processing. Eds. Shan, J., Toth, C., Boca Raton, Fl, USA: CRC Press, 307-333.

Podobnikar, T., Vrecko, A., 2012. Digital elevation model from the best results of different filtering of a LiDAR point cloud. Transactions in GIS 16 (5), 603-617.

Sampath, A., Shan, J., 2010. Segmentation and reconstruction of polyhedral building roofs from aerial LiDAR point clouds. IEEE Transactions on Geoscience and Remote Sensing 48 (3), 1554-1567.

Sithole, G., Vosselman, G. 2004. Experimental comparison of filter algorithms for bare-Earth extraction from airborne laser scanning point clouds. Journal of Photogrammetry and Remote Sensing 59 (1-2), 85-101.

Stal, C., De Wulf, A., De Maeyer, P., Goossens, R., Nuttens, T., Tack, F., 2012. Statistical comparison of urban 3D models from photo modeling and airborne laser scanning. Paper presented at the SGEM, Albena, Bulgaria, pp. 8.

Stal, C., Tack, F., De Maeyer, P., De Wulf, A., Goossens, R. 2013. Airborne photogrammetry and LiDAR for DSM extraction and 3D change detection over an urban area: a comparative study. International Journal of Remote Sensing 34 (4), 1087-1110.

Stine, R., 1995. Graphical interpretation of variance inflation factors. The American Statistician 49 (1), 53-56.

Wagner, W., Ullrich, A., Ducic, V., Melzer, T., Studnicka, N., 2006. Gaussian decomposition and calibration of a novel small-footprint full-waveform digitising airborne laser scanner. ISPRS Journal of Photogrammetry and Remote Sensing 60 (12), 100-112.

Xu, S., Oude Elberink, S., Vosselman, G. 2012. Entities and features for classification of airborne laser scanning data in urban area. ISPRS Annals of the Photogrammetry, Remote Sensing and Spatial Information Sciences 1 (4), 257-262.

Chapter 7

Integrating geomatics in archaeological research at the site of Thorikos (Greece)

7. Integrating geomatics in archaeological research at the site of Thorikos (Greece)[7]

Abstract

Archaeological excavation is a destructive process, making accurate, fast and efficient 3D documentation of information essential. With this in mind, our research uses an integrated workflow of topographic measurements and image-based 3D modelling to generate highly accurate reconstructions of archaeological features at the site of Thorikos, Greece. Topographic ground control points and images are acquired using a total station and consumer digital camera respectively, and processed in a highly automated workflow using Structure from Motion and Multiview Stereo reconstruction software. These models were generated on a daily basis in order to map the on-going of a field campaign at this archaeological site in 2012. Moreover, a management system is presented as a consultation and analysis application, enabling the interaction with the 3D models, accompanied with attribute data and metadata. For the efficiency of the management system it was essential to integrate the 3D models in a Harris matrix. This matrix functions as an intermediate between a graphical user interface and the database system. Additionally, two applications of these 3D models are presented, focussing on capacity calculations and in situ mapping (orthophoto mapping) of stone wall remains. The presented management system, the linking of 3D models with excavation data, and the use of 3D models as a scientific tool demonstrate the huge potential of 3D data for archaeological research.

Keywords: 3D modelling; data management; excavation; Geomatics; SfM-MVS; Thorikos

7.1. *Introduction*

Next to range-based 3D modelling techniques (Pavlidis et al., 2007), image-based 3D modelling is increasingly applied in archaeology and heritage studies in recent years (e.g. Plets et al., 2012; Koutsoudis et al., 2013a, Koutsoudis et al., 2013b, Verhoeven et al., 2012a and Verhoeven et al., 2012b). Among these, several studies have already illustrated the potential of image-based 3D modelling for the recording of archaeological excavations (De Reu et al., 2013, De Smedt et al., 2013, Dellepiane et al., 2013, Doneus et al., 2011, Forte et al., 2012, Pollefeys et al., 2000 and Pollefeys et al., 2003). Many studies have also shown that 3D modelling is a useful alternative when excavation is not an option or when it is not required. Airborne data acquisition is well known for archaeology and cultural heritage (Hendrickx et al., 2011, Koller et al., 2009 and Remondino, 2011). Furthermore, terrestrial laser scanning and close-range photogrammetry are frequently used for the documentation, reconstruction and management of archaeological sites and cultural heritage (Boehler and Marbs, 2004 and Tack et al., 2005). The flexibility of both techniques allows to generate high quality 3D models of a wide range of different relicts and artefacts. Even when sites have contaminated or when sites are politically sensitive or environmentally sensitive, it is possible to generate 3D models. The ability to perform contact-free measurements is therefore a huge advantage for these techniques. Specifically for close-range

[7] Modified from: Stal, C., Van Liefferinge, K., De Reu, J., Docter, R., Dierkens, G., De Maeyer, P., Mortier, S., et al. (2013), Integrating geomatics in archaeological research at the site of Thorikos (Greece). *Journal of Archaeological Science. 45* (May), 112–125.

photogrammetry, additional advantages of the methodology are the high geometric accuracy of the 3D models, the clear procedure for the recordings and the photorealistic texture. Furthermore, one can proceed from a traditional 2D documentation to a more realistic 3D documentation of the archaeological heritage (e.g. De Reu et al., 2013). And finally, 3D excavation data often have an important and attractive visual character (Hermon, 2008). Because an archaeological excavation is a destructive process (Lucas, 2001), it requires highly accurate visual and scientific recording techniques. Besides its visual value, the scientific value of 3D modelling for the study of archaeological excavations is significant.

Although 3D models have already been used in archaeological research for some years, the construction of these models has sometimes been restricted to the finalisation phase of the archaeological excavation. However, there are examples of the construction of 3D models during excavations, where the advantages of this technique are stress out (Losier et al., 2007 and De Reu et al., 2014). An important question we have to answer is how this 3D data can be made accessible, manageable and usable among the excavators during the excavation and in the post-processing phase of the excavation. Large amounts of data are difficult to manage without a powerful database system, especially when a sufficient infrastructure is absent. Therefore, this paper investigates the implementation of a user-friendly management system for very large 3D data sets, by linking the models with the Harris-matrix of the excavation. The combination of the Harris matrix with 3D models allows a better insight on the site formation processes. A thorough understanding of the different relations between features in time and space, as presented by these 3D models, is facilitated by a solid data management. Consequently, the human interactions on the site can be understood during the occupancy of the site. Furthermore, we explore two different applications on how the 3D models can be used as base data for spatial analysis related to excavators. First, the calculation of the volume or capacity of the cistern is explored and discussed. These calculations enable the estimation of the volume or capacity of the reservoir. Second, the generation of orthophotomaps, extracted from the 3D models, is explored as a tool for the contour mapping of stone walls. These orthophotomaps are augmenting the traditional 2D manual recordings (e.g. drawings) to be used as an excavation plan during the archaeological fieldwork and enable off-site feature digitalization.

7.2. *The archaeological site of Thorikos, Greece*

The archaeological site of Thorikos is located on the Velatouri Hill in southeast Attica (Greece, Figure 7-1), an area known for the presence of rich silver deposits. Since the late Neolithic, the history of the region was largely determined by the exploitation and processing of these mineral resources. Mining activities boomed especially during the Classical (400–323 BC) and the Early Hellenistic period (323–250 BC), but also during the Late Classical period (400–500 AD) (Kakavoyiannis, 2005), when a large amount of ore processing workshops consisting of an ore washery, a cistern and living quarters, were scattered over the Laurion. Especially cisterns were vital, since water was an indispensable resource in the silver production process.

To date, thirteen of such workshops have been recorded in Thorikos. In this paper, focus will be on the so-called 'Cistern no.1 workshop', named after its eye-catching water reservoir and located north of the 'Industrial Quarter' (Figure 7-2, red ellipse). Thoroughly studied parts of this workshop were excavated during three short campaigns (2010–2012, e.g. Van Liefferinge et al., 2011a) within the framework of a wider research project on water use and management at Thorikos and the Laurion region (Van Liefferinge et al., 2014). Given that the cistern of this workshop is by far the largest water reservoir of the site, its closer study is particularly valuable for this project.

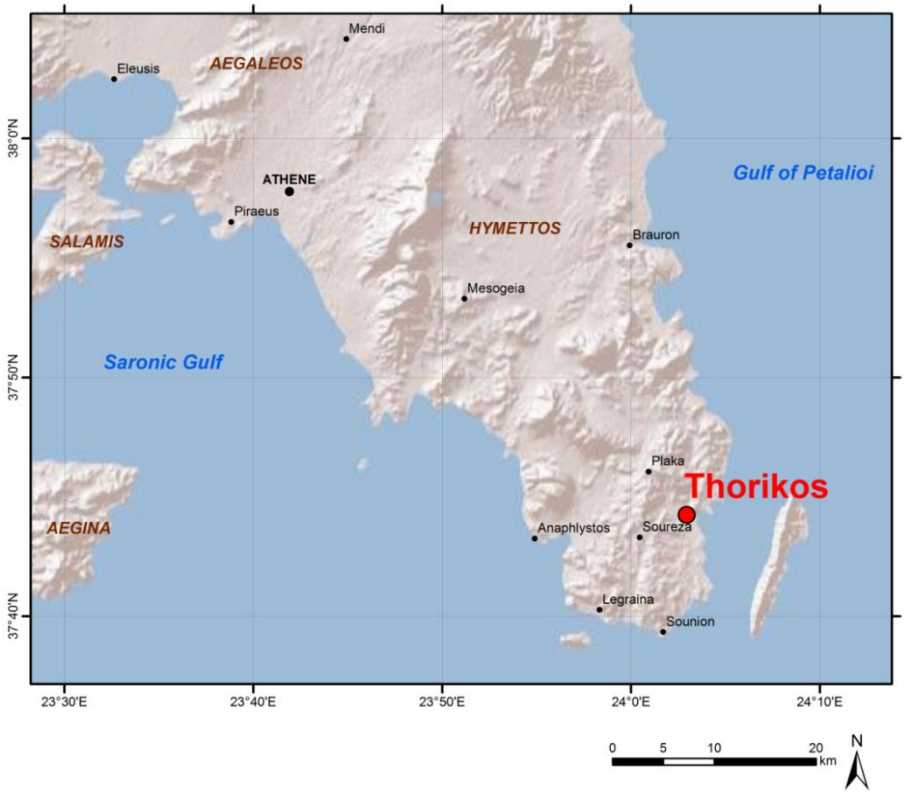

Figure 7-1: Overview of the Attica province in Greece

In the summer of 2012, an intensive archaeological campaign was organized on the ancient site of Thorikos (Greece) by the department of Archaeology of Ghent University (Belgium) and the department of History of the University of Utrecht (the Netherlands). One of the aims of this campaign was to finish the documentation of a large cistern and its surroundings north of the 'Industrial quarter'. To be more precise, work was concentrated on two zones. First, a sounding was dug in the basin of the cistern in order to establish its capacity and date of abandonment. Given its extensive size and the nature of the filling (primarily consisting of large rocks tumbled into the cistern), it was not feasible to clear the entire basin. Therefore, work was concentrated on one zone (A) only (Figure 7-3). Secondly, a room built against the south wall of the cistern was investigated, with the aim to recover dates on the chronology of the cistern (construction date and date of use). Light would be shed on the use of two overflow channels. Two small trenches were dug in this room, focussing on each of these channels: Zone F was located in the east and Zone G in the west.

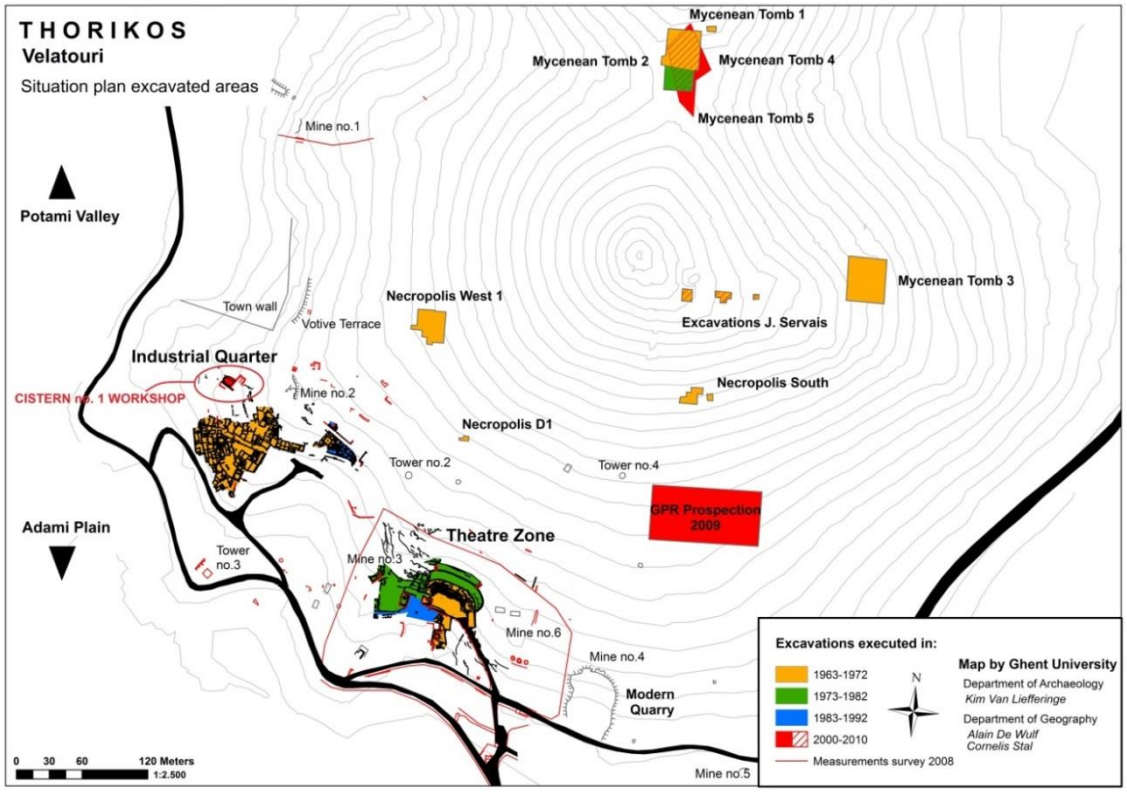

Figure 7-2: Overview of the Thorikos archaeological site

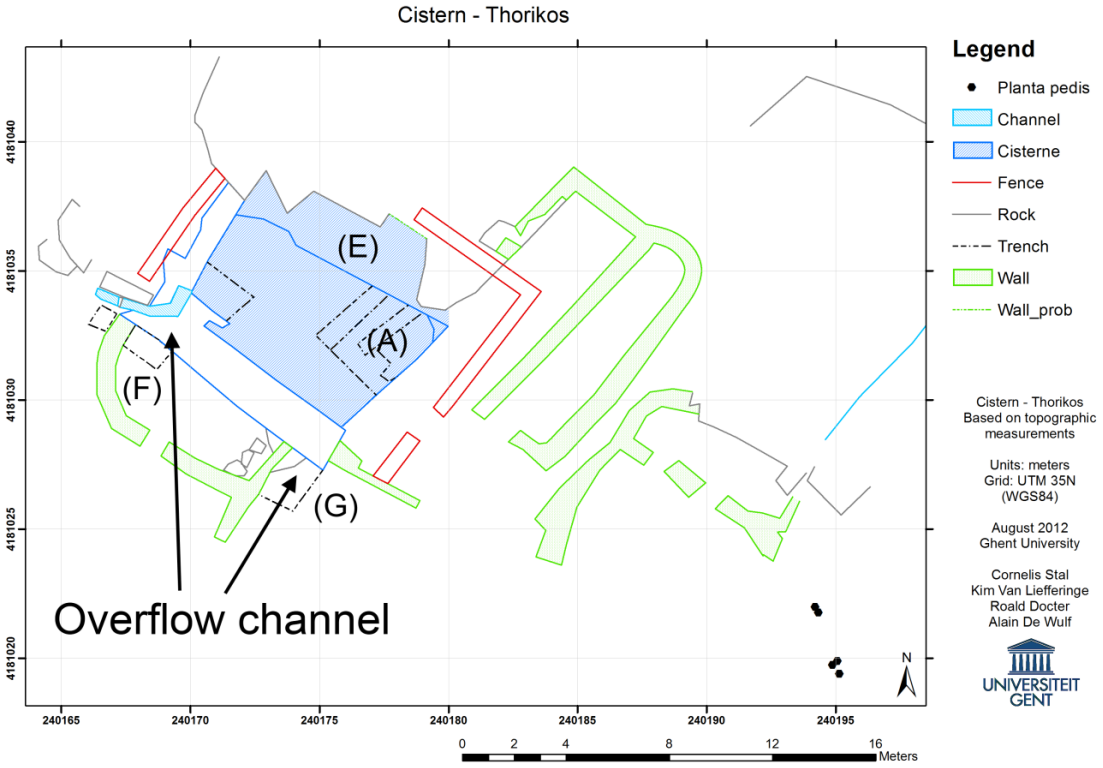

Figure 7-3: Detailed map of the Cistern no 1 workshop.

In general, the stratigraphic conditions of the excavations in Thorikos are very complex. Being a multi-period site, the majority of the houses and workshops knew multiple occupation phases, during which many adjustments to the buildings were made. Since the investigated zone is no exception, it is imperative to record the excavated contexts meticulously, in order to make a sound interpretation of the stratigraphy. Furthermore, the partial excavation of the cistern involves some problems. The cistern has an irregular outline, with planimetric dimensions of approximately 9.0 m × 7.5 m and an estimated depth of 4.9 m. The shape of the basin is rather unconventional in comparison with other cisterns in the region. The cistern is subdivided in two parts: the actual basin, which was nicely carved into the rock, and a higher zone in the north, which consists of unadjusted bedrock (E), likely to be used for drawing water out of the basin by low water level. As a result, establishing the capacity of the cistern would not prove to be an easy task. However, by introducing 3D modelling in the archaeological workflow, both discussed issues can be approached in a comprehensive and more accurate way than in the case of traditional archaeological methods.

7.3. ***Virtual reconstruction procedure***

7.3.1. Data acquisition

During the excavation, a systematic series of images was taken and topographic measurements were performed. At the beginning of the campaign, 30 ground control points (GCPs) were materialised using a water resistant felt-tip pen and chalk. These markers were put on solid rock and an approximately equal spatial distribution of the GCPs was guaranteed in all directions. Besides, the targets are situated in and around the site, and especially in and around possible areas of special interest. After installing all GCPs, these points were measured using a Trimble S6 robotic total station. A maximal absolute error of 1 cm for the free stationing was respected, which is acceptable considering the field conditions. This configuration resulted in an absolute error of only a few cm, although the relative accuracy is related to the image pixels, corresponding with a few mm. At the last day of the campaign, an intensive survey was performed in order to get the overall picture of the exposed structures in the immediate neighbourhood of the cistern. It was important that these GCPs were photographed from at least two camera positions, in order to perform a model referencing. The targets were measured using a total station and oriented within the local grid of the Thorikos site. The concrete poles on the edges of this grid had already been measured during previous fieldwork (De Wulf et al., 2000). The transformation parameters for the conversion between the local grid and UTM 35N coordinates were defined during the 2000 field campaign. Control measurements on the physical condition of the grid were performed in 2008 (Van Liefferinge et al., 2011b).

A large number of images were taken on a daily basis between 6 and 7 AM, in order to avoid cast shadows on the excavated structures. A thorough cleaning was also performed, in order to avoid unwanted elements in the models. The images were taken with a Canon EOS 400D digital single lens reflex camera with a 10.1 Mp CMOS sensor and a Canon EF-S 18–55 mm lens. In order to use the images for 3D modelling, it is required that the images are taken from different positions. Varying the positions will yield a parallax and enables the calculation of object coordinates in a

3D space. A systematic linear movement of the camera around the site (as visualized in Figure 7-4), is preferred for the fast image processing, but this is not an absolute requirement. Randomly taken images may result in correct 3D models as well, as long as each spot is covered by at least two images (Shashua and Werman, 1995), even for very complex structures. A constant quality check should be performed during the acquisition and a surplus of images is advisable.

7.3.2. Structure from motion and multi-view stereo software

The 3D models are based on a Structure from Motion – Multi-View Stereo (SfM-MVS) processing workflow (Lourakis and Argyros, 2009). SfM-MVS is implemented in different software, such as Agisoft PhotoScan, and enables the generation of 3D models based on a large series of images. SfM-MVS is a technique to reconstruct the camera acquisition parameters and to calculate a sparse point set of the scene (SfM). Moreover, it is a technique to acquire the 3D geometry of an object, or a series of objects (MVS), using a series of 2D images. Agisoft PhotoScan is used during this project and covers the entire workflow from the impact of the original images to the highly accurate and textured 3D meshes. In order to construct these 3D meshes, three basic steps are performed (Verhoeven, 2011): photo alignment (SfM), geometry reconstruction (MVS) and texture mapping.

The first step in the SfM process is the automatic detection of feature points. Characteristic points have to be localised on each image. Thereafter, corresponding points are detected on other images, resulting in a set of matching points. Different methods have been developed for image matching, e.g. methods based on region growing algorithms using seeding points (Heipke et al., 1992), or the use of a GCP database (Chen et al., 2000). The algorithms are based on a least squares estimation, so the solution is obtained by an error minimisation estimator (Gruen, 1985). In order to detect feature points and to perform the image matching, local contrasts or non-equally coloured textures and non-shininess surfaces on the objects are required. This is not a problem for the site of Thorikos, but can be problematic in other projects, e.g. with white limestone or glass. Next to these feature points, the intrinsic image parameters, like the image size and the focal length of the camera, are used to perform the iterative bundle adjustment. The solution of this adjustment corresponds with the best fitting virtual reconstruction of the image scene in a 3D space. By adding GPCs to this scene, external parameters are calculated and accurately metric measurements will be possible in the model.

An initial visualization of the scene structure and the position and the orientation of the images is illustrated in Figure 7-4, which already gives a good geometrical impression by the 3D visualization of the feature points. This scene represents the zones F and G of the excavated site. The rectangles represent each image used for the reconstruction, numbered by the name of the corresponding image. Based on this figure, it is clear that the requirement of different positions is respected. The numbered dots with flags represent the measured GCPs.

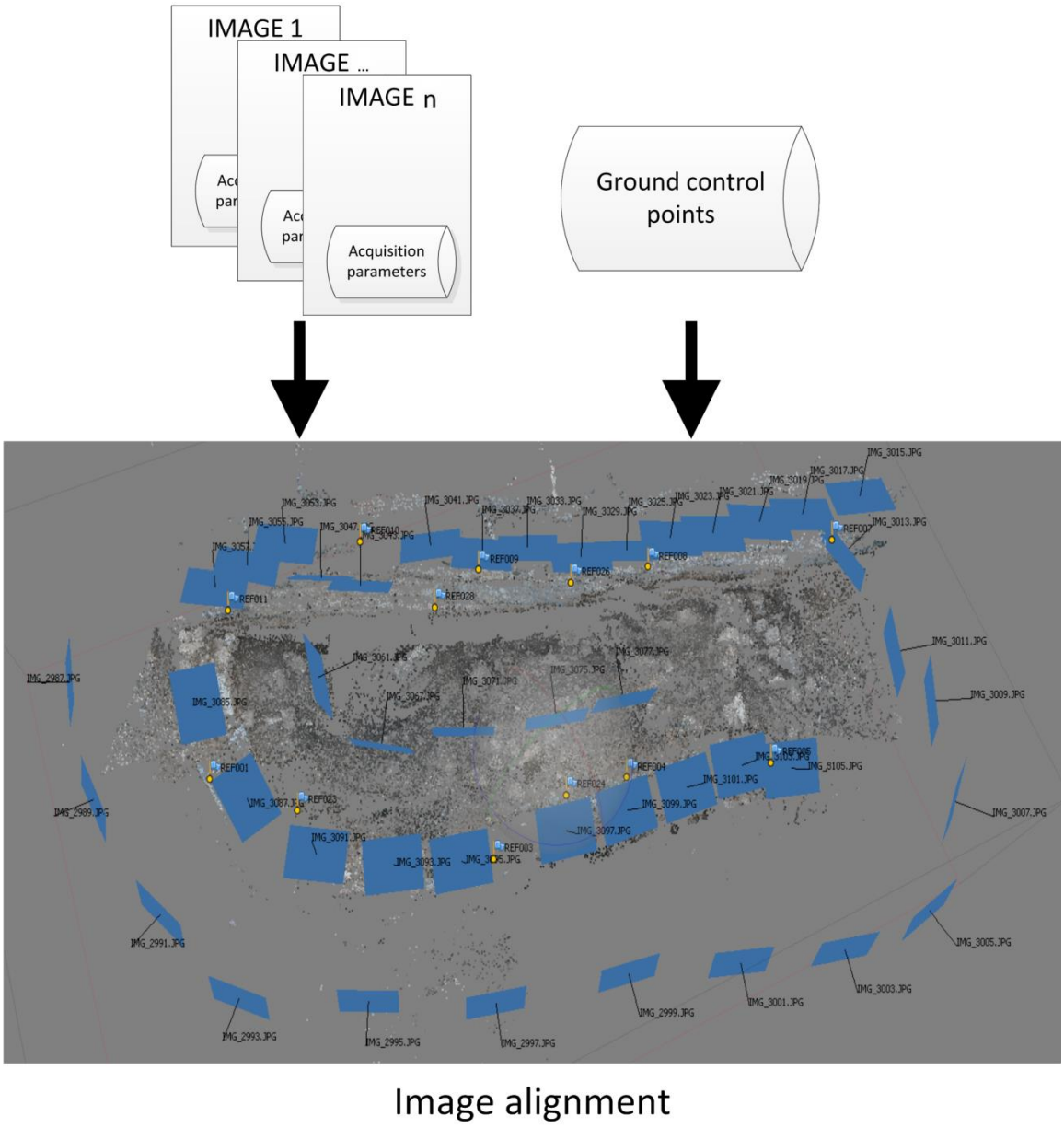

Figure 7-4: Scene structure with matched feature points and positioned and oriented images

The 3D feature points are not used for the actual 3D reconstruction. A 3D mesh is generated based on the intersection of perspective pixel rays, which is the actual MVS. These rays are projected according to the image frames. The orientation and position of these frames are determined after the image alignment. The focal lengths of the cameras are also used to define the linear projection parameters of the 2D image pixel rays in a 3D space. The result of this project is a series of depth maps, representing the distance between the focal centre of the camera and the intersection of perspective rays. A dense point set is then created by combining these depth maps from differently oriented positions. These points are hereafter triangulated into a mesh. A mesh simplification could be performed for computational performance reasons. More detailed information about SfM-MVS is presented in an extensive discussion by Robertson and Cipolla (2009) and Seitz et al. (2006).

During the geometric 3D reconstruction, a single colour value, based on averaged colour values of all corresponding pixels from the different images, is assigned to each face in the mesh. A detailed and photorealistic texture map is obtained using uv-mapping (Hülksen et al., 2007). The geometry is textured by projecting the original images on the mesh. Each pixel of the resulting texture map is assigned to a position on the mesh. The colour of this pixel is defined by a function of the weighted value of the corresponding pixels from the original images (Wang et al., 2001). Figure 7-5 illustrates the concept of UV-mapping, where the geometry of the site (1) is draped with the texture map of the site (2), in order to have the textured 3D mesh (3). The model can be exported as a 3D virtual model in combination with a separate texture map, in order to use the model in other software.

Alignment parameters, like the number of feature points, and geometry reconstruction parameters, like the number of faces and accuracy thresholds, were chosen so that the software would give the highest possible quality. However, for the sake of performance of the visualisation of the 3D models in the management system, the 3D mesh was limited to two million faces. The 3D models were described by the Virtual Reality Modelling Language (VRML), with compressed JPEGs as separate texture maps with 100 megapixels. Finally, digital elevation models (DEMs) or orthophotos were generated to facilitate capacity calculations and conventional site interpretations.

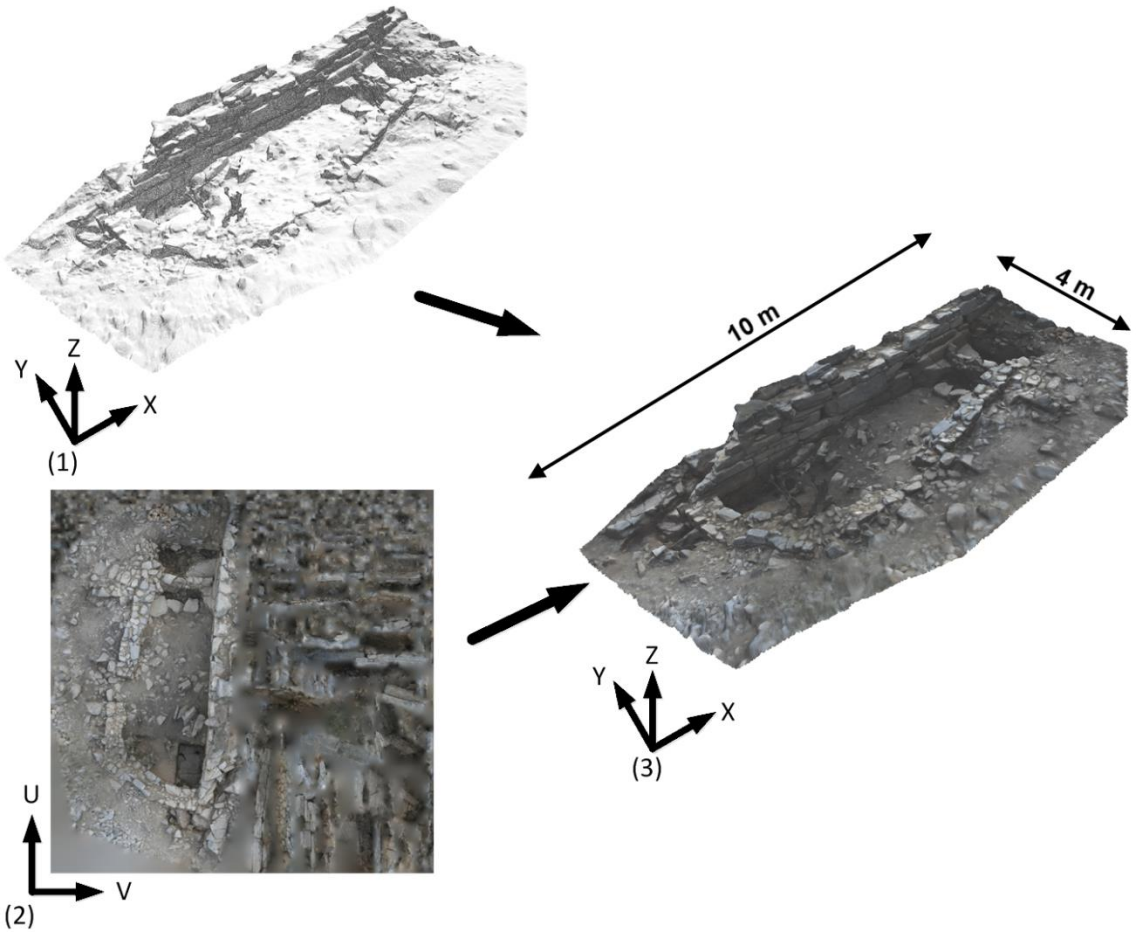

Figure 7-5: Geometry (1) and texture (2) result in a textured 3D model (3)

7.4. *Towards an archaeological management system*

During the campaign, a total of 38 3D models were generated. These models covered the cistern, as well as the room immediately to its south with a different level of detail. Special attention was given to two trial trenches (Zone F and G). Apart from the 3D models, the data was supplemented with attribute data, describing the non-spatial properties of the model. These data were processed in a time dependent manner. It was obvious that this large amount of data required an efficient way of storing and consulting the data. In this context, it was vital that the performance of the management system and the degree of detail of the models were in equilibrium. An example of a random time series, representing the evolution of the excavation in Zone G, is presented in Figure 7-6.

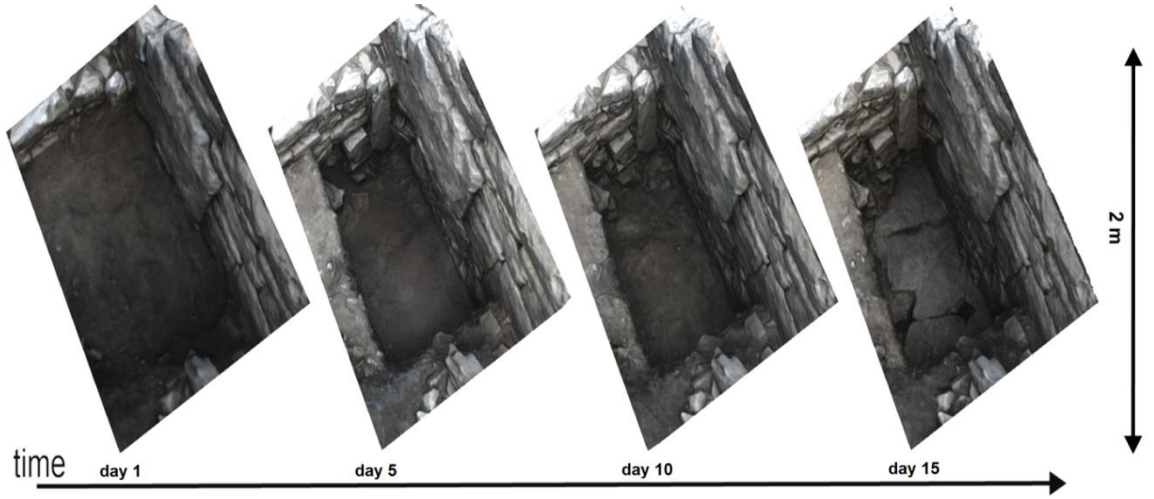

Figure 7-6: Exemplary time series of Zone G

The graphic user interface (GUI) of the management system was split in four sections (Figure 7-7, left): the Harris matrix, the actual 3D model, an overview map and a metadata table. The main feature within the management and consultation system was the Harris matrix. This graph-based matrix structure enabled the description of topological and chronological relations between archaeological objects and stratigraphic units (Harris, 1989). During the field campaign, both elements were recorded as contexts and documented by a large number of images. The relations between contexts were modelled and visualised by the creation of a diagram, where nodes represented each context. The sequence of the context and relation between other contexts were represented by directed graphs and by the layered order of the nodes. Some useful software tools exist for the composition of a Harris matrix (Hundack et al., 1997 and Traxler et al., 2008). However, MS Visio was used for the composition, in order to enable the visualisation of the model in a browser, without required plug-ins. The software also enabled to put a hyperlink on every feature within the model, which enabled interaction between the model and different objects in the interface.

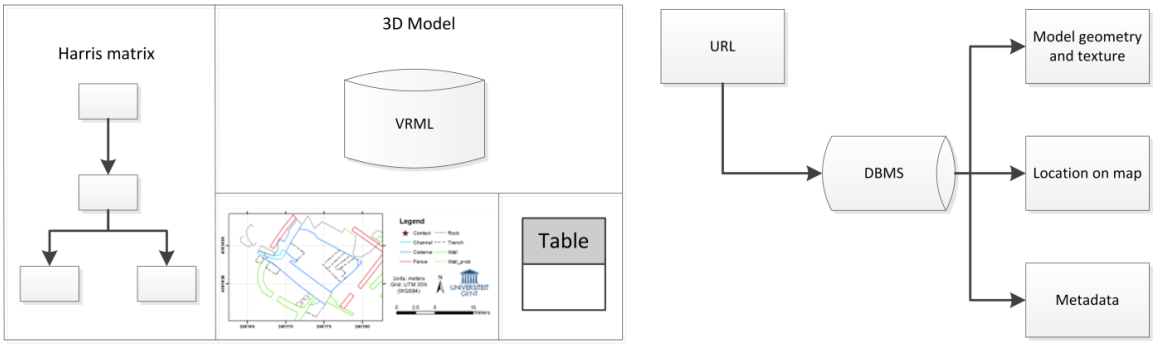

Figure 7-7: Sketch (left) and conceptual view (right) of the management system

The static Harris matrix provided the actual interaction between the user and the management system. Each node contained a Uniform Recourse Locator (URL) linking features in different databases that were related to the specific context. The URL was processed as a query and controls the 3D model view, the location on the map and the metadata view within the database management system (DBMS, Figure 7-7, right). The 3D model viewer received a URL and will manage the geometry and texture in the appropriate container, pointing to a certain 3D visualisation plug-in. The URL may optionally contain of a view point definition, defining the virtual camera position, orientation and coordinates of the focus point, where the camera points should aim at. The Virtual Reality Modelling Language (VRML) was chosen to describe the 3D models. Although this language is already succeeded by X3D, VRML is still a frequently used language for the description of virtual reality in archaeology and cultural heritage (Mendes et al., 2012 and Rua and Alvito, 2011). Because of its frequent usage, VRML is supported by many commercial and non-commercial 3D viewers. When a specific context is selected, the corresponding 3D model will be loaded using a 3D visualization browser plug-in.

The URL also requests for a map, which is loaded as a static image of the site provided with a marker at the context's location. The map window represents the precise location. In a later stadium, it should be possible to manipulate the database using an interactive map interface. Such system may be implemented as a web feature service (WFS) or web mapping service (WMS). For this pilot study, the static map was used, loaded as portable network graphic (PNG). The base layer of this map was equal to the topographic measurement map of Figure 7-3. An overview of the architecture of the prototype management system is presented in Figure 7-8. The Harris matrix is used by the client to request data. Each node is linked with its corresponding context. This context is the main identifier to a date, a series of topographic measurements and metadata. The coordinates are linked with a GIS (Geographic Information System), in order to generate a map. In further steps, the implementation of a WFS or WMS is foreseen, as well as the assignment of a viewpoint to each coordinate (Koutsoudis et al., 2013b).

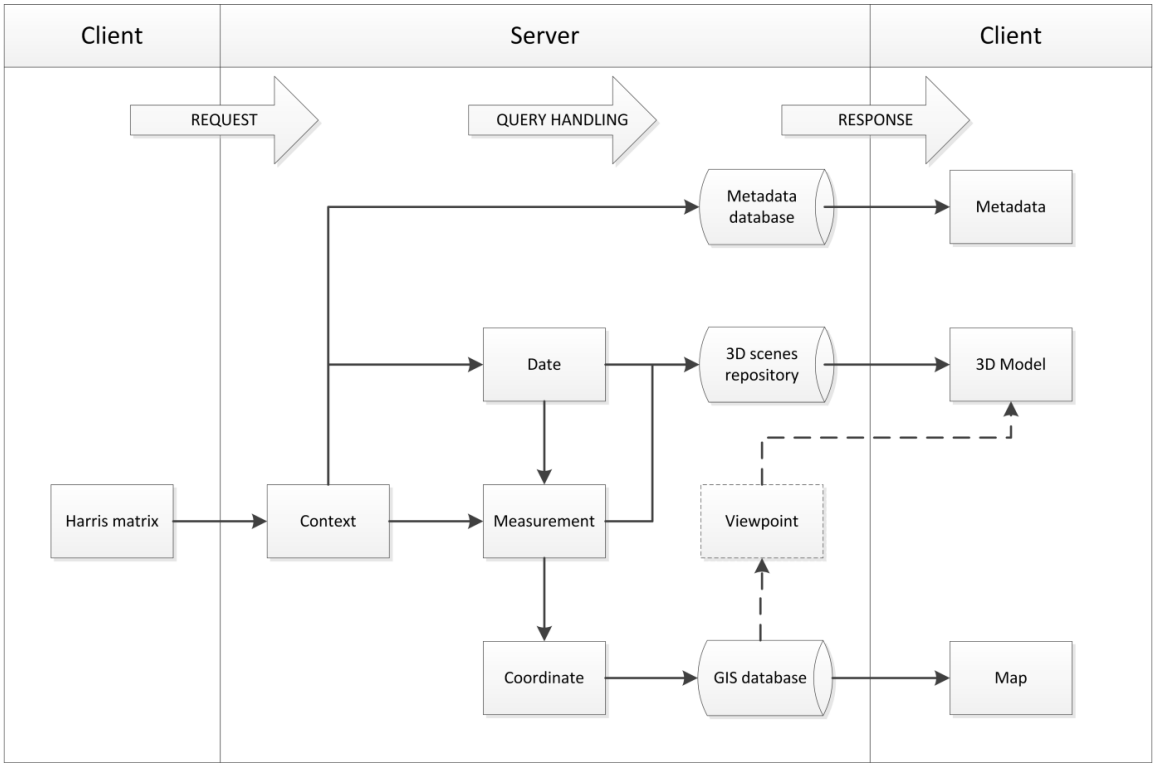

Figure 7-8: Architecture of the prototype management system

These viewpoints may highlight objects of special interest in the 3D model, but in the current implementation, an overview point suffices. The implementation of these concepts resulted in the actual version of the management system, with a graphical user interface presented in Figure 7-9.

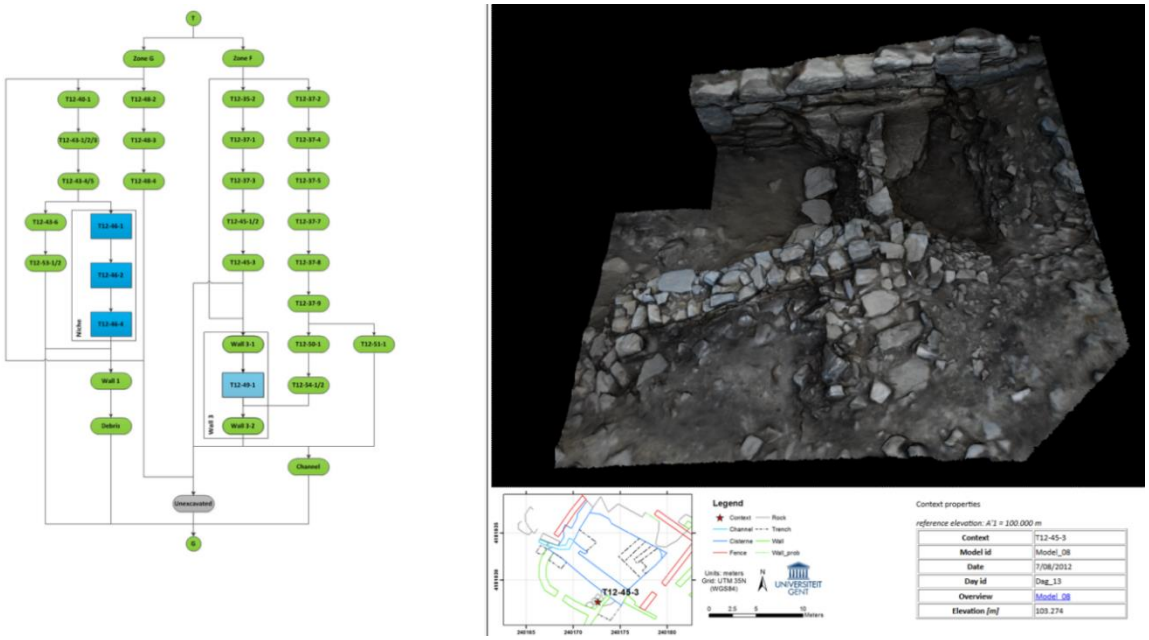

Figure 7-9: Screenshot of the management system, as implemented in the current version

In contrast with many other management systems, the presented implementation is not a final product for the analysis and visualisation of the data. During the excavation and the post-

processing of the finds, many more data can be added to the system, from the field sheets of the excavated contexts to the artefact database. This requires a large degree of flexibility of the management system for adding, removing and modifying data. This important aspect is respected by implementing more complex protocols, like PHP and SQL.

7.5. ***Other advanced applications***

Besides the advantages of 3D modelling in the archaeological workflow of an excavation, it can also have its use in more specific applications.

7.5.1. Capacity calculation of the cistern

In the context of this excavation and the wider research questions, a capacity calculation was a particularly valuable technique. As mentioned above, a careful water management was crucial for the metallurgical activities at Thorikos. A definition of the capacity of the site's largest water reservoir will contribute to our knowledge on the production output of the individual workshop and on a larger scale, of Thorikos as an industrial site.

Figure 7-10: Screenshots of 3D model of the cistern after partial excavation (for dimensions: Figure 7-11)

Figure 7-10 shows several viewpoints of the 3D model of the cistern, built by using image-based 3D modelling and total station measurements. Since the 3D model was constructed using a series of GCPs, a horizontal reference plane could be defined. The elevation values were then projected on this plane, in order to generate a Digital Elevation Model (DEM). This DEM and some characteristic elevation points are visualised in Figure 7-11. Elevations (or depths) in this figure are related to the original surface, which is used as a reference level. By converting the 3D model to a DEM, the geometric complexity was reduced to 2.5D. This implies that every planimetric position had only one elevation value. Thus, it was not possible to model overhanging parts in the DEM and volumes covered by these overhangs were not included in the total capacity calculation.

The cistern can be divided into two zones, both used for water storage, as demonstrated in Figure 7-11. The first zone (I) was excavated until an elevation of −6.0 m, where the bottom of the cistern was reached, corresponding with zone A in Figure 7-2. Other points in this zone, with an

elevation of up to −3.5 m, remained unexcavated. Based on other fully excavated cisterns elsewhere in the region, it was assumed that the elevation of the entire bottom of the cistern is equal to −6.0 m. The second zone (II) consisted of bare rock with elevations between −2.5 m and −1.7 m and corresponds with zone E in Figure 7-2. The total capacity was calculated as the sum of the two separate volumes of zone (I) and zone (II), with an a priori reference plane at an elevation of −1.1 m. This was the elevation of the highest stone at the southern partition wall. It was assumed that this reference plane is horizontal and perpendicular to the gravity normal.

The volume of zone (I) was calculated by taking the area of the convex hull of this zone, which was 39.02 m^2. The a priori maximal elevation was -1.1 m, whereas the minimal elevation was -6.0 m, corresponding with a range of 4.9 m. The volume of zone (I) was then equal to 191.2 m^3. The solid rock surface of zone (II) was totally excavated and sloping, so a grid-wise volume calculation was used. For each pixel within the convex hull, the difference between the elevation of that pixel and the elevation of the reference plane was calculated. The resolution of the DEM was equal to 0.01 m^2 and the total area of zone (II) was equal to 17.9 m^2. The volume of zone (II) was thus equal to the sum of all elevation differences times the area of the zone, corresponding with 18.42 m^3. Consequently, the total capacity of the cistern was equal to 209.6 m^3.

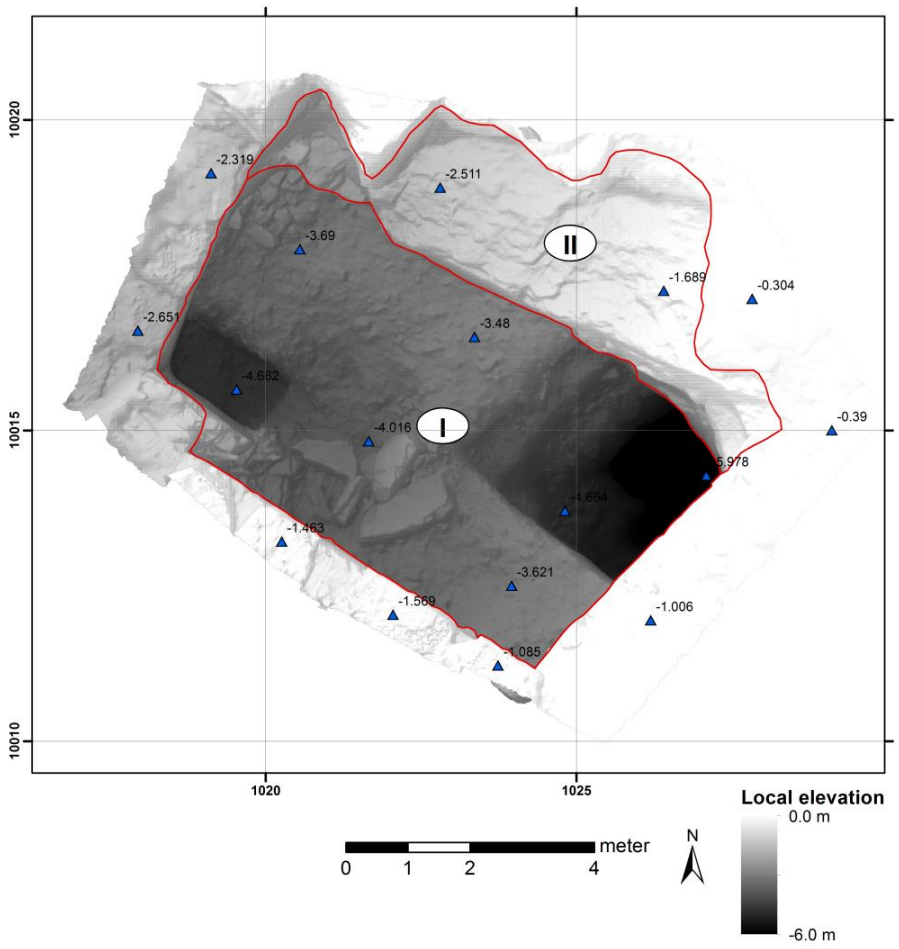

Figure 7-11: Digital elevation model of the cistern and zonal division (grid: local coordinates)

7.5.2. Detailed wall mapping

The composition of stone suffers from important errors, which are caused by, inter alia, erroneous grid construction and usage, human subjectivity and, environmental conditions in terms of temperature, humidity and comfort, etc.

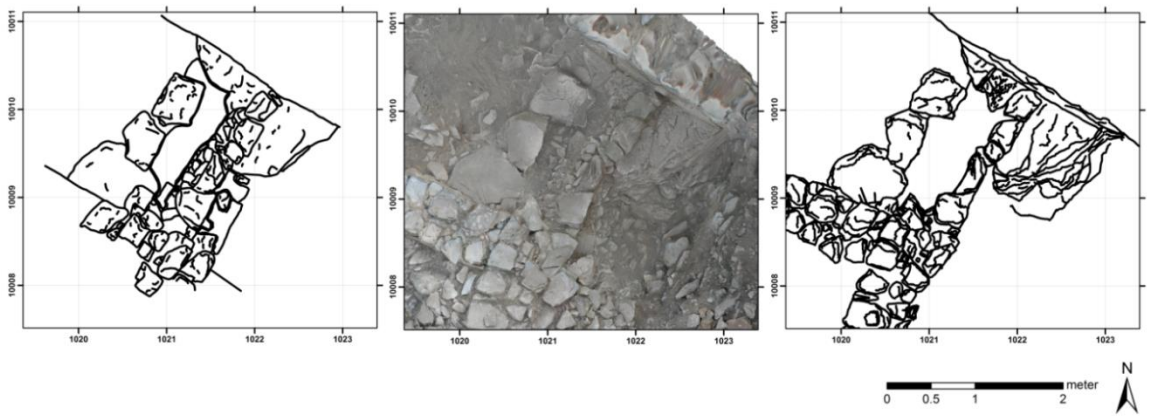

Figure 7-12: Stone plan and orthophoto (middle) of the intersecting area of Wall 2 and Wall 3, manual (left) and orthophoto digitising (right)

As mentioned in section 3, one of the products of a SfM-MVS workflow is an orthophoto. In contrast with a conventional image, containing a central perspective, the advantage of such an image is the absence of geometrical deformations, caused by the orthogonal projection of the image on a DEM. As a result, orthophotos are very useful for in situ mapping. Characteristic lines were traced manually or with the use of edge detection filters. The result of this procedure is demonstrated in Figure 7-12 (right), where the lines represent the stone outlines.

A visual comparison between the manual stone mapping and orthophoto-based stone mapping states the difference of the two approaches. In spite of the much smoother polylines in the manual map, a misalignment with the orthophoto was apparent. This is most clear in the southernmost part of the image. Furthermore, several break lines or marginal ridges were not or not correctly mapped, due to the often difficult conditions on field (visibility, heat, time, etc.) … The orthophoto-based vector map had a much better correspondence with the degree of detail of the orthophoto itself. This stresses out the user dependency of the results of both techniques. However, since these maps could be made in post-processing, and thus off-site, the extra time required for the orthophoto generation is partially compensated by a significant saving of time during the excavation itself.

7.6. ***Discussion***

Virtual 3D models were generated systematically on a daily base sequence, in order to evaluate the excavation process and to place the archaeological contexts in a correct spatial neighbourhood. During the campaign, almost 3000 images were taken and topographic measurements were performed. These data were used for the construction of 38 digital 3D models of the excavation

site. As demonstrated in this paper, the advantages of using 3D models are manifold and apply on all phases of the archaeological workflow. In contrast with conventional archaeological data processing, the entire processing chain was digital and the research results in a systematic DEM of the evolution of the excavation during the three-week campaign. The models allowed the archaeologist to perform intensive research on different contexts in a digital 3D environment, even when this context had been removed. As a result, the presented DEMs were useful for in situ documentation, interpretation and management. Besides, the absolute orientation of the models by topographic means enabled geometric evaluation archaeological objects in post processing, the definition of topological relations between contexts and the construction of a wide range of derivatives, like orthophoto plans, wall drawings and contour line maps.

The 3D data facilitated to correlate, re-assess and re-assembly the sometimes fragmented information obtained during the excavation and the post-processing of the acquired data (Katsianis et al., 2008). Purely practically speaking, it guaranteed a smoother continuation of the activities on site, since a large part of the drawing was consciously postponed to the post-processing phase. Especially in Mediterranean excavations, where a regular day of an archaeological campaign is usually divided in excavating before noon and data processing in the afternoon, this methodology could easily be adopted. Newly recorded walls were for example photographed during the excavation in the early morning and subsequently modelled and drawn in the office in the afternoon. Furthermore, excavation units could more easily be investigated. Measurements could be performed from all angles, section cuttings could fluently be created and volumes calculated. Vertical sections were an extremely important tool in archaeology to record stratigraphic sequence (Zhukovsky, 2002). 3D models enabled to cut cross-sections off-site and wherever they were considered to be profitable, whereas on field only a restricted amount of cross-sections can be created due to time constraints. Another important advantage of the use of 3D models is the fact that visual obstacles can be removed easily. The only requirement is that the study object behind the obstacle is photographed in accordance with the rules (e.g. enough contrast, overlap and different acquisition positions or non-zero baselines) of image-based modelling. An example from this case study is the fact that the Greek Heritage Authorities were reluctant to grant the removal of olive tries on the site. One of these trees is in the middle of zone F, obscuring some important structures in a wider context from different viewpoints. It is easy to ignore this tree during the 3D reconstruction, resulting in an obstacle-free visualisation. This concept is clearly visible in Figure 7-13, where the original photograph (left) and the 3D reconstruction (right) correspond with the same viewpoint.

It must be mentioned that the proposed methodology may suffer from some drawbacks. The environmental conditions at the Greek site oblige to take the images at a limited time frame at dawn and after carefully cleaning the site. This implies that the excavation should be put on hold for a few moments. The quality of the markers has to be verified frequently and all objects on the site have to be terrestrially photographed. This is also an advantage of the methodology, since this systematic coverage is guaranteed with high accuracy and high resolution. Furthermore, since it is not preferred to perform the excavations as a function of the 3D data acquisition, the images can also be taken using sun screens in order to avoid shades. In the case of the Thorikos excavation in 2012, the working area was limited and could be fully covered by terrestrial images. If the site has

larger dimensions or if the objects on the site are too complex to fully cover terrestrially, the use of a low cost Unmanned Aerial Vehicle (UAV) would be a very useful alternative (Perez et al., 2013). Such a flying platform extends the spatial extend of the image acquisition and also enables to cover difficultly reachable areas. Notwithstanding these two different acquisition methodologies, the result is a series of images that have to be processed using the same workflow. In our case, both the site cleaning and the acquisition of the images required only twenty to thirty minutes. The excavation started immediately after the image acquisition, altering the entire scene. The image acquisitions should be immediately successful, as the recording can only be done once. This requires profound training and photogrammetric expertise.

The post-processing of the images is frequently considered as a time consuming process, motivated by the performance of conventional photogrammetric procedures. Earlier research demonstrates that the image processing workflow require a few minutes to a few hours, depending on the desired processing parameters (Doneus et al., 2011). After selecting correct images, defining GCPs on the images and fine-tuning the parameters, most of this time goes to the reconstruction itself, which does not require human interaction but is fully automated.

During many excavation campaigns, a total station and a digital camera are standard equipment. Consequently, no extra on-site hardware and resulting costs are needed. Agisoft Photoscan, which is commercial software, was used for the 3D reconstruction and requires a powerful computer. In fact, this is the only additional cost, but one could also opt for open-source software (Kersten and Lindstaedt, 2010). Next to the expertise on the data acquisition, a thorough knowledge about the processing is indispensable. Recent publications about the use of 3D modelling in archaeological research indicate 3D modelling is already applied for entire sites (Verhoeven et al., 2012a and Verhoeven et al., 2012b), but also for soil profiles (De Reu et al., 2014) or rock art (Fritz and Tosello, 2007). These projects are just an example of the much recent projects where 3D models and digital orthophotos facilitate archaeological research.

Capacity calculations were employed to estimate volumes of soil samples in relation to the excavation unit volume and to calculate the amount of earth still to dig (Losier et al., 2007). The geometric accuracy of these products is high, especially in comparison with many manually generated equivalents. Within the framework of the Thorikos excavation, it proved to be a particularly useful tool to define the capacity of ‘Cistern no.1’. Due to the restricted time frame in which the campaign had to be conducted, it was only possible to clear one zone of the basin (zone A). Nonetheless, the model allowed the creation of an accurate assessment of its capacity. An extra advantage of working with image-based 3D modelling was that the texture and colour of the soil and archaeological features is also recorded. Investigating archaeological contexts through 3D models was therefore not only more accurate, but also more realistic.

Figure 7-13: Photograph (left) and 3D reconstruction (right) of zone F, demonstrating the advantageous effect of virtual obstruction removal

Up-to-date 3D information about the progress of the excavation is essential for various reasons:

- It facilitates the decision making about the further continuation of the campaign: new areas of interest, additions to existing areas or even adjustments on the excavation strategy can be defined by the interpretation of the latest DEMs and orthophotos.
- It enables fast exchange of information between the excavators and finds processors: on the one hand, excavators can assign their findings to specific context by creating a digital link between the feature and the model. On the other hand, finds processors can directly implement the results of their analysis in the model allowing a better focus on specific areas of the site.
- It allows the extension of a temporal GIS: contexts are modelled as closed 3D models. When a Harris matrix is used as a conceptual model of the topological relations between

features, the 3D GIS with temporal attribute forms the physical representation of the site. Temporal attributes enables the easy definition of relations between different features and they may assist in a better understanding of the spatial distribution of phenomenon.

The large number of 3D models requires the implementation of some management environment, in order to enhance flexibility of the consultation and analysis of the models. Parallel with the daily construction of the 3D models, a Harris matrix was generated for the documentation of different topological and chronological relations. Since the same relations exist between different successive 3D models, it would be obvious to generate a link between the Harris matrix and the virtual reconstructions. Not only is the Harris matrix simultaneously generated during the campaign, its interpretation is common practice in archaeological sciences. As a result, the conceptual file structure of the models within the matrix does not require much effort for the field expert. Implementing the system in an online server-client based environment improves the efficiently of the research work, as well as the visibility of the Thorikos-project for a wider public.

7.7. ***Conclusion***

In this paper, we demonstrated the use and management of archaeological 3D data. The 3D data were collected during an excavation campaign of the Cistern no.1 workshop in Thorikos, Greece in 2012. It involved topographic measurements and a large series of images. The data were processed in a SfM-MVS based workflow, resulting in a series of daily 3D models of specific areas of interest. The large number of models enabled the monitoring of the course of the excavation in a highly detailed and accurate way, enhancing the interpretation of the contexts. However, the efficient and clear management of these data was indispensable. We presented a management system focussing on the requirements of fast model visualisation, clear metadata consultation and the ability to use the data for advanced analysis. Using the system's architecture, it was also possible to add, remove and modify data in a transparent way. The implementation of more advanced protocols, like PHP and SQL, in the presented prototype, improves the performance of the system and will be done in the near future.

We also demonstrated the advanced use of 3D models to answer archaeological research questions or to improve the quality of the archaeological excavation documentation. Two examples were presented, focussing on capacity calculations and in situ mapping of stone wall remains. Within the framework of the Thorikos site, the calculation of the capacity of the cistern was essential for the research on the water management within its industrial context. An accurate and mobile procedure of calculating capacity was therefore indispensable. The presented SfM-MVS approach fitted these requirements. A second application was the use of SfM-MVS-based orthophotos for mapping. Based on a visual comparison, the orthophoto-based digitalisation of stone outlines tended to give significantly better results than its manual-visual counterpart.

Acknowledgement

This research is part of the research project “3D CAD modelling of spatial architectural volumes, using terrestrial laser scanning and LiDAR” (G082309N of the Fund for Scientific Research Flanders (FWO). This project is promoted by Prof. Dr. Ir. A. De Wulf, Prof. Dr. Ph. De Maeyer, Prof. Dr. N. Van De Weghe, Prof. Dr. S. Gautama, Prof. Dr. R. De Meyer and Arch. M. Mattys. The authors would like to acknowledge the support of FWO-Flanders.

References

Boehler, W., Marbs, A., 2004. 3D scanning and photogrammetry for heritage recording: a comparison, 12th Conference of Geoinformatics - Geospatial Information Research: Bridging the Pacific and Atlantic, Gävle, Sweden, pp. 291-298.

Chen, L., Lo, C., Liu, C., Chen, A., 2000. Orientation modeling by matching image templates of a GCP database, 21th Asian Conference on Remote Sensing, Kuala Lumpur, Malaysia, pp. 6 (on CD-ROM)

De Reu, J., Plets, G., Verhoeven, G., De Smedt, P., Bats, M., Cherretté, B., De Maeyer, W., Deconynck, J., Herremans, D., Laloo, P., Van Meirvenne, M., De Clercq, W., 2013. Towards a three-dimensional cost-effective registration of the archaeological record. Journal of Archaeological science 40(2), 1108-1121.

De Reu, J., De Smedt, P., Herremans, D., Van Meirvenne, M., Laloo, P., De Clercq, W., 2014. On introducing an image-based 3D reconstruction method in archaeological excavation practice. Journal of Archaeological Science 41 (January), 251-262.

De Smedt P., Van Meirvenne M., Herremans D., De Reu J., Saey T., Meerschman E., Crombé P., De Clercq W., 2013. The 3-D reconstruction of medieval wetland reclamation through electromagnetic induction survey. Scientific Reports, 3 (1517). pp. 5.

De Wulf, A., Van Herck, T., De Dapper, M., De Vliegher, B.M., 2000. Analysis of the efficiency in archaeology of GPS satellite surveying versus classical surveying using totalstations: Applications in the Thorikos region and on the Pyrgari (Greece), in: Vermeulen, F., De Dapper, M. (Eds.), Geoarchaeology of the Landscapes of Classical Antiquity, pp. 197-207.

Dellepiane M., Dell’Unto N., Callieri M., Lindgren S., Scopigno R., 2013. Archeological excavation monitoring using dense stereo matching techniques. Journal of Cultural Heritage 14 (3), 201-210.

Doneus M., Verhoeven G., Fera M., Briese C., Kucera M., Neubauer W., 2011. From Deposit to Point Cloud - A Study of Low-Cost Computer Vision Approaches for the Straightforward Documentation of Archaeological Excavations. In: Čepek A. (Ed.). XXIIIrd International CIPA Symposium, Prague, 12-16 September 2011. Geoinformatics, 6. Faculty of Civil Engineering, Czech Technical University, Prague: 81-88.

Forte M., Dell'Unto N., Issavi J., Onsurez L., Lercari N., 2012. 3D Archaeology at Çatalhöyük. International Journal of Heritage in the Digital Era, 1 (3): 351-378.

Fritz, C., Tosello, G., 2007. The hidden meaning of forms: methods of recording Paleolithic parietal art. Journal of Archaeological Method and Theory 14 (1), 48-80.

Gruen, A., 1985. Adaptive least squares correlation: a powerful image matching technique. South Africa Journal of Photogrammetry, Remote Sensing and Cartography 14 (3), 175-187.

Harris, E., 1989. Principles of archaeological stratigraphy. Academic Press, London, UK.

Heipke, C., Kornus, W., Strunz, G., Thiemann, R., Colomina, I., 1992. Automatic photogrammetric processing of Spot imagery for point determination, DTM generation and orthoprojection. International Archives of Photogrammetry and Remote Sensing 29 (4), 465-471.

Hendrickx, M., Gheyle, W., Bonne, J., Bourgeois, J., De Wulf, A., Goossens, R., 2011. The use of stereoscopic images taken from a microdrone for the documentation of heritage - An example from the Tuekta burial mounds in the Russian Altay. Journal of Archaeological Science 38 (11), 2968-2978.

Hermon, S., 2008. Reasoning in 3D: a critical appraisal of the role of 3D modelling and virtual reconstructions in archaeology. in: Frischer, B., Dakouri-Hild, A. (Eds.), Beyond Illustration: 2D and 3D Digital Technologies as Tools for Discovery in Archaeology, BAR International Series 1805, Archaeopress, Oxford, pp. 35–44.

Hülksen, F., Eckes, C., Kuck, R., Unterberg, J., Jörg, S., 2007. Modeling and animating virtual humans for real-time applications. International Journal of Virtual Reality 6 (4), 11-20.

Hundack, C., Mutzel, P., Pouchkarev, I., Thome, S., 1997. ArchE: A graph drawing system for archaeology, in: Di Battista, G. (Ed.), Graph Drawing. Springer-Verlag, Heidelberg, Germany, pp. 297-302.

Kakavoyiannis, E., 2005. Μέταλλα συγκεχωρημένα: η οργάνωση της εκμετάλλευσης του ορυκτού πλούτου της Λαυρεωτικής από την Αθηναική Δημοκρατία (Metals "ergasima" and "synkechoremena". The exploitation of the mineral wealth of the Lavrion mines by the Athenian Democracy). Archaeological Receipts, Athens, Greece.

Katsianis, M., Tsipidis, S., Kotsakis, K., Kousoulakou, A., 2008. A 3D digital workflow for archaeological intra-site research using GIS. Journal of Archaeological science 35(3), 655-667.

Kersten, T., Lindstaedt, M., 2010. Reality-based 3D modeling, segmentation and web-based visualization, in: Ioannides, M. (Ed.), 3rd International Euro-Mediterranean Conference on Digital Heritage (EuroMed 2010). Springer, Limassol, Cyprus, pp. 140-152.

Koller, D., Frischer, B., Humphreys, G., 2009. Research challanges for digital archives of 3D cultural heritage models. Journal on Computing and Cultural Heritage 2 (3), 1-17.

Koutsoudis, A., Stravroglou, K., Pavlidis, G., Chamzas, C., 2013. 3DSSE: A 3D scene search engine, exploring 3D scenes using keywords. Journal of Cultural Heritage 13 (2), 187-194.

Koutsoudis A., Vidmar B., Ioannakis G., Arnaoutoglou F., Pavlidis G., Chamzas C., 2013. Multi-image 3D reconstruction data evaluation. Journal of Cultural Heritage: http://dx.doi.org/10.1016/j.culher.2012.1012.1003.

Losier, L.-M., Pouliot, J., Fortin, M., 2007. ED geometrical modeling of excavation units at the archaeological site of Tell 'Acharneh (Syria). Journal of Archaeological science 34, 272-288

Lourakis, M., Argyros, A., 2009. SBA: A software package for generic sparse bundle adjustment. ACM Transactions on Mathematical Software 36 (1), 1-30.

Lucas G., 2001. Destruction and the Rhetoric of Excavation. Norwegian Archaeological Review 34(1), 35-46.

Mendes, C., Silva, L., Bellon, O., 2012. IMAGO Visualization System: an interactive web-based 3D visualization system for cultural heritage applications. Journal of Multimedia 7 (2), 205-210.

Pavlidis, G., Koutsoudis, A., Arnaoutoglou, F., Tsioukas, V., Chamzas, C., 2007, Methods for 3D digitization of cultural heritage. Journal of Cultural Heritage 8 (1), 93-98.

Pérez, M., Agüera, F., Carvajal, F., 2013. Low cost surveying using an unmanned aerial vehicle. International Archives of Photogrammetry and Remote Sensing and Spatial Information Sciences 40 (1/W2), 311-315.

Plets G., Gheyle W., Verhoeven G., De Reu J., Bourgeois J., Verhegge J., Stichelbaut B., 2012a. Towards a Three-Dimensional Registration of the Archaeological Heritage of the Altai Mountains. Antiquity, 86(333): 884–897.

Pollefeys M., Koch R., Vergauwen M., Van Gool L., 2000. Automated reconstruction of 3D scenes from sequences of images. ISPRS Journal of Photogrammetry and Remote Sensing, 55(4), 251-267.

Pollefeys M., Van Gool L., Vergauwen M., Cornelis K., Verbiest F., Tops J., 2003. 3D recording for archaeological fieldwork. Computer Graphics and Applications, IEEE, 23(3), 20-27.

Remondino, F., 2011. Heritage recording and 3D modeling with photogrammetry and 3D scanning. Remote Sensing 3 (6), 1104-1138.

Robertson, D., Cipolla, R., 2009. Structure from motion, in: Varga, M. (Ed.), Practical image processing and computer vision. John Wiley, Hoboken, NJ, USA., p. 49.

Rottensteiner, F., Trinder, J., Clode, S., Kubik, K., 2007. Building detection by fusion of airborne laser scanner data and multi-spectral images: performance, evaluation and sensitivity analysis. ISPRS Journal of Photogrammetry and Remote Sensing 62 (2), 135-149.

Rua, H., Alvito, P., 2011. Living the past: 3D models, virtual reality and game engines as tools for supporting archaeology and the recontruction of cultural heritage: the case-study of the Roma villa of Casa de Freiria. Journal of Archaeological Science 38 (12), 3296-3308.

Shashua, A., Werman, M., 1995. Trilinearity of three perspective views and its associated tensor, Fifth International Conference on Computer Vision. IEEE, Boston, MA, USA, pp. 920-925.

Seitz, S., Curless, B., Diebel, J., Scharstein, D., Szeliski, R., 2006. A comparison and evaluation of multi-view stereo reconstruction algorithms, IEEE Computer Society Conference on Computer Vision and Pattern Recognition, New York, NY, USA, 17-22 June, pp. 519-528

Tack, F., Debie, J., Goossens, R., De Meulemeester, J., Devriendt, D., 2005. A feasible methodology for the use of close range photogrammetry for the recording of archaeological excavations, Proceedings of the CIPA 2005 XX International Symposium, Torino, Italy, pp. 561-565.

Tack, F., Buyuksalih, G., Goossens, R., 2012. 3D building reconstruction improvement based on given ground plan information and surface models extracted from spaceborne imagery. ISPRS Journal of Photogrammetry and Remote Sensing 67 (1), 52-64.

Traxler, C., Neubauer, W., 2008. The Harris matrix momposer: a new tool to manage archaeological stratigraphy, in: Börner W., U.S. (Ed.), Archäologie und Computer: Kulturelles Erbe und Neue Technologien, Vienna, Austria, pp. 12 (on CD-ROM)

Van Liefferinge, K., Docter, R., Pieters, T., van den Eijnde, F., 2011a. The excavation of Cistern no.1 at Thorikos, in: Docter, R., De Wulf, A., Monsieur, P., van den Eijnde, F., van de Put, W., Van Gelder, K. (Eds.), Thorikos 10, Reports and Studies. University Press, Ghent, Belgium.

Van Liefferinge, K., Stal, C., De Wulf, A., 2011b. The Thorikos excavations 1963-2010 in maps, in: Docter, R., De Wulf, A., Monsieur, P., van den Eijnde, F., van de Put, W., Van Gelder, K. (Eds.), Thorikos 10, Reports and Studies. University Press, Ghent, Belgium.

Van Liefferinge, K., van den Berg, M., Stal, C., Docter, R., De Wulf, A., Verhoest, N., 2014. Reconstructing the position of Thorikos in the Laurion silver mining district (Attica, Greece) through hydrological analyses. Journal of Archaeological Science 41, 272-284.

Verhoeven, G., 2011. Taking computer vision aloft - archaeological three-dimensional reconstruction from aerial photographs with PhotoScan. Archaeological Prospection 18 (1), 67-73.

Verhoeven G., Taelman D., Vermeulen F., 2012. Computer vision-based orthophoto mapping of complex archaeological sites: the ancient quarry of Pitaranha (Portugal-Spain). Archaeometry, 54(6), 1114-1129.

Verhoeven, G., Doneus, M., Briese, C., Vermeulen, F., 2012. Mapping by matching: a computer vision-based approach to fast and accurate georeferencing of archaeological aerial photographs. Journal of Archaeological Science 39 (7), 2060-2070.

Wang, L., Kang, S., Szeliski, R., Shum, H., 2001. Optimal texture map reconstruction from multiple views. IEEE Computer Vision and Pattern Recognition 1 (1), 1-8.

Zhukovsky, M., 2002. Handling digital 3-D record of archaeological excavation data. Archaeological Informatics: Pushing the Envelope. CAA2001, BAR International Series 1016, 431-438.

Chapter 8

3D city mapping and data management using interconnected GI-software and Python

8. 3D city mapping and data management using interconnected GI-software and Python[8]

Abstract

Most current digital 3D city mapping procedures have either a low degree of automation or require much specialized skills. Moreover, the construction process is the result of an equilibrium between the desired level of detail on the one hand and model performance on the other hand. Although environmental 3D models and 3D city models in particular are essential for a wide range of applications and disciplines, these difficulties are substantial bottle necks for the availability of the models. As a result, spatial data users are able to obtain very large 3D data sets, but the use of city models derived from these data is frequently out of range.

In this paper, a new approach for the construction of 3D city models is presented using different spatial data sets. An Airborne Laser Scanning (ALS) point cloud, airborne imagery and standard digital 2D cadastre data are used for the 3D modelling. The novelty of this approach is the fact that various widely used software applications in geographic sciences are used and that the different processing steps are integrated into one single workflow. Different python scripts are written to automatically perform tasks in the software. Notwithstanding the use of quotidian software applications, the procedure itself is not a black box and much parameter adjustment is allowed through the entire workflow. The first step involves point processing and feature detection on an ALS point cloud, resulting in the separation of building and ground points from vegetation and other points in the point cloud. Second, the detected building features are described by a simplified triangular model. Thereafter, a texture map is generated for each feature and a 3D city model is finally produced. The presented workflow is illustrated by the construction of city models of some parts of Ghent and Geraardsbergen (Belgium). For this construction, two high density ALS point clouds were used, together with high-resolution airborne imagery, which was obtained during a recent photogrammetric campaign. The results of the presented procedure can be managed and analysed in a CityGML database, and different visualisations can be generated in standard 3D viewers. Moreover, kml files can be generated, significantly increasing the usability of these city models. The city model might be further enriched with building information models of the individual buildings in the model, if they are available.

Keywords: city modelling, 3D mapping, CityGML, processing, data management

8.1. *Introduction*

Digital 3D models of urban environments and landscapes play an essential role in a large range of applications. Urban planning, city management, calamity control, solar panel potential mapping, noise mapping or the development of the G4 network require virtual models with various Levels of Detail (LoD), attribute contents and spatial scale. Especially for higher LoDs, the manual

[8] Modified from: Stal, C., De Maeyer., P., De Meyer, R., Pauwels, P., Nuttens, T., Verstraeten, R. & De Wulf, A. (2014), 3D city mapping and data management using interconnected GI-software and Python. *Journal of Maps, Under review.*

production of these models is common practice (Heo et al., 2013), whereas the automatic construction of urban city models using airborne imagery and Airborne Laser Scanning (ALS) is still a challenging task (Nguyen et al., 2012). It is frequently required to describe geometry in the digital urban model by a limited number of features, while the study area is frequently oversampled by a point cloud. Thus, two types of 3D models can be developed starting from an urban point cloud. On the one hand, the simplest type contains a triangulation or tetrahedonation of the ALS point cloud, possibly after a point classification is performed (Penninga et al., 2006). This type of models is easy to construct, but is hard to use because of the considerable amount of data involved. On the other hand, 3D models built using geometric solid primitives are very easy to describe, but they require complex detection techniques and they result in a significant loss of detail. Notwithstanding the kind of 3D model that is aimed for, 3D urban environmental models are mostly generated using multiple spatial data sources. 3D city mapping using aggregates of spatial data is based on a chain of multiple processes. These processes have been discussed for many decades and involve filtering, classification, detection, modelling and simplification of geometric features, as well as texture mapping and semantic enrichment of these features (Haala and Kada, 2010). The modelling workflow presented in this paper is based on the geometric reconstruction using ALS point clouds, texture mapping using airborne imagery and semantic enrichment using a large scale digital map. ALS is a common 3D data acquisition technique for the modelling of urban and rural environments (Doneus et al., 2008; Oude Elberink and Vosselman, 2011; Stal et al., 2013b). Next to ALS, it is also possible to reconstruct the geometry of environments by processing airborne imagery in a photogrammetric workflow. However, this topic will not be covered in this paper. Here, airborne imagery is only used to generate the appearance of the model by texture mapping.

Although 3D city mapping is still a dynamic research topic, it appears that most contributions mainly focus on data acquisition, data processing, or data management. In this paper, an integrated approach on data processing and data management is presented. Different governmentally acquired large scale data sets will be used for the construction of a 3D virtual model, described by CityGML. CityGML is a standard for the modelling and exchange of virtual 3D city maps (Kolbe et al., 2005). Interesting attempts to use such data in a national or state context are presented for the Netherlands (van den Brink et al., 2013) and Germany (Over et al., 2010). In a Belgian context, challenges on the implementation of CityGML for the Flemish large scale map (GRB: *Grootschalig Referentie Bestand* or Large Scale Reference File) are discussed (De Cubber and Van Orshoven, 2012). These authors mainly focus on the different approaches in defining relations between features and on the rather diverge ontology.

An innovative approach is presented in this paper for the construction of 3D city maps. The workflow is illustrated by a case study on the city of Ghent and Geraardsbergen, both situated in Belgium. It will be clear that this procedure results in very good models with LoD1 and LoD2 using the integrated approach. The workflow is implemented using different well-known software for geo-scientists in combination with *Python* scripting (Stal et al., 2010). The novelty of the procedure is the ability to generate 3D city models from scratch, with many options to manipulate processing parameters. This approach enables a smooth integration of city modelling projects in other projects where spatial data are used for environmental studies, planning or management. For

example, the data could efficiently be used in smart cities projects, especially if the city models are further enriched with available data sets of a different kind, including, for instance, building information, public transport data, electricity grid data, and so forth. We will specifically look into a combination of the city model with possibly available Building Information Models (BIM) (Eastman et al., 2008).

In the following section, the presented workflow is elaborated, covering an overview of the methodology (2.1) and the used data (2.2). Thereafter, each separate part of the process is discussed, focussing on the point cloud processing (2.3), the feature modelling (2.4) and the model appearance (2.5). The management system for exchanging, visualizing and analysing the model is discussed in section 2.6, followed by some results in section 3. These findings are also used to motivate the extension of the model to LoD3 and LoD4 in section 4. This extension allows the development of smart city management systems.

8.2. ***Methods***

8.2.1. General overview of the approach

The presented workflow is based on the decision to process the geometry, the semantics and the appearance of the model in a sequential order. In order to use a 3D model as a map, geometric objects require an appearance as a function of both the spatial and non-spatial properties. The latter can consist of attribute data, radiometric data or a combination of both. The 3D mapping techniques are implemented in a semi-automatic workflow for processing and managing data. In the suggested workflow, ALS data are used as a starting point for the urban reconstruction, as schematized in Figure 8-1. It is assumed that these data are already pre-processed (in terms of geometric adjustment) and that they can be used as-is for the modelling process. However, these data require point cloud post-processing, which concern the removal of outliers and the classification of the point cloud in ground points and building points. Next to the use of a point classifier, a building point can be validated by a point-in-polygon test (Ooms et al., 2009), using the cadastre data. This test also enables to start the feature modelling, meaning that attribute data from the cadastre database can be assigned to a series of corresponding points. Moreover, the integrated use of these two data sources enables to perform a feature-based object simplification (Cignoni et al., 1998). The final data processing step involves the texture mapping or image draping of the building and non-building features, using a series of correctly positioned and oriented images in a 3D space.

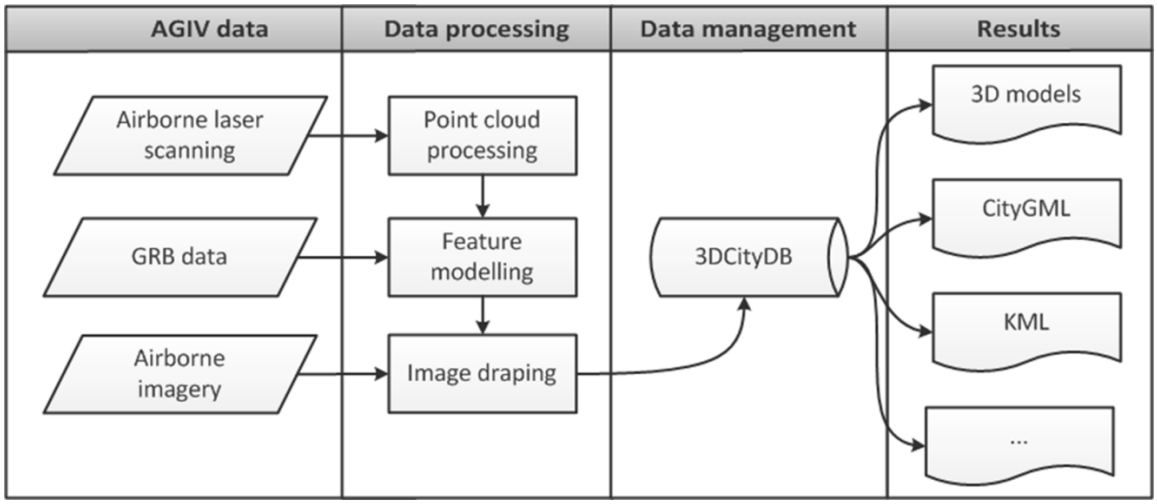

Figure 8-1: General 3D city mapping workflow

After processing the data, a system for data management is required. The proposed data management system should allow the construction of various virtual 3D representations, like X3D or VRML, and geographic products, like models described by CityGML or KML. Ideally, such a data management system allows the incorporation of data coming from other sources, such as building information or public transport information. Using a query language and CityGML manipulation libraries, like SQL and CityGML4J, it is possible to generate dynamic 3D mapping results. The data processing step and data management chain are further elaborated below.

8.2.2. Used data

The data of the Ghent study area have been acquired during two flights in 2008 (ALS) and 2009 (airborne imagery). These data were used for the geometrical 3D reconstruction of the city centre, within the context of the 'Gent in 3D' project (Ghent, 2009). The city of Geraardsbergen was covered in April 2012, when a test campaign was organized by the Flemish Geographical Information Agency (AGIV) for updating the already existing ALS and imagery data set. The test area has a size of approximately 30 km^2 and has a great variability of rural landscapes (AGIV, 2013). A summary of the metadata of the airborne images is presented in Table 8-1 and a summary of the ALS data is presented in Table 8-2. Two samples of the ALS data are presented in Figure 8-2. Although the data set covering the city of Geraardsbergen contains a colour value for each measured point, these colour data are not used for this procedure. The semantic data for the city models are gathered from the GRB, which is a Flemish kind of a cadastre. However, the GRB is not a cadaste sensu stricto, since it has no legal or fiscal meaning. For this research, only the layer containing buildings is used.

It is important to mention that the procedure starts with the assumption that all the data are already pre-processed, and thus ready for usage. The use of spatial data from different sensors irrevocably results in inconsistencies (Veregin, 1999) or geometrical offsets (Bretar et al., 2006) between these data sets. Inconsistencies refer to spatial redundancies and to violations of topological rules. Offsets are mainly caused by the misalignment of data acquisition sensors, by

the accuracy of the sensors and by the workflow for data processing. In both cases, the resulting incoherence of the data can be reduced through the different steps in the processing workflow (Stal et al., 2013a). Since the used data sets are intensively validated by the contracting authority, it is assumed that the different data sources are already geometrically coherent.

Table 8-1: Metadata of the airborne images

Study area		Ghent (Belgium)		Geraardsbergen (Belgium)	
Flight date		April 2008		April 2012	
Measuring system		*Microsoft UltraCamX*		*IGI DigiCAM*	
Altitude (above ground) [m]		2250		400	
Image format	long track [mm][pixel]	67.8	9420	36.8	5412
	cross track [mm][pixel]	103.9	14430	49.1	7216
Pixel size [µm]		7.2 x 7.2		6.8 x 6.7	
GSD [m]		0.15		0.08	
Focal length [mm]		100.5		35.1	

Table 8-2: Metadata of the ALS data

Study area	Ghent (Belgium)	Geraardsbergen (Belgium)
Flight period	July 2009	April 2012
Measuring system	*FUGRO Fli-Map 1000*	*IGI LiteMapper 6800*
Altitude (above ground) [m]	290	390
Measuring frequency [Hz]	250 000	266 000
Average point density [P/m²]	20	27

Figure 8-2: Illustrative bird's eye view of the ALS point cloud for Ghent (left) and Geraardsbergen (right)

8.2.3. Point cloud processing

One of the main requirements when dealing with an ALS point cloud is an accurate and efficient point classification or filtering (Briese, 2010; Pfeifer and Mandlburger, 2008). Using ALS sensors, the backscatter of the laser signal can occur on either ground or non-ground objects, resulting in a

single point per transmitted signal. Moreover, due to the laser beam footprint size, several objects at different distances may contribute to the echo waveform, e.g. by the canopy of a tree and the underlying ground. In this case, it is useful to distinct first, second,… echoes. Since point sets are frequently just a large list of point coordinates without further attributes, most classification algorithms are typically based on geometrical properties and neighbourhood functions (Sithole and Vosselman, 2004). In the 3D city mapping workflow presented in this paper, the point classifier of *LASTools* is used (Isenburg and Shewchuk, 2013). An overview and comparison of different ground point extraction algorithms is presented by (Chen et al., 2013). Although the results of the *LASTools* classifier are good, the algorithms behind the classification modules are not known (Podobnikar and Vrecko, 2012). However, the software has the ability to perform the entire point processing workflow in a batch process (Hug et al., 2004) or in a *Python* script in *ESRI ArcGIS*. Based on generated messages during the point classification, the following pseudo-code can be formulated:

```
Input unclassified point cloud
Set units, step size, spike size and offset size (m, 5, 1+10, 0.05)
Find initial ground points
Generate initial ground estimate
Refine ground points
Add terrain features
Integrate points higher than the threshold
Calculate elevation of non-ground points above the ground
Classify non-ground points
   If point in planar neighbourhood then roof
   Else if Point in rough neighbourhood than vegetation
   Else set unknown
```

The resulting point cloud contains ground points and points classified as buildings (actually as roofs, since building façades are ignored) and vegetation. If no class can be assigned to a point with a certain probability, the class of this point remains unknown. Only the ground points and the points assigned to the roof class are used for the city modelling process. Thus, it is not required to extract generic classes and the use of a standard point cloud classification procedure is sufficient. An example classified point cloud is presented in Figure 8-3.

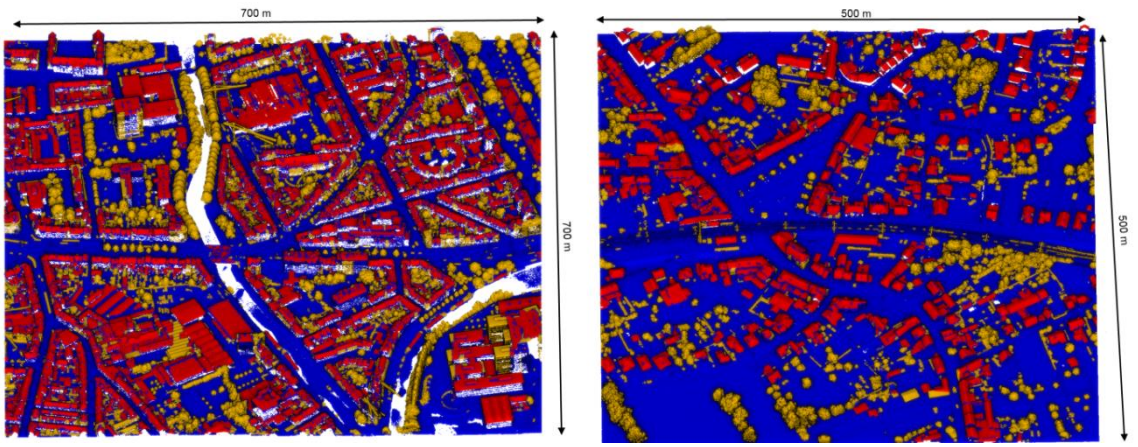

Figure 8-3: Illustrative bird's eye view of the classified ALS point cloud for Ghent (left) and Geraardsbergen (right), with separated ground (blue) building (red) and vegetation (yellow) points

8.2.4. Feature modelling

The feature modelling phase is implemented in *ESRI ArcGIS* and illustrated in Figure 8-4. This phase covers the construction of a triangular model of the ground surface and a large series of meshes for each building feature in the GRB data set. The first step in the feature modelling phase is the definition of a data link between a series of ALS points (A) and the corresponding building feature (B). Roof points are already classified in the point processing phase, so the next step is consequently a point-in-polygon test. Performing this test avoids the presence of non-building points inside a building polygon as well as the presence of roof points outside the building polygon. Possible anomalies within a building polygon are avoided with this procedure, while the walls of the building can be generalized by vertical planes, corresponding with LoD2. For example, ALS-points measured on façades will heavily distort the model of the roof structures, since a Delaunay triangulation is used here (De Wulf et al., 2006). Therefore, these points have to be removed from the point cloud. After refining the building point set, the ground points are converted to a Digital Terrain Model (DTM) and the roof points are triangulated to a Digital Surface Model (DSM) as well, using the building polygons as inside clipper (C). By then subtracting these two models, the final 3D model of all building features can be obtained, represented by Multipatches (D). The separated geometric features in this file as well as the DTM (E) are converted to *Wavefront Object* files (OBJ) for texturing.

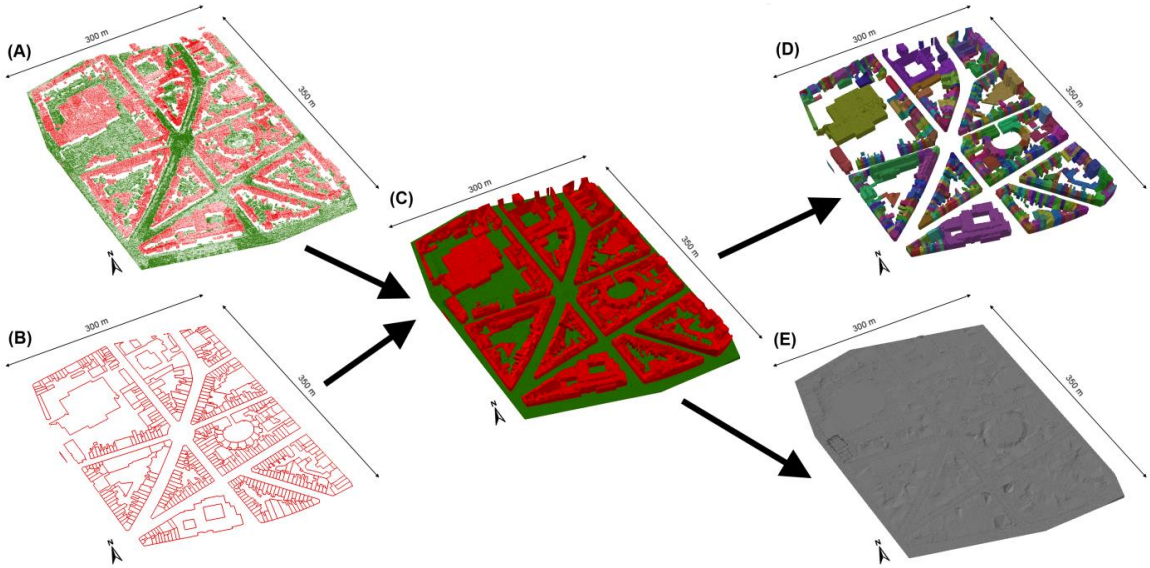

Figure 8-4: Overview of the feature modelling step with the Ghent data set

8.2.5. Model appearance

After reconstructing the geometry of the scene, a photorealistic model appearance is calculated by image-based texturing, also called projective texture mapping (Rüther et al., 2012). A texture map is calculated for each building feature using *Agisoft PhotoScan*. This software is frequently used for the image-based 3D reconstruction of objects using Structure from Motion (SfM) and Multiview Stereo (MVS). Instead of using the entire 3D mapping workflow, the software is used to perform a bundle adjustment on the airborne images, corresponding with the SfM step

(Robertson and Cipolla, 2009). Then, the actual texture mapping will be performed for each separate 3D model of a building. Obviously, an image-based geometrical 3D reconstruction (MVS) is not required, since the geometry of the features are derived from the ALS data. Therefore, only the correct and refined image acquisition parameters are relevant for the texture mapping of the georeferenced features. The first step in the SfM process is the automatic detection of matching points. Characteristic points have to be localised on each image. Then, corresponding points are detected on other images, resulting in a set of matching points (Dellaert et al., 2000). Next to these matching points, the intrinsic image parameters, like the image size and the focal length of the camera, are used to initiate the iterative bundle adjustment. The solution of this adjustment corresponds with the best fitting virtual reconstruction of the image scene in a 3D space and results in a sparse point cloud and corrected image acquisition parameters. Finally, the reconstructed image scene is used for the texture mapping by projecting the images on each separate building model. An example of the reconstructed image scene is presented in Figure 8-5.

Airborne imagery frequently only allows the calculation of orthophotos. Motivated by the large coverage of the study areas and the large overlap between images, it was chosen to perform an adaptive orthophoto-projection of the images on the models. By doing so, the facades of the buildings, which are assumed to be vertical, are now also textured using local vertical planes as a collection of a certain number of building feature surfaces. In order to increase the model performance and to retain the data volume of the final model, a mesh simplification is performed just before the texture mapping. The entire procedure is implemented in a Python script, and described in pseudo-code below:

```
   make new project in same coordinate system as image acquisition
parameters
   load images and accompanying acquisition parameters
   align images using acquisition parameters
   for each building model in building model list do:
      import building model as mesh
      perform texture mapping with adapted orthophoto geometry
      export building model as textured mesh with same name
   loop
```

Although the number of final faces is arbitrary, the mesh simplification step obviously results in a significant data reduction, but also a loss of accuracy and detail of the models. Furthermore, the decision to use only well-known software and as little complex programming as possible implies the usage of built-in simplifiers. It is clear that this approach for data reduction can be substituted with more intelligent techniques. A good choice would be the implementation of some plane detection and plane fitting algorithm, like connected component analysis (Novacheva, 2008) or Random Sample Consensus (RANSAC) (Haala and Kada, 2010).

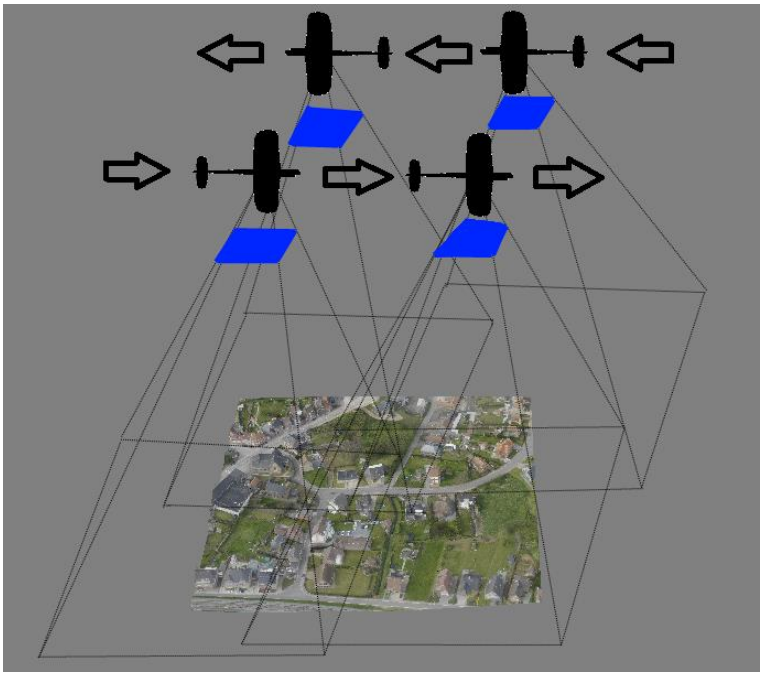

Figure 8-5: Example of an image scene and texture mapping of the terrain

8.2.6. CityGML and city database

Each building in the test site is described by a textured 3D model, with a file nomenclature referring to the corresponding attributes in the GRB database. *Safe FME* is used for the conversion of these textured models to CityGML and to explicitly define the attributes for each geometric feature. This open data model supports the geometric properties of virtual cities, as well as their attributes or semantics and the description of their physical appearance. CityGML is built on top of the Geographic Markup Language version 3.0 (GML), which is, in turn, built on top of the eXchange Markup Language (XML). Both languages are recognised as standards by the Open Geospatial Consortium (OGC) and the World Wide Web Consortium (W3C) respectively. CityGML has a modular structure, allowing the definition of different features by the standard, without the obligation to implement the entire language. Another key aspect of CityGML is the multiscale representation of features in accordance with well-defined Levels of Detail (LoDs) and accompanying accuracies (Kolbe, 2009). The workflow presented in this paper covers the first three LoDs of CityGML (Löwner et al., 2013):

- LoD0: covers the topographic modelling at a regional or landscape scale. In this LoD, buildings are represented as flat surfaces in a general DTM.
- LoD1: buildings are modelled as solids, which imply an extrusion of the building polygons. As a result, the roofs of these objects are flat. In some implementations of the model, the terrain is kept flat and the height of the building is simply derived from the elevation above the ground;
- LoD2: the real shapes of the roofs or buildings are described in this LoD and the geometry is represented by a composite surface or closed boundary representation

(BREP). As with LoD1, the function of the exterior shell of a building feature can be specified by a ground surface, roof surface or wall surface.

With LoD3, the façades are modelled and with LoD4, the interiors of the buildings are modelled. These LoDs are not implemented in the presented workflow. For all LoDs, it is possible to define a separate appearance for each geometrical feature in the model, or to calculate texture maps for the model or parts of the model. The functions or types (wall, roof, ground) of the different planes belonging to a building feature are simply determined by the direction of the normal vector of that surface and by the relative position of other surfaces belonging to that building feature. If the z-component of the normal vector of a plane is equal to zero, this plane will be vertical, corresponding with a wall surface. If the elevations of a building surface coincide with the range of elevations of the DTM, this building surface is a ground surface. Non-vertical surfaces with a high elevation are finally defined as roof surfaces. These formulations can be implemented in a simple script.

The *3D City Database* program (Kolbe et al., 2013; Stadler et al., 2009) is used for the management of the final models in combination with *PostgreSQL*. *PostgreSQL* is an open-source object-relational database management system (ORDBMS) and supports a large part of the SQL standard. After initializing an empty spatial database, it is possible to add new features to this database. In the current version of the procedure, only terrain and building features are implemented in accordance with the standard CityGML definition. However, the modularity of the workflow allows the implementation of other CityGML features of even new schemas easily. Exporting the entire model or parts of the model as CityGML or KML is possible using the 3D City Database user interface, whereas the *PostgreSQL* software allows the analysis of the database using SQL queries.

8.3. ***Results***

In Figure 8-6, a conceptualization of the presented 3D city modelling procedure is illustrated. The four layers of the procedure are covered by different software. The point processing is performed using *LASTools*, which can be used as stand-alone application or as a plug-in for *ESRI ArcGIS*. The feature modelling is performed using *ESRI ArcGIS*. Thereafter, *Agisoft PhotoScan* is used for the texture mapping and *Safe FME* is used for most of the data conversion and the assignment of attributes to spatial features. The final 3D city model is managed using the *3DCityDB* software.

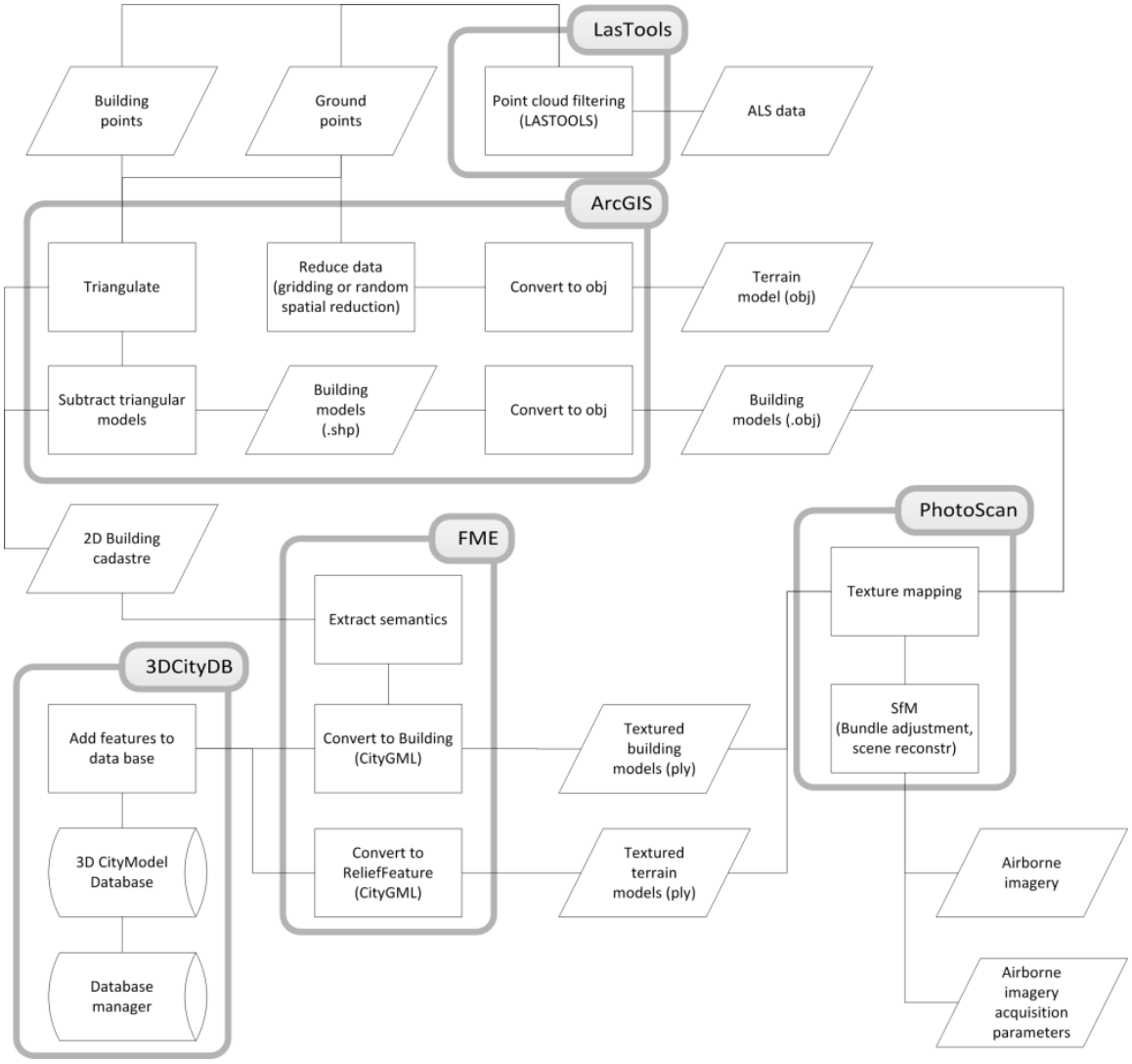

Figure 8-6: Implementation of the workflow in different software applications

The results of this workflow can be consulted using different analysis and visualization applications. An obvious choice for the visualization of the models, translated to KML-files, is *Google Earth* (Figure 8-7 and Figure 8-8). An alternative visualization example is given in Figure 8-9. Each building is visualized as a function of the relative height above the ground (traditional housing in blue; middle- to high-rise buildings in red). The *FZKViewer* (K.I.T., 2013) is used for this visualization and allows to access the attributes of each feature in the model.

Figure 8-7: Screenshot of a kml rendering of the Ghent study area using *Google Earth*

Figure 8-8: Screenshot of a KML rendering of the Geraardsbergen study area using *Google Earth*

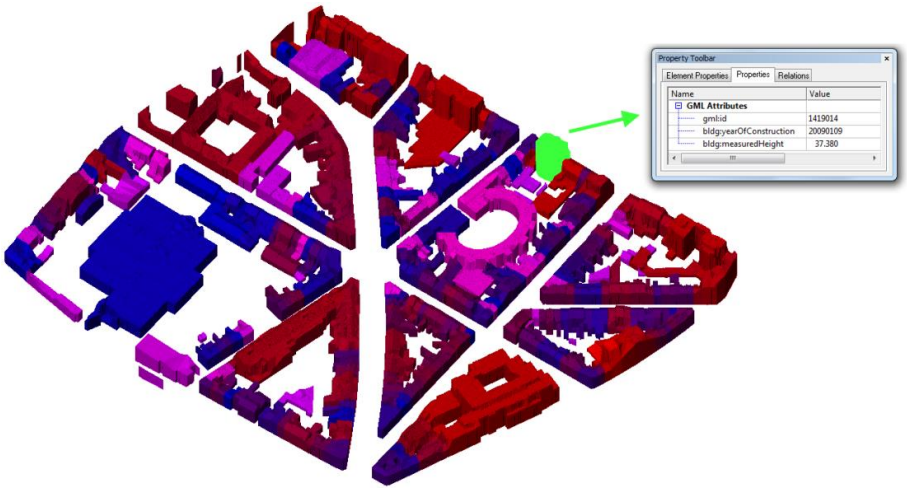

Figure 8-9: Screenshot of the Ghent test site in the *FZKViewer*, with each building coloured by its relative height

8.4. *Making the combination with linked building data*

The procedure documented above results in an interesting and useful basis for smart city management. At the moment, all buildings in the model are available up to LoD2. Consequently, the model can already be used for urban planning at building block scale, for building permit handling (in which cadastre data are to be compared with incoming building permit requests), and for visualization purposes (public transport network visualization, organisation and movement simulation during mass events, and so forth). In order to further enhance smart city management, it would be useful to make individual building information available up to LoD3 and LoD4. This information would enable, for instance, smart management of electricity grid or power consumption within building blocks, informed emergency interventions by fire fighter or healthcare services, and so forth. In this section, a brief prospect is elaborated on the ways this LoD3 and LoD4 information can be generated and integrated in the 3D City Database. The 3D City Database provides identifiers for each of the buildings in a building block. These identifiers are already associated to a limited number of data and metadata, like:

- Basic 2D and 3D information: height, building outline, situation;
- Cadastre information: cadastre identifier, building owner, etc.:
- Appearance data: texture maps.

In order to obtain LoD3 and LoD4 information, additional procedures are required. For a 3D city model with LoD3, it might be useful to rely on the available texture maps. These images are currently used for draping the 3D volumes that were obtained in the conversion procedure, and façade information can be extracted from these images. However, it will most likely not be possible to automatically generate fully correct and detailed 3D models of building façades using vertical imagery only. Therefore, terrestrial imagery or laser scanning data can be acquired to facilitate façade mapping. Relying on image analysis, pattern recognition techniques or feature grammars, these data allow the recognition of individual 3D building elements, such as windows, doors, façade columns, and so forth (Becker, 2009). Based on the recognized features, a more detailed façade geometry might be generated. This geometry can be added to the building identifier in the 3D City Database, so that a LoD3 visualization can be provided if required.

For a 3D city model in LoD4, we suggest to combine the GIS information in the 3D City Database with BIM models that could be available for some of the buildings in the building block (Eastman et al., 2008). A BIM model is typically modelled by an architect or by a building contractor during the design and construction phase of a building. The information in a BIM model is typically highly detailed and specific. Building elements are described in all their aspects (materials used, geometry, composition, structural function, cost, and so forth) using semantic representations. The inner spaces of a building are represented using geometric features and semantic annotations about the function and use of the space. All information is closely linked together using a standardized language (ISO, 2013; Liebich et al., 2013). It is clear that the level of detail of BIM models surpasses the targeted LoD4. Therefore, if a BIM model is available for one of the buildings in the digitized building block, it will be possible (1) to link the identifier in the 3D City Database to an identifier of a publicly available BIM model, but also (2) to generate a

simplified (LoD4) representation of the building from the BIM model and link that building representation as well to the corresponding identifier in the 3D City Database.

It is important to mention that BIM models are frequently not publicly available. First of all, these models are typically not available if the building has not gone through a construction process recently. Second, preparing BIM models is a labour-intensive work, so it is often done only for larger and more complex buildings, where the use of a BIM model provides a larger return on investment. Third, even if a BIM model is available, it is often not fully shared (internally) among partners in a construction process, due to responsibility issues and legislative/jurisdictional issues. Moreover, due to privacy regulations, the publication of highly detailed building plans is not required, although this could be desirable for security reasons (e.g. in case of emergency situations). From this small portion of internally shared BIM models, only a limited number is made publicly available, for security or privacy reasons. Consequently, it is not a recommended approach to link building identifiers in the 3D City Database to identifiers of publicly available BIM models, as long as BIM models are seldom made publicly available. The construction of simplified (LoD4) representations of buildings from BIM models and linking that building representation to corresponding building identifiers in the 3D City Database is a more viable approach. This approach can be implemented by:

- providing a service that calculates a LoD4 representation of a building, based on a BIM model;
- allowing to link a building identifier in the 3D City Database to an identifier of the LoD4 representation;
- making the required simplification procedures available to BIM modellers and allowing them to easily export a simplified (LoD4) representation of their building model.

The LoD4 representation of the building can be made available in diverse ways. It may be included in the 3D City Database, it can be published separately on the internet, it may be generated on-demand, and so forth. At this moment, it is recommended to keep the LoD4 representation separate in a distinct and publicly accessible database. In this case, the links between this database and the 3D City Database must be provided. The conversion procedures that allow a simplification of the BIM model to a LoD4 representation requires a more detailed review of the specifications of LoD4 representations than currently provided in this paper. Assuming that the LoD4 representation is less detailed than the BIM model, the required representation can easily be extracted from the BIM model using various implementation approaches and programming languages. Central to this approach should be (1) the conversion of the building façade geometry from its representation by diverse building elements (BIM model) into one combined 3D mesh geometry that can be used in a LoD3 and LoD4 building model in the 3D City Database; and (2) the conversion of the geometric representations of the building spaces into corresponding LoD4 geometric models.

8.5. ***Conclusion***

In this paper, a procedure for the combination of different spatial data sources is presented for the construction of 3D city maps. Central in this procedure is the proposal of a novel city modelling workflow. The city modelling workflow is based on the use of well-established software applications. These applications are developed for remote sensing applications or GIS and allow the definition and use of scripts and macros. As a result, the proposed 3D city modelling procedure can be implemented in the available software applications and production flows can be used by spatial data specialists. The project requirements and processing results can be combined into one 3D City Database using well-known software.

The proposed procedure is demonstrated for two test areas in Ghent and Geraardsbergen (Belgium). ALS data, airborne imagery and 2D maps data are used for the environmental modelling, covering the two test areas. Remote sensing and general GIS applications are used, covering the geometrical reconnection, the assignment of attribute data to building features and the model appearance by the calculation of texture maps. The used software applications (*LasTools, ESRI ArcGIS, Safe FME* and *Agisoft PhotoScan*) are well-known for many geoscientists and allow *Python* scripting. Each application is used for specific parts of the modelling procedure and the resulting intermediates can serve various derivative applications. After the last step of the reconstruction, the models are loaded into a *3D City Database*. This management program is a plug-in for *PostGreSQL*, consequently allowing the management of the diverse parts of the city model. Furthermore, this software allows performing SQL queries on the city models, as well as exporting KML-files or CityGML-files. These file formats are standards in the exchange of urban spatial data, significantly increasing the interoperability of the results. The documented procedure allows to build 3D city models to level of detail 2 (LoD2: overall representation of roof and building geometry). These city models have their value in smart city management. Adding more detail to the available building models, up to LoD3 (façade geometry) and LoD4 (internal spaces), would further increase the value of the 3D city models for smart city management. Therefore, an outlook on how to make such detailed building models and thus city models available was also presented. A special focus was on the option of generating LoD4 building representations from models available in building information modelling (BIM) applications. Such applications provide highly detailed models of buildings, and, presumably, a LoD4 representation can thus be extracted.

Acknowledgement

This research is part of the research project “3D CAD modelling of spatial architectural volumes, using terrestrial laser scanning and LiDAR”, supported by the Research Foundation Flanders (FWO). The authors would like to express their gratitude to the Flemish Geographical Information Agency (AGIV) for providing the various data sets.

References

AGIV, 2013. www.agiv.be, Ghent, Belgium

Becker, S., 2009. Generation and application of rules for quality dependent façade reconstruction. ISPRS Journal of Photogrammetry and Remote Sensing 64 (6), 640-653.

Bretar, F., Rouxb, M., Pierrot-Deseillignya, M., 2006. Matching topographic surfaces: application to LiDAR and photogrammetric surfaces. Revue française de photogrammétrie et de télédétection 182 (2006), 41-46.

Briese, C., 2010. Extraction of digital terrain models, in: Vosselman, G., Maas, H. (Eds.), Airborne and terrestrial laser scanning. Whittles Publishing, Dunbeath, UK, pp. 135-167.

Chen, C., Li, C., Li, W., Dai, H., 2013. A multiresolution classification algorithm for filtering airborne LiDAR data. ISPRS Journal for Photogrammetry and Remote Sensing 82 (1), 1-9.

Cignoni, P., Montani, C., Scopigno, R., 1998. A comparison of mesh simplification algorithms. Computers & Graphics 22 (1), 37-54.

De Cubber, I., Van Orshoven, J., 2012. Towards an internationally more accessible data model for the GRB, the 2D-large scale topographic inventory of Flanders, in: Billen, R.E., Binard, M. (Ed.), Hallot, P. (Ed.), Donnay, J. (Ed.), (Ed.), USB-Proceedings of the Spatial Analysis and Geomatics, Liège, Belgium, pp. 145-157

De Wulf, A., Hennau, M., Constales, D., 2006. Processing and filtering of multibeam data: grid modelling versus TIN based modelling. Hydrographic Journal 55 (2006), 9-12.

Dellaert, F., Seitz, S., Thorpe, C., Thrun, S., 2000. Structure from motion without correspondence, IEEE Computer Society Conference on Computer Vision and Pattern Recognition, Pittsburgh, PA, USA, pp. 238-248

Doneus, M., Briese, C., Fera, M., Janner, M., 2008. Archaeological prospection of forested areas using full-waveform airborne laser scanning. Journal of Archaeological Science 35 (4), 882-893.

Eastman, C., Teicholz, P., Sacks, R., Liston, K., 2008. BIM handbook: a guide to building information modeling for owners, managers, architects, engineers, contractors, and fabricators. Wiley, New York, NY, USA.

Ghent, B., 2009. www.gent.be, Ghent, Belgium

Haala, N., Kada, M., 2010. An update on automatic 3D building reconstruction. ISPRS Journal of Photogrammetry and Remote Sensing 65 (6), 570-580.

Heo, J., Jeong, S., Park, H., Jung, J., Han, S., Hong, S., Sohn, H., 2013. Productive high-complexity 3D city modeling with point clouds collected from terrestrial LiDAR. Computers, Environment and Urban Systems 41 (5), 26-38.

Hug, C., Krzystek, P., Fuchs, W., 2004. Advances LiDAR data processing with LASTools. International Archives of Photogrammetry and Remote Sensing 35 (B2), 832-837.

Isenburg, M., Shewchuk, J., 2013. LAStools, 1.2 ed, http://lastools.org, pp. Converting, viewing and compressing LIDAR data in LAS format

ISO, 2013. Industry Foundation Classes (IFC) for data sharing in the construction and facility management industries. International Organization for Standardization (ISO) Geneva, Switserland

K.I.T., 2013. FZKViewer. Karlsruhe Institut für Technologie, Germany

Kolbe, T., 2009. Representing and exchanging 3D city models with CityGML, in: Lee, J., Zlatanova, S. (Eds.), 3D Geo-Information Sciences. Springer-Verlag, Berlin, Germany.

Kolbe, T., Nagel, C., Herreruela, J., 2013. 3D City Database for CityGML. Addendum to the 3D City Database Documentation 2 (1).

Kolbe, T.H., Gröger, G., Plümer, L., 2005. CityGML: interoperable access to 3D city models, First International Symposium in Geo-Information for Disaster Management. Springer Verlag, Delft, the Netherlands, pp. 883–899

Liebich, T., Adachi, Y., Forester, J., Hyvarinen, J., Richter, S., Chipman, T., Weise, M., Wix, J., 2013. Industry Foundation Classes. Building Smart, Northamptonshire, UK

Löwner, M., Benner, J., Gröger, G., Häfele, K., 2013. New concepts for structuring 3D city models, an extended level of detail concept for CityGML buildings, in: Murgante, B., et, a. (Eds.), Lecture Notes on Computer Sciences. Springer, Heidelberg, Germany, pp. 466-480.

Nguyen, H., Pearce, J., Harrap, R., Barber, G., 2012. The application of LiDAR to assessment of rooftop solar photovoltaic deployment potential in a municipal district unit. Sensors 12 (4), 4534-4558.

Novacheva, A., 2008. Building roof reconstruction from LiDAR data and aerial images through plane extraction and colour edge detection. International Archives of Photogrammetry, Remote Sensing and Spatial Information Sciences 37 (B6), 53-58.

Ooms, K., De Maeyer, P., Neutens, T., 2009. A 3D inclusion test on large datasets, in: Neutens, T., De Maeyer, P. (Eds.), Lecture Notes in Geoinformation and Cartography. Springer-Verlag, Heidelberg, Germany, pp. 181-199.

Oude Elberink, S., Vosselman, G., 2011. Quality analysis on 3D building models reconstructed from airborne laser scanning data. ISPRS Journal of Photogrammetry and Remote Sensing 66 (2), 157-165.

Over, M., Schilling, A., Neubauer, S., Zipf, A., 2010. Generating web-based 3D city models from OpenStreeMap: the current situation in Germany. Computers, Environment and Urban Systems 34 (6), 496-507.

Penninga, F., van Oosterom, P., Kazar, B., 2006. A tetrahedronized irregular network based dbms approach for 3D topographic data modeling, in: Riedl, A., Kainz, W., Elmes, G. (Eds.), Progress in Spatial Data Handling. Springer, Heidelberg, Germany, pp. 581-598.

Pfeifer, N., Mandlburger, G., 2008. LiDAR data filtering and DTM generation, in: Shan, J., Toth, C. (Eds.), Topographic laser ranging and scanning: principles and processing. CRC Press, Boca Raton, Fl, USA, pp. 307-333.

Podobnikar, T., Vrecko, A., 2012. Digital elevation model from the best results of different filtering of a LiDAR point cloud. Transactions in GIS 16 (5), 603-617.

Robertson, D., Cipolla, R., 2009. Structure from motion, in: Varga, M. (Ed.), Practical image processing and computer vision. John Wiley, Hoboken, NJ, USA., p. 49.

Rüther, H., Held, C., Bhurtha, R., Schroeder, R., Wessels, S., 2012. From point cloud to textured model, the Zamani laser scanning pipeline in heritage documentation. South African Journal of Geomatics 1 (1), 44-59.

Sithole, G., Vosselman, G., 2004. Experimental comparison of filter algorithms for bare-Earth extraction from airborne laser scanning point clouds. ISPRS Journal of Photogrammetry and Remote Sensing 59 (1-2), 85-101.

Stadler, A., Nagel, C., König, G., Kolbe, T., 2009. Making interoperability persistent: A 3D geo database based on CityGML, in: Lee, J., Zlatanova, S. (Eds.), 3D Geo-Information Sciences. Springer-Verlag, Berlin, Germany, pp. 175-192.

Stal, C., De Maeyer, P., De Wulf, A., Nuttens, T., Vanclooster, A., Van de Weghe, N., 2010. An optimized workflow for processing airborne laserscan data in a GIS-based environment. International Archives of Photogrammetry, Remote Sensing and Spatial Information Sciences 38 (4), 163-167.

Stal, C., De Roo, B., De Maeyer, P., Nuttens, T., De Wulf, A., 2013a. Considerations on the fusion of multi-sensor spatial data for cultural heritage. In 16th AGILE conference on Geographic Information Science (AGILE 2013): Geographic information science at the heart of Europe., in: De Roo, B. (Ed.), 16th AGILE conference on Geographic Information Science, Leuven, Belgium, p. 3

Stal, C., Tack, F., De Maeyer, P., De Wulf, A., Goossens, R., 2013b. Airborne photogrammetry and LiDAR for DSM extraction and 3D change detection over an urban area: a comparative study. International Journal of Remote Sensing 34 (4), 1087-1110.

van den Brink, L., Stoter, J., Zlatanova, S., 2013. Establishing a national standard for 3D topographic data compliant to CityGML. International Journal of Geographic Information Science 27 (1), 92-113.

Veregin, H., 1999. Data quality parameters, in: Longley, P., Goodchild, M., Maguire, D., Rhind, D. (Eds.), Geographical Information Systems. Wiley, New York, NY, USA.

Chapter 9

Discussion and general conclusions

9. Discussion and general conclusions

This concluding chapter starts with a general summary of the research, where the different aspects and conclusions from previous chapters are resumed. Three key-elements of 3D modelling are elaborated in section 9.1, focussing on the data acquisition, processing and management. In this section, the first four research questions are also explicitly recapitulated (RQ1-4). The findings regarding the spatial data acquisition cover different data acquisition platforms and methods (RQ1), combined with a number of quality assessments and feasibility studies (RQ2). Various aspects on data processing, with a special focus on point cloud filtering (RQ3), and data conceptualization (RQ4) are also elaborated. The relevance of the findings of this dissertation is presented in section 9.2 as a continuation of the discussion on RQ4. However, this section also focusses on the strengths and opportunities of this work for spatial planning and management (in the context of RQ5), cultural heritage and archaeology, as well as spatio-temporal applications. This section is presented from a pragmatic attitude, thus an insight on RQ6 is given as well. In section 9.3, the limitations and opportunities of the work are discussed, aiming at the formulation of recommendations for further research and perspectives. Some concluding remarks are given in section.

9.1. *Analysis of the data acquisition, processing and management*

RQ1: Which data acquisition platforms and methods are able to acquire spatial data for the construction of 3D models?

The 3D modelling process obviously starts with the 3D data acquisition. A whole gamut of different sensors and techniques are already available and the most optimal methodology should be selected based on multiple factors, like the size of the area to be covered, the spatial density and accuracy of the data, the availability of hardware, software, human ware and financial resources … Under ideal circumstances, the properties of the application for which the data is acquired should obviously be the most constraining factor. Nevertheless, the theoretical and practical study of 3D data acquisition is required to facilitate the discussion making process. Therefore, a thorough theoretical elaboration and comparison of different state-of-the-art sensors and techniques was presented in chapter 2.

The use of laser scanning (section 2.1) was elaborated, focussing on topographical airborne applications (ALS) and bathymetrical airborne applications (ALB), but also on the difference between static (STLS) and mobile (MTLS) laser scanning for terrestrial applications. The selection of a sensor or technique is an equilibrium between various aspects: while a manned airborne platform is able to acquire data over large areas, static terrestrial platforms are able to measure massive data sets with a very high accuracy of limited areas. However, a large number of scanning setups have to be prepared and an even larger number of reference points have to be materialized when STLS is used for topographic surface modelling. Kinematic laser scanning overcomes this issue by measuring a point cloud in a systematic way, using integrated positioning and orientation sensors (GNSS and INS). When ALS configurations are used in data acquisition campaigns for topographic mapping, gridded elevation models are frequently requested with a

2.5D geometry. STLS is mainly deployed for civil engineering, architectural or cultural heritage applications, like façade mapping or construction measurements of bridges and tunnels. Both STLS and MTLS are considered as full-3D data acquisition techniques, whereas MLTS allows the generation of point clouds for large parts of cities in a much more limited time frame than STLS.

Next to different laser scanning techniques, image based 3D modelling was discussed in section 2.2. Conventional photogrammetry and SfM-MVS-based 3D reconstruction techniques were elaborated, indicating the great potential of the latter for relatively fast and accurate environmental modelling. Current conventional photogrammetric workflows are based on the stereoscopic processing of images, resulting in a number of 2.5D DEMs that are merged in a final modelling phase. SfM-MVS enables to process a large number of images in an integrated way for both terrestrial and airborne applications. The image matching, sparse point generation and image scene reconstruction (SfM), as well as the dense point reconstruction and mesh (or TIN) calculation (MVS) are possible using SfM-MVS processing software.

Finally, the use of conventional topographic measurement techniques (GNSS and total station measurements) was briefly discussed in section 2.3. It became clear that these techniques are very suitable for single point measurements with very high accuracies. However, each point has to be measured explicitly and manually. Therefore, it is advised to use these techniques to measure GCPs and reference point sets. As such, topographically measured points facilitate the quality improvement and the assessment of laser scanning based models and image based models.

A theoretical summary of optimal GSD and vertical accuracies of DEMs was presented in Table 2-1. Based on the theoretical evaluation of the different 3D data acquisition techniques, it was possible to select the most suitable modelling methodology for a wide range of applications. ALS and conventional airborne photogrammetry were also used in chapter 5 for a comparative study and to explore the possibility to use these data sets for urban change detection. The point cloud classification technique presented in chapter 6 and the integrated 3D city modelling workflow in chapter 8 were based on the sole use of ALS data. The limited size of the archaeological structures, described in chapter 7, allowed the use of terrestrial close-range imagery in a SfM-MVS workflow.

RQ2: What geometric accuracies and precisions can be reached using the different data acquisition methods and what are the performances of these methods in view of further data processing?

Another comparison of different 3D data modelling methodologies for the reconstruction of historical globes was elaborated in chapter 3. This chapter concludes with an innovative procedure for the 3D documentation of this kind of cultural heritage. The aim of this project was on highly accurate 3D modelling using optimized procedures. The results of this research were presented at an exhibition on the 500th birthday of Mercator. Hence, high quality textures were the initial requirement for the modelling process. However, during the evaluation of different procedures, the geometric quality was also considered. A large number of images were taken from two globes, constructed by Mercator in the 16th century. These images were processed in a SfM-MVS workflow for the construction of fully 3D visualizations. The images were also

georeferenced in a GIS and placed in a sequential series for pseudo-3D or dynamic imaging. Furthermore, STLS measurements were performed as well, in order to evaluate the performance of laser scanning for globe modelling. The results based on manual georeferencing were acquired in a time consuming process and were of much lower quality than the results generated by dynamic imaging and SfM-MVS. STLS resulted in a highly accurate geometric reconstruction of the globes, but no textural information was incorporated in the models. Therefore, the manual georeferencing of images and the use of STLS were not suitable for this project. However, it can be concluded that for the modelling of historical globes, the dynamic imaging and the SfM-MVS technique are the most suitable for the generation of 3D models of globes aimed at public exhibitions and cartographic research. The results from the dynamic imaging are very useful for further semantic and historical research of the globes. Globe details, like compass cards, cartouches and toponyms in general, are clearly represented in the model. The resolution of the original images is retained and the constant angular increment of the globe still results in a 3D impression. Some of the image resolution will be lost by SfM-MVS processing, but this reduction is manageable by the optimization of the processing parameters. Therefore, this 3D modelling technique offered very satisfactory visual results (Figure 9-1).

Figure 9-1: Screenshot of a 3D view on Mercator's terrestrial globe (1551), hosted by the Mercatormuseum in Sint-Niklaas, Belgium

The geometric quality of DEMs derived from ALS, conventional photogrammetry and SfM-MVS was evaluated in chapter 4. For both image based techniques, the same airborne images and GCPs were used. Two different study areas were modelled using these three techniques: one area covered a heavily built-up part of the city of Ghent and another area was situated in a rural area in the municipality of Kooigem (both in Belgium). The ALS data set was used as a reference for a point-to-point comparison and for a point-to-mesh comparison after triangulation of this reference data set. The evaluation was thus based on the distances between the data sets. Based on the

results of this comparative study, it could be concluded that conventional photogrammetric modelling would result in lower planimetric errors than using the SfM-MVS-based workflow for both urban study areas and rural study areas. However, no significant difference appeared between the altimetric errors of the two image-based data sets. Furthermore, it was stated that conventional photogrammetry suffered more from outliers in the model, especially for the urban area. Nevertheless, this did not affect the overall comparison between the models. It could also be concluded that both conventional photogrammetric and SfM-MVS image based reconstruction techniques were very suitable for the 3D modelling of complex urban areas and rural areas. For the conventional photogrammetric workflow, the usability of airborne imagery for 3D city modelling was also stated in chapter 5. The results of the qualitative comparison in this chapter corresponded with the results from chapter 4, stating methodological consistency. However, SfM-MVS was preferred for its processing performance and the ability to use the point clouds for accurate point cloud classification, as discussed in the next paragraph. Based on this research, it can be stated that ALS data are geometrically comparable with conventional airborne photogrammetry and SfM-MVS. This statement is very useful for environmental 3D modelling when the availability of spatial data is limited.

RQ3: Under the assumption that point clouds are used for 3D city modelling, how can information be extracted from these point clouds?

The data processing phase is an important link between the data acquisition and the final 3D city model. In the previous discussion on the quality assessment of the different data sets, a certain degree of data processing was already required in order to make the data conceptually coherent. Of course, point cloud generation from images and even from laser scanning require data processing, like strip adjustment, noise removal or point interpolation. Nevertheless, the results of more complex data processing were recapitulated in this section. For the three modelling techniques (ALS, conventional photogrammetry and SfM-MVS), the previously discussed geometrical comparison of DEMs was extended with a pair-wise comparison of the results of point cloud filtering for DTM construction in chapter 3. The potential of using airborne imagery based point clouds for the extraction of DTMs with point cloud filtering was also assessed. The filtering resulted in a series of ground-points and non-ground points, which were evaluated by the calculation of Cohen's kappa-values. For the urban study area, the difference between the conventional photogrammetric DTM (k = 0.52) and the SfM-MVS-based DTM (k = 0.67) was not large. The difference was much larger for the rural study area, where the quality of the filtering of the conventional photogrammetric data is much lower (k = 0.18) than the SfM-MVS-based filtering (k = 0.75). This large difference is mainly caused by the spatial distribution of the two point clouds which is more or less regular for the urban study area, but dissimilar for the rural area. For the rural area, dominated with large farming fields, the SfM-MVS processing results in a point cloud with a regular spatial distribution, whereas the conventional photogrammetry results in an aggregated spatial distributed point cloud. Next to the geometrical comparability of different spatial data, the suitability of image based modelling techniques for point cloud classification has been proven. As a results, it can be stated that the SfM-MVS-based reconstruction techniques do not only result in highly accurate 3D models, but the technique can also be applied as a reliable alternative for conventional photogrammetry and for ALS, when the resulting point cloud is filtered and thus used for semantic 3D city modelling.

For the first comparative study, a standard point cloud filtering software package was used. In order to validate the accuracy of the filtering itself, and to enable a full point cloud classification, a new classification technique was presented in chapter 6, based on BLR analysis. Current classification techniques make use of one or a limited number of geometric criteria or neighbourhood functions for the assignment of a point to a certain class. The proposed method makes use of a large feature space of which the parameters were also based on the geometry of the neighbourhood. The entire feature space was used for the estimation of a series of logistic models defining the probability that a point with a given feature space belongs to a certain class. The idea behind the proposed filtering technique is very similar with the gestalt laws of grouping (Sarkar and Boyer, 1993), where individual features are clustered by a set of similar properties. Thus, a set of probabilities was calculated for each point belonging to each class and the final class assignment would be based on the highest probability. Because of the fact that probabilities were used, model evaluation by statistical inference was allowed. The ability to generate many generic classes was the biggest strength of the proposed method. The user adaptability of the algorithm, depending on the characteristics of the measurement area and the user's experience, allowed a very wide range of applications in the field of point classification. This classification was supported by a thorough statistical analysis to interpret the performance of the results. Moreover, not only the BLR procedure itself could be optimized, also the model adjustment constraints could be fine-tuned in a Java tool, depending on the application. If the training sets were defined correctly, the ratio of misclassified points would improve with 5-12%. The procedure was explained by the classification of two different ALS data sets. The first was a dense point cloud of an urban area covering the city of Ghent, Belgium. For this area, a ground- and non-ground filtering with a Type-I error of 4% and an overall correctness of 95% were achieved. For the second test site, located around the rural village of Ctiněves (Czech Republic), a Type-I error of 8% and an overall correctness of 96% were reached. These values were in line with other state-of-the-art classification methods for ground point extraction. However, in contrast with most other classification methods, multiple classes could be extracted from an ALS point cloud. Next to the mentioned parameters in this research, it was possible to use many other parameters to define the feature space. For example, the presented results look very promising to improve the classification procedure, e.g. by taking the neighbourhood of the class assignment into account or by the use of a rough DTM for the calculation of a preparatory normalized elevation model. Though, with the presented classification technique, promising steps were taken to use BLR for ALS point cloud classification.

RQ4: How can 3D data be managed, more specifically in a spatio-temporal database with multiple data sources and in accordance with a certain data model?

Through the entire dissertation, spatial data management played a very important role for the use of these data. The importance of the role of spatial data management is suggested in chapter 4 and 5, but in chapter 7 and 8 various aspects of spatial data management were explicitly covered. In these chapters, different (independent) data set were processed and analysed in one and the same database. Hence, spatial data management involves the implementation of an SDI related to the data model specifications. The data model specifications are determining the way the data are acquired, stored and exchanged. Besides, abstract rules on the conceptual model conformity and data validation rules are defined by the data model specifications. As an example, CityGML

defines different levels of detail as a kind of quality labels, XML schemas for data interoperability or for the definition of completeness requirements. Based on the findings of this research, two conditions for a correct spatial data management can be defined (Stal et al., 2013):

- **Conceptual conformity:** if a single real-world object is represented by different features in various databases, or measured by different sensors, it must be clear how to describe this feature in the final database. In chapter 7, the conceptual model for the 3D models is clearly defined and also in chapter 8, the use of CityGML is promoted to support the conceptual 3D city model. The way features are geometrically and semantically described, depends on the used ontology as formulated by conceptual database schemas. The question arises how to define the common attributes of objects and how to guarantee or qualify the coherence in different schemas. Multiple reasons for this issue are identified: databases are initially acquired for different purposes, they are built-up from different data sources and suffer from various ways of interpretation (e.g. during digitizing or other manual object interpretations). The multi-temporality and inhomogeneity in scale obviously play a differentiating role in spatial data representation. In general, the integration of different spatial data sets is problematic because of the difference of object models and semantic description of features in these sets;
- **Data validation:** the different aspects of data validation concern the data accuracy, completeness and up-to-date-ness. As with the data acquisition, data may be used to improve one of these aspects. Feature matching is performed by fusing objects with corresponding geometrical, topological and/or semantic properties. The evaluation of data sets is usually performed by the comparison of data with a reference data set, or to face the temporal data with the original data. However, the validity of the reference data set and the influence of this analysis on the final data evaluation pose an interesting issue. Besides, during the data integration, the final error of the aggregates needs to be defined and tracked as a function of the different separate data sets. By doing so, the final error will be calculated by mathematical rules of error propagation.

In order to enhance flexibility of the consultation and analysis of a large number of 3D models, the models require the implementation of some management environment, as elaborated in chapter 6. Parallel with the construction of the daily 3D models, a Harris matrix is generated for the documentation of different topological and chronological relations. Since the same type of relations exist between different successive 3D models, it is obvious to generate a link between the Harris matrix and the virtual reconstructions. Not only is the Harris matrix simultaneously generated during the campaign, its interpretation is common practice in archaeological sciences. As a result, the conceptual file structure of the models within the matrix does not require much effort for the field expert. Implementing the system in an online server-client based environment improves the efficiency of the research work, as well as the visibility of archaeological projects for a wider public.

9.2. ***Relevance of the research***

9.2.1. Spatial planning and management

Urban planning and the management of space is a hot topic for European policy makers on all spatial levels. Especially on a local scale and landscape scale, 3D models are a very important tool for sustainable planning and management. Interaction between a virtual 3D model of the environment and its actors allow a better understanding of the environment, the elements within the environment and the relations between these elements. Moreover, a digital 3D model enables the implementation of changes to the environment in a virtual way. The impact of proposed changes can be simulated and evaluated with high accuracy on forehand, allowing the development of additions and modifications for the plans, but also allowing the reduction or avoiding of negative impact of these plans. Moreover, the internet can be used for making the 3D models accessible for the wide public, increasing the awareness of certain spatially related decisions. The construction of these models is a challenging task, especially when the models are used for more than just visualization. Next to a large series of geometrical features, a 3D city model contains semantics and appearance. Topological relations between these features are not explicitly elaborated in this dissertation, but nevertheless, these relations are very important. Instead, a strong focus is on the acquisition and processing of spatial data for geometric reconstruction of features using different sensors and techniques. Since airborne data acquisition techniques are frequently used for 3D city modelling in governmental, legal and lifesaving applications, the need for a quality assessment emerges. Chapter 2, 4 and 5 are directly related to the use and evaluation of 3D data acquisition techniques for environmental mapping and 3D city modelling. The advantages of airborne techniques are obvious and it has been demonstrated that conventional spatial data allow the construction of innovative, attractive and highly accurate 3D models. The innovative classification technique in chapter 6 extends the modelling of well-known classes that are originally extracted form ALS point clouds, like buildings, vegetation and ground points to the detection of generic classes. The proposed classification methodology has the potential to extend these classes to a large number of user-defined classes, like fences, antennas or electricity poles. This allows a great flexibility in the modelling process. The findings of these chapters come together in chapter 8, where an entire 3D city modelling process is presented. Since much 3D spatial data is already made available for governmental organizations, the 3D models that can be derived from these data are within reach, even for smaller organizations with limited budgets. The presented 3D city modelling approach is very accessible as it uses only well-known geo-software packages. As a result, these models open the door to a wide range of new applications, but many of these applications also require further research, as elaborated in the next section.

9.2.2. Cultural heritage and archaeology

Chapter 3 and 7 are dedicated to the construction and use of 3D models for applications in cultural heritage and archaeology. For both the research of historical artefacts, as well as for archaeological excavations, image-based 3D modelling plays an important role for object documentation. The reconstruction of small and fragile cultural heritage requires a fast 3D

modelling methodology with minimal human contact and with nice textural appearance. For globes, the use of laser scanning (Adami, 2009) and the georeferencing of images (Hruby et al., 2006) were discussed earlier. These methods were also evaluated in chapter 3, and it becomes clear that they are either lacking proper visualization, or that they are very time consuming. Since the ability to use digital 3D representations is essential for a thorough study of the globes, the need for more efficient reconstruction techniques emerges. The presented method makes use of a static camera emplacement with studio lightning conditions and a globe rotating around its axis. The result of this configuration is a series of high quality imagery which can be used for SfM-MVS-based 3D reconstruction. Although this method was only applied on globes, it is possible to use it for all kinds of small objects, like the Maoi-statues of the Rapa Nui (Figure 9-2) or many other objects. Image-based 3D modelling is therefore a fast and low-cost alternative for cultural heritage applications, but also for other reverse engineering techniques.

Figure 9-2: Digital representation of a replica of a Maoi-statue. From left to right: original image, point cloud, triangular model and textured 3D model (own processing, in collaboration with Prof. Dr. Morgan De Dapper)

The advantage of image based modelling is already stated by other authors, aiming at the virtual reconstruction of a wide range of archaeological objects using airborne platforms or close-range photography (Brutto and Spera, 2011; Plets et al., 2012; Remondino, 2011). In the two case studies presented in this dissertation, an innovative procedure based on SfM-MVS was developed for the reconstruction, as discussed by Verhoeven et al. (2012). In addition to the work presented by these authors, the purposes of the projects presented in this dissertation were not limited to the sole visualization of archaeological data. A fully operational management system was developed for a large number of 3D models, covering the entire on-going of the archaeological excavation. Moreover, some advanced applications were presented as examples on the extended usage of these models. The results integrate geomatics and archaeology in a multidisciplinary research approach, allowing a more efficient and effective data management and data analysis.

9.2.3. Time and space

In chapter 5 and 7, spatial data were used for describing geometrical difference of features over time. The management of large time series of spatial data and the development of meaningful data analysis procedures is a challenging task. In chapter 5, an automated 3D building change detection approach was introduced in addition to the geometrical comparison of ALS and conventional photogrammetry. The novel change detection procedure for urban areas has a special focus on spatial coherence and meaning and significance of detected features. In chapter 7, a large number of image based 3D models were generated for the daily monitoring of archaeological excavations and for the facilitation of the virtual registration of findings. In both cases, the elevation values of a series of cells in a raster or nodes in a TIN were compared with the elevation values in another raster or TIN. 3D models in a time series allow the recursive evaluation of spatial processes, as well as the prediction of these processes by spatio-temporal extrapolation. As a result, the following advantages of these time series are formulated:

- The management of spatio-temporal data fits within the current scientific interest in a full 4D GIS (3D GIS with temporal component). The spatial registration of features in time enables a better understanding of these features (Dubovyk et al., 2011). The next advantages on predictive modelling, monitoring and reference definition are all extensions or applications of the use of such a 4D GIS;
- Time series facilitate the decision making based on predictive modelling (Mironga, 2004). Structured knowledge of the past enables to generate prognoses, which can be statistically evaluated, using advanced tools;
- Time series also allow the explicit definition of a starting point or reference of a phenomenon (t_o). For example, the calculation of an absolute volume requires the establishment of a reference surface. Moreover, changes over time can be indexed to (or compared with) a reference layer;
- Up-to-date or real-time data allow the monitoring of spatial phenomenon (Martin et al., 2004). If these data are processed and exchanged using GIS and web services, the monitoring system can be used as a centralized information point for the assisting department in case of serious calamities or disasters (Louhisuo et al., 2007). In this case, high quality and continuous data flows for the acquisition, processing, analysis and exchanges of data are required. Automated reporting and alerting systems facilitate the information exchange between different interested parties. Organizations will all have the same knowledge of a phenomenon avoiding much discussion and vagueness. Another application where accurate data about a phenomenon in terms of time and space are required, is the monitoring of newly built tunnels, as discussed by Nuttens et al. (2010).

Consequently, it has been demonstrated that the use of 3D models in large time series for archaeological site monitoring is possible when an efficient management system is used. The novel management system presented in this dissertation facilitates archaeological site monitoring and supports a thorough analysis of large data sets.

9.3. *Recommendations for further research and perspectives*

Different important aspects of environmental modelling or 3D city modelling were elaborated in this dissertation. These aspects were illustrated with theoretical studies and facilitated by the development of new data processing and data management procedures. Notwithstanding the promising results of this research, much work still has to be done and there are still open issues to be solved.

In the introductory chapter, the importance of spatial data was emphasized. These data facilitate various domains, like spatial management focussing on sustainability (Naess, 2001) or biodiversity (Sandström et al., 2006). Moreover, spatial data are indispensable for water management (Niemczynowicz, 1999), crisis and calamity management (Vakalis et al., 2004), cadastre mapping (Bartoněk et al., 2011), noise mapping (de Kluijver and Stoter, 2003) or air pollution modelling (Merbitz et al., 2012). As a matter of fact, the sole use of classic GIS and 2D maps is no longer sufficient for decision making processes and spatial analysis. The increased complexity of these issues emerges for high quality environmental models and 3D city models. Until recently, the development of these models was hampered by the lack of processing automation, data integration, standards, … (Döllner et al., 2006). The last few years, many work is done on many aspects of city modelling, like the assignment of attributes to geometric features using external databases (Smart et al., 2011), geometric reconstruction procedures using primitive fitting (Haala and Kada, 2010) or texture mapping of 3D models (Grammatikopoulos et al., 2007). With regard to the managing, storing and exchanging of 3D city models, the development of CityGML plays an essential role in the technological progress (Gröger et al., 2008). Linking these developments with the wide range of applications is still a challenging task, since no comprehensive and hands-on 3D GIS tools are yet available and most tools are limited to 2.5D cases. This dimensional simplification of reality is sufficient for many applications, but sophisticated tools are required for complex geometric analyses, like pollution problems where pedological or meteorological models need to be implemented. In this cases, the behaviour of a phenomenon is influenced by a large number of factors in a 3D space.

The use of full-3D city models as a land policy tool is required for governmental organizations responsible for urban development, from a practical, legal and financial point of view. For example, the Flemish government has put considerable effort into the construction of a large scale topographic map in 2D. If this model is extended to 3D, the above mentioned applications can be implemented in a Flemish context. Both the governmental organizations, private companies and the general public will significantly benefit from such a model. An interesting example is proposed by the city of Ghent, where policy makers are visioning a 3D city model that can be used for the (visual) evaluation of construction proposals (Matthys et al., 2005). The 3D modelling projects could facilitate these kinds of ambitions. However, the formulation of a statutory context for these models and its applications is required. Among others, a legal framework should consider responsibility and accessibility layers for the model content, as well as for the legal extend of the model as defined in institutional arrangements and land policy laws (Enemark et al., 2005). Notwithstanding the lack of legal regulations on 3D land policy and cadastre applications, the acquisition, use and circulation of 2D spatial data is already arranged in

different directives and legislation, like the European directive regarding the establishment of an Infrastructure for Spatial Information in the European Community (INSPIRE) (EuropeanCommission, 2007) or the United States law coordinating geographic data acquisition and access: the national spatial data infrastructure (UnitedStatesPresident, 1994). Whereas INSPIRE aims at the integration of spatial information for policies or activities that have an impact on the environment in member states of the European Union, the United States Geological Survey (USGS) has made a huge amount of worldwide spatial data (ALS data, topographic maps, satellite imagery, …) available for the public (USGS, 2013). Increasing the amount, quality and coverage of these data sets, especially 3D spatial data, would enhance the use of these data in a large number of new and innovative applications. The easy accessibility of spatial data is therefore a prerequisite for application development in both developing and developed countries. In a Flemish context, the AGIV has made their spatial data available for education purposes and scientific research. Other users can have access to the data using a web-based viewer (AGIV, 2013).

Most 3D city modelling projects make use of already existing airborne spatial data, as described above. This is a big advantage for both the data suppliers and the data users. The first will have an additional application where the data are used; the second will not have to generate the data by themselves. This idea is fully in correspondence with the idea of 're-using' spatial data, as supported by a SDI (Steiniger and Hunter, 2012). If no sufficient spatial data are available, or if the data do not fit with a-priori requirements, a cost-benefit analysis has to be performed. Although airborne data has a relatively lower cost than terrestrial data acquisition (assuming the same data quality and density or resolution), the general cost for airborne spatial data remains high (Bennett et al., 2011). Moreover, the usage of regular airborne techniques (ALS and conventional photogrammetry) is frequently ruled out for practical or organizational reasons. An alternative could be the use of lightweight, flexible, compact and low-cost UAVs (Ortiz et al., 2013). These flying platforms allow the easy and fast deployment of the system in more remote areas. Besides, the compactness of these systems would even allow the deployment in forested areas. For terrestrial applications, the use of structured light sensors could be an alternative (Kourosh and Oude Elberink, 2012). The development, refinement and usage of these low cost platforms and 3D reconstruction techniques are very active research fields with much potential. Open questions in these fields remain on sensor positioning and calibration, data accuracy, data acquisition optimization, etcetera. Archaeological projects, like the one discussed in chapter 7, would directly benefit from the results of this research.

The lack of a systematic approach for the qualitative evaluation of spatial data is an important issue for the work presented in this dissertation. This is obviously caused by the variation of data models and resulting conceptual inconsistency. In chapter 4 and 5, a geometrical comparison between airborne spatial data was presented for raster data, based on the projection of one data set on another reference data set. The quality of a data set was then evaluated as a function of the deviation between them. This methodology is straightforward, but has a significant drawback in the fact that it does not take the resolution parameters correctly into account. This issue becomes even more obvious when inconsistent data sets are compared, like discrete raster data sets with continuous vector data sets or TINs (Goodchild, 1992). Moreover, it is also important to have

tools to evaluate the attribute data, topology and appearance of a model. The CityGML standard gives accuracy criteria for the geometric evaluation of features in the different LoDs, but does not define tools for non-geometric evaluation. However, in chapter 4 and 6, the semantical quality of a point cloud was evaluated against a reference point cloud using cross comparisons, kappa values and classification error matrices, as suggested by Veregin (1999). For the rest of this dissertation, and especially in chapter 8, the quality evaluation of attribute data was ignored by assuming that the thematic resolution and accuracy were not relevant for the test cases. Consequently, for a full comprehension of the different quality layers of spatial data, further research and framework standardization is required for uniform quality assessment and description.

In chapter 6, a point cloud classification was presented based on class allocation using BLR analysis. The probability that a point can be assigned to a certain class is estimated with a logit function, which is defined by the best fitting solution of a series of feature space parameters for that class. Consequently, it is required to define training samples for all classes in the supervised classification (Foody and Mathur, 2004). The biggest drawbacks of this approach are twofold, since the training set definition is a manual process and will only cover the characteristics of the training sample. As a result, the sample size, which is related to the complexity of the sample, plays an important role (McCaffrey and Franklin, 1993). Further research on this topic should focus on the implementation of automated classification using unsupervised algorithms and cluster analysis (Lu and Weng, 2007). Unsupervised point cloud classification would overcome these issues, and has the potential to enable the detection of unconventional classes, like antennas, garden sheds or other features.

In chapter 8, a procedure for semi-automated 3D city modelling was presented using ALS data, airborne imagery and 2D cadastre data. A classification procedure was executed for the extraction of building points and ground points from the ALS point cloud. A point-in-polygon test, using the cadastre data set, was also performed to generate a series of point clouds per building. The geometry of a building is defined by a triangular model, which is simplified in the final texture mapping phase. Although the number of final faces per building is arbitrary, the mesh simplification step obviously results in a significant data reduction, but also in a loss of accuracy and detail of the models. Furthermore, the decision to use only well-known software and only limited programming implies the usage of build-in simplifiers. It is clear that this approach for data reduction can be substituted with more intelligent techniques. Such as the implementation of some plane detection and plane fitting algorithms, like Connected Component Analysis (CCA) (Novacheva, 2008) or Random Sample Consensus (RANSAC) (Schnabel et al., 2007). The importance of such feature extraction procedure or primitive fitting algorithm becomes clear with the following example: the celestial globe that was constructed in chapter 3 consists of an obj-file with a file size of 91,798 kB, containing a geometric representation with 444,835 vertices and 889,411 faces. A best-fitting sphere was generated using all vertices from the original model, resulting in a geometric primitive with a file size of only 64 kB, containing 554 vertices and 1104 faces (Figure 9-3, left). A point to mesh comparison, in accordance with chapter 4, demonstrates that the mean distance between the two data sets is only a millimetre (Figure 9-3, right). The data reduction for urban objects in a 3D model will not be that impressive, but still has a large potential for more efficient data management and exchange.

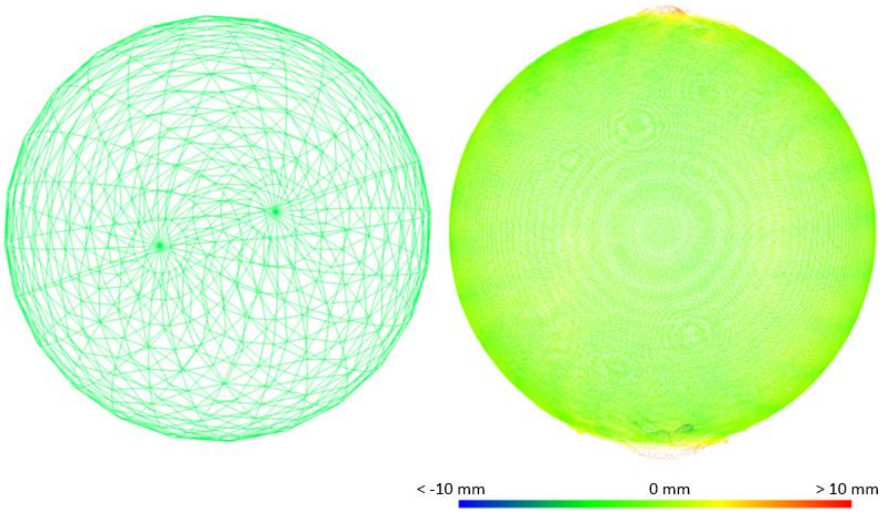

Figure 9-3: Best fitting sphere of a historical globe (left) and original point cloud with distances between this point cloud and the simplified geometry (right)

9.4. *Final thoughts*

Notwithstanding the potential and opportunities for further research, it has been demonstrated that the current state-of-the-art in 3D modelling already offers a wide range of solutions for the virtual 3D modelling. Different elements of the acquisition, processing, analysis and management of spatial data for 3D modelling were covered in this dissertation. The knowledge of this research enabled to optimize the different acquisition and processing steps for environmental models, 3D city models and 3D models of small objects. The most suitable sensor or (integrated) series of sensors and processing techniques could be selected, based on this research. Furthermore, it is possible to perform thorough geometrical and semantical quality analyses on the data, using various statistical tools. This dissertation contains some practical elaborations on the use of spatial 3D data. These applications were made possible using the above mentioned research results, but also by the implementation of intelligent and innovative management systems and automated procedures for enriched 3D modelling.

It can be concluded that this work contributed to different scientific research fields, dealing with 3D models for various applications. Data acquisition sensors are becoming smaller and lighter, whereas computers and software are becoming more powerful and sophisticated. Since the proposed methods, techniques and approaches are in fact application and platform independent, it can be hoped that the findings of this dissertation support the increasing availability and quality of 3D models of the environment, cities or features for expert users of the wide public.

References

Adami, A., 2009. From real to virtual globe: new technologies for digital cartographic representation. E-Perimetron 4 (3), 144-160.

AGIV, 2013. www.geopunt.be, Ghent, Belgium

Bartoněk, D., Bureš, J., Dráb, A., 2011. Usage of GIS technology in civil engineering. Journal of Environmental Science and Engineering 5 (2), 177-183.

Bennett, R., Welham, K., Hill, R., Ford, A., 2011. Making the most of airborne remote sensing techniques for archaeological survey and interpretation, in: Cowley, D. (Ed.), Remote Sensing for Archaeological Heritage Management. Europae Archaeologia Consilium (EAC), Brussels, Belgium, pp. 99-107.

Brutto, M., Spera, M., 2011. Image-based and range-based 3D modelling of archaeological cultural heritage: the Telamon of the temple of Olympian Zeus in Agrigento (Italy). International Archives of Photogrammetry, Remote Sensing and Spatial Information Sciences 37 (Part 5), 8 p. (on CD-ROM).

de Kluijver, H., Stoter, J., 2003. Noise mapping and GIS: optimising quality and efficiency of noise effect studies. Computers, Environment and Urban Systems 27 (1), 85-102.

Döllner, J., Kolbe, T., Liecke, F., Sgouros, T., Teichmann, K., 2006. The virtual 3D city model of Berlin: managing, integrating, and communicating complex urban information, Urban Data Management Symposium (UDMS), Aalborg, Denemark, 15-17 May, pp. 12 (on CD-ROM)

Dubovyk, O., Sliuzas, R., Flacke, J., 2011. Spatio-temporal modelling of informal settlement development in Sancaktepe district, Istanbul, Turkey. ISPRS Journal of Photogrammetry and Remote Sensing 66 (2), 235-246.

Enemark, S., Williamson, I., Wallace, J., 2005. Building modern land administration systems in developed economies. Journal of Spatial Science 50 (2), 51-68.

EuropeanCommission, 2007. Establishment of an Infrastructure for Spatial Information in the European Community (INSPIRE) 108. European Parliament and of the Council, Brussels, Belgium, pp. 1-14

Foody, G., Mathur, A., 2004. Toward intelligent training of supervised image classifications: directing training data acquisition for SVM classification. Remote Sensing of Environment 93 (1), 107-117.

Goodchild, M., 1992. Geographical data modeling. Computers & Geosciences 18 (4), 401-408.

Grammatikopoulos, L., Kalisperakis, I., Karras, G., Petsa, E., 2007. Automatic multi-view texture mapping of 3D surface projections. International Archives of Photogrammetry and Remote Sensing and Spatial Information Sciences 36 (5), 6.

Gröger, G., Kolbe, T., Czerwinski, A., Nager, C., 2008. Open City Geography Markup Language (CityGML) encoding standard, Open GIS Encoding Standard. Open Geospatial Consortium Inc., p. 234

Haala, N., Kada, M., 2010. An update on automatic 3D building reconstruction. ISPRS Journal of Photogrammetry and Remote Sensing 65 (6), 570-580.

Hruby, F., Plank, I., Riedl, A., 2006. Cartographic heritage as shared experience in virtual space: a digital representation of the earth globe of Gerard Mercator (1541). e-Perimetron 1 (2), 88-98.

Kourosh, K., Oude Elberink, S., 2012. Accuracy and resolution of kinect depth data for indoor mapping applications. Sensors 12 (2), 1437-1454.

Louhisuo, M., Veijonen, T., Ahola, J., Morohoshi, T., 2007. A disaster information and monitoring system utilizing earth observation. Management of Environmental Quality: An International Journal 18 (3), 246-262.

Lu, D., Weng, Q., 2007. A survey of image classification methods and techniques for improving classification performance. International Journal of Remote Sensing `28 (5), 823-870.

Martin, P., LeBoeuf, E., Daniel, E., Dobbins, J., Abkowitz, M., 2004. Development of a GIS-based spill management information system. Journal of Hazardous Materials 112 (3), 239-252.

Matthys, M., De Maeyer, P., Bogaert, P., Brondeel, M., Collard, C., 2005. A Belgian 3D cadastre (in dutch), L'information patrimoniale, une opportunité pour le monde académique, Brussels, Belgium

McCaffrey, T., Franklin, S., 1993. Automated training site selection for large-area remote-sensing image analysis. Computers & Geosciences 19 (10), 1413-1428.

Merbitz, H., Buttstädt, M., Michael, S., Dott, W., Schneider, C., 2012. GIS-based identification of spatial variables enhancing heat and poor air quality in urban areas. Applied Geography 33 (3), 94-106.

Mironga, J., 2004. Geographic information systems (GIS) and remote sensing in the management of shallow tropical lakes. Applied Ecology and Environmental Research 2 (1), 83-103.

Naess, P., 2001. Urban planning and sustainable development. European Planning Studies 9 (4), 503-524.

Niemczynowicz, J., 1999. Urban hydrology and water management: present and future challenges. Urban Water 1 (1), 1-14.

Novacheva, A., 2008. Building roof reconstruction from LiDAR data and aerial images through plane extraction and colour edge detection. International Archives of Photogrammetry, Remote Sensing and Spatial Information Sciences 37 (B6), 53-58.

Nuttens, T., De Wulf, A., Bral, L., De Wit, B., Carlier, L., De Ryck, M., Stal, C., Constales, D., De Backer, H., 2010. High resolution terrestrial laser scanning for tunnel deformation measurements, XXIV FIG International Congress, Sydney, Australia (on CD ROM).

Ortiz, J., Gil, M., Martínez, S., Rego, T., Meijide, G., 2013. Three-dimensional modelling of archaeological sites using close-range automatic correlation photogrammetry and low-altitude imagery. Archaeological Prospection 20 (2).

Plets, G., Gheyle, W., Verhoeven, G., De Reu, J., Bourgeois, J., Verhegge, J., Stichelbaut, B., 2012. Three-dimensional recording of archaeological remains in the Altai Mountains. Antiquity 86 (333), 1-14.

Remondino, F., 2011. Heritage recording and 3D modeling with photogrammetry and 3D scanning. Remote Sensing 3 (6), 1104-1138.

Sandström, U., Angelstam, P., Khakee, A., 2006. Urban comprehensive planning: identifying barriers for the maintenance of functional habitat networks. Landscape and Urban Planning 75 (1-2), 43-57.

Sarkar, S., Boyer, K., 1993. Perceptual organization in computer vision: a review and a proposal for a classificatory structure. IEEE Transactions on Systems, Man and Cybernetics 23 (2), 382-399.

Schnabel, R., Wahl, R., Klein, R., 2007. Efficient RANSAC for point-cloud shape detection. Computer Graphics Forum 26 (2), 214-226.

Smart, P., Quinn, J., Jones, C., 2011. City model enrichment. ISPRS Journal of Photogrammetry and Remote Sensing 66 (2), 223-234.

Stal, C., De Roo, B., De Maeyer, P., Nuttens, T., De Wulf, A., 2013. Considerations on the fusion of multi-sensor spatial data for cultural heritage. In 16th AGILE conference on Geographic Information Science (AGILE 2013): Geographic information science at the heart of Europe., in: De Roo, B. (Ed.), 16th AGILE conference on Geographic Information Science, Leuven, Belgium, p. 3

Steiniger, S., Hunter, A.J.I.p.-S.B.H., 2012. Free and open source GIS software for building a spatial data infrastructure, in: Ruas, A. (Ed.), Geospatial Free and Open Source Software in the 21st Century. Springer, Heidelberg, Germany, pp. 247-261.

UnitedStatesPresident, 1994. Coordinating geographic data acquisition and access: the national spatial data infrastructure, in: House, t.W. (Ed.), 12906, Washington D.C., USA, p. 4

USGS, 2013. EarthExplorer, http://earthexplorer.usgs.gov, in: Survey, U.S.G. (Ed.), Reston, VA, USA

Vakalis, D., Sarimveis, H., Kiranoudis, C., Alexandridis, A., Bafas, G., 2004. A GIS based operational system for wildland fire crisis management II. System architecture and case studies, Applied Mathematical Modelling 28 (4), 411-425.

Veregin, H., 1999. Data quality parameters, in: Longley, P., Goodchild, M., Maguire, D., Rhind, D. (Eds.), Geographical Information Systems. Wiley, New York, NY, USA.

Verhoeven, G., Doneus, M., Briese, C., Vermeulen, F., 2012. Mapping by matching: a computer vision-based approach to fast and accurate georeferencing of archaeological aerial photographs. Journal of Archaeological Science 39 (7), 2060-2070.

Chapter10

References and scientific contributions

10. References and scientific contributions

Journal papers used for this dissertation

Stal, C., De Wulf, A., De Coene, K., De Maeyer, P., Nuttens, T., & Ongena, T. (2012). Digital representation of historical globes : methods to make 3D and pseudo-3D models of sixteenth century Mercator globes. *Cartographic Journal*, *49*(2), 107–117.

Stal, C., Briese, C., De Maeyer, P., Goossens, R., Hendrickx, M., Nuttens, T., Pfeifer, N. & De Wulf, A. (2013), Comparison of airborne laser scanning and image based modelling technique. *The Photogrammetric Journal, Under review.*

Stal, C., Tack, F., De Maeyer, P., De Wulf, A., & Goossens, R. (2013). Airborne photogrammetry and LIDAR for DSM extraction and 3D change detection over an urban area : a comparative study. *International Journal of Remote Sensing*, *34*(4), 1087–1110.

Stal, C., Briese, C., De Maeyer, P., Dorninger, P., Nuttens, T., Pfeifer, N. & De Wulf A. (2013) Classification of airborne laser scanning point clouds based on binomial logistic regression analysis, *International Journal of Remote Sensing, 35* (9), 3219-3236

Stal, C., Van Liefferinge, K., De Reu, J., Docter, R., Dierkens, G., De Maeyer, P., Mortier, S., et al. (2013), Integrating geomatics in archaeological research at the site of Thorikos (Greece). *Journal of Archaeological Science, 45* (May), 112–125

Stal, C., De Maeyer., P., De Meyer, R., Pauwels, P., Nuttens, T., Verstraeten, R. & De Wulf, A. (2014), 3D city mapping and data management using interconnected GI-software and Python. *Journal of Maps, Under review.*

Complete list of scientific publications (2014)

A1 (Referenced on ISI Web of Science)

Stal, C., Tack, F., De Maeyer, P., De Wulf, A., & Goossens, R. (2013). Airborne photogrammetry and LIDAR for DSM extraction and 3D change detection over an urban area : a comparative study. *International Journal of Remote Sensing*, *34*(4), 1087–1110.

Stal, C., De Wulf, A., De Coene, K., De Maeyer, P., Nuttens, T., & Ongena, T. (2012). Digital representation of historical globes : methods to make 3D and pseudo-3D models of sixteenth century Mercator globes. *Cartographic Journal*, *49*(2), 107–117.

Werbrouck, I., Antrop, M., Van Eetvelde, V., **Stal, C**., De Maeyer, P., Bats, M., Bourgeois, J., et al. (2011). Digital elevation model generation for historical landscape analysis based on LiDAR data : a case study in Flanders (Belgium). *Expert Systems with Applications*, *38*(7), 8178–8185.

Van Liefferinge, K., Van Den Berg, M., **Stal, C**., Docter, R., De Wulf, A., & Verhoest N. (2014), Reconstructing the position of Thorikos in the Laurion silver mining district (Attica, Greece) through hydrological analyses. *Journal of Archaeological Science, 41 (January)*, Pages 272-284.

Stal, C., Van Liefferinge, K., De Reu, J., Docter, R., Dierkens, G., De Maeyer, P., Mortier, S., et al. (2013), Integrating geomatics in archaeological research at the site of Thorikos (Greece). Journal of Archaeological Science. 45 (May), 112–125

Stal, C., Briese, C., De Maeyer, P., Dorninger, P., Nuttens, T., Pfeifer, N. & De Wulf A. (2013) Classification of airborne laser scanning point clouds based on binomial logistic regression analysis, *International Journal of Remote Sensing*, *35* (9), 3219-3236

Submitted A1

Nuttens, T., **Stal, C**., De Backer, H., Deruyter, G., Schotte, K., Van Bogaert, Ph. & De Wulf, A. (2013), Laser scanning for ovalization measurements: experimental standard deviations and optimal smoothing levels (Diabolo project, Belgium). *ASCE Journal of Civil Engineering. Under review.*

Badreldin, N., Uria-Diez, J., Mateu, J., Youssef, A., **Stal, C**., El-Bana, M., Magdy, A., Goossens, R., 2014. Object-based image analysis for monitoring the spatial distribution of a halophytic species in an arid coastal environment. *Applied Geography, Under review.*

Stal, C., Frankl, A., Abraha, A., Poesen, J., Rieke-Zapp, D., De Wulf, A. & Nyssen, J. (2013), Quantifying volumes of gullies and river channels: a rapid and detailed approach by image-based 3D modelling. *Progress in Physical Geography, Under review.*

Nuttens, T., **Stal, C**., Constales, D. & De Wulf A. (2014), Processing laser scanning data of cylindrical tunnels for deformation measurements: Automatic point cloud filtering and cylinder fitting. *ASCE Journal of Civil Engineering, Under review.*

Stal, C., De Maeyer., P., De Meyer, R., Pauwels, P., Nuttens, T., Verstraeten, R. & De Wulf, A. (2014), 3D city mapping and data management using interconnected GI-software and Python. *Journal of Maps, Under review.*

Stal, C., Briese, C., De Maeyer, P., Goossens, R., Hendrickx, M., Nuttens, T., Pfeifer, N. & De Wulf, A. (2013), Comparison of airborne laser scanning and image based modelling technique. *Expert Systems with Applications, Under review.*

P1 (Conference papers on ISI Web of Science)

Stal, C., De Wulf, A., De Maeyer, P., Deruyter, G., Goossens, R., Hendrickx, M., & Nuttens, T. (2013). Change detection on cultural heritage by radiometric comparison of terrestrial photos and terrestrial laser scanning. *International Multidisciplinary Scientific GeoConference-SGEM* (pp. 587–594). Presented at the 13th International multidisciplinary scientific Geoconference SGEM (SGEM 2013), Sofia, Bulgaria: International Scientific Conference SGEM.

Deruyter, G., Van Quickelberghe, A., Nuttens, T., **Stal, C**., & De Wulf, A. (2013). Risk assessment: a comparison between the use of laser scanners and total stations in a situation where time is the critical factor. *International Multidisciplinary Scientific GeoConference-SGEM* (pp. 687–694). Presented at the 13th International multidisciplinary scientific Geoconference SGEM (SGEM 2013), Sofia, Bulgaria: International Scientific Conference SGEM.

De Wulf, A., De Maeyer, P., De Ryck, M., Nuttens, T., **Stal, C**., Libert, M., & Annaert, A. (2013). Higher hydrography education in Belgium. *International Multidisciplinary Scientific GeoConference-SGEM* (pp. 429–436). Presented at the 13th International multidisciplinary scientific Geoconference SGEM (SGEM 2013), Sofia, Bulgaria: International Scientific Conference SGEM.

De Wulf, A., Nuttens, T., **Stal, C**., & Deruyter, G. (2013). Renewed (2013) geomatics Bachelor, Master and PhD programs at Belgian academic universities. *International Multidisciplinary Scientific GeoConference-SGEM* (pp. 497–504). Presented at the 13th International multidisciplinary scientific Geoconference SGEM (SGEM 2013), Sofia, Bulgaria: International Scientific Conference SGEM.

Deruyter, G., Vandedrinck, F., Nuttens, T., **Stal, C**., & De Wulf, A. (2013). The evolution of education in land surveying in Flanders, Belgium: a work in progress. *International Multidisciplinary Scientific GeoConference-SGEM* (pp. 557–564). Presented at the 13th International multidisciplinary scientific Geoconference SGEM (SGEM 2013), Sofia, Bulgaria: International Scientific Conference SGEM.

Nuttens, T., De Wulf, A., Deruyter, G., & **Stal, C**. (2012). Deformation monitoring with terrestrial laser scanning: measurement and processing optimization through experience. *International Multidisciplinary Scientific GeoConference-SGEM* (pp. 707–714). Presented at the 12th International Multidisciplinary Scientific GeoConference SGEM 2012, Sofia, Bulgaria: STEF92 Technology.

Stal, C., De Wulf, A., De Maeyer, P., Goossens, R., Nuttens, T., & Tack, F. (2012). Statistical comparison of urban 3D models from photo modeling and airborne laser scanning. *International Multidisciplinary Scientific GeoConference-SGEM* (pp. 901–908). Presented at the 12th International Multidisciplinary Scientific GeoConference SGEM 2012, Sofia, Bulgaria: STEF92 Technology.

Nuttens, T., De Wulf, A., **Stal, C**., Constales, D., De Backer, H., & Schotte, K. (2011). Ovalisation measurements of newly built concrete tunnels by means of terrestrial laser scanning. *International Multidisciplinary Scientific GeoConference-SGEM* (pp. 287–294). Presented at the 11th International Multidisciplinary Scientific GeoConference (SGEM 2011), Sofia, Bulgaria: International Scientific Conference SGEM.

Other scientific contributions per category

A2

Docter, R., Vella, N., Cutajar, N., Bonanno, A., Pace, A., Anastasi, M., Bechtold, B., **Stal, C**., et al. (2012). Rural Malta : first results of the joint Belgo-Maltese survey project. *BABESCH : Bulletin Antieke Beschaving*, *87*, 1–47.

Stal, C., Nuttens, T., Bourgeois, J., Carlier, L., De Maeyer, P., & De Wulf, A. (2011). Accuracy assessment of a LiDAR digital terrain model by using RTK GPS and total station. *Earsel Eproceedings*, *10*(8), 1–8.

A4

Nuttens, T., De Wulf, A., Bral, L., De Wit, B., Carlier, L., De Ryck, M., **Stal, C**., et al. (2012). Terrestrial laser scanning for tunnel deformation measurements. *PositionIT*, (April-May), 24–32.

Stal, C., De Wulf, A., & Nuttens, T. (2012). Tunnel measurements and point filtering : automated point set filtering of cylindrical tunnel point sets. *GIM International*, *26*(8), 30–35.

B2

Stal, C., De Wulf, A. & De Maeyer, P. (2013). Digitale representative van historische globes: methoden voor het maken van 3D- en pseudo-3D-modellen van globes van Mercator uit de 16de eeuw. In H. Van Royen (Ed.), *Mercator Cartograaf*. Sint Niklaas, Belgium: Snoeck Uitgeverij

Van Liefferinge, K., **Stal, C**., & De Wulf, A. (2011). The Thorikos excavations 1963-2010 in maps. In R. Docter (Ed.), *Thorikos 10 Reports & Studies* (Vol. 10, pp. 15–50). Ghent, Belgium: Ghent University Department of Archaeology.

C1

Stal, C., Goossens, R., Carlier, L., Debie, J., Haoudy, K., Nuttens, T., & De Wulf, A. (2013). Cultural heritage documentation and integrated geomatics techniques in an educational context: case Bois-du-Luc (Belgium). In P. Grussenmeyer (Ed.), *International Archives of the Photogrammetry, Remote Sensing and Spatial Information Sciences* (Vol. XL-5/W2, pp. 611–615). Presented at the 24th International CIPA Symposium, International Society for Photogrammetry and Remote Sensing (ISPRS).

Stal, C., De Roo, B., De Maeyer, P., Nuttens, T., & De Wulf, A. (2013). Considerations on the fusion of multi-sensor spatial data for cultural heritage. *Geographic Information Science, 16th AGILE conference, Proceedings*. Presented at the 16th AGILE conference on Geographic Information Science (AGILE 2013): Geographic information science at the heart of Europe.

De Wulf, A., Constales, D., **Stal, C**., & Nuttens, T. (2012). Accuracy aspects of processing and filtering of multibeam data: grid modeling versus TIN based modeling. *FIG working week 2012, 6-10 May 2012, Rome, Italy : Knowing to manage the territory, protect the environment, evaluate the cultural heritage : proceedings*. Presented at the FIG Working Week 2012, International Federation of Surveyors (FIG).

Nuttens, T., Vandendriessche, B., Tytgat, C., De Wulf, A., **Stal, C**., Van Damme, D., & Goossens, R. (2012). Photogrammetric restitution of a presumed ancient Asclepius temple in Titani, Peloponnesos, Greece. *Advances in Remote Sensing for Archaeology and Cultural Heritage Management, 3rd International EARSeL workshop, Proceedings*. Presented at the 3rd International EARSeL workshop on the Advances in Remote Sensing for Archaeology and Cultural Heritage Management.

Seube, N., De Wulf, A., Böder, V., Touzé, T., Debese, N., Moitié, R., Probst, I., **Stal, C**., et al. (2012). International cooperation in education: the Vassivière Erasmus Intensive Training Program (2011-2013) on hydrography and geomatics. *Hydro12 proceedings*. Presented at the Hydro-12 : Taking care of the sea, Hydrographic Society Benelux.

De Wulf, A., Constales, D., Nuttens, T., & **Stal, C**. (2012). Grid models versus TIN: geometric accuracy of multibeam data processing. *Hydro12 proceedings*. Presented at the Hydro-12 : Taking care of the sea, Hydrographic Society Benelux.

Stal, C., De Maeyer, P., De Wulf, A., Goossens, R., Maddens, R., & Nuttens, T. (2012). Virtual reconstruction of a Maya temple using total station and photo modelling. *Computer Applications and Quantitative Methods in Archaeology, 40th International conference, Proceedings* (pp. 26–30). Presented at the 40th International conference on Computer Applications and Quantitative Methods in Archaeology (CAA 2012).

Nuttens, T., De Wulf, A., Deruyter, G., **Stal, C**., De Backer, H., & Schotte, K. (2012). Application of laser scanning for deformation measurements: a comparison between different types of scanning instruments. *FIG working week 2012, 6-10 May 2012, Rome, Italy : Knowing to*

manage the territory, protect the environment, evaluate the cultural heritage : proceedings. Presented at the FIG Working Week 2012, International Federation of Surveyors (FIG).

Stal, C., Nuttens, T., Constales, D., Schotte, K., De Backer, H., & De Wulf, A. (2012). Automatic filtering of terrestrial laser scanner data from cylindrical tunnels. *FIG working week 2012, 6-10 May 2012, Rome, Italy : Knowing to manage the territory, protect the environment, evaluate the cultural heritage : proceedings*. Presented at the FIG Working Week 2012, International Federation of Surveyors (FIG).

De Wulf, A., Nuttens, T., **Stal, C**., De Wit, B., Seube, N., & Boder, V. (2012). Erasmus intensive program (2011-2013) in hydrography and geomatics. *FIG working week 2012, 6-10 May 2012, Rome, Italy : Knowing to manage the territory, protect the environment, evaluate the cultural heritage : proceedings*. Presented at the FIG Working Week 2012, International Federation of Surveyors (FIG).

Stal, C., Bourgeois, J., De Maeyer, P., De Mulder, G., De Wulf, A., Goossens, R., Hendrickx, M., et al. (2012). Test case on the quality analysis of structure from motion in airborne applications. In K. Perakis (Ed.), *Advances in geosciences : proceedings of the 32nd EARSeL symposium*. Presented at the 32nd EARSeL Symposium : Advances in geosciences, European Association of Remote Sensing Laboratories (EARSeL).

Stal, C., De Wulf, A., De Maeyer, P., Goossens, R., & Nuttens, T. (2012). Evaluation of the accuracy of 3D data acquisition techniques for the documentation of cultural heritage. *Advances in Remote Sensing for Archaeology and Cultural Heritage Management, 3rd International EARSeL workshop, Proceedings*. Presented at the 3rd International EARSeL workshop on the Advances in Remote Sensing for Archaeology and Cultural Heritage Management.

Nuttens, T., De Maeyer, P., De Wulf, A., Goossens, R., & **Stal, C**. (2011). Comparison of 3D accuracy of terrestrial laser scanning and digital photogrammetry : an archaeological case study. In L. Halounová (Ed.), *Remote sensing and geoinformation not only for scientific cooperation : proceedings of the 31st EARSeL symposium* (pp. 66–74). Presented at the 31th EARSeL symposium : Remote sensing and geoinformation not only for scientific cooperation, European Association of Remote Sensing Laboratories (EARSeL).

De Wulf, A., Docter, R., **Stal, C**., Goossens, R., Nuttens, T., & Vella, N. (2011). Integrated 3D geomatics for archaeology : case study Malta. In L. Halounová (Ed.), *Remote sensing and geoinformation not only for scientific cooperation : proceedings of the 31st EARSeL symposium* (pp. 604–612). Presented at the 31th EARSeL symposium : Remote sensing and geoinformation not only for scientific cooperation, European Association of Remote Sensing Laboratories (EARSeL).

Stal, C., De Wulf, A., Nuttens, T., De Maeyer, P., & Goossens, R. (2011). Reconstruction of a medieval wall : photogrammetric mapping and quality analysis by terrestrial laser scanning. In L. Halounová (Ed.), *Remote sensing and geoinformation not only for scientific cooperation :*

proceedings of the 31st EARSeL symposium (pp. 54–65). Presented at the 31th EARSeL symposium : Remote sensing and geoinformation not only for scientific cooperation, European Association of Remote Sensing Laboratories (EARSeL).

Nuttens, T., De Maeyer, P., De Wulf, A., Goossens, R., & **Stal, C**. (2011). Terrestrial laser scanning and digital photogrammetry for cultural heritage : an accuracy assessment. *FIG Working Week 2011 and 6th national congress of ONIGT : proceedings*. Presented at the FIG Working Week 2011 : Bridging the gap between cultures, International Federation of Surveyors (FIG).

De Wulf, A., Constales, D., Meskens, J., Nuttens, T., & **Stal, C**. (2011). Procedure for analyzing geometrical characteristics of an EDM calibration bench. *FIG Working Week 2011 and 6th national congress of ONIGT : proceedings*. Presented at the FIG Working Week 2011 : Bridging the gap between cultures, International Federation of Surveyors (FIG).

De Wulf, A., Nuttens, T., **Stal, C**., & De Maeyer, P. (2011). Geomatics education in Belgium : 2011 program reformation at Belgian universities. *FIG Working Week 2011 and 6th national congress of ONIGT : proceedings*. Presented at the FIG Working Week 2011 : Bridging the gap between cultures, International Federation of Surveyors (FIG).

Stal, C., De Maeyer, P., De Ryck, M., De Wulf, A., Goossens, R., & Nuttens, T. (2011). Comparison of geometric and radiometric information from photogrammetry and color-enriched laser scanning. *FIG Working Week 2011 and 6th national congress of ONIGT : proceedings*. Presented at the FIG Working Week 2011 : Bridging the gap between cultures, International Federation of Surveyors (FIG).

De Wulf, A., Nuttens, T., **Stal, C**., & De Maeyer, P. (2011). Evaluation and reformation (2011) of the geomatics education programs at Belgium academic universities. *INTED 2011 proceedings* (pp. 3183–3192). Presented at the 5th International Technology, Education and Development conference (INTED 2011), International Association of Technology, Education and Development (IATED).

Stal, C., Bourgeois, J., De Maeyer, P., De Mulder, G., De Wulf, A., Goossens, R., Nuttens, T., et al. (2010). Kemmelberg (Belgium) case study : comparison of DTM analysis methods for the detection of relicts from the First World War. In R. Reuter (Ed.), *Remote sensing for science, education, and natural and cultural heritage : proceedings of the EARSeL Symposium 2010* (pp. 65–72). Presented at the 30th EARSeL symposium : Remote sensing for science, education, and natural and cultural heritage, European Association of Remote Sensing Laboratories (EARSeL).

Stal, C., De Maeyer, P., De Wulf, A., Nuttens, T., Vanclooster, A., & Van de Weghe, N. (2010). An optimized workflow for processing airborne laserscan data in a GIS-based environment. In Thomas Kolbe, G. König, & C. Nagels (Eds.), *International Archives Of The Photogrammetry, Remote Sensing And Spatial Information Sciences* (Vol. 38, pp. 163–167). Presented at the 5th International conference on 3D GeoInformation.

Nuttens, T., De Wulf, A., Bral, L., De Wit, B., Carlier, L., De Ryck, M., **Stal, C**., et al. (2010). High resolution terrestrial laser scanning for tunnel deformation measurements. *The XXIV FIG International Congress 2010 : proceedings*. Presented at the 24th FIG International Congress (FIG Congress 2010) : Facing the challenges, building the capacity, FIG (Fédération Internationale des Géomètres).

C3

Frankl, A., **Stal, C.,** Poesen, J., Amanuel Abraha, De Wulf, A., Nyssen, J. (2013). Recording erosion features in 3D: the use of image-based modelling. *GAPSYM, Abstracts* (pp. 50-50). Poster presented at the 7th symposium of Ghent Africa Platform (GAPSYM), Ghent, Belgium, 6 December 2013.

Docter, R., Verdonck, L., Dierkens, G., van de Put, W., Vella, N., Bonanno, A., Anastasi, M., **Stal, C**., et al. (2013). Rural sites in Northwest Malta: results of the Belgo-Maltese survey project. *Radio-Past colloquium, Abstracts* (pp. 40–40). Presented at the Radio-Past colloquium : Non-destructive approaches to complex archaeological sites in Europe : a round-up.

Hendrickx, M., De Laet, V., **Stal, C**., De Wulf, A., & Goossens, R. (2013). The use of high resolution digital surface models for change detection and viewshed analysis in the area around the pyramids of Giza, Egypt. *JURSE, Book of abstracts*. Presented at the JURSE 2013 : Joint Urban Remote Sensing Event.

Stal, C., De Wulf, A., De Coene, K., De Maeyer, P., Nuttens, T., & Ongena, T. (2012). Digital representation of historical globes : methods to make 3D and semi-3D models of 16th century Mercator globes. In S. Vervust, B. Ooghe, & P. De Maeyer (Eds.), *Mercator revisited : cartography in the age of discovery : conference proceedings* (pp. 117–117). Presented at the Mercator revisited : cartography in the age of discovery.

Stal, C., De Wulf, A., De Maeyer, P., Goossens, R., & Nuttens, T. (2012). Evaluation of the accuracy of 3D data acquisition techniques for the documentation of cultural heritage. *Advances in Remote Sensing for Archaeology and Cultural Heritage Management, 3rd International EARSeL workshop, Abstracts*. Presented at the 3rd International EARSeL workshop on the Advances in Remote Sensing for Archaeology and Cultural Heritage Management.

Hendrickx, M., De Laet, V., **Stal, C**., De Wulf, A., & Goossens, R. (2012). Urban expansion around the pyramids of Giza, Egypt: 3D change detection based on high resolution digital surface models. *EARSeL, 32nd Symposium, Book of abstracts* (pp. 115–115). Presented at the 32nd EARSeL Symposium : Advances in geosciences.

Hendrickx, M., De Laet, V., **Stal, C**., De Wulf, A., & Goossens, R. (2012). Landscape evolution in the Nile Valley: physical and anthropogenic 3D changes in the last 40 years in Dayr al-Barsha. *EARSeL, 32nd Symposium, Book of abstracts*. Presented at the 32nd EARSeL Symposium : Advances in geosciences.

Hendrickx, M., De Laet, V., **Stal, C**., De Wulf, A., & Goossens, R. (2012). Evolution of the river Nile as derived from CORONS DSMs in the region of Dayr al-Barsha, Middle Egypt. *Advances in Remote Sensing for Archaeology and Cultural Heritage Management, 3rd International EARSeL workshop, Abstracts* (pp. 36–37). Presented at the 3rd International EARSeL workshop on the Advances in Remote Sensing for Archaeology and Cultural Heritage Management.